Engineering troponin C with altered Ca^{2+} binding properties to study mechanisms of enhanced contraction of cardiac muscle from healthy and infarcted hearts

Erik Russell Feest

A dissertation submitted in partial fulfillment of the requirements for the degree of:

Doctor of Philosophy

University of Washington

2013

Supervisory Committee:

Michael Regnier, Advisor

William Mahoney, Jr. (GSR)

Fernando Santana

Rong Tian

Program Authorized to Offer Degree:

Bioengineering

University of Washington

ABSTRACT

Engineering troponin C with altered Ca^{2+} binding properties to study mechanisms of enhanced contraction of cardiac muscle from healthy and infarcted hearts

Erik Feest

Chair of the Supervisory Committee:

Professor Michael Regnier

Department of Bioengineering

Heart failure is the leading cause of morbidity and mortality in developed nations. It is responsible for 1 in every 3 deaths while costing over $500 billion annually in the United States alone. Unfortunately, most current treatments for heart failure are palliative approaches that fail to restore any functional capacity to the heart. This significant lack of effective clinical treatments underscores the need to develop new therapies for heart failure focused on recovery of cardiac function.

Motivated by this need, the long-term goal of this dissertation was to improve the mechanistic understanding of how modulating myofilament Ca^{2+} binding properties affects cardiac muscle contraction and apply it to the development of a novel cardiac muscle-targeted gene therapy to improve heart function. From both mechanistic and therapeutic perspectives, it was important to understand how manipulating thin and thick filament properties impacted cardiomyocyte and whole heart function. I demonstrated that altering myofilament Ca^{2+} binding properties via troponin modulations with L48Q cTnC or phosphorylation states of cTnI sets cardiac thin filament activation

levels and the SL dependence of Ca^{2+} sensitivity of force. I also improved healthy and diseased intact cardiomyocyte contractility without perturbing relaxation or Ca^{2+} transient properties by increasing myofilament Ca^{2+} binding properties (via L48Q cTnC) or crossbridge cycle kinetics (via dATP). Based on these promising results in intact cardiomyocytes, I engineered a novel cardiac muscle-specific AAV6 gene delivery system to investigate the effects of *in vivo* expression of L48Q cTnC on whole heart function.

This dissertation translated the insights gained from basic science research to the development a potential strategy to treat heart failure. In doing so, it established the foundation for a number of on-going collaborations in the lab and additional studies, including evaluation of the AAV6 L48Q cTnC system as a therapeutic strategy to enhance whole heart function.

Acknowledgements

I would like to begin by expressing my thanks and gratitude to my principal supervisor, Dr. Michael Regnier. Your support, guidance, insights, willingness to challenge me, and openness to being challenged by me were crucial to the development and completion of this work. I would also like to thank my supervisory committee members, Drs. Fernando Santana, Kenneth Schenkman, and Rong Tian for your valuable perspectives, advice, flexibility, and willingness to help at each step. I would also like to thank Dr. William Mahoney, Jr. for doing me a big scheduling favor late in this process and joining my committee. Also, thank you to all the faculty, department staff, especially Dorian Varga, and graduate students that compose the Bioengineering department at UW.

This work would not have been possible without the help and support of the research team in the Heart and Muscle Mechanics Lab (HAMM lab). The entire lab was very helpful in providing the proper perspectives when they were needed most, both scientifically and emotionally. My sincere thanks go to Maria Razumova, Galina Flint, Zhixiong (Charles) Luo, An-yue Tu, Jin Dai, and Martha Mathaison, for your technical help and countless things you taught me over the long years. Many thanks also go to my fellow graduate students – Anthony Rodriquez, Sarah Nowakowski, Kassandra Thomson, Scott Lundy, Dave Williams and Dan Wang – for being my comrades through the highs and lows in the process, and for your friendship, humor, and advice. Thank you to the undergraduate student, Elizabeth Gay, for your help and perseverance through very challenging science times. I would like to thank post-doctoral fellow Vijay Rao for your advice and insights both scientifically and professionally. Importantly, I would like to convey my deepest gratitude, respect, and admiration to Dr. F. Steven Korte for the invaluable and immeasurable impact you have made on my life and career as a true mentor, colleague, scientist, friend, and person. You have helped me more than you can ever imagine, and this work would not have been completed without you.

I would like to thank all of my collaborators for the help and opportunities to learn they provided me. Thanks goes to the entire Charles Murry lab. Also, thank you to the members of Jeff Chamberlain's lab for letting me learn far more than I imagined about *in vivo* studies and viral development. A special thanks goes to Guy Odom in the Chamberlain lab for your humor, support, experimental advice, and flexibility. My thanks also goes to many other labs throughout the country that I collaborated with: Tom Irving's lab, Jeff Molkentin's lab, and Steven Hauschka's lab.

I owe many thanks to all of my many wonderful friends here in Seattle, back in California, and all across the world now. You have been more than amazing with your support, understanding, and belief in me throughout this process. You have no idea how much your love and support has meant to me; you are all forever part of my extended family.

Finally, I would like to wholeheartedly express my sincerest gratitude to my beloved family. Words cannot describe how much your unwavering love, support, and willingness to deal with me at my best and worst has meant to me. Thank you from the bottom of my heart to my mother, Kathryn Feest, my late father, Ronald Feest, my brother, Alex Feest, and the newer part of my family – the entire Allen family. I would like to give an extremely special thank you to my girlfriend, Jessica Allen, for your consistent and strong love, belief in me and our relationship, willingness to deal with me during one of the most challenging times in my life, and understanding throughout this process all from 800+ miles away. Without all the unconditional love, help, and support from all of you, it would have been impossible to complete this work.

Dedication

I dedicate this work to my late father, Ronald Feest, who at the young age of 51 lost a courageous, admirable, and incredible battle with leukemia when I was 16 years old. This battle forever changed the lives of everyone he knew, and those he didn't get a chance to know. Experiencing his battle with leukemia served as one of my biggest motivations for becoming a bioengineer; I did so in hopes of tackling the challenges that take so many loved ones away from their families and friends sooner than they deserve. Despite not being able to be present with me throughout this process and many others in life, I have always known that his unwavering love and support was, and will be, with me. I have been told on a number of occasions that we share many qualities, and that is one of the most honorable compliments I could ever be paid. Regardless of the situation, I will continue to do my very best to always be your rock, Dad.

Table of Contents

List of Figures and Tables

Abbreviations

ΔEC_{50}	difference in EC_{50} between SL 2.3 μm and 2.0 μm
ΔpCa_{50}	difference in pCa_{50} between SL 2.3 μm and 2.0 μm
$[Ca^{2+}]_i$	intracellular Ca^{2+} concentration
A	actin
AAV	adeno-associated virus
AAV6	adeno-associated virus serotype 6
ARC	adult rat cardiomyocyte
AV	adenovirus
CB	crossbridge
CMV	cytomegalovirus
cMyBP-C	cardiac myosin binding protein-C
cTm	tropomyosin
cTn	troponin complex
cTnC	cardiac troponin C
cTnC-cTn	recombinant cardiac troponin complex containing a cTnC variant
cTnI	cardiac troponin I
cTnT	cardiac troponin T
$d_{1,0}$	inter-thick filament spacing;
dATP	2 deoxy-ATP
DCM	dilated cardiomyopathy
DT_{50}, DT^{90}	time to 50% and 90% Ca^{2+} transient decay
F_{MAX}	maximum steady-state force (mN/mm^2)
F_{pass}	resting tension (mN/mm^2)
GFP	green fluorescent protein
HCM	hypertrophic cardiomyopathy
$I_{1.1}/I_{1,0}$	equatorial intensity ratio of 1,1 and 1,0 peaks of x-ray diffraction pattern
k_{tr}	force redevelopment rate
L48Q cTnC	recombinant cardiac troponin C with point the mutation of luecine (L) to glutamine (Q) at position 48

M	myosin
mCherry	red fluorescent protein
MI	myocardial infarction
MI+L48Q cTnC	cardiomyocyte from infarcted hearts transduced with L48Q cTnC
MI+WT cTnC	cardiomyocyte from infarcted hearts transduced with WT cTnC
NA	Non-transduced cardiomyocytes
n_H	Hill coefficient
pCa	$-\log[Ca^{2+}]$
pCa_{50}	Ca^{2+} sensitivity of force
P_i	norganic phosphate
PKA	protein kinase A
PKC	protein kinase C
RLC	myosin regulatory light chain 2
Rrm1	muscle ribonucleotide reductase 1
Rrm2	muscle ribonucleotide reductase 2
RT_{50}, RT_{90}	time to 50% and 90% relaxation
S23/24A	recombinant troponin complex containing S23/24A cTnI
S23/24D	recombinant troponin complex containing S23/24D cTnI
SERCA2a	sarco-endoplasmic reticulum Ca^{2+} ATPase
SL	sarcomere length
vg	vector genomes
WT cTn	recombinant wild-type troponin complex
WT cTnC	recombinant wild-type cardiac troponin

Chapter 1. Introduction

The heart is truly a remarkable organ and biological engineering feat. The heart is a mechanical pump driven by an electrical system composed of many different types of cells that work in concert without ever requiring conscious management from the individual. It is responsible for continually supplying the entire body with blood carrying oxygen and nutrients throughout the lifetime of the individual without ever taking a break. It does this by continuously and cyclically contracting and relaxing – generating over 3 billion beats over an individual's lifetime – while adapting to changes in physiological demands of the body that occur throughout the day during work, rest, and exercise. Despite possessing these extraordinary characteristics, it can still fail and malfunction. When it does, it can result in progression to the fatal state of heart failure. Heart failure has a variety of etiologies including myocardial infarction (MI), ischemia/reperfusion injury, diabetes, high blood pressure, and hypertrophic (HCM) and dilated cardiomyopathy (DCM). The impact of these cardiovascular related diseases is shocking. Heart failure is the leading cause of morbidity and mortality in developed nations, and is responsible for 1 in every 3 deaths. Furthermore, the costs associated with treating heart failure total over $500 billion annually in the United States alone [1]. The impact of heart failure is increasing dramatically around the world, and it is no longer only a "developed world" issue.

1.1 MYOCARDIAL INFARCTION AND HEART FAILURE

Heart failure is most commonly caused by myocardial infarction (MI) [1]. Inadequate blood flow carrying oxygen and nutrients to myocardium caused by a partial or complete occlusion of a coronary artery rapidly results in an MI. Much of the cardiac tissue downstream of the blockage is irreversibly damaged and often dies forming a non-contractile fibrotic scar, which ultimately results in less functional cardiac muscle to support the physiological demands of the body [2]. The tissue that does

survive the initial insult activates many compensatory mechanisms in an attempt to preserve cardiac output to meet the cardiovascular demands of the body. In most cases, these efforts fail to sufficiently preserve cardiac pumping capacity, and the heart then enters a vicious cycle of decompensated function called heart failure. Heart failure is characterized by chronic β-adrenergic stimulation, which exhausts contractile reserves and can elevate diastolic Ca^{2+} levels, loss of the Frank-Starling length-tension relationship, and left ventricular dilation [3–5]. Current clinical treatments for heart failure are primarily palliative and attempt to manage the progression of the disease rather than restore cardiac function. In extreme and rare cases, heart transplants and left ventricular assist devices are able to completely replace the failing heart with a new pump and "restore function". These treatments, however, are cost-prohibitive, require additional drug therapies for the rest of the recipient's life, and only help a very small fraction (< 1%) of the patient population. The available pharmacologic therapies, such as inotropic agents, β-adrenergic blockers, or angiotensin-converting enzyme inhibitors, fail to treat the pathology and improve heart function. Furthermore, they can cause significant side-effects, including arrhythmias and/or impaired diastolic function from ventricular dilation or elevated intracellular Ca^{2+} ($[Ca^{2+}]_i$) during diastole [6]. The significant lack of effective clinical treatments underscores the need to develop new therapeutic strategies for heart failure focused on recovery of cardiac function.

1.2 CURRENT PHARMACOLOGICAL TREATMENTS

There are a number of available pharmacological agents used as treatment strategies for heart failure, and most of them modulate cardiac muscle contractility through the manipulation of intracellular Ca^{2+}. Dobutamine is a β-adrenergic agonist similar to isoproterenol that was developed to selectively activate β_1-adrenergic receptors to increase cardiac contractility while minimizing the off-target effects on β_2-adrenergic receptors [7]. Milrinone is a drug that also targets the β-adrenergic pathway to increase inotropy, but has a different mechanism of action. Milrinone is a

phosphodiesterase-3 inhibitor that increases the activation of protein kinase A (PKA) and subsequent PKA-mediated phosphorylation of myofilament and Ca^{2+} handling proteins including L-type Ca^{2+} channels, which leads to increased Ca^{2+} influx and contractility [8]. Ca^{2+} sensitizing agents have also been developed, such as calmidazolium, bepridil, and levosiemenden, that increase Ca^{2+} binding to the N-terminus of cardiac troponin C (cTnC) and enhance contractile activation. These agents, however, are not highly specific to cTnC and can have off-target effects on other similar EF-hand Ca^{2+} binding proteins and on other aspects of excitation-contraction coupling [9,10]. One pharmacological treatment currently under development is omecantiv mecabril, which is a small molecule capable of directly activating myosin and thus modulating cardiac contractility [11,12]. This treatment does not manipulate intracellular Ca^{2+} in order to increase contractility; instead, it interacts with myosin and enhances the transition to the strongly actin-bound state [13]. Because of the direct interaction with myosin to enhance contraction and systolic function, there are many concerns with the molecule's potential negative effects on diastolic function. While these pharmacological treatments are able to increase cardiac output in the short term, they still fail to improve mortality rates in patients [14], and in some cases, even end up accelerating heart failure progression [15]. Development of novel approaches to modulate contractility for lifetime of the patient and in a more targeted manner, such as the potential gene therapy explored in this dissertation, may offer a true therapy for heart failure.

1.3 CARDIAC GENE THERAPY

Gene therapy is an alternative therapeutic strategy to treat heart failure that is being investigated and has the potential to overcome many the shortcomings of pharmacological treatments. The guiding principle behind gene therapy is to deliver and express a chosen gene in dysfunctional or diseased tissue and thereby restore normal function to the tissue. In the context of cardiac muscle, a gene therapy is well-suited to overcome many of the inherent challenges associated with targeting

the heart. These challenges include, but are not limited to, the difficulty achieving uptake and expression of genes in non-proliferative cells like cardiomyocytes, transducing only a sub-population of cells in a tissue that contains multiple different cell types like the myocardium, and accomplishing long-term enhancement of myocardial function [16,17]. Employing a myocardium-targeted gene delivery system could effectively address and overcome all of these challenges. Delivery of genes that are capable of modulating heart function has been accomplished using viral (adenovirus (AV), adeno-associated virus (AAV), or lentivirus) and non-viral delivery (polymer-based, lipid-based, or naked plasmid DNA) strategies [16,17]. Viral delivery strategies have been shown to be effective at transducing the myocardium, but they still face challenges with achieving the desired duration of expression, the potential elicitation of an immune responses, and/or potential oncogenesis with viruses that require insertion into the host genome for expression. Non-viral delivery strategies are considered safer but face their own hurdles, including very low transfection efficiency, weak transient gene expression profiles, and potential toxicity from the gene delivery vehicle degradation products [16,17].

Considering the advantages and limitations of both strategies, many cardiac gene therapy approaches have focused on viral transduction strategies. A number of groups have published evidence that expression of important cardiac genes can indeed improve cardiac muscle function following an MI. These strategies have focused on genes associated with different components involved in excitation-contraction coupling. Unfortunately, like many of the inotropic agents, most of these approaches modulate intracellular Ca^{2+} handling to achieve their effects on cardiac contractility, such as over-expression of sarco-endoplasmic reticulum Ca^{2+} ATPase (SERCA2a) [18], phospholamban [19], or the Ca^{2+} binding molecule S100A1 [20]. The strategy of over-expressing SERCA2a has been the most successful gene therapy approach to date, and recently completed Phase II clinical trials with promising results. This approach employed an AAV1 system to effectively

maintain long-term (12 months) SERCA2a over-expression and reduce major cardiac events without adverse effects [21,22]. Larger clinical trials will be necessary to determine if these early successes will translate into a viable therapy for heart failure.

Another gene therapy approach that is garnering excitement about its potential as a treatment for heart failure was developed in our laboratory and is focused on increasing the 2'-deoxyadenosine triphosphate (dATP) content in cardiac muscle cells. dATP is a naturally occurring nucleotide ubiquitously used for DNA synthesis. Its content in cells can be increased via over-expression of the enzyme, ribonucleotide reductase (Rrm1 Rrm2), which removes the 2' oxygen from adenosine diphosphate (ADP) generating dADP, which is rapidly phosphorylated to create dATP [23]. Small increases in dATP levels have been shown to increase maximal force and rate of force production in demembranted cardiac muscle [24], and acute increases in dATP in intact cardiomyocytes via over-expression of Rrm1/Rrm2 have increased the magnitude and rate of cellular shortening with minimal effects on relaxation or intracellular Ca^{2+} handling (discussed in more detail in Chapter 6) [25]. Chronic over-expression of Rrm1/Rrm2 in a transgenic mouse model has also demonstrated that increased dATP concentrations elevated systolic function *in vivo* also with minimal effects on relaxation or intracellular Ca^{2+} handling [26]. While these results are very promising, it still needs to be determined if increased cardiomyocyte dATP concentrations can improve heart function in diseased hearts, if there are any off-target effects in cardiac muscle, and if the improved heart function from increased dATP can be recapitulated in larger animal models and human trials.

1.4 CARDIAC MUSCLE CONTRACTION REGULATION

When attempting to develop novel therapies for heart failure that actually restore functional capacity to the heart, it is important to understand and consider how cardiac muscle contraction is regulated.

Cardiac muscle contraction is a regulated process that is dependent on myofilament Ca^{2+} binding for initiation, potentiation, and regulation. Cardiac muscle is composed of tubular myofibrils, which contain repeating structural units known as sarcomeres. The sarcomere is the smallest contractile unit of muscle and is composed of myofilaments. The myofilaments are composed of thin and thick filaments, and interactions between the thin filament and myosin motor on the thick filament generate sarcomere/muscle shortening and force [27].

The thin filament is composed of actin and the regulatory proteins troponin (cTn) and tropomyosin (cTm). These regulatory proteins act in a Ca^{2+}-dependent manner to regulate the availability of myosin crossbridge binding sites on actin. cTn consists of three subunits, the Ca^{2+} binding subunit (cTnC), the inhibitory subunit (cTnI), and a subunit that associates cTn with cTm (cTnT) (Figure 1.1 [28]). Each cTm spans 7 actin monomers and is associated with a single cTn complex. The position of cTm and cTn on the thin filament determines the exposure of the myosin binding sites on actin. These binding sites can be considered as blocked, closed, or open. When intracellular Ca^{2+} concentration is low, cTm, together with the C-terminus of cTnI, blocks the myosin binding sites on actin and is referred as the blocked state because it is unable to bind crossbridges. When $[Ca^{2+}]_i$ rises during systole, Ca^{2+} binds to the single *N*-terminal regulatory site on cTnC and initiates activation of the thin filament. This increases cTnC's affinity for cTnI and shifts the binding of cTnI away from its inhibitory interaction with actin [29]. The Ca^{2+} activation signal is then translated through the cTnT subunit of cTn, allowing movement of cTm towards positions that expose myosin crossbridge binding sites on actin that are available for weak binding. The availability of weak binding sites on actin is known as the closed state of the thin filament. The subsequent transition of the myosin-actin interaction from the weakly bound state to the strongly bound state is responsible for force generation and additional displacement of cTm, which increases the availability of additional myosin crossbridge binding sites and is known as cooperativity. This state of the thin filament is known as

the open state since it is able to strongly bind multiple myosin crossbridges. This dynamic three state model of thin filament activation is supported by extensive biochemical and structural studies [30–32]. Once strong crossbridges are formed, myosin will go through the power stroke generating force and sarcomere and cardiomyocyte shortening. During diastole, intracellular Ca^{2+} concentrations return to low levels via ion pumps and exchangers in the sarcolemma and sarcoplasmic reticulum (SR) and Ca^{2+} dissociates from cTnC [33]. The dissociation of Ca^{2+} from cTnC results in detachment of strong myosin crossbridges from actin and relaxation of the sarcomeres and cardiac muscle.

While thin filament activation is known to be regulated by both Ca^{2+} binding to cTnC and strong myosin crossbridges binding to actin, some of the mechanisms of regulation are still being investigated. Modulation of cardiac muscle contraction and regulation has been shown to be greatly impacted by phosphorylation of myofilament proteins, such as cTnI, cTnT, myosin binding protein C, and myosin light chain [34–38]. Changes in myosin binding to actin and the formation of strong crossbridges, which constitute a positive and cooperative feedback on thin filament activation [27], can also have significant effects on cardiac muscle regulation and is something we will explore further in this dissertation [25]. In cardiac muscle this feedback is particularly strong, as strong crossbridges can increase cTnC Ca^{2+} binding affinity [39,40]. Similarly, changes in Ca^{2+} binding to cTnC haVE profound effects on thin filament activation and regulation, cardiac muscle contractility, and the dependence on myosin crossbridge formation for full contractile activation.

The central role cTnC plays in cardiac muscle contraction as the Ca^{2+} sensor of the thin filament makes it an intriguing target to study for both mechanistic understanding and potential therapeutic applications. Recent work in our lab [41,42] and by others [43,44] with an engineered cTnC variant (Figure 1.2 [44]) has shown that the point mutation of luecine (L) to glutamine (Q) at position 48 in

cTnC, L48Q, can have profound effects on both cTn and myofilament Ca^{2+} binding properties, and on the contractile properties of cardiac muscle. L48Q cTnC has been shown to increase the Ca^{2+} binding affinity of the cTn complex [41], and it does so by enhancing both the binding of Ca^{2+} to cTnC and the interaction of cTnC with cTnI [42]. Additionally, when L48Q cTnC was exchanged into cardiac myofibrils and demembranated trabeculae, it increased thin filament activation [45], the Ca^{2+} sensitivity of force, and the rate of force development without perturbing maximal force generation or relaxation properties [41]. The effects of alterations to cTnC Ca^{2+} binding properties on cardiac contractility will explored further at sub-cellular, cellular, and whole heart levels in this dissertation.

1.5 MYOSIN POWER STROKE

The myosin crossbridge cycle is responsible for force generation in cardiac muscle. Myosin heads bind adenosine triphosphate (ATP) and enzymatically hydrolyze the gamma phosphate, and the energy released during this hydrolysis is used to generate contractile work. This reaction is catalyzed by actin, and the interaction of actin and myosin is regulated through cTn and cTm on the thin filament. The cyclic interaction of myosin binding to actin and hydrolyzing ATP is known as the crossbridge cycle, or chemo-mechanical cycle. The products of the crossbridge cycle are the hydrolysis products ADP and inorganic phosphate (P_i), and shortening of the sarcomere, which results in force generation. Figure 1.3 illustrates the eight-step representation of the crossbridge cycle [46].

The cycle begins when ATP binds to myosin (M) (step 1), which causes rapid dissociation of myosin from actin (A) (step 2) [47]. Once myosin has detached from actin, it then hydrolyzes ATP to ADP and P_i once (step 3) and quickly re-associates with actin (step 4) to form a weakly bound A∼M state through electrostatic interactions. The transition from a weakly bound state to strongly bound state

(step 5) is regulated by the thin filament, its Ca^{2+} handling properties, and its subsequent activation by Ca^{2+} [48,49]. Exposure of the myosin binding sites on actin permits strong myosin binding via hydrophobic interactions between myosin and actin, which precedes force generation (step 6) and P_i release (step 7; [50,51]). Once strongly bound to actin, the myosin head undergoes the force generating isomerization (step 6), which is followed by P_i release (step 7) [52]. Then ADP is released from myosin (step 8), which is rate-limiting for unloaded conditions (*in vitro* or during unloaded shortening). Once ADP is released from myosin, the actomyosin complex remains until ATP binds to myosin again to repeat the cycle. The availability of ATP and binding sites on actin (via thin filament regulation), as well as the buildup of hydrolysis products ADP and P_i, are just some of the limitations of crossbridge cycling. Both the properties of the thin filament and the different nucleotides that myosin binds, such as dATP instead of ATP, can have significant effects on crossbridge cycling, and their effects on intact cardiomyocyte contractility will be explored in more detail in this dissertation.

1.6 EXCITATION-CONTRACTION COUPLING AND CA^{2+} REGULATION IN CARDIAC MUSCLE

Intracellular Ca^{2+} ($[Ca^{2+}]_i$) handling is central to the process of excitation-contraction coupling and relaxation in ventricular cardiomyocytes. During systole, membrane depolarization from the resting membrane potential (~-90 mV) causes an influx of Ca^{2+} via the voltage-sensitive L-type Ca^{2+} channel in the T-tubule membrane. This influx of Ca^{2+} produces an increase in the local Ca^{2+} concentration near the ryanodine receptor (RyR) triggering release of intracellular stores of Ca^{2+} from the sarcoplasmic reticulum (SR), a process known as Ca^{2+}-induced Ca^{2+} release (CICR). The resulting rise in $[Ca^{2+}]_i$ to ~100 μM is sensed by cTnC, resulting in sarcomere shortening and muscle contraction. Conversely, muscle relaxation is initiated as the membrane repolarizes and causes a decrease in $[Ca^{2+}]_i$, which is a process primarily driven by the concerted actions of the SR Ca^{2+} ATPase pump (SERCA) and the sarcolemma Na^+/Ca^{2+} exchanger (NCX). SERCA-mediated reuptake of Ca^{2+} accounts for ~80-90% of the intracellular Ca^{2+} removal and replenishes Ca^{2+} stores in the SR for the next

excitation. The sarcolemma NCX extrudes most of the remaining ~10-20% intracellular Ca^{2+} by exporting one Ca^{2+} ion to the extracellular space in exchange for three Na^{+} ions [53]. In this way, the NCX extrudes the amount of Ca^{2+} that entered the cell via L-type Ca^{2+} channels, and is primarily responsible for maintenance of low intracellular Ca^{2+} concentrations during diastole (~0.1 uM $[Ca^{2+}]_i$) [33,54,55]. The sarcolemma Ca^{2+}-ATPase pump also helps lower intracellular Ca^{2+} concentrations by pumping Ca^{2+} to the extracellular space, but its contributions are much less than SERCA and NCX (Figure 1.4 [53]). Ultimately, the lowering $[Ca^{2+}]_i$ causes dissociation of Ca^{2+} from the myofilaments and relaxation of the sarcomere. Additionally, β-adrenergic stimulation enhances contractile force and relaxation rate in cardiac muscle by phosphorylation myofilament contractile proteins (cTnI, myosin binding protein C, myosin light chain) and the channels and pumps involved in Ca^{2+} cycling. Specifically, phosphorylation of the L-type Ca^{2+} channels and RyRs increases Ca^{2+} flux into the cytosol of the cardiomyocyte, and phosphorylation of phospholamban (PLB) increases the resequestration of Ca^{2+} by the SR via increased the pump activity of SERCA [56]. When the combination of excitation-contraction coupling and thin and thick filament regulation and interactions at the single cardiomyocyte level are carried out in concert at the tissue level, they are responsible for and regulate the pump function at the whole heart level.

1.7 SARCOMERE LENGTH DEPENDENCE OF CARDIAC MUSCLE FUNCTION

Another way myocardial performance is tightly regulated is at the cardiomyocyte level by sarcomere length (SL), whereby increases in SL sharply increase force generation. This capability is the cellular basis of the Frank-Starling relationship, which allows the heart to match venous return and stroke volume of the right and left ventricles and to match systemic demand of the body on a beat-to-beat basis. Loss of this relationship significantly comprises the ability of the heart to meet the cardiovascular demands of the body. Furthermore, there is significant evidence demonstrating that the Frank-Starling mechanism is compromised in human [57–59] and other animal models of heart

failure [60–63]. The molecular mechanisms of this SL dependent effect are currently debated but thought to result, at least in part, from changes in lattice spacing between the thin and thick filaments, and/or changes in myosin crossbridge orientation that increase the probability of myosin binding to actin at longer SLs [27,64–69]. Moreover, crossbridge binding enhances Ca^{2+} binding to cTn in cardiac muscle, which is a unique form of cooperative thin filament activation whose mechanism is currently not well understood [65,70–72]. The net result of these interactions is an apparent increase in the Ca^{2+} sensitivity of thin filament activation at longer SLs, whereby a given submaximal Ca^{2+} concentration results in greater contractile force development. Thus, SL-dependent changes in Ca^{2+}-sensitivity of force generation result from the intrinsic properties of the thin filament [69,73] as well as from complex interactions between thin and thick filament proteins. This is especially important to understand in cardiac muscle since the intracellular Ca^{2+} concentration during activation is known to be submaximal [27,74] and loss of SL-dependence of contraction can occur during heart failure [57,59,60]. The work in this dissertation examines how changes in the properties of the thin filament through modulation of cTn Ca^{2+} binding properties (via cTnC and cTnI variants) affect the SL dependent force-Ca^{2+} relationships in cardiac muscle.

1.8 STUDY MOTIVATION

The heart is a complex organ, and its responsibilities of meeting and sustaining the physiological demands of the body are equally as complex. When the myocardium becomes diseased or damaged, as is commonly the cause of heart failure, the same properties of the heart that make it so adaptable to the changing demands of the body are the ones that can cause additional dysfunction and eventual failure. The heart has a number of compensatory mechanisms it employs to meet the acute physiological demands (i.e. Frank-Starling relationship, changing heart rate, neurohormonal activation, etc.); however, chronic reliance on these compensatory mechanisms eventually contributes to heart failure [3–5]. Because the heart has limited capacity to regenerate damage

and/or diseased cardiomyocytes and is thus unable to regain its full functional capacity after an insult, various treatment approaches have been developed to attempt to treat the failing heart. Unfortunately, most of the current treatments are palliative approaches that do not restore any functional capacity to the heart and end up simply slowing the progression of the disease. This significant lack of effective clinical treatments underscores the need to develop new therapeutic strategies for heart failure focused on recovery of cardiac function.

While extensive research into heart failure and treatments for it have been conducted, none of the work (to date) has produced a treatment strategy that improves the functional capacity of the heart over the long-term. When attempting to address this critical unmet need and develop novel therapeutic strategies to improve cardiac dysfunction, it is essential to have a thorough understanding of the mechanisms of healthy cardiac muscle function and regulation, and how healthy muscle responds to small perturbations to the contractile system. The manner in which healthy cardiac muscle responds to changes in the healthy system may elucidate new potential targets and mechanisms that novel therapies can focus on as strategies to improve cardiac performance in failing hearts. In this dissertation, a wide variety of work in cardiac muscle was completed with that hypothesis in mind. Examination of sub-cellular, cellular, tissue, and organ levels of cardiac muscle contraction enabled the development of a project that coupled novel insights into the mechanisms of muscle contraction regulation with the application of these insights to the challenge of improving cardiac muscle contraction in diseased/damage myocardium. While many of the current pharmacological treatments are drugs that achieve their effects on cardiac function through changes intracellular Ca^{2+} [7,8], this work focused on understanding cardiac thin and think filament properties and directly modulating these properties. The properties of the thin and thick filaments play key roles in cardiac muscle contraction regulation and offer novel targets for methods to improve cardiac muscle function through manipulation of these properties.

Changes in myofilament Ca^{2+} sensitivity and/or modulating the crossbridge cycle can have profound effects on the overall activation of cardiac muscle [25,75,76]. Altering myofilament Ca^{2+} sensitivity may have effects on SL dependence of Ca^{2+} sensitivity of force, which is thought to be cellular mechanism that underlies, at least in part, the Frank-Starling relationship. On the thin filament side, it is beneficial to understand how acutely increasing (via cTn exchange with L48Q cTnC-cTn) and decreasing (via PKA phosphorylation and cTn exchange containing different phosphorylated states of cTnI) myofilament Ca^{2+} sensitivity affects the SL dependence of Ca^{2+} sensitivity of force. Additionally, based on the previous results in cardiac myofibrils and demembranated trabeculae [41], acute increases to myofilament Ca^{2+} sensitivity via incorporation of L48Q cTnC-cTn may also have important effects on intact cardiomyocyte contractile properties and whole heart function, which has not been investigated until this work. On the thick filament side, changes in the crossbridge cycle rates through the use of dATP as the myosin substrate have greatly increased the magnitude and rate of force development, and increased the Ca^{2+} sensitivity of the force-pCa relationship in cardiac trabeculae [74,77,78]. It is important to investigate if these enhancements in myofilament contractility, either from L48Q cTnC or dATP, are recapitulated by acute expression in intact cardiomyocytes.

From both mechanistic and heart failure treatment perspectives, it is important to understand how manipulations of thin and thick filament properties impact individual cardiomyocyte and whole heart function. It is equally important to understand if any of these manipulations have off-target effects and what the effects may be. The long-term goal of this work, therefore, is to apply the improved mechanistic understanding of how modulating myofilament Ca^{2+} binding properties affects cardiac muscle contraction to the development of a novel cardiac muscle-targeted gene therapy to

improve heart function. Significant progress toward this long-term goal was made by completing the following aims and goals:

1 Investigate how changes in myofilament Ca^{2+} binding properties via troponin modulations affect the SL dependence of Ca^{2+} sensitivity of force in demembranated cardiac muscle

2 Examine the effects of acute changes to myofilament Ca^{2+} binding properties (via L48Q cTnC) or crossbridge cycle kinetics (via dATP) on healthy and diseased intact cardiomyocyte contractility

3 Engineer a cardiac muscle-specific *in vivo* gene delivery system to investigate how acute changes in myofilament Ca^{2+} binding properties (via L48Q cTnC expression) affect whole heart function

By completing these aims and goals, this work has combined the investigation of basic science questions and the translation of these findings to the development of a potential therapeutic strategy to treat heart failure. Improvement of the mechanistic understanding of cardiac muscle contraction regulation and the role modulation of cTn Ca^{2+} binding affinity via cTnC properties plays in thin filament activation provided unique insights into an innovative target for therapeutic strategies. These insights motivated the engineering of a potential cardiac-muscle targeted gene therapy that may actually provide a method to improve heart function in failing hearts without the off-target effects of current therapies. The work in this dissertation has set the stage for a number of future studies, and one of the most crucial set of studies is to more rigorously determine how expression of L48Q cTnC (via the engineered cardiac-muscle targeted gene delivery system) affects healthy and diseased whole heart function.

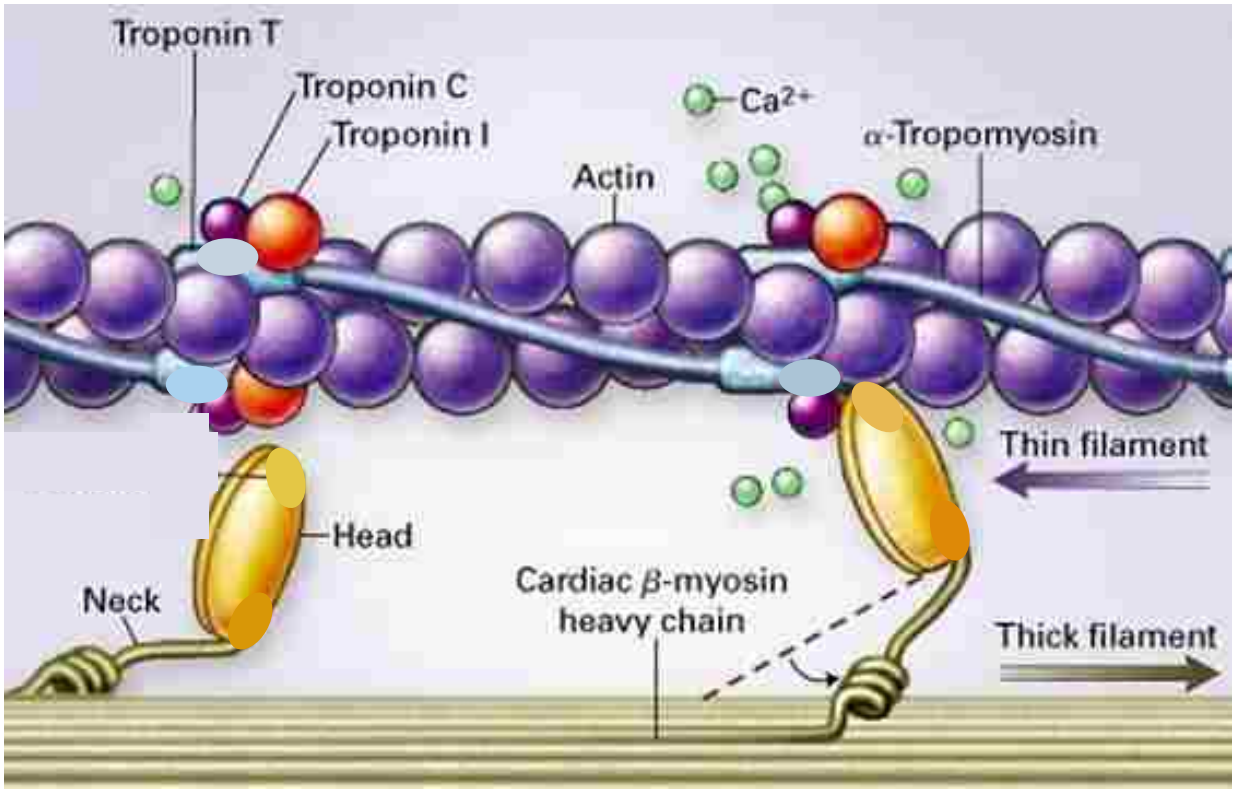

Figure 1.1: The thin and thick filament proteins involved in muscle contraction regulation. Modified from [196].

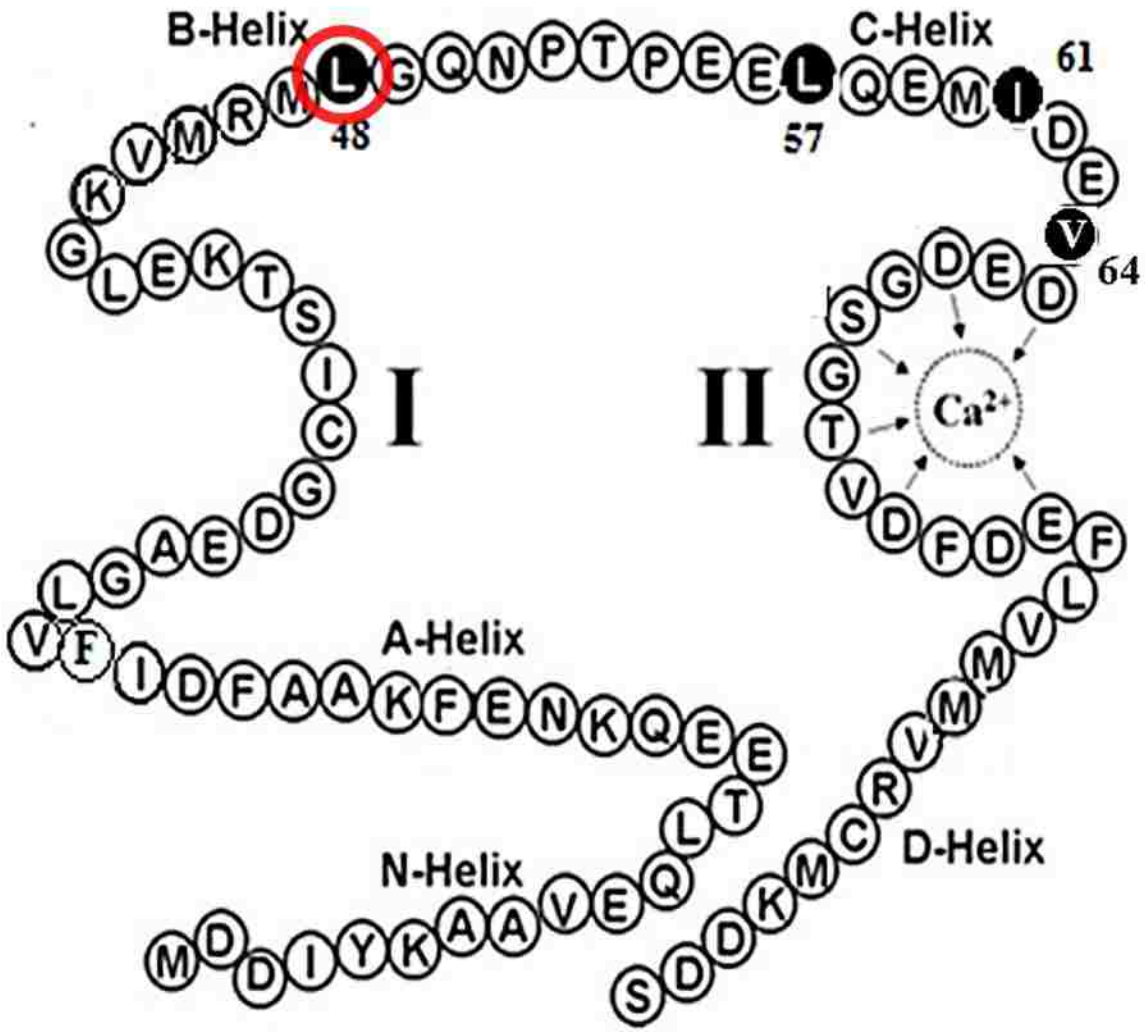

Figure 1.2: Amino acid sequence in the regulatory domain of cTnC including Ca^{2+} binding site I (defunct) and site II. The circled residue shows the location of the point mutation of luecine (L) to glutamine (Q) at position 48 in L48Q cTnC. Modified from [44].

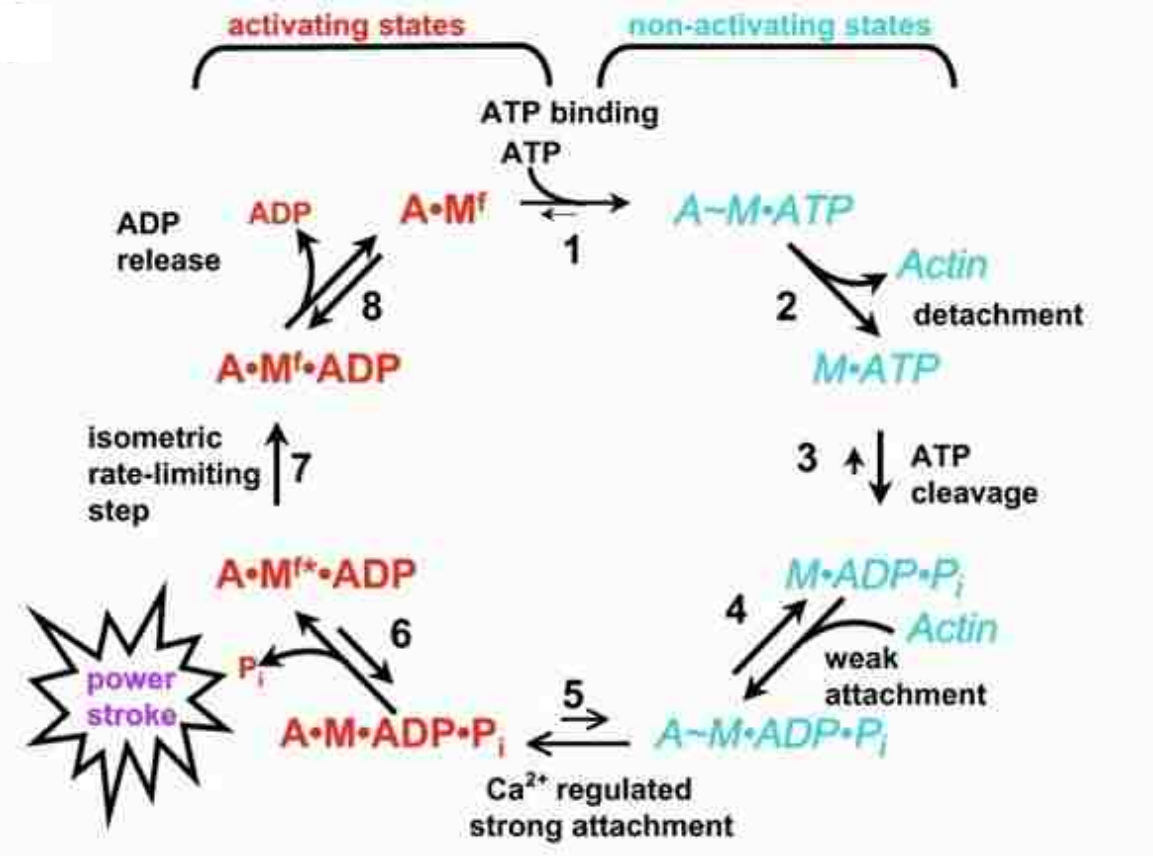

Figure 1.3: The 8 steps that compose the crossbridge cycle [46].

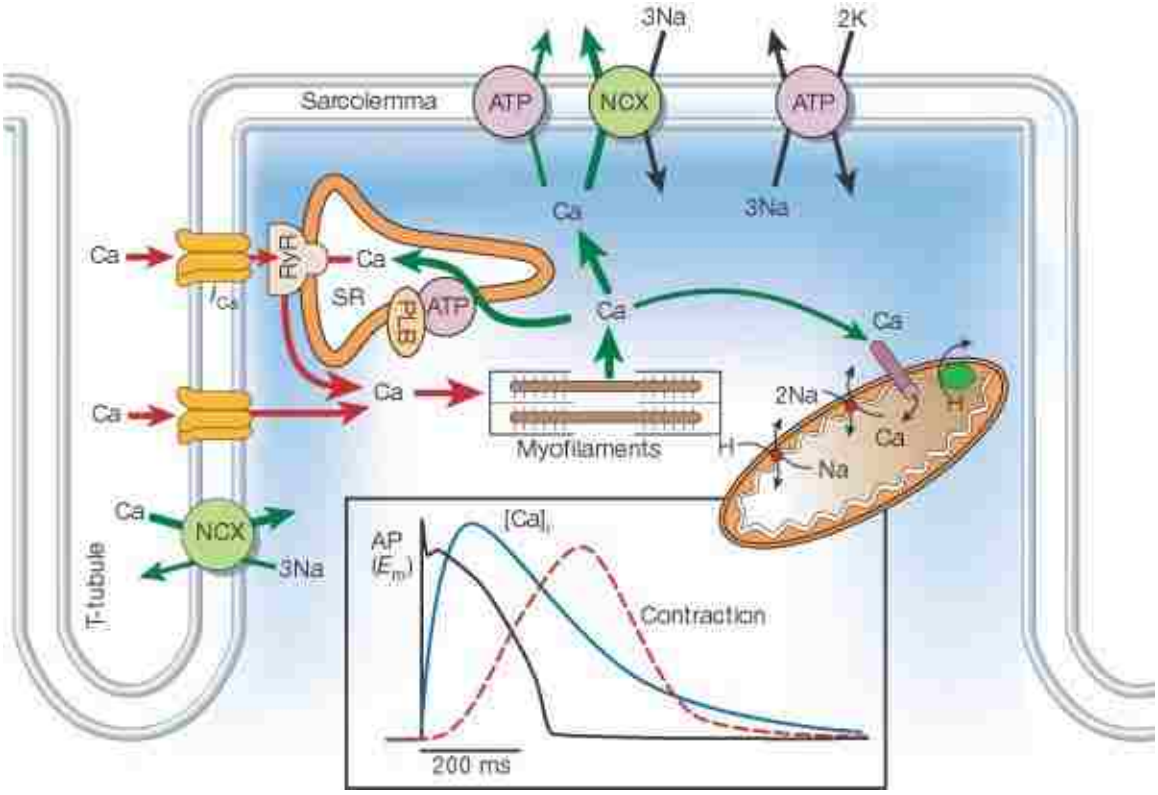

Figure 1.4: Ca^{2+} transport during excitation-contraction coupling [53].

Chapter 2. Materials and Methods

Because of the breadth and depth of the work in this dissertation, many different experimental approaches were used to investigate the different hypotheses and accomplish the various goals. The use of a myriad of techniques enabled the study of cardiac muscle function to span all levels of physiology from engineering at the amino acid level of individual proteins, to sub-cellular study of myofilament properties, to individual intact cardiomyocyte contractile properties, and finally at the whole organ level by studying the overall cardiac performance of the heart. The ability to employ so many different tools and techniques led to the creation of a diverse and well-balanced work that tackled the unanswered basic questions as well as the challenges of translating these discoveries into a potential therapeutic strategy to treat heart failure. Because many of these techniques were used in multiple components of this project, the purpose of this chapter is to summarize these techniques and methods while the subsequent chapters will focus on the results and implications of this work.

2.1 TRABECULAR MECHANICS

2.1.1 Experimental animals and tissue preparations

All animal procedures were conducted in accordance with the US National Institutes of Health Policy on Humane Care and Use of Laboratory Animals and were approved by the University of Washington (UW) Animal Care Committee. For trabecular mechanics experiments, male Sprague-Dawley rats (200–250 g) were housed in the Department of Comparative Medicine at UW and cared for in accordance with the UW Institutional Animal Care and Use Committee (IACUC) procedures. Rats were anesthetized by intraperitoneal injection of sodium pentobarbital (50-100 mg/kg). When the animals had no reflexive response, the heart was rapidly excised and the right ventricles were

dissected in oxygenated Ringer's solution containing (in mM): 100 NaCl, 24 $NaHCO_3$, 2.5 KCl, 1 $MgSO_4*7H_2O$, 1 Na_2HPO_4, and 1 $CaCl_2$. Trabeculae were permeabilized *in situ* by incubation of splayed ventricles overnight in a relaxing solution (in mM: 100 KCl, 10 imidazole, 2 EGTA, 5 $MgCl_2$, and 4 ATP) containing 50% glycerol and 1% Triton X-100 (Sigma-Aldrich) at 4°C. Individual trabeculae were then dissected from ventricular free walls, pinned to the bottom of a sylgar-coated Petri dish, and stored for up to 1 week in glycerinated relaxing solution at 4°C. All skinning and storage solutions contained protease inhibitor cocktail (P8340; Sigma-Aldrich).

2.1.2 Recombinant protein generation and purification

Construction and expression of rat recombinant WT cTnC, cTnI and cTnT were done as previously described [79]. Site directed mutagenesis was performed using the QuikChange II Site-Directed Mutagenesis Kit (Stratagene, La Jolla, CA) to substitute to produce the following cTn subunit variants: L48Q cTnC, serines 23, 24 in cTnI with either alanine, to mimic the N-terminal unphosphorylated state of cTnI (cTnI (S23/24A)), or with aspartic acid (cTnI (S23/24D) to mimic the N-terminal phosphorylated cTnI state (Chapter 4, Supplemental Figure S4.1). A pET-24 (Novagen, Madison, Wisc.) vector containing the T7 promoter, lac operator, and a kanamycin resistant gene was used for expression of WT and mutant proteins in E. coli (BL21). The DNA sequences of the expression constructs were verified by DNA sequencing. The expressed protein was extracted from bacterial cells as previously described (4) and purified on a DE 52 or CM 52 (Whatman) column equilibrated by 6M Urea, 25mM Tris at pH 8.0, 1mM EDTA and 15mM 2-Mercaptoethanol. Proteins were eluted with a salt gradient by washing in the same buffer from 0 to 0.3M NaCl. The fractions containing the desired protein and their concentrations were monitored by SDS polyacrylamide gel electrophoresis and DU 800 Spectrophotometer. Super pure proteins were stored in a -80°C freezer before use.

2.1.3 Passive whole cardiac troponin exchange

Cardiac Tn (cTn) complex was reconstituted from isolated recombinant subunits (1:1:1), using a modification of published protocols [80]. In brief, after subunits were complexed in a 1:1:1 molar ratio, cTn was gradually dialyzed into buffer containing, (mM): KCl 200, MOPS 20, EGTA 5, $MgCl_2$ 5, β-mercapto-ethanol 15, pH 7.0; Tn concentration was ~ 1.0 mg/ml. Exchange of whole cTn complex into detergent skinned trabeculae was accomplished via passive exchange by incubating trabeculae overnight on a mechanical rocker (Beckman) at 4°C in a protein buffer solution with addition of 4 mM ATP, 1mg/ml DTT, and protease inhibitor cocktail. Following the exchange procedure, preparations were then washed several times in relaxing solutions containing 1 mg/ml BSA to remove any non-specifically bound exogenous cTn and transferred to the glycerinated (50% v/v) relaxing solution for storage at -20°C. Exchanged trabeculae were used within two days after the procedure.

2.1.4 Ca^{2+} solutions and mechanical measurements

Solution composition was determined by an iterative computer program that calculates the equilibrium concentration of ligands and ions based on published affinity constants [81]. Relaxing and activating solutions were prepared using a custom software package as described previously [82,83]. Solutions were maintained pH 7.0 at 15°C and contained (in mM): 15 phosphocreatine, 15 EGTA, 80 MOPS, 1 free Mg^{2+}, 1 DTT, and 5 Mg_2ATP, and 135 (Na^+ + K^+). For activating and relaxing solutions, Ca^{2+} concentration (reported as pCa = −log[Ca^{2+}]) was adjusted by varying amounts of $CaCl_2$. Ionic strength was set to 0.17 M with KCl.

Demembranated trabeculae were mounted between a high-speed length controller (Model 312B servo motor (Aurora Scientific)) tuned for a 350 μs step response and a force transducer (Aurora

Model 400A) via aluminum t-clips as previously described [41]. Trabecuale were placed in 200 µL temperature controlled wells at 15°C that could be moved to expose preparations to different solutions. SL was measured by image analysis using a MyoCam (Ion Optix, Inc. Boston, MA) and set at either 2.3 µm or 2.0 µm in relaxing solution (pCa 9.0). Trabeculae were then fully activated in pCa 4.0 to determine maximum force (F_{max}) prior to exposure to increasing Ca^{2+} concentrations (decreasing pCa). Passive force was determined at pCa 9.0 and subtracted from total force to obtain the active force values reported. After determining the passive force at SL 2.3 or 2.0 µm, trabeculae were exposed to increasing Ca^{2+} concentration (decreasing pCa) in a step-wise manner. At each pCa a slack-re-stretch maneuver was performed to measure steady state force and the rate of force redevelopment (k_{tr}, [84]) followed by stiffness measurements obtained from applying small (0.1%) sinusoidal changes in length at 1000 Hz for 0.5 sec. SL was then set to 2.0 or 2.3 µm, which ever was not set as the initial SL since the order of initial SL was reversed in some trabeculae, and the protocol was repeated. Results from either SL sequence were rejected if force at pCa 4.0 (F_{max}) declined by more than 15% at SL 2.3 µm at the end of the pCa curve.

In other experiments with dextran T500 or 2,3-butanedione monoxime (BDM), the following conditions were used. For experiments with 3% dextran T500, SL was set to 2.0 µm and initial force–pCa data were obtained. The same trabeculae were then exposed to pCa solutions containing 3% dextran T500 to obtain additional force–pCa data. For experiments with 7 mM BDM, SL was set to 2.3 µm and initial force–pCa data were obtained. The same trabeculae were then exposed to pCa solutions containing 7 mM BDM to obtain additional force–pCa data. For PKA treatment, skinned trabeculae were exposed to 200 µL relaxing solution containing 100 units of the catalytic subunit of PKA (Sigma-Aldrich, St. Louis, MO) and 6 mM DTT for 45 minutes at 20°C.

2.1.5 Data processing and statistical analysis

Force–pCa data were fitted with the Hill Equation (Eq. 1) where F_{MAX} is the maximal Ca^{2+} activated force, n_H is the Hill coefficient, or slope of the relationship, and pCa_{50} is the pCa at which force is half-maximal [41]. The k_{tr} was determined from release-restretch transient, with the resulting force redevelopment trace fit using a monoexponential equation (4).

$$F = F_{MAX} \Big/ (1 + 10^{n_H (pCa_{50} - pCa)}) \qquad \text{(Equation 1)}$$

The reported pCa_{50} and n_H values represent the means of the values from the individual fits, ± standard error of the means (SEM). Means are compared with Student's T-test with significance at the 95% confidence level ($p<0.05$). Statistical analysis was performed using Excel (Microsoft, Redmond, WA), SigmaPlot (Systat, Richmond, CA), and Fityk [85].

2.1.6 X-ray diffraction

Low-angle X-ray diffraction measurements were performed on the small-angle BioCAT instrument on beamline 18-D at the Advanced Photon Source, Argonne National Laboratory [86] using trabeculae mounted in a simple plexiglass X-ray chamber containing pCa 9.0 relaxing solution at a SL of 2.3 µm. X-ray exposures were 1 sec. at an incident flux of ~$1x10^{12}$ photons/sec. with 12 keV photon energy. Camera length was 2.8 m. Diffraction patterns were collected on a CCD-based X-ray detector (Mar 165, Rayonix Inc. Evanston Il, USA) and the spacing's of the 1,0 and 1,1 equatorial reflections were acquired [87,88]. The distance between the 1,0 and 1,1 reflections were converted to the $d_{1,0}$ lattice spacing using Bragg's law. This may be converted to the inter-thick filament spacing ($d_{1,0}$) by multiplying by $2/\sqrt{3}$ [89]. Intensities of the 1,0 and 1,1 equatorial reflections were determined from non-linear least square fits to one-dimensional projections of the integrated intensity along the

equator [88]. All data were analyzed independently by three individuals and the results were averaged.

2.1.7 SDS-PAGE and Western blots on trabeculae

To monitor the extent of mutant cTn incorporation into trabeculae, we used cTn where cTnT contained a 9 amino acid myc-tag at the N-terminus, which was similar to previous studies [90]. The exchange efficiency was determined through Western blot analysis after the proteins were extracted by SDS sample buffer and separated by 12.5% SDS-PAGE. The presence of the myc-tag allowed us to visibly separate the exchanged protein from endogenous (Figure 4.1 in Chapter 4). Exchange efficiency was determined by calculating the percent of myc-tagged cTnT (top band) and endogenous cTnT (bottom band) present in the sample. Protein bands were quantified using ImageJ gel analysis toolkit (NIH).

SDS-PAGE and concurrent phosphoprotein and total protein staining were performed on exchanged trabeculae (n = 3 gels, 10 trabeculae/lane collected from 8 hearts) with and without PKA treatment. Each gel represents data collected from 2-3 hearts. Trabeculae populations were mixed (i.e. each lane represents trabeculae from multiple hearts) to reduce bias from a single animal. Gels were stained with Pro-Q Diamond (Invitrogen) phosphoprotein staining solution and imaged using a BioSpectrum AC Imaging System (UVP). Following phosphoprotein staining and imaging, gels were stained for total protein with Coomassie Blue. Densitometry analysis was performed using the ImageJ gel analysis toolkit (NIH).

2.2 *IN VITRO* INTACT CARDIOMYOCYTE CONTRACTILITY

2.2.1 Experimental animals and cell preparations

All animal procedures were conducted in accordance with the US National Institutes of Health Policy on Humane Care and Use of Laboratory Animals and were approved by the University of Washington (UW) Animal Care Committee. Animals were housed in the Department of Comparative Medicine at UW and cared for in accordance with the UW Institutional Animal Care and Use Committee (IACUC) procedures.

Adult rat cardiomyocytes (ARCs) were isolated from 6-8 week old female Fischer 344 rat hearts using aortic retrograde perfusion for enzymatic (collagenase/protease) dispersion of cells [91]. Rats were anesthetized with intraperitoneal injection of sodium pentobarbital at 50-100mg/kg (using sodium Nembutal or Beuthanasia-D Special) then heparin (1mg/kg) was injected intravenously and allowed to circulate for ~ 5 minutes. The hearts were then rapidly excised and rinsed in cold (on ice) DE buffer (in mmol/L: NaCl 116.4, Pyruvate 5, HEPES 20, NaH_2PO_4 1, glucose 5.5, $MgCl_2$ 0.8; pH 7.4) containing 100 mM EGTA, then cannulated through the aorta and perfused with warm (37°C) DE buffer until cleared of blood. To increase the yield, 10 mM 2,3-butanedione monoxime (BDM) was added to all solutions except the plating and culture media. The heart was then perfused with warm (37°C) digestion buffer (DE buffer plus colleganase type II (~200 U/mL; Worthington)) for 20-30 minutes. The ventricles were then cut into four sections that remained connected at the apex of the heart and then placed in fresh digestion buffer. The ventricles were then gently agitated and shaken for 3-5 minuntes to mechanically release the cardiomyocytes from the extracellular matrix of the digested ventricles. The cardiomyocytes were then allowed to settle and pellet by gravity for 15 minutes. The supernatant was then removed and discarded and the digestion reaction was quenched by washing the cells in DE buffer plus 2.5% bovine serum albumin (BSA; Sigma, St. Louis, MO) and

100 μM $CaCl_2$. Cells were again allowed to settle by gravity, the supernatant was removed and discarded, and cells were reintroduced to Ca^{2+} by resuspending in DE buffer plus 5% BSA and 125 μM $CaCl_2$. This was repeated three separate times. Finally after the third Ca^{2+} wash and gravity pelleting, the supernatant removed and discarded, and the cells were resuspended in plating media (DMEM/M199 (4:1) supplemented with 10% horse serum (ICN Flow), 5% fetal bovine serum (HyClone), penicillin G (100 U/mL) and streptomycin (100 μg/mL) (Gibco)). The cells were then plated on to 25 mm^2 glass coverslips (1.0 thickness) for contractility analysis, or 6-well tissue culture dishes for myofilament cTnC-Flag incorporation analysis, that were pre-coated with laminin at 20-25 ug/mL in PBS. After 2-4 hours, adenovirus was added to the media and cells for ~2 hours (~200-250 viral particles per cardiomyocyte). After 2 hours, additional unmodified DMEM was added to the wells. DMEM containing the adenovirus was removed the following day after 24 hours incubation, and cardiomyocytes were maintained and fed daily with DMEM for 48-60 hours before contractility and protein expression analyses were made.

For cardiomyocytes isolated from infarcted hearts (MI), adult female rats (Fischer 344) 6-8 weeks old were infarcted via permanent ligation of the left descending coronary artery using a surgical suture. Access to the heart was obtained via thoracotomy [92]. Sham control animals received only the thoracotomy procedure. ARCs were isolated from MI hearts once systolic and/or diastolic dysfunction developed (4-6 weeks post-infarction), which was monitored by echocardiography. Cardiomyocytes were subsequently transduced and cultured for 48-60 hours as described above to allow sufficient transgene expression before contractility measurements were made.

When neonatal rat cardiomyocytes (NRCs) were used for some assays, they were isolated by enzymatic dispersion from 1-3-day old newborn Fischer 344 rats as previously described [92].

Neonatal Rat Cardiomyocytes (NRCs) were isolated by enzymatic dispersion from 1- 3-day old newborn Fischer 344 rats as previously described [15]. Briefly, neonatal rats were decapitated and their hearts rapidly removed and placed into an ice-cold buffer (in mmol/L: NaCl 116.4, HEPES 20, NaH_2PO_4 1, glucose 5.5, KCl 5.4, MgSO4 0.8; pH 7.4). The ventricles were trimmed of atria and large vessels and cut in 2 to 3 mm pieces for repeated incubation (5-6 times at 37°C for 25 minutes) in buffer containing collagenase type II (95 U/mL; Worthington) and pancreatin (0.6 mg/mL; Gibco BRL). After each incubation the supernatant was collected and centrifuged (600 x g for 5 minutes), then the resulting cell pellet was resuspended in DMEM/M199 (4:1) supplemented with 10% horse serum (ICN Flow), 5% fetal bovine serum (HyClone), penicillin G (100 U/mL) and streptomycin (100 μg/mL) (Gibco) and preplated for 30 minutes to reduce contaminating non-myocytes. Cardiomyocytes were pooled and counted with a typical cell yield of ~$1x10^6$ per neonatal heart. The cells were then plated in media onto sterile, gel-coated 6-well dishes at a concentration of ~$2x10^5$ cells per well for culturing and infection. After 2-4 hours, plating media was removed and cells were transduced with plating media containing adenovirus (~200-250 viral particles per cardiomyocyte) for Rrm1 + GFP and Rrm2 + GFP or GFP-only, or left untreated.

For demembranted trabeculae experiments with dATP, rat cardiac trabeculae were dissected from the right ventricle of male Sprague-Dawley rats, chemically demembranated, and prepared for mechanical measurements as previously described above and in [92]. Trabeculae averaged 1.3 ± 0.2 mm in length by 170 ± 30 μm in width.

2.2.2 Plasmid design and adenovirus production

The AdEasy™ system was used as originally described [93,94] to generate recombinant adenoviral vectors to express Rrm1, Rrm2, histidine-tagged (C-terminal 6-His tag) WT cTnC and L48Q cTnC, and

Flag tagged (C-terminal Flag tag) WT cTnC and L48Q cTnC from the cytomegalovirus (CMV) promoter. The viruses containing histidine-tagged (C-terminal 6-His tag) WT cTnC and L48Q cTnC were used for contractility measurements with cTnC over-expression, but the His tag was not well-suited for determination of myofilament incorporation of tagged cTnC via Western blot. A second set of viruses containing WT cTnC-Flag and L48Q cTnC-Flag were made using a more effective tag system to determine myofilament incorporation of cTnC-Flag via Western blot. There were no differences in the effects on cardiomyocyte function or Ca^{2+} transient properties from transduction with either His tag or Flag tag viral systems (Supplemental Figure 5.S1, Tables 5.S6-9, Chapter 5). For all sets of viruses, the genes were first cloned into the shuttle vector pAdTrack-CMV, which contained green fluorescent protein (GFP) also driven by CMV as a reporter protein to identify transduced cells via fluorescence microscopy. A GFP-only vector was also produced as a viral control. The resultant plasmid was linearized by digesting with restriction endonuclease PmeI, and subsequently co-transformed into E. coli. BJ5183 cells with an adenoviral backbone plasmid pAdEasy-1. Recombinants were selected for kanamycin resistance, and recombination confirmed by restriction endonuclease analysis. Linearized recombinant plasmid was transduced into adenovirus packaging HEK 293 cell lines to produce high titer adenoviral preparations. Viral titers of 10^8-10^9 were generated. Cardiomyocytes were transduced at ~200-250 infectious units per cell (MOI) for 48-60 hours. We achieved nearly 100% transfection efficiency and gene transfer as grossly indicated by green fluorescence with microscopy (Figure 2.1 [25]). This is consistent with previous studies using cardiomyocytes [92,95]. The cell survival over this period assessed by the percentage of rod-shaped cells prior to contractile and intracellular Ca^{2+} transient measurements was similar in all groups, including non-transduced control cells, which suggests that these viral vectors did not compromise cardiomyocyte viability.

2.2.3 Cardiomyocyte contractile assessments

Cell shortening and relengthening of arbitrarily selected stimulated cardiomyocytes was monitored and recorded using IonOptix SarcLen system video microscopy. (IonOptix, Milton, MA, USA). For all cells, video microscopy was completed using a 40x objective (Olympus UWD 40) and 25x intermediate lenses. Contractile assessments were performed at room temperature (22-24°C) and at 37°C in fresh modified Tyrodes buffer (in mmol/L: $CaCl_2$ 1.8, MgCl2 1.0, KCl 5.4, NaCl 140, HEPES 10, NaH_2PO_4 0.33, glucose 5,; pH 7.4). We chose to perform these experiments at room temperature (22-24° C) to compare with the predominant number of reports for cultured cardiomyocytes in the literature [25,96–100]. However, a subset of measurements was made at 37°C to determine if the effects persist at physiological temperature as well. For adult cardiomyocytes, only cells that followed field stimulation 1:1 and with resting sarcomere lengths above 1.65 μm were measured. Average cardiomyocyte length and sarcomere length is reported, and there was no difference in either length between transduced and non-transduced cells. Experiments were performed by 3 different experimentalists, with at least 2 rotating on a given day, and all data has been analyzed in duplicate by 3 different analysts. No differences were found between experimentalists or analysts. Single cardiomyocytes in the cell bath were field-stimulated with a 4 ms square supra- threshold (at least 10V) pulse at 0.5, 1 and 2 Hz through parallel platinum electrodes. Cell shortening was recorded by illuminating the cardiomyocytes with red transmitted light (> 600 nm).

Ca^{2+} transients induced by electrical stimulation were measured in Fura-2AM loaded adult cardiomyocytes using IonOptix equipment as described [101]. Briefly, Ca^{2+} transients were recorded by measuring Fura-2 fluorescence passed through a 510 nm emission filter to a photomultiplier tube using the interpolated pseudo-ratiometric method with 380 nm excitation during, and 360 nm excitation at the onset and end of 20 second recording events. Fura-2 fluorescence was measured

using an IonOptix spectrophotometer (Stepper Switch) attached to a fluorescence microscope. Emitted Fura-2 fluorescence was collected by the 40X objective, passed through a 510nm filter and detected by a photomultiplier tube. The cell, sarcomere length, and fluorescent signals were recorded simultaneously by computer acquisition, and were analyzed later using proprietary software (IonOptix). Contractile measurements of adult cardiomyocytes were taken at 0.5 Hz, 1 Hz and 2 Hz stimulation frequencies.

For neonatal rat cardiomyocytes used in the Rrm1+Rrm2 and dATP studies, spontaneously beating cardiomyocytes were arbitrarily selected. Due to typical neonatal cardiomyocyte asymmetry, care was taken to align contraction along the major axis of cardiomyocyte movement, and all measurements were normalized to "resting" length. Experiments showed that neonatal cardiomyocytes maintain beating rate and amplitude for over an hour under the conditions noted above. There was no difference in the intrinsic beating frequency between non-transduced and transduced cardiomyocytes. This implies that exposure to adenovirus and/or overexpression of GFP or Rrm1+Rrm2 did not alter the intrinsic cardiomyocyte pacemaker potential.

2.2.4 Contractile assessment data processing and statistical analysis

Cardiomyocyte shortening and relengthening and Ca^{2+} transient rise and decay parameters were calculated offline using IonOptix software to determine the maximum of the first derivative of these transients in some cases. Times to peak shortening and 50% and 90% return to baseline were also calculated offline. An example contractile trace with analysis is shown in Figure 2.2. Statistical differences were determined by ANOVA, with Student-Newman-Keuls as a *post-hoc* pairwise test (SigmaPlot, Systat, Richmond, CA). Trabeculae were compared using paired t-tests. Differences at p-value < 0.05 were considered statistically significant. Data are displayed as mean ± S.E.M.

Where fluorescence data were converted to $[Ca^{2+}]_i$ an *in vitro* calibration of the measured ratio (R) was performed using the Grynkiewicz equation [102]: $[Ca^{2+}] = K_d * (R-R_{min}) / (R_{max} - R) * Sf_2 / Sb_2$. The values of R_{max} and R_{min} are the ratio values measured under conditions of saturating Ca^{2+} levels and in the absence of Ca^{2+}, respectively. The values of Sb_2 and Sf_2 are proportional to the fluorescence excited by the denominator wavelength (380nm) again under conditions of saturating (b, bound) Ca^{2+} levels and in the absence (f, free) of Ca^{2+}, respectively. A value of 225 nmol/L was assumed for the dissociation constant for the Fura-2 Ca^{2+} binding (K_d). Values for minimal and maximal $[Ca^{2+}]_i$ as determined from this equation and differences between groups are statistically identical to those determined from the ratiometric values [25]. Furthermore, these $[Ca^{2+}]_i$ values are in agreement with those previously reported by Herron et al., using similar conditions (i.e., adenovirally transduced adult rat cardiomyocytes after at least 48 hours in culture) [101].

2.2.5 Nucleotide binding affinity and kinetic assays

Rapid kinetic measurements of nucleotide binding and actin-myosin dissociation were taken at 10°C and 20°C (Hi-Tech Scientific SF-61 DX2 stopped-flow system) as previously described [103] using pyrene labeled actin and myosin S1. Myosin was purified from mouse hearts, rabbit soleus, and rabbit bulk fast muscle as previously described [104,105]. Actin was purified from rabbit skeletal muscle [106]. The stopped-flow transients were fitted to one or two exponentials by non-linear least squares curve fitting using the Kinetic Studio software (TgK Scientific). All experiments were carried out in 20 mM Cacodylate buffer, pH 7.0 containing 100 mM KCl, and 5 mM $MgCl_2$. The rate constant for ATP-induced actin-S1 dissociation (k_{obs}) was determined from Equation 2:

$$k_{obs} = k_{+2} K_1 \frac{[ATP]}{1 + K_1[ATP]}$$ (Equation 2)

2.2.6 Reverse transcriptase-polymerase chain reaction, SDS-PAGE, and Western blot analysis of intact cardiomyocytes

For experiments with Rrm1+Rrm2 and dATP, RT-PCR and Western blot analysis of Rrm transcript and protein abundance was performed in NRCs. NRCs were cultured at ~1-2x10^5 cells per well and were harvested from individual wells from a 6-well tissue culture dish by mild (0.05%) trypsin treatment. NRCs were transduced using the same MOI (~200-250) that was used for contractility measurements. For determination of total cellular Rrm content, intact NRCs were immediately stored in Laemmli sample buffer at -80°C until SDS-PAGE. SDS-PAGE separated proteins were transferred to nitrocellulose membrane and probed with monoclonal antibodies specific to Rrm1 or Rrm2 (Santa Cruz Biotechnology, Santa Cruz, CA), after blocking with 5% milk (w/v in Tris-buffered saline), which showed significant over-expression of Rrm1 and Rrm2 in transduced cells. Protein bands were quantified using open ImageJ gel analysis toolkit (NIH) and expression of each Rrm isoform was expressed relative to the housekeeping protein GAPDH.

For experiments with WT and L48Q cTnC-Flag expression in ARCs, SDS-PAGE and Western blot were used to analyze cTnC-Flag myofilament incorporation. ARCs were plated at 6-9x10^4 cells per well, and were cultured under the same conditions that were used for the contractility analysis [25]: MOI of ~200-250 infectious units/cell and cultured for 48-60 hours. To determine the amount of Flag tagged cTnC that was incorporated into the myofilaments, ARCs were harvested and demebranated to leave only myofilament proteins. Briefly, once cells were harvested and the trypsin EDTA reaction was quenched with media containing FBS, 0.1% v/v Triton X-100 was added to the cell suspension

for 5 min. The cells were then spun down at 500x gravity and the supernatant was discarded, which left just the cardiac myofibrils. The myofibrils were rinsed briefly in 1X PBS to remove and residual sarcolemma and cytosolic milieu. The demembranated cells were then spun again 500x gravity, and the supernatant was again removed. The cardiomyocyte myofibrils were then resuspended in lysis buffer [25] using 2X volume of lysis buffer as compared to the volume of the myofibril pellet. The samples were stored at -20°C until they were used. In preparation for SDS-PAGE and Western blotting, total protein content from the myofibril preparations was measured using the Bradford colormetric protein assay where the protein content is determined by measuring the absorbance of 595nm light. The amount of absorbance at this wavelength is proportional to the amount of Coomassie blue dye bound to protein [107,108]. Once total protein content for each sample was determined, the myofibril preparations were resuspended in Laemmli sample and boiled for 2 min before SDS-PAGE. Determination of total protein content before SDS-PAGE allowed loading of equal amounts of total protein (20 μg). SDS-PAGE separated proteins were transferred to a nitrocellulose membrane and probed with rabbit polyclonal anti-TnC (Santa Cruz Biotechnology, Santa Cruz, CA) and rabbit polyclonal anti-Flag (Sigma-Aldrich, St. Louis, MO) after blocking with 5% milk (w/v in Tris-buffered saline containing 0.1% v/v Twee-20). Antibody incubations were carried out in 1% milk (w/v in Tris-buffered saline containing 0.1% v/v Twee-20). The same nitrocellulose membrane was probed with one antibody, either anti-TnC or anti-Flag, and was then stripped and reblocked with 5% milk before probing with the second antibody, which ever was not used first. The order of probing did not affect either antibody signal. The same membrane was probed twice to confirm that the higher molecular weight band in the anti-TnC blot was indeed cTnC-Flag. Protein bands were quantified using ImageJ gel analysis toolkit (NIH), and the expression of each cTnC-Flag was calculated relative to the amount of native cTnC present in the anti-TnC Western blot. This analysis generated a relative amount (%) of the total cTnC (native + cTnC-Flag) of cTnC-Flag that was incorporated into the myofilaments of transduced ARCs.

2.3 *IN VIVO* ANIMAL STUDIES AND VIRAL EXPRESSION ANALYSIS

2.3.1 Adeno-associated virus (AAV6) development and administration

The design and development of the adeno-associated virus (AAV6) *in vivo* gene delivery system is covered in detail in Chapter 7. All animal procedures were conducted in accordance with the US National Institutes of Health Policy on Humane Care and Use of Laboratory Animals and were approved by the University of Washington (UW) Animal Care Committee. Animals were housed in the Department of Comparative Medicine at UW and cared for in accordance with the UW Institutional Animal Care and Use Committee (IACUC) procedures. Young adult (6-8 weeks old) male wildtype C57Bl/6J mice (The Jackson Laboratory, Bar Harbor, ME) were used for the *in vivo* studies. Five mice each received $6x10^{12}$ vector genomes of rAAV6 cTnT_{455} mCherry-P2a-L48Q cTnC-Flag in a single 200 µL bolus intravenous injection via retro-orbital injection [109]; 5 control mice received 200 µL Hank's balanced salt solution (HBSS) via retro-orbital injection. Mice were then monitored over the next 4 weeks and were sacrificed at the end of the 4 week period for biodistribution and tissue analysis.

2.3.2 Echocardiography

In vivo cardiac function assessments were made non-invasively with echocardiography at 1 week before AAV6 delivery (baseline cardiac function), and then at 1, 2, 3, and 4 weeks post-injection as previously described [92]. Briefly, mice were weighed and then lightly sedated with isoflurane while being monitored continuously using electrocardiography (ECG) via three limb leads. Baseline function was evaluated to determine if L48Q cTnC expression enhanced healthy heart function. Measurements were taken using a GE Vivid7 echocardiography system (GE, Piscataway, NJ) with an 11 MHz convex transducer of parasternal long-axis and short-axis images at the mid-papillary muscle

level to ensure accurate evaluation of heart function. Short axis 2-D views at the mid-ventricular (papillary muscle) level were used to generate M-mode measurements of the left ventricular (LV) end-systolic (LVESD) and end-diastolic (LVEDD) diameters, and anterior and posterior wall (PW) dimensions. These were used to calculate percent fractional shortening (FS) [(LVEDD-LVESD)/LVEDD x 100%] (schematic shown in Figure 2.3). Quality control was achieved by determining intra-observer and inter-observer variability for a single reader during two different sessions and two blinded readers obtaining measurements for several images.

2.3.3 Ventricular cross-section fluorescence imaging

At the conclusion of the 4 week *in vivo* study, animals were sacrificed for analysis of AAV6 expression in the heart and other tissues. Hearts were separated into the ventricles and atria for additional analysis. The ventricles were weighed and then cut approximately in half to enable use of tissue in multiple assays. One half of the ventricle was used for cross-sectional tissue analysis and the other half was used for Western blot and quantitative PCR (RT-PCR) analyses of vector expression. The cross-section tissue analysis was performed to determine the uniformity and robustness of AAV6 expression via the fluorescent mCherry reporter. The ventricle cross-section images were acquired at 18X using a fluorescent dissection microscope (Leica MZ 16FA) capable of capturing bright light images, GFP-like excitations and emissions, and red fluorescent protein (RFP)-like excitations and emissions.

2.3.4 SDS-PAGE and Western blot on ventricular tissue

The other half of the ventricles not used for cross-sectional images were snap frozen in liquid N_2 and stored at -80°C until prepared for SDS-PAGE and Western blot analysis. Before preparing the ventricles for SDS-PAGE and Western blot analysis, the tissue was ground up and pulverized on liquid

N_2 using a mortar and pestle. The ground up ventricles were then placed in lysis buffer, frozen and thawed three times at -20°C, and then sonicated for 10 minutes to fully lyse the cells in the tissue. Once the lysate was collected, total protein content from the ventricular preparations was measured using the Bradford colormetric protein assay where the protein content is determined by measuring the absorbance of 595nm light. The amount of absorbance at this wavelength is proportional to the amount of Coomassie blue dye bound to protein [107,108]. Once total protein content for each sample was determined, the ventricular preparations were resuspended in Laemmli sample and boiled for ~2 min before SDS-PAGE. Determination of total protein content before SDS-PAGE allowed loading of equal amounts of total protein (20 μg). SDS-PAGE separated proteins were transferred to a nitrocellulose membrane and probed with rabbit polyclonal anti-Flag (Sigma-Aldrich, St. Louis, MO) or rabbit polyclonal anti-2A peptide (Millipore, Temecula, CA) after blocking with 5% milk (w/v in Tris-buffered saline). Antibody incubations were carried out in 1% milk (w/v in Tris-buffered saline).

2.3.5 RT-PCR analysis of AAV6 vector genomes in tissue samples

Collection of tissues for analysis of AAV6 vector genome transduction enabled the determination of the biodistribution of the AAV6 expression system through the quantification of the number of vector genomes in cardiac and non-cardiac tissue. Ventricular tissue and other tissues (atria, lung, liver, gastrocnemius, soleus, tibialis anterior, extensor digitorum longus) were snap frozen in liquid N_2 and stored at -80°C until they was ground up and pulverized for DNA extraction. DNA was extracted from 10-15 mg of tissue after digestion with proteinase K using the Qiagen DNAeasy Blood & Tissue Kit. All RT- PCRs were performed on a ABI 7500 Real Time PCR System (Applied Biosystems, Foster City, CA) in a total volume of 15 μl, consisting of 5 μl sample DNA, 7.5 μl 2x iTaq Universal PCR SuperMix (Applied Biosystems, Foster City, CA), 0.15 μM of each primer, 0.075 μM TaqMan custom probe (Applied Biosystems, Foster City, CA), and 2.215 μl dH_2O. Reaction conditions were 50°C for 2

minutes, 95°C for 10 minutes, and 40 cycles of [95°C for 15 seconds followed by 60°C for 1 minute]. Each sample was analyzed in triplicate for concentration of total vector genome detection, the probe and primer set was targeted to the mCherry region of the vector genome. mCherry Primers: 5′-GACCACCTACAAGGCCAAGAAG-3′, 5′-GGGAGGTGATGTCCAACTTGA-3′, TaqMan Probe: 5′-6-FAM-TGCCCGGCGCCTACAACGTC-BHQ1a-6FAM-3′. The pAAV human Pax7 herII plasmid was used as standard in order to obtain absolute genome copy numbers obtained for each tissue sample. Pax7 primers: 5'-CAAGGCCGGGTCAATCAG-3'; 5'- AGATGACACAGGGCCGGA-3'; Probe: 5'-5HEX-CGACCCCTGCCTAACCACATCCG-BHQ1a-5HEX-3'. The number of AAV6 vector genomes was normalized to the total number of genome copies in each tissue. Data are displayed as mean ± S.D.

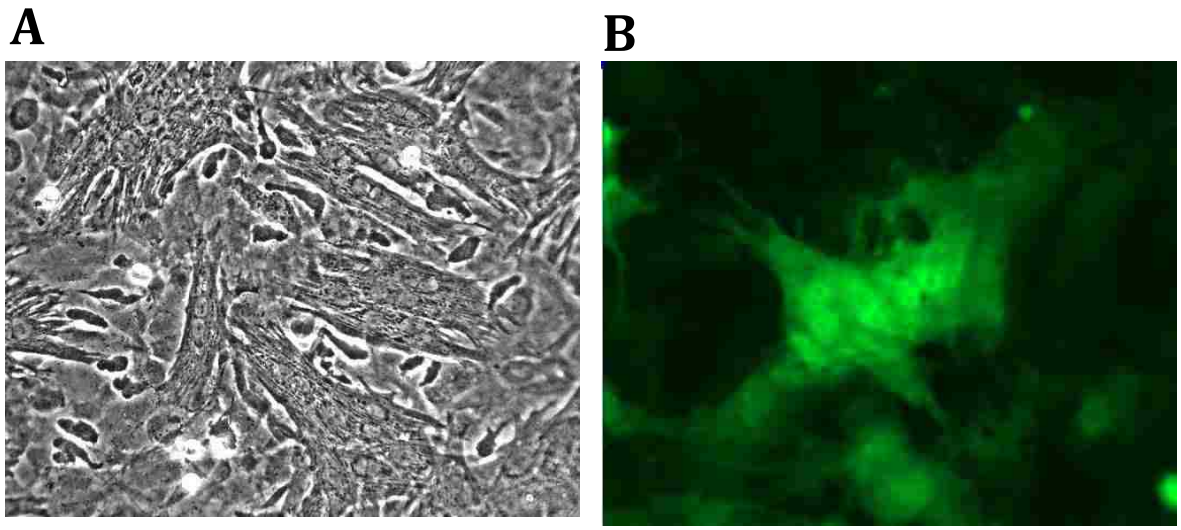

Figure 2.1: Cultured NRCs following adenoviral transduction of Rrm1+GFP and Rrm2+GFP under white light **(A)** and fluorescence microscopy **(B)** at 20X magnification. [25]

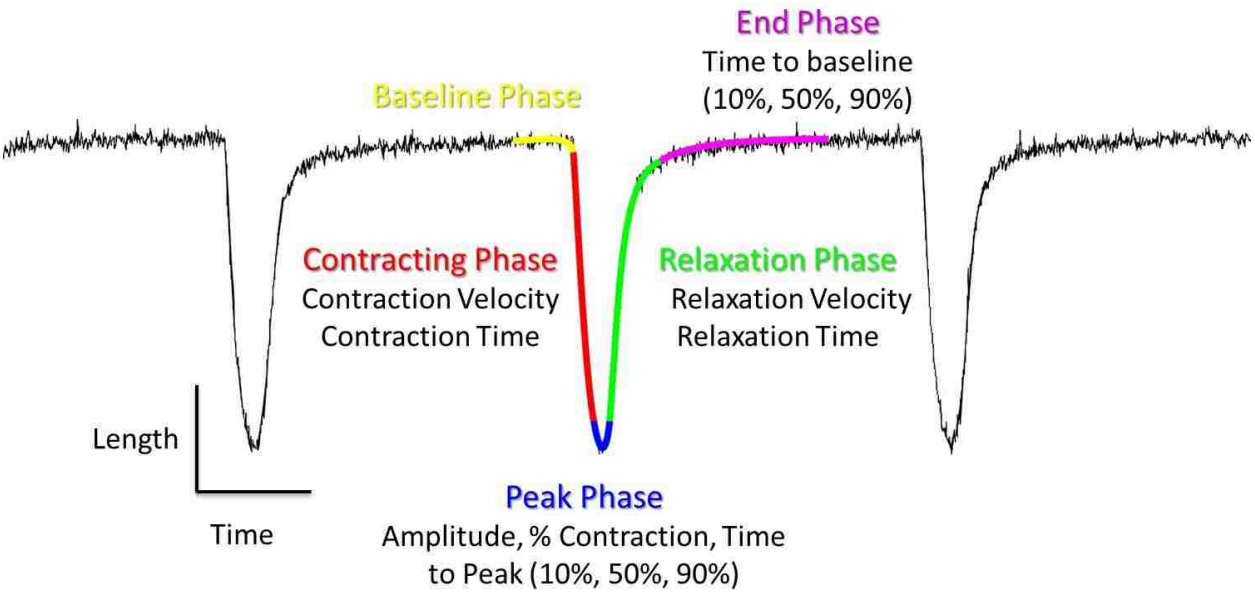

Figure 2.2: Example videomicroscopy cardiomyocyte contraction trace demonstrating contraction and relaxation parameters measured using IonOptix software.

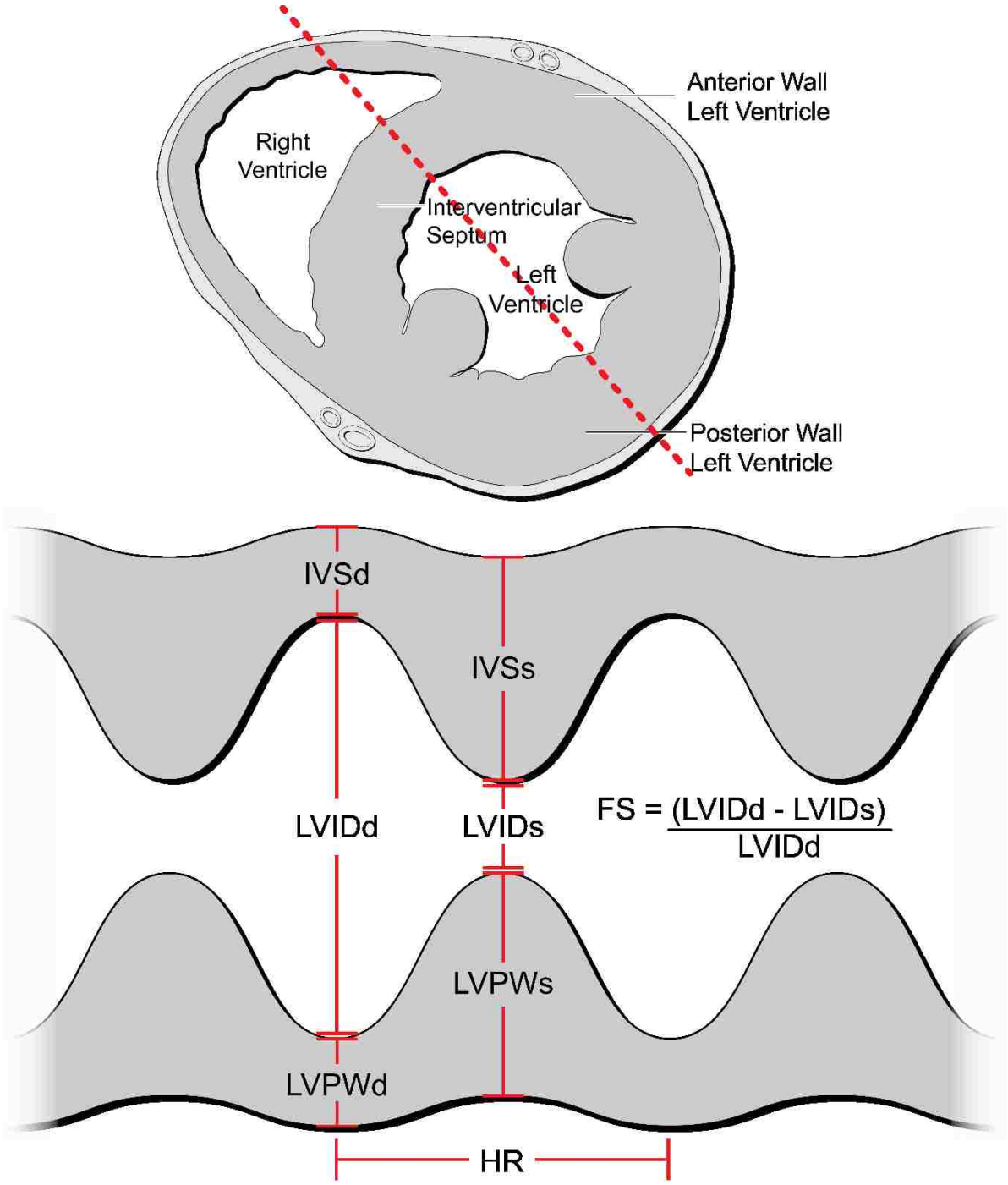

Figure 2.3: Example echocardiography illustrating how and where the different cardiac physiology and functional measurements were obtained. Image courtesy of Scott David Lundy ©2013.

Chapter 3. Enhanced Ca^{2+} binding of cardiac troponin reduces sarcomere length-dependence of contractile activation independently of strong crossbridges

F. Steven Korte, Erik R. Feest, Maria V. Razumova, An-Yue Tu, Michael Regnier. 2012. *AJP Heart and Circulatory Physiology*: Vol. 303 no. 7 H863-H870.

3.1 ABSTRACT

Ca^{2+} sensitivity of the force-pCa relationship depends strongly on sarcomere length (SL) in cardiac muscle, and is considered to be the cellular basis of the Frank-Starling law of the heart. SL-dependence may involve changes in myofilament lattice spacing and/or myosin crossbridge orientation to increase probability of binding to actin at longer SLs. We used the L48Q cTnC variant, which has enhanced Ca^{2+} binding affinity, to test the hypotheses that the intrinsic properties of cardiac troponin C (cTnC) are important in determining 1) thin filament binding site availability and responsiveness to crossbridge activation and 2) SL-dependence of force in cardiac muscle. Trabeculae containing L48Q cTnC-cTn lost SL-dependence of the Ca^{2+} sensitivity of force. This occurred despite maintaining the typical SL-dependent changes in maximal force (F_{max}). Osmotic compression of preparations at SL 2.0 μm with 3% dextran T500 increased F_{max} but not pCa_{50} in L48Q cTnC-cTn exchanged trabeculae, while WT-cTn exchanged trabeculae exhibited increases in both F_{max} and pCa_{50}. Furthermore, crossbridge inhibition with BDM at SL 2.3 μm decreased F_{max} and pCa_{50} in WT cTnC-cTn trabeculae to levels measured at SL 2.0 μm, whereas only F_{max} was decreased with L48Q cTnC-cTn. Overall, these results suggest that L48Q cTnC confers reduced crossbridge dependence of thin filament activation in cardiac muscle, and that changes in the Ca^{2+} sensitivity of force in response to changes in SL are at least partially dependent on properties of thin filament troponin.

3.2 INTRODUCTION

Myocardial performance is tightly regulated at the cardiomyocyte level by sarcomere length (SL), whereby increases in SL sharply increase force generation. This capability is the cellular basis of the Frank-Starling relationship, which allows the heart to match venous return and stroke volume of the right and left ventricles and to match systemic demand of the body on a beat-to-beat basis. The molecular mechanisms of this SL dependent effect are currently debated but thought to result, at least in part, from changes in lattice spacing between the thin and thick filaments, and/or changes in myosin crossbridge orientation that increase the probability of myosin binding to actin at longer SLs [27,64–69]. Furthermore, crossbridge binding enhances Ca^{2+} binding to troponin (cTn) in cardiac muscle, a unique form of cooperative thin filament activation whose mechanism is currently not well understood [65,70–72]. The net result of these interactions is an apparent increase in Ca^{2+} sensitivity of thin filament activation at longer SLs, whereby a given submaximal Ca^{2+} concentration ($[Ca^{2+}]$) results in greater contractile force development. Thus, SL-dependent changes in Ca^{2+}-sensitivity of force generation result from the intrinsic properties of the thin filament [69,73] as well as from complex interactions between thin and thick filament proteins. This is especially important to understand in cardiac muscle, as intracellular $[Ca^{2+}]$ during activation is known to be submaximal [27,74] and loss of SL-dependence of contraction can occur during heart failure [57,59,60].

Under normal conditions, contractile activation is initiated by Ca^{2+}-binding to the cTn complex on cardiac thin filaments, allowing tropomyosin movement that exposes myosin binding sites on actin. Myosin initially forms crossbridges with actin in a weak, electrostatic conformation, then transitions to a strong, hydrophobic conformation that generates force [110]. Transition to a strong binding state further activates cardiac thin filaments and increases Ca^{2+} affinity for cTn, demonstrating a thick-filament mediated influence on thin filament Ca^{2+} binding properties [64,111]. This suggests the inherent Ca^{2+} binding properties of cTn may be relatively weak (compared with skeletal muscle

Tn), and raises the question as to whether thin filaments containing cTn with greater Ca^{2+} affinity would be less dependent on myosin for activation. This, in turn, should confer Ca^{2+}-sensitivity of force that is less responsive to changes in SL.

In the current study we tested the hypotheses that the intrinsic properties of cTn are important in determining Ca^{2+} sensitivity of thin filament activation in response to crossbridge binding, and thus the SL dependence of force in cardiac muscle. We compared the Ca^{2+} dependence of force generation at long (2.3 μm) and short (2.0 μm) SL for demembranated trabeculae exchanged with WT cTn vs. cTn containing a mutant (L48Q) cTnC with enhanced Ca^{2+} affinity [41,43]. To separate the direct influence of strongly bound crossbridges, we compared changes in Ca^{2+} sensitivity at short SL (2.0 μm) with and without osmotic compression by 3% dextran T500, which is sufficient to compress trabeculae and increase maximal force to levels observed at SL 2.3 μm. Finally, we examined crossbridge influence on Ca^{2+} sensitivity of force at long SL using the crossbridge inhibitor BDM at a concentration (7 mM) sufficient to decrease maximal force to levels approximately observed at short SL.

Our results, described below, imply that in cardiac muscle thin filament activation by Ca^{2+} alone is limited, perhaps due to a limited ability to expose crossbridge binding sites on F-actin. More complete activation requires strong binding crossbridges, and this crossbridge dependent component of activation steepens the cardiac force-length relationship. Our data suggest that increasing the Ca^{2+} binding affinity and/or cTnC-cTnI interaction properties of cTn, via L48Q cTnC-cTn, can reduce or eliminate this limitation, by improving thin filament activation at any given submaximal Ca^{2+}. This, in turn, reduces or eliminates crossbridge induced changes in Ca^{2+} sensitivity. Perhaps most importantly, the data suggest that the SL-dependence of cardiac force development is greatly influenced by the properties of native cTn. This is likely to have implications for many familial

inherited cardiomyopathies associated with mutations in thin filament proteins that result in altered Ca^{2+} affinity and/or Ca^{2+} sensitivity of force.

3.3 RESULTS

The Ca^{2+} dependence of isometric steady-state force and force redevelopment rate (k_{tr}) at SL 2.0 (short) and 2.3 μm (long) were determined for demembranated cardiac trabeculae at 15° C (Figure 3.1) following exchange of native cTn with WT cTn or cTn containing L48Q cTnC. We have previously demonstrated that our exchange protocol results in ~90% exchange of native cTn, and that excess cTn was completely removed prior to experiments [41]. In each trabecula, after an initial activation at SL 2.3 μm, trabeculae were exposed to increasing Ca^{2+} concentration (decreasing pCa) at either long (2.3 μm) or short (2.0 μm) SL to obtain measurements of steady-state force, rate of force redevelopment (k_{tr}) and stiffness, then SL was changed and the protocols were repeated. This varying of initial SL helps account for any run down of the preparation, and results from either SL sequence were rejected if force at pCa 4.0 (F_{max}) declined by more than 15% at the end of the force-pCa curve.

3.3.1 SL dependence of steady-state force and stiffness

Force-pCa relationships at SL 2.0 and 2.3 μm for trabeculae with either WT or L48Q cTnC-cTn are summarized in Figure 3.1. A concomitant increase in stiffness with force occurred as Ca^{2+} was increased at short and long SL with both WT and L48Q cTnC-cTn (Figure 3.1A). This suggests that force varied proportionally in all conditions as a result of changes in strong crossbridge binding, and not a change in force produced per crossbridge. In Figure 3.1B the data were compared by plotting force-pCa relationships normalized to F_{max} at SL 2.0 or 2.3 μm. The absolute values for F_{max} are

summarized in Figure 3.1C. The data from individual force-pCa curves were fit with the Hill equation for determination of pCa_{50} and $n_{H,}$ and the mean (±SEM) of these values for each condition are listed in Table 3.1. Decreasing SL from 2.3 to 2.0 μm in WT trabeculae decreased F_{max} from 30±7 mN/mm^2 to 17±3 mN/mm^2, and right shifted pCa_{50} by 0.09±0.01 (ΔpCa_{50}) (Figure 3.1C; Table 3.1). These results are similar to our previous report [78].

For trabeculae containing L48Q cTnC-cTn, decreasing SL from 2.3 to 2.0 μm reduced F_{max} from 33±7 mN/mm^2 to 20±3 mN/mm^2 (Figure 1C; Table 3.1). These values were not different from WT cTnC-cTn exchanged trabeculae. Increasing SL from 2.0 to 2.3 μm in L48Q cTnC-cTn trabeculae increased the passive force, similar to results for WT cTnC-cTn trabeculae (Table 3.1). Additionally, there was no difference in stiffness at 2.3 and 2.0 μm in relaxing solution between WT and L48Q cTnC-cTn trabeculae (data not shown), which indicates L48Q cTnC-cTn does not allow Ca^{2+}-independent activation of the thin filament at pCa 9.0. However, in L48Q cTnC-cTn trabeculae, there was a dramatically different effect on the SL-dependence of pCa_{50}. As previously reported [41], L48Q cTnC-cTn increased Ca^{2+} sensitivity of force at SL 2.3 μm compared to WT. Interestingly, when SL was decreased from 2.3 to 2.0 μm, there was no significant change in pCa_{50} (Figure 3.1B; Table 3.1), demonstrating a much larger effect of L48Q cTnC-cTn on pCa_{50} at short SL. In effect, this means that L48Q cTnC-cTn greatly reduced, and very likely eliminated, the SL dependence of Ca^{2+} sensitivity of thin filament activation in cardiac muscle. However, the influence of SL on maximal strong crossbridge binding (F_{max}) remains. Similar results have been reported by others, i.e. a decrease in SL dependence of the Ca^{2+} sensitivity of force in myocardium containing L29Q-cTnC (decrease in ΔpCa_{50} [112]) or ssTnI (decrease in ΔEC_{50} [113]), both of which left-shifted the force-pCa curve.

3.3.2 Role of lattice spacing in the loss of SL dependence of force generation with L48Q cTnC-cTn

To determine if loss of the SL-dependence of Ca^{2+} sensitivity of force with L48Q cTnC-cTn is sensitive to changes in thin-thick filament spacing or actin-myosin proximity, myofilament lattice spacing was osmotically compressed using 3% dextran T500 (w/v) at SL 2.0 μm. This dextran concentration was selected because it increased F_{max} values at SL 2.0 μm to those measured at SL 2.3 μm without dextran. Force-pCa relationships for these trabeculae are summarized in Figure 3.2. Trabeculae with WT cTnC-cTn exhibited an increase in pCa_{50} and F_{max} when osmotically compressed at SL 2.0 μm (Figure 3.2A; Table 3.2). This is consistent with our previous work (1), which demonstrated that osmotic compression of lattice spacing at SL 2.0 μm results in force and Ca^{2+} sensitivity of force similar to that seen at SL 2.3 μm without dextran. However, with L48Q cTnC-cTn, 3% dextran increased F_{max} at SL 2.0 μm without any significant change in pCa_{50} (Figure 2B; Table 3.2). The increase in pCa_{50} with L48Q cTnC-cTn (relative to WT cTnC-cTn) was maintained, but there was no additional increase in pCa_{50} with osmotic compression. These results suggest that actin-myosin proximity may have little to no effect on myofilament Ca^{2+} sensitivity of force when L48Q cTnC-cTn is present in thin filaments.

3.3.3 Role of strong cross-bridge binding in the loss of SL dependence of force generation with L48Q cTnC-cTn

To determine if the loss of SL dependence of the Ca^{2+} sensitivity of force with L48Q cTnC-cTn is reliant on the number of strongly bound cross-bridges, strong cross-bridge formation was inhibited using BDM at SL 2.3 μm. The BMD concentration was selected such that F_{max} at SL 2.3 μm with BDM was similar to F_{max} values at SL 2.0 μm without BDM for each muscle preparation. Force-pCa relationships for these trabeculae are summarized in Figure 3.3 and Table 3.2. The passive force in L48Q cTnC-cTn trabeculae was unchanged in the presence of BDM indicating no active crossbridge cycling while at rest (pCa 9.0). With WT cTnC-cTn, BDM caused a right shift in force-pCa curve and a decrease of F_{max}, both of which were similar to the levels observed when SL was reduced from 2.3 to 2.0 μm

without BDM (Figure 3.3A, Table 3.1, 3.2). Trabeculae containing L48Q cTnC-cTn also exhibited a decrease in F_{max} with BDM (Figure 3.3B; Table 3.1, 3.2); however, there was no significant right shift of the force-pCa curve. L48Q cTnC-cTn trabeculae still exhibited an increase in the Ca^{2+} sensitivity of force compared to WT cTnC-cTn at SL 2.3 μm, with and without BDM. These results suggest that improved myofilament Ca^{2+} binding, via incorporation of L48Q cTnC-cTn, reduces the dependence of thin filament activation on the number of strongly bound cross-bridges.

3.3.4 Ca^{2+} and SL dependence of force redevelopment (k_{tr})

In a previous study we demonstrated that L48Q cTnC-cTn enhances the Ca^{2+} sensitivity of the rate of force redevelopment (k_{tr}), but not the maximal rate [41]. In the current study, we determined how L48Q cTnC-cTn influences the SL dependence of the k_{tr}-pCa and k_{tr}-force relationships. These results are summarized in Figure 3.4. Example representative traces of force redevelopment during the k_{tr} slack-re-stretch protocol at pCa 4.0 for WT and L48Q cTnC-cTn trabeculae are shown in Figure 3.4A. These traces and the summarized data demonstrate that at maximal Ca^{2+} (pCa 4.0) k_{tr} was similar for both WT and L48Q cTnC-cTn at SL 2.0 and 2.3 μm. The Ca^{2+} dependence of k_{tr} was not affected by SL for either WT (Figure 3.4B) or L48Q (Figure 3.4C). At submaximal Ca^{2+} (between pCa 6.0 and 5.4), k_{tr} was significantly faster for L48Q cTnC-cTn (vs. WT cTnC-cTn) at both SL 2.0 and 2.3 μm. However, when k_{tr} was compared at a given force level for WT and L48Q cTnC-cTn trabeculae, there was no difference between them at either SL 2.0 or 2.3 μm. This is demonstrated in Figure 3.4D, were k_{tr} values for WT and L48Q cTn containing trabeculae at SL 2.3 μm are re-plotted vs. the steady state force produced at each pCa. These results suggest that L48Q cTnC-cTn increases the activation level of the thin filament at sub-maximal forces independent of SL, but that at similar levels of thin filament activation, L48Q cTnC-cTn does not increase the rate of force development.

3.4 DISCUSSION

The SL-dependence of the Ca^{2+} sensitivity of force is thought to be the molecular mechanism behind Frank-Starling relationship of the heart, and it has been shown to be influenced by various components of the contractile apparatus. Changes in thin filament properties, such as substitution of ssTnI for cTnI [113–115] or point mutations in cTnC [112] and cTnT [116,117], as well as changes in thick filament properties [118] and factors affecting thin and thick filament interactions (lattice spacing [65,67,78,119–122], pH [118]) or the cross bridge cycle [70,123] have all been shown to influence the SL dependence of contraction. However, no single mechanism has emerged as the primary determinant of the Frank-Starling relationship.

In this study, we independently altered properties of the thin and thick filament that are responsible for thin filament activation and contraction of cardiac muscle. We demonstrated that a cTnC variant with increased Ca^{2+} affinity (L48Q) eliminated crossbridge-mediated effects on the apparent Ca^{2+} sensitivity of thin filament activation as the Ca^{2+} concentration required to produce half-maximal force (pCa_{50}) for L48Q cTnC-cTn exchanged trabeculae was unaffected by perturbations of crossbridge activity/number. In contrast, these perturbations did produce changes in pCa_{50} of native or WT cTnC-cTn trabeculae. The concomitant increase in stiffness with force as Ca^{2+} is increased at short and long SL with both WT and L48Q cTnC-cTn (Figure 3.1A) suggests that force varied proportionally in all conditions as a result of changes in strong crossbridge binding, and not a change in force produced by each cross-bridge. These results corroborate the evidence presented by Sun YB et al. [69] that the intrinsic properties of the thin filament play a very significant role in the cooperative Ca^{2+} activation and regulation of cardiac contractility, and suggest that by sensitizing the thin filament to Ca^{2+}, L48Q cTnC greatly reduces the crossbridge assistance required for thin filament activation in cardiac muscle.

The reliance on strong crossbridges for thin filament activation is a hallmark of cardiac contraction. Ca^{2+} binding to troponin initiates thin filament activation exposing myosin binding sites on actin. However, unlike in skeletal muscle, thin filament activation in cardiac muscle is not achieved primarily by Ca^{2+} binding alone [27,77,124]. Numerous studies have shown that crossbridge binding in cardiac muscle increases Ca^{2+} binding to cTnC [27,40,65,68,78,119,122] and induces structural changes in fluorescently-tagged cTnC as measured by dichroism [125]. Furthermore, rigor-myosin subfragment -1 crossbridges (NEM S-1) and Ca^{2+} can greatly increase the rate of product release from pre-power stroke myosin bound to thin filaments over Ca^{2+} alone [70,123]. This effect was not observed in skeletal muscle, where Ca^{2+} alone was sufficient to achieve accelerated product release. A similar difference was observed between skeletal and cardiac myosin where S1-thin filament binding assays showed a Ca^{2+}-induced 4-fold change in closed-open equilibria of the skeletal vs. cardiac system, which is indicative of a fundamental difference in the actin-TnI-TnC binding equilibria. Overall, the results suggest that situations that increase or decrease the number of strongly bound crossbridges (such as SL) increase or decrease the apparent Ca^{2+} sensitivity of cardiac muscle contraction.

We introduced perturbations to crossbridge binding that are generally accepted to affect pCa_{50}, to determine whether they would have the same effect on pCa_{50} and SL-dependence of the Ca^{2+} sensitivity of force in the presence of L48Q cTnC-cTn. Several studies [65,67,78,118,119,122] have concluded that acto-myosin interaction distance, at least in part, is responsible for an increased contractile activation at longer SL in cardiac muscle. Martyn et al. [121] showed that compression with 3% osmotic solute dextran T-500 at SL 2.0 μm results in thick filament spacing observed at SL 2.3 μm with 0% dextran. In this manner, we matched the overall force generating capacity of myofilaments at a short SL to that at long SL via modulations in actin-myosin proximity. Despite

increased crossbridge binding and force in the presence of dextran, pCa_{50} was unchanged for L48Q cTnC-cTn trabeculae, but was significantly increased for native and WT cTnC-cTn trabeculae, as previously demonstrated [65,67,78,118,119,122]. This suggests crossbridge binding induced increases of Ca^{2+} sensitivity with WT cTnC-cTn, but not with L48Q cTnC-cTn, and suggests that L48Q cTnC-cTn sufficiently increases the Ca^{2+} sensitivity of the thin filament to a level that no longer requires crossbridge contributions to achieve full activation.

To test this hypothesis, we inhibited crossbridge binding with BDM at SL 2.3 μm to decrease force to levels approximately equal to those seen at SL 2.0 μm. Thus, a similar number of force generating cross-bridges were likely involved at SL 2.0 and SL 2.3 μm in the presence of BDM [50], while the remaining myofilament environment characteristic of SL 2.3 μm was maintained (e.g. actin-myosin proximity, passive tension, etc.) With BDM, even though F_{max} was reduced, little to no change in pCa_{50} was observed with L48Q cTnC-cTn, while there was a decrease in both F_{max} and pCa_{50} with WT cTnC-cTn. All of these crossbridge perturbations resulted in the expected increases (longer SLs, dextran) and decreases (shorter SLs, BDM) in F_{max} for both WT and L48Q cTnC-cTn exchanged trabeculae. This indicates that the numbers of strongly bound crossbridges was changing accordingly. Together our results and those of others [70] suggest that Ca^{2+} only partially activates thin filaments containing native cTnC, where more complete activation requires strongly bound crossbridges, and this cross-bridge dependent component of activation may underlie the steep SL dependence of Ca^{2+} sensitivity in cardiac muscle. Furthermore, our results indicate that the crossbridge-induced feedback on thin filament Ca^{2+} sensitivity was eliminated with L48Q cTnC-cTn.

It is interesting to speculate on how L48Q cTnC might lessen the cross-bridge dependent component of cardiac thin filament activation. In a recent study, we examined how the L48Q variant might affect the intrinsic properties of the thin filament by investigating the ability of L48Q cTnC to bind Ca^{2+} and

cTnI using a combination of solution protein studies, nuclear magnetic resonance spectroscopy (NMR), and molecular dynamic (MD) simulation approaches [42]. Our solution studies, and studies by others [43], have shown that L48Q cTnC has a significantly higher affinity for Ca^{2+}, compared to WT cTnC alone or in cTn complex. We also demonstrated that L48Q cTnC has a higher affinity for cTnI in both the presence and absence of Ca^{2+}. Both NMR and MD simulation data indicate that the N-terminal lobe of L48Q cTnC has a more open structure and exposure of the cTnC hydrophobic patch is stabilized following Ca^{2+} binding. This should increase cTnC-cTnI interaction, allowing enhanced movement of Tm and access to myosin binding sites on actin for a given submaximal [Ca^{2+}]. It is likely that this is the cause of increased Ca^{2+} sensitivity of thin filament activation and force development in cardiac muscle containing L48Q cTnC, and it may also reduce the requirement for crossbridges to [126] stabilize the cTnC-cTnI state. This effect should be more pronounced at lower [Ca^{2+}], where the slower dissociation rate of L48Q cTnC [41,43] should result in Ca^{2+} being bound to more cTn in thin filaments at any given time. This is in contrast to behavior at higher [Ca^{2+}] where thin filament activation is more complete, and thus dissociation rate of Ca^{2+} is not limiting. Indeed, F_{max} appears to be similar with WT and L48Q cTnC at both long and short SL, and the greatest effect of L48Q cTnC on force is when $pCa_{50} < 5.3$ at both short and long SL. A recent study [112] examining L29Q cTnC, a mutation reported to be associated with hypertrophic cardiomyopathy, demonstrated increased Ca^{2+} binding affinity and, interestingly, also a decrease in Ca^{2+} sensitivity responsiveness to changes in SL. Additionally, others have shown that replacement of native TnI with ssTnI increased Ca^{2+} sensitivity of force and reduced SL dependent activation [115]. Our experiments using 2-deoxy-ATP that increases Ca^{2+} sensitivity of force production have shown no effect on the SL-dependence of pCa_{50} [78]. Because Ca^{2+} binding affinity *per se* and cTnC-cTnI interaction strength are coupled processes, it is difficult to discern which may be responsible for the loss of SL-dependence of the Ca^{2+} sensitivity of thin filament activation and force development.

Further studies will be necessary to determine the relative importance of Ca^{2+} binding affinity and the strength of cTnC-cTnI interaction in the mechanism of the SL dependence of the force-pCa relationship in cardiac muscle. Use of other variants with altered Ca^{2+} sensitivity, Ca^{2+} sensitizing agents [78,127] and/or altered strength of cTnC-cTnI interaction or factors changing C-I interactions, like PKA phosphorylation of cTnI that lowers cTnC affinity for cTnI, can be important tools in determining this. Regardless of the mechanism behind our results, this work demonstrates that alteration of intrinsic properties of troponin can have dramatic effect on thin filament activation in response to crossbridge binding, and thus, in determining SL dependence of force in cardiac muscle. Perhaps most importantly, the properties of cTn are likely to have implications for many familial inherited cardiomyopathies that are associated with mutations in thin filament proteins.

3.5 AKNOWLEDGEMENTS

We acknowledge Zhaoxiong Luo for preparation of recombinant troponin complexes.

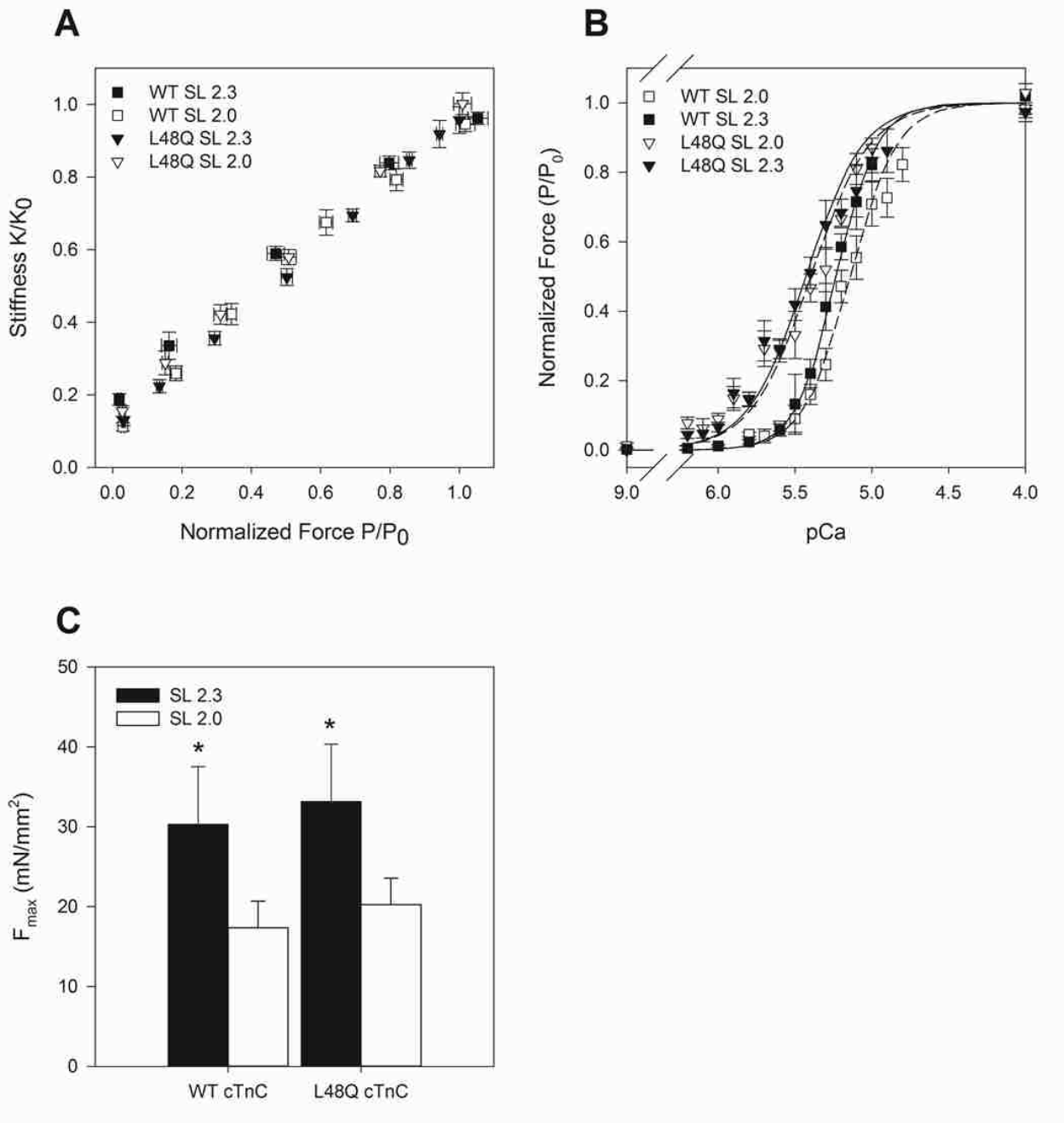

Figure 3.1: Normalized SL dependence of Ca^{2+} sensitivity of force and stiffness after whole cTn exchange containing WT or L48Q cTnC. A) Normalized force vs. stiffness as Ca^{2+} was varied at SL 2.0 (open symbols) and 2.3 μm (closed symbols) for trabeculae containing WT (squares) and L48Q cTnC-cTn (triangles) B) normalized force-pCa and C) absolute maximal force (F_{max}) values for WT (squares) and L48Q (triangles) cTnC-cTn exchanged trabeculae at SL 2.0 (open symbols) and 2.3 μm (closed symbols). The error bars represent ± S.E.M. and in some cases are contained within the symbol. The data were fit with the Hill equation and corresponding fit values are included in Table 3.1.

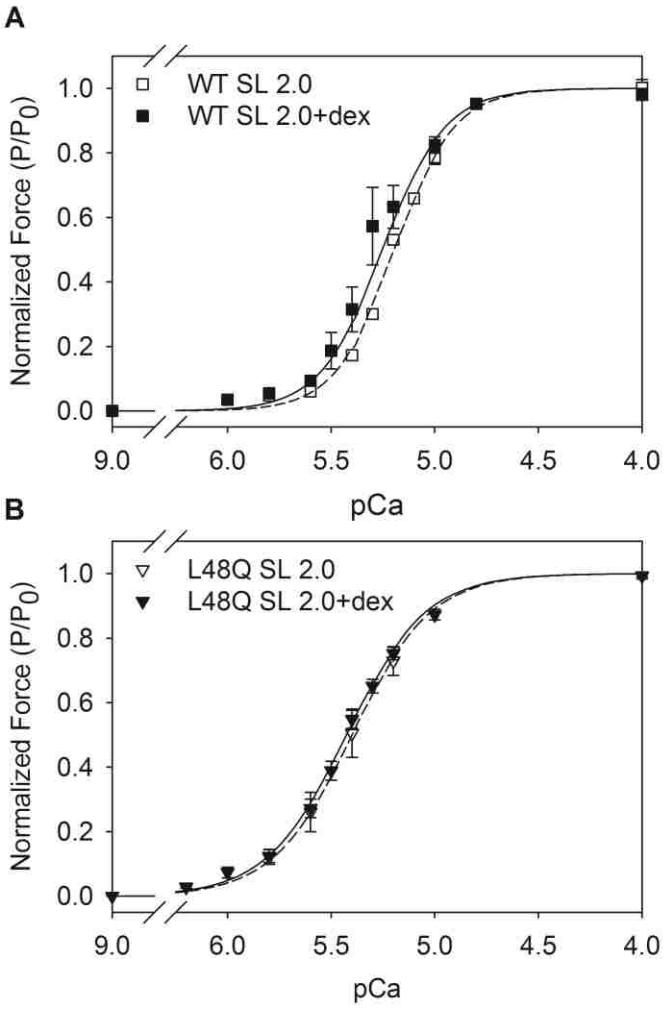

Figure 3.2: Normalized force-pCa relationship at SL 2.0 μm ± 3% dextran for trabeculae containing WT or L48Q cTnC-cTn A) WT cTnC-cTn at SL 2.0 (open symbols) and SL 2.0 + 3% dextran (closed symbols) B) L48Q cTnC-cTn at SL 2.0 (open symbols) and SL 2.0 + 3% dextran (closed symbols). The error bars represent ± S.E.M. and in some cases are contained within the symbol. The data were fit with the Hill equation and corresponding fit values are included in Table 3.2.

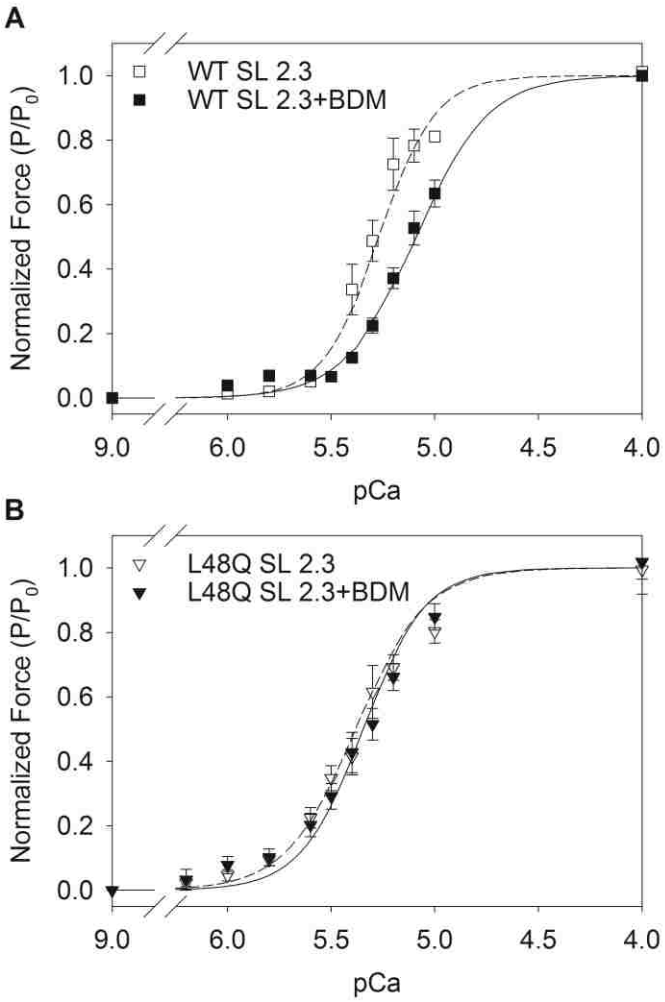

Figure 3.3: Normalized force-pCa relationship at SL 2.3 μm ± 7mM BDM for trabeculae containing WT or L48Q cTnC-cTn A) WT cTnC-cTn at SL 2.3 (open symbols) and SL 2.3 + 7mM BDM (closed symbols) B) L48Q cTnC-cTn at SL 2.3 (open symbols) and SL 2.3 + 7mM BDM (closed symbols). The error bars represent ± S.E.M. and in some cases are contained within the symbol. The data were fit with the Hill equation and corresponding fit values are included in Table 3.2.

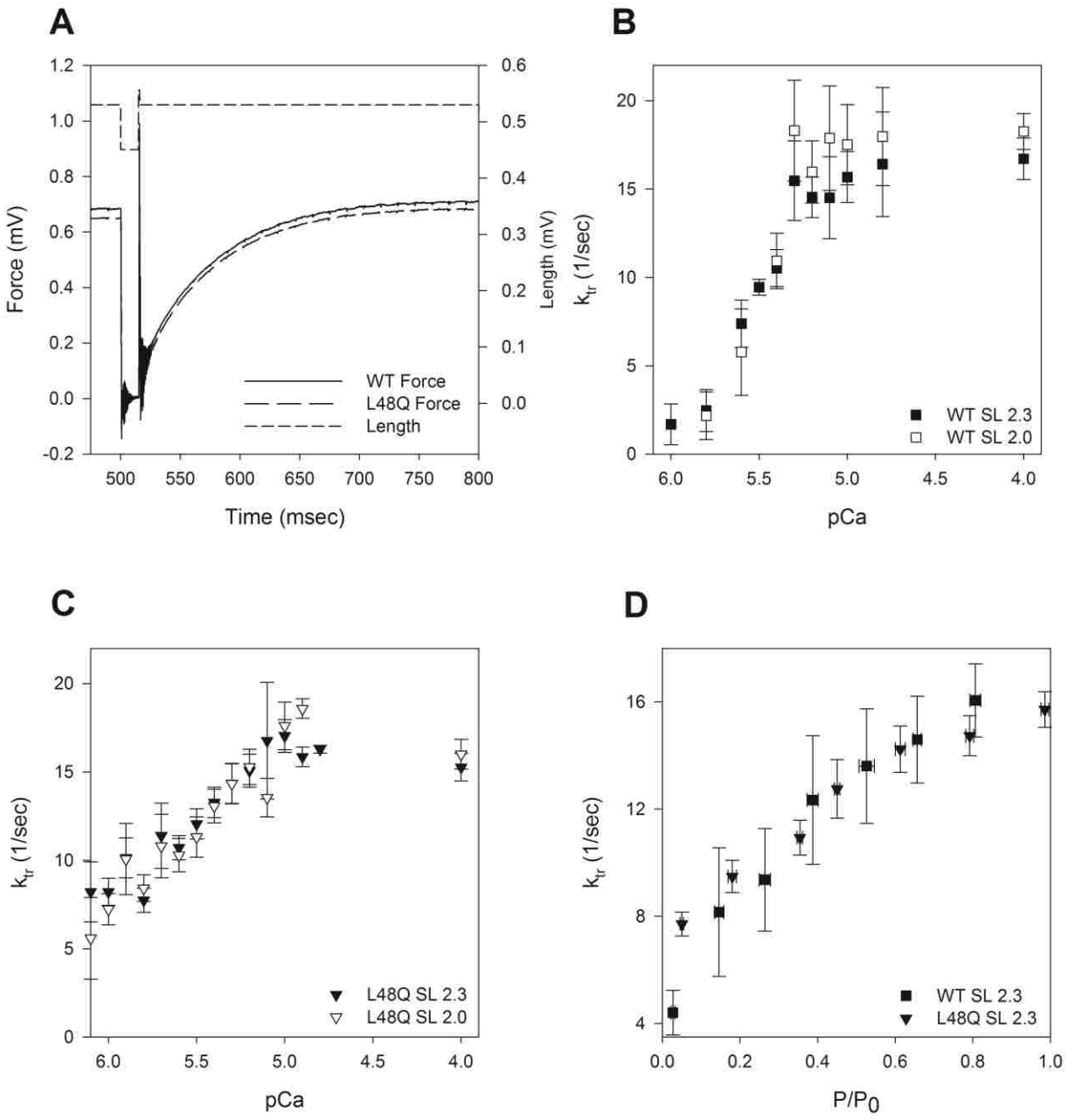

Figure 3.4: ktr-pCa and ktr-force relationships during steady-state activation for trabeculae containing WT or L48Q cTnC-cTn at SL 2.0 and 2.3 μm. A) WT (solid) and L48Q (dashed) cTnC-cTn example force traces after a slack-restretch procedure. The corresponding length trace is shown in dotted line. B) WT cTnC-cTn ktr-pCa relationships at SL 2.0 (open symbols) and 2.3 μm (closed symbols) C) L48Q cTnC-cTn ktr-pCa relationships at SL 2.0 (open symbols) and 2.3 μm (closed symbols) D) WT (open symbols) and L48Q (closed symbols) cTnC-cTn ktr-force relationships at SL 2.3 μm. The error bars represent ± S.E.M. and in some cases are contained within the symbol.

Table 3.1: Summary of steady-state force-pCa parameters after whole cTn exchange in cardiac trabeculae at SL 2.0 and 2.3 μm. Values are means ± S.E.M., and * = $p<0.05$ as compared to SL 2.0 μm.

	N	SL, μm	F_{max}, mN/mm²	$F_{passive}$, mN/mm²	pCa_{50}	nH
WT cTnC	8	2.3	30 ± 7	4.8 ± 1.0*	5.23 ± 0.03*	3.2 ± 0.2
		2	17 ± 3	0.9 ± 0.1	5.14 ± 0.04	2.8 ± 0.1
L48Q cTnC	17	2.3	33 ± 7*	7.6 ± 1.6*	5.43 ± 0.03	2.3 ± 0.1
		2	20 ± 3	1.8 ± 0.3	5.40 ± 0.03	2.2 ± 0.1
Native	15	2.3	39 ± 4*	3.8 ± 0.8*	5.45 ± 0.03*	4.2 ± 0.2
		2	24 ± 2	1.3 ± 0.3	5.32 ± 0.03	4.2 ± 0.3

Table 3.2: Summary of steady-state force-pCa parameters after whole cTn exchange in cardiac trabeculae at SL 2.0 μm + 3% dextran or SL 2.3 μm + 7mM BDM. Values are means ± S.E.M., and * = $p<0.05$ as compared to control condition for WT or L48Q cTnC-cTn.

		N	SL, μm	F_{max}, mN/mm²	$F_{passive}$, mN/mm²	pCa_{50}	nH
WT cTnC	Control	4	2	15 ± 3	1.0 ± 0.2	5.19 ± 0.00	3.0 ± 0.1
	+ 3% Dex		2	23 ± 4*	1.2 ± 0.2	5.25 ± 0.02	2.9 ± 0.1
L48Q cTnC	Control	9	2	18 ± 3	1.7 ± 0.4	5.40 ± 0.05	2.3 ± 0.1
	+ 3% Dex		2	28 ± 5*	2.2 ± 0.4	5.43 ± 0.02	2.3 ± 0.1
WT cTnC	Control	4	2.3	27 ± 8	5.4 ± 2.0	5.27 ± 0.02	3.2 ± 0.3
	+BDM 7mm		2.3	17 ± 3	6.1 ± 2.8	5.09 ± 0.02 *	2.5 ± 0.1
L48Q cTnC	Control	11	2.3	35 ± 5	10.6 ± 2.0	5.38 ± 0.03	2.6 ± 0.2
	+BDM 7mm		2.3	19 ± 3*	8.2 ± 1.4	5.35 ± 0.03	2.9 ± 0.5

Chapter 4. N-terminal phosphorylation of cardiac troponin-I reduces length dependent Ca^{2+} sensitivity of contraction in cardiac muscle

Vijay S. Rao, F. Steven Korte, Maria V. Razumova, Erik R. Feest, Hsiao Man Hsu, Thomas Irving, Michael Regnier, Donald A. Martyn. 2013. *J. Physiology*: Vol. 591; 475-490.

4.1 ABSTRACT

Protein kinase A (PKA) phosphorylation of myofibrillar proteins constitutes an important pathway for β-adrenergic modulation of cardiac contractility. In myofilaments PKA targets troponin I (cTnI), myosin binding protein-C (cMyBP-C) and titin. We studied how this affects the sarcomere length (SL) dependence of force-pCa relations in demembranated cardiac muscle. To distinguish cTnI from cMyBP-C/titin phosphorylation effects on the force-pCa relationship, endogenous troponin (Tn) was exchanged in rat ventricular trabeculae with either wild-type (WT) Tn, nonphosphorylatable cTnI (S23/24A) Tn or phosphomimetic cTnI (S23/24D) Tn. PKA cannot phosphorylate either cTnI S23/24 variant, leaving cMyBP-C/titin as PKA targets. Force was measured at 2.3 and 2.0 μm SL. Decreasing SL reduced maximal force (F_{MAX}) and Ca^{2+}-sensitivity of force (pCa_{50}) similarly with WT and S23/24A trabeculae. PKA treatment of WT and S23/24A trabeculae reduced pCa_{50} at 2.3, but not 2.0 μm SL, thus eliminating the SL-dependence of pCa_{50}. In contrast, S23/24D trabeculae reduced pCa_{50} at both SL, primarily at 2.3 μm, also eliminating SL-dependence of pCa_{50}. Subsequent PKA treatment moderately reduced pCa_{50} at both SL. At each SL F_{MAX} was unaffected by either Tn exchange and/or PKA treatment. Low angle x-ray diffraction was performed to determine whether pCa_{50} shifts were associated with changes in myofilament spacing ($d_{1,0}$) or thick-thin filament interaction. PKA increased $d_{1,0}$ slightly under all conditions. The ratios of the integrated intensities of the equatorial x-ray reflections ($I_{1,1}/I_{1,0}$) indicate that PKA treatment increased crossbridge proximity to thin filaments under all conditions. The results suggest that phosphorylation by PKA of either cTnI or

cMyBP-C/titin independently reduces the pCa_{50} preferentially at long SL, possibly through reduced availability of thin filament binding sites (cTnI) or altered crossbridge recruitment (cMyBP-C/titin). Preferential reduction of pCa_{50} at long SL may not reduce cardiac output during periods of high metabolic demand because of increased intracellular Ca^{2+} during β-adrenergic stimulation.

4.2 INTRODUCTION

Increasing sarcomere length (SL) of cardiac myocytes with increased ventricular filling results in a steep increase in force generation that underlies the heart's ability to match ventricular output to venous return (i.e. the Frank-Starling relation). Elevated force from increasing SL results in part from an accompanying increase in sensitivity of the contractile regulatory apparatus to intracellular Ca^{2+}, particularly important since Ca^{2+} activation is sub-maximal during a cardiac twitch [27,74]. During increased metabolic demand, β-adrenergic stimulation of the heart and subsequent activation of protein kinase A (PKA) phosphorylates several myofilament and Ca^{2+} handling proteins, allowing an adaptive increase of cardiac contractility and ventricular output. β-adrenergic stimulation enhances intracellular Ca^{2+} transients during cardiac contractions, decreases the sensitivity of the myofilament contractile apparatus to Ca^{2+}, and increases the rate of intracellular Ca^{2+} return to sub-activation threshold levels to initiate diastole [53]. While cardiac contraction is enhanced by β-adrenergic stimulation, it is not clear whether (or how) the myofilament basis for the Frank-Starling mechanism is altered by β -adrenergic activation via PKA. Literature reports are contradictory, with reports that PKA treatment either increased [87,115,128], decreased [129], or did not change [37] the influence of SL on the Ca^{2+}-sensitivity of force . Our approach to resolve this disparity is based on previous studies suggesting that the actin-binding inhibitory subunit of cardiac troponin (cTnI) may play an important role in determining the SL-dependence of the Ca^{2+}-sensitivity of contractile force in

demembranated (skinned) cardiac muscle [113–115] via phosphorylation of the N-terminal serines (Ser 23, 24) by PKA [130].

The influence of SL on the Ca^{2+}-sensitivity of force results from complex interactions between both thin and thick filament associated regulatory proteins. These interactions include 1) Ca^{2+}-binding to the troponin complex (Tn) to initiate contractile activation of thin filaments, 2) strong myosin crossbridge (CB) binding to further activate cardiac thin filaments, and 3) the intrinsic properties of the troponin regulatory subunits [27,65]. The interactions between these contractile regulatory proteins are additionally modulated by phosphorylation of specific amino acids by a host of protein kinases, including PKA [130–133]. Central to these interactions is the phosphorylation of cTnI [134–137]. By itself, PKA phosphorylation of cTnI decreases the Ca^{2+}-sensitivity of force in skinned cardiac trabeculae and increases the rate of myofibril relaxation [137,138]. N-terminal phosphorylation of cTnI weakens interaction between the C-terminus of cTnI and the N-terminus of cardiac troponin C (cTnC) during Ca^{2+}-activation [126,131,136,139,140] and increases the Ca^{2+} dissociation rate from cTnC [135,141]. This results in more rapid dissociation of Ca^{2+} from cTnC to begin diastole, increasing the rate of relaxation to subsequently enhance ventricular filling.

The interactions of CBs with thin filaments may also be influenced by the myosin-associated proteins including myosin-binding protein C (cMyBP-C) [142,143] and regulatory light chain 2 (RLC2) [38,144,145], as well as the giant sarcomeric protein titin [145–147]. Thick filament targets for PKA phosphorylation include the cardiac specific motif of cMyBP-C [142,143] and the N2B domain of titin [148,149]. PKA phosphorylation within the motif region of cMyBP-C reduces binding to the S2 domain of myosin and increases the proximity of CBs to thin filaments [88,142,150,151]. PKA

phosphorylation of the cardiac N2B titin domain and reduces passive tension in skinned cardiac preparations [148,149,152].

Because PKA targets cTnI, cMyBP-C and titin it has been difficult to determine the precise mechanistic role that phosphorylation of each protein plays in myofilament force regulation and the Frank-Starling mechanism. The goal of this study was to determine the specific role of PKA phosphorylation of cTnI (vs. cMyBP-C and titin). This was accomplished by exchanging endogenous cTn in skinned right ventricular trabeculae from rats with recombinant cTn containing either a cTnI variant in which serines 23, 24 represent a nonphosphorylatable state, cTnI (S23/24A) [153], or a constitutively phosphorylated state cTnI (S23/24D) [154]. Neither of these cTnI variants can be phosphorylated by PKA. Thus with either cTnI variant, PKA treatment primarily targets both cMyBP-C and titin, so that any additional effects could be attributed to phosphorylation at sites on those proteins. However, it is important to understand that these experiments do not allow separation of the individual influences of cMyBP-C or titin phosphorylation by PKA.

Using a combination of phosphomimetic cTnI mutants and PKA treatment, we found that the SL-dependence of the pCa_{50} of force (but not maximal force) could be reduced by phosphorylation of cTnI Ser23/24 or cMyBP-C/titin. Combined with X-ray diffraction studies of myofilament lattice structure these results point to separate length dependent effects of PKA on cTnI and cMyBP-C/titin that are most evident at long SL where the probability of crossbridge formation increases. PKA phosphorylation of cTnI may reduce cTnC-cTnI interaction, leading to decreased Ca^{2+} sensitivity and reduced thin filament access for CB's, particularly at the longer SL. In contrast, PKA phosphorylation of cMyBP-C may reduce the SL dependence of contraction by promoting weak myosin binding to the

thin filament. The net effect of PKA phosphorylation is to attenuate the effect of SL on force generation over the physiologically relevant range of intracellular [Ca^{2+}].

4.3 RESULTS

4.3.1 Recombinant troponin exchange and phosphorylation profiles

To quantify the extent of cTn exchange, recombinant cTn complex containing cTnT labeled at the N-terminus with a c-myc tag (Figure 4.1A) was exchanged into skinned right ventricular trabeculae from rat hearts. Densitometry analysis of Western blots using cTnT specific antibodies indicated that 80% of endogenous Tn was replaced by Tn containing the c-myc tagged cTnT, similar to exchange efficiency values reported previously [90,136]. This suggests the exchange protocol was efficient and that the resulting changes in contractility can primarily be attributed to the exchanged cTn containing either WT cTnI or cTnI variants. Consistent with previously published reports from our group [124], no evidence was found for extraction of myosin regulatory light chains (Supplemental Figure 4.S2A).

Phosphoprotein analysis confirmed that recombinant cTn had no measurable levels of cTnI or cTnT phosphorylation prior to exchange (Supplemental Figure 4.S1). Endogenous cTnI phosphorylation levels in native trabeculae were relatively low according to Pro-Q signal intensity (un-normalized Pro-Q signal: total protein signal =1.2), which likely reflects low overall cTnI phosphorylation. Following exchange of unphosphorylated recombinant WT Tn or S23/24A Tn, phosphorylation levels of Tn from trabeculae were further reduced (WT Tn = 0.6±0.2 and S23/24A Tn = 0.8±0.3). PKA treatment of trabeculae significantly increased cTnI phosphorylation in native (Figure 4.1B) and WT trabeculae (Figure 4.1C), exhibiting a ~3-fold increase in cTnI phosphorylation signal over endogenous levels. S23/24A trabeculae had no change in the cTnI phosphorylation signal following treatment with PKA, which demonstrates this variant was effective in suppressing PKA

phosphorylation of cTnI, and confirms that Tn exchange was nearly complete (Figure 4.1D). cMyBP-C phosphorylation levels were relatively low and were significantly increased following PKA treatment in all experimental conditions, which is consistent with previous observations by others [38]. PKA treatment increased cMyBP-C phosphorylation by ~50% (Figure 4.1B) for native trabeculae, approximately 2-fold for WT trabeculae (Figure 4.1C) and ~2.5 fold for S23/24A trabeculae (Figure 4.1D). Although PKA is known to phosphorylate titin in skinned cardiac myocytes [148,149,152] we did not attempt to determine titin phosphorylation levels in this study.

Because exchange of recombinant cTn for native cTn was not 100%, some residual cTnI phosphorylation was evident in every exchange condition. This residual phosphorylation can be attributed to N-terminal sites on cTnI (S23 and S24), as well as the cTnI PKC sites (S43, S45, and T144). Furthermore, phosphorylation of serines 23 and 24 would represent both mono- and bisphosphorylated cTnI; the bisphosphorylated N-terminal form is required to decrease Ca^{2+}-sensitivity of force (pCa_{50}) [135]. Regulatory light chain (RLC; Supplemental Figure S2A), cTnT (Supplemental Figure 4.S2B), and tropomyosin (Tm; Supplemental Figure 4.S2C) phosphorylation levels were also assessed by densitometry (normalized for protein loading) and did not change significantly following PKA treatment for any condition tested.

4.3.2 PKA effects on SL-dependent activation in Wild-type cTn exchanged trabeculae

To determine how phosphorylation of myofibrillar proteins by PKA influences SL-dependence of force generation of cardiac muscle, we measured force-pCa relations at long (2.3 μm) and short (2.0 μm) SL in WT trabeculae before and after treatment with the catalytic subunit of PKA. Data from each experiment was fit by the Hill equation (Eq. 1) to obtain the Ca^{2+}-sensitivity of force (pCa_{50}) and slope (n_H) of the force-pCa relationship (see Table 4.1). For comparison with previous studies, EC_{50} were

also calculated and reported in Table 4.1. Prior to PKA treatment, increasing SL increased pCa_{50} and EC_{50} compared to the short SL (Figure 4.2A, Table 4.1). Following PKA treatment (in relaxing solution), pCa_{50} (and EC_{50}) at long SL was significantly decreased, while the pCa_{50} at the short SL was not altered. As a result, the SL dependence of pCa_{50} was greatly reduced. In contrast, PKA treatment did not affect maximum force (F_{MAX}; pCa 4.5) at either SL (Figure 4.2C). Put another way, PKA treatment resulted in a loss of SL influence on pCa_{50}, but at any given [Ca^{2+}] increasing SL still resulted in a corresponding increase in force (Table 4.1). Thus the Frank-Starling effect was reduced by PKA, but not eliminated.

To verify our WT cTn exchanged results, we measured the force-pCa relationship in native cardiac trabeculae at long and short SL, before and after PKA treatment. Consistent with other groups and our WT trabeculae results, the pCa_{50} of native trabeculae increased with increasing SL (Supplemental Figure 4.S3). Also similar to WT trabeculae, the length dependence of maximum force (F_{MAX}) production was maintained before and after PKA treatment. In a subset of experiments, measurements were made with native trabeculae only following PKA treatment, to check for biases related to the order of treatment. No differences were found between these post-PKA treatment groups. It is worth noting that we observed a 0.28 pCa unit decrease at both long and short SL following exchange of recombinant cTn into skinned trabeculae. Despite this decrease in the absolute value of pCa_{50}, physiological effects were maintained as the length-dependent difference in Ca^{2+} sensitivity, $\Delta pCa_{50,}$ and force levels were equal to native samples before and after PKA treatment.

4.3.3 PKA effects on SL-dependent activation with cTnI phosphorylation mutants

To investigate the role of cTnI phosphorylation independent of PKA mediated effects on cMyBP-C and titin, we substituted endogenous Tn with nonphosphorylatable cTnI (S23/24A) Tn or

phosphomimetic cTnI (S23/24D) Tn into demembranated rat cardiac trabeculae. S23/24A trabeculae exhibited similar SL dependent effects as WT preparations, with a greater pCa_{50} and F_{MAX} at the long SL (Figure 4.3A). To determine the influence of cMyBP-C/titin phosphorylation, S23/24A trabeculae were treated with PKA. This significantly decreased pCa_{50} at the long SL but had no effect at the short SL (Figure 4.3C), effectively eliminating the SL-dependence of $pCa_{50,}$ similar to results for WT trabeculae (Table 4.1). Because Tn exchange efficiency was high, and cTnI (S23/24A) cannot be phosphorylated by PKA, these results imply that PKA phosphorylation of cMyBP-C/titin was likely the main contributor to both decreased Ca^{2+}-sensitivity of force and elimination of its SL-dependence. However, the possible contribution of a small fraction of remaining native, phosphorylatable cTnI cannot be ruled out.

When trabeculae were exchanged with the N-terminal cTnI phosphomimetic S23/24D, we observed a significantly decreased pCa_{50} at both SL, with a greater effect at long (-0.18 pCa units) *vs.* short SL (-0.11 units) when compared to S23/24A trabeculae. This effectively eliminated the SL dependence of pCa_{50} (Figure 4.3B). Together with the maintained SL-dependence of pCa_{50} for S23/24A trabeculae, the data strongly indicates that phosphorylation of cTnI serines 23 and 24 alone can eliminate the SL dependence of myofilament Ca^{2+} sensitivity. PKA treatment of S23/24D trabeculae caused a small, but statistically insignificant further decrease in pCa_{50} (Figure 4.3B; Table 4.1). This implies the possible contribution of cMyBP-C/titin phosphorylation to decreasing the Ca^{2+}-sensitivity of force that we observed with S23/24A trabeculae. In total, these data suggest potential overlapping roles of both cMyBP-C/titin and cTnI in modulating length dependence of force during PKA phosphorylation. It also worth noting that there was little to no phosphatase activity in our demembranated preparations. As a result, the exchange of S23/24D or phosphorylation by PKA treatment was assumed to be irreversible. Physiologically, we would expect that phosphorylation

turnover (i.e. balance of kinase and phosphatase activity) would impact how cTnI and/or cMyBP-C phosphorylation influences SL-dependence.

4.3.4 Effects of cTnI variants and PKA treatment on myofilament structure by low-angle X-ray diffraction

To determine if changes in the SL-dependence of the force-pCa relationship were correlated with myofilament structural changes, we performed low angle X-ray diffraction experiments in resting trabeculae (pCa 9.0) under all conditions for which mechanical data were obtained. Measurements included the inter-thick filament spacing ($d_{1,0}$) and the ratio of the integrated intensities of the 1,0 and 1,1 equatorial x-ray reflections ($I_{1,1}/I_{1,0}$) at 2.3 μm SL. Representative low angle x-ray diffraction patterns from a skinned WT trabeculae before and after PKA treatment are illustrated in Figure 4.4A, along with a scan of the integrated intensity along the equator from the diffraction patterns (Figure 4.4B). $d_{1,0,}$ was not significantly different for any experimental conditions. Notably, $d_{1,0}$ was not different between S23/24A trabeculae or S23/24D trabeculae, suggesting that altered myofilament lattice spacing did not contribute to the loss of SL-dependence of pCa_{50} with cTnI (S23/24D) Tn. In all cases PKA treatment cause a small (~1) nm increase in $d_{1,0}$ (Figure 4.5A), as observed by others [88,150].

The equatorial intensity ratio, $I_{1,1}/I_{1,0}$ provides information on the distribution of crossbridge mass between the thick and thin filaments [155], with increasing $I_{1,1}/I_{1,0}$ indicating a redistribution of crossbridge mass from thick towards thin filaments. Recent evidence from low-angle X-ray diffraction experiments shows an increase in $I_{1,1}/I_{1,0}$ following PKA phosphorylation of cMyBP-C [88,150]. In the current study, prior to PKA treatment, equatorial intensity ratios were not significantly different for any condition (Figure 4.5B). PKA treatment increased $I_{1,1}/I_{1,0}$ for WT and

S23/24D trabeculae, while the intensity ratio appeared to increase slightly (but not significantly) following PKA treatment of S23/24A and native trabeculae (Figure 4.5B).

4.4 DISCUSSION

The goal of this study was to determine the specific role of PKA phosphorylation of cTnI (vs. cMyBP-C and titin) in modulating the sarcomere length (SL) dependence of myocardial force generation, i.e. the sarcomere level basis of the Frank-Starling relation. PKA phosphorylates both the thin filament cardiac troponin (cTn) subunit cTnI [133] and thick filament associated proteins, myosin binding protein-C (cMyBP-C) [143,156] and titin [157], all of which have been shown to modulate cardiac contractility. By replacing endogenous Tn with recombinant WT Tn, a nonphosphorylatable cTnI (S23/24A) Tn, or the phosphomimetic cTnI (S23/24D) Tn, we determined that phosphorylation of cTnI or cMyBP-C/titin, individually or in combination, significantly reduced the SL dependence of Ca^{2+} sensitivity (pCa_{50}). This occurred primarily through a reduction of pCa_{50} at the long SL where the propensity for strong crossbridge formation is greater. However, PKA phosphorylation did not alter the SL-dependence of F_{MAX}, suggesting the SL-dependence of CB binding and force was maintained. X-ray diffraction studies showed that CB mass movement under relaxing conditions was increased by PKA treatment. Taken together, our findings point to cTnC-cTnI interactions as a switch that sets the length dependence of Ca^{2+} sensitivity in cardiac muscle, in conjunction with PKA induced changes in crossbridge structure.

4.4.1 Effects of cTnI and cMyBP-C/titin phosphorylation state on the Ca^{2+}-sensitivity of cardiac force

Decreased pCa_{50} in cardiac muscle occurs in response to β-adrenergic stimulation [133,158] and following PKA treatment (Figure 4.2, Supplemental Figure 4.S3), and has been attributed primarily

to phosphorylation of serines 23 and 24 (S23/24) in the N-terminus of cTnI [135,138]. At the protein level, cTnI S23/24 phosphorylation decreases the Ca^{2+}-affinity of cTnC when complexed with cTnI and weakens the interaction between cTnI and the regulatory domain of cTnC [139,159,160]. Structural data suggest that in the unphosphorylated state the cardiac specific N-terminal extension of cTnI interacts with the N-terminal regulatory domain of cTnC, stabilizing the "open" or Ca^{2+}-activated cTnC state [159]. Our finding that S23/24D trabeculae have reduced Ca^{2+}-sensitivity of force (Figure 4.3), relative to non-phosphorylatable S23/24A trabeculae, supports previous observations that alterations in cTnC-cTnI interaction by PKA phosphorylation can decrease the Ca^{2+}-sensitivity of force [135]. Furthermore since PKA treatment of S23/24D trabeculae, which allows phosphorylation primarily of cMyBP-C/titin (and not cTnI), had a no significant additional effect on pCa_{50}, the data confirms a significant role for cTnI S23/24 phosphorylation in regulating the Ca^{2+}-sensitivity of force [161].

PKA phosphorylation of the cardiac specific motif of cMyBP-C reduces cMyBP-C interaction with the S2 domain of myosin [162] and is associated with a redistribution of myosin crossbridge mass towards thin filaments [88,150]. This implies the potential for increased myosin-thin filament interaction, which is supported by observations that increased force development kinetics following PKA treatment is specific to cMyBP-C phosphorylation [163,164]. In this study, PKA treatment of S23/24A trabeculae increased cMyBP-C phosphorylation 3-fold (Figure 4.1D) and was associated with reduced Ca^{2+}-sensitivity of force (Figure 4.3C); there was no corresponding PKA induced elevation of cTnI phosphorylation. Reduction of pCa_{50} by cMyBP-C phosphorylation is consistent with previous studies where RLC2 phosphorylation was controlled [164]. In addition to effects on cMyBP-C, PKA phosphorylation increases the compliance of titin and is associated with increased $d_{1,0}$ in skinned cardiac trabeculae and reduced passive force, at least at longer SL [149]. Here we found

that PKA treatment induced a small (~ 1.0 nm) increase of $d_{1,0}$ under all conditions tested (Figure 4.5A). By itself increasing $d_{1,0}$ would be expected to reduce pCa_{50} [65], although this should have contributed similarly to pCa_{50} reduction under all conditions tested. However, it must be considered that the relationship between PKA treatment, Ca^{2+}-sensitivity, and lattice spacing may not be unique. For example, PKA treatment does not always result in increased lattice spacing and changes in lattice spacing do not always have an inverse relationship with pCa_{50} [115]. PKA treatment of skinned trabeculae from transgenic mice that expressed the slow skeletal isoform of cTnI decreased myofilament lattice spacing, with no change in pCa_{50}. In contrast, PKA treatment increased lattice spacing and reduced pCa_{50} in trabeculae of non-transgenic animals. These observations emphasize the complexity of the molecular interactions that underlie the coupling between lattice spacing and Ca^{2+}-sensitivity in cardiac muscle.

4.4.2 Effects of cTnI and cMyBP-C phosphorylation state on the SL-dependence of force-[Ca^{2+}] relations

Previous studies to determine the effects of PKA-treatment on the length-dependent force activation in cardiac muscle have produced complex and often contradictory results. PKA treatment of skinned cardiac muscle preparations was found to either increase [87,115,128] or decrease [129] the SL-dependence of Ca^{2+}-sensitivity. Furthermore, PKA treatment was found to either not change or decrease the SL-dependence of Ca^{2+}-sensitivity (ΔpCa_{50}) when measured in younger or older mice, respectively [37]. Similar to our studies, Kajiwara *et. al.* [129] found that PKA treatment reduced ΔpCa_{50}, primarily by a greater reduction of Ca^{2+}-sensitivity at longer SL. In contrast, others [115] have observed an increase in ΔEC_{50} following PKA treatment of skinned trabeculae from non-transgenic mice, although ΔpCa_{50} was unaffected. Recent studies have also shown that PKA phosphorylation of cMyBP-C and cTnI increases the SL-dependence of power output [128]. Additional complexity is indicated by observations that in younger transgenic cMyBP-C knock-out

mice ΔpCa_{50} was increased by PKA, relative to younger non-transgenic preparations in which PKA had no significant effect on ΔpCa_{50} [37]. In the same study ΔpCa_{50} was reduced by PKA treatment in older non-transgenic animals, while in older cMyBP-C knock-out mice both ΔpCa_{50} and the effect of PKA on ΔpCa_{50} was reduced relative to non-transgenic controls.

The source of these disparities between multiple studies is not clear, but a speculative explanation could be that the effect of PKA on length-dependent activation is a complex function of differences in the relative phosphorylation levels of RLC, cTnI and cMyBP-C. For example, RLC phosphorylation was not controlled in these earlier studies, and has subsequently been shown to impact the contractile response to PKA activation. Verduyn *et al.* [164,165] observed a larger decrease in Ca^{2+}-sensitivity following PKA treatment in skinned myocardium when RLC and cMyBP-C phosphorylation were reduced. While Chen *et al.* [164] found that following PKA treatment Ca^{2+}-sensitivity decreased most when both cTnI and cMyBP-C could be phosphorylated. Additionally, Colson *et al.* [88] found that while phosphorylation of both RLC-2 and cMyBP-C increase myosin crossbridge proximity to thin filaments, elevation of RLC-2 phosphorylation alone increased Ca^{2+}-sensitivity, while PKA treatment and phosphorylation of cTnI and cMyBP-C decreased the Ca^{2+}-sensitivity of force. Unfortunately, the isolated effects of RLC and cMyBP-C phosphorylation levels on length-dependent activation have not been determined alone or in combination. In our study RLC phosphorylation level was unaffected by cTn exchange or by PKA treatment (Supplemental Figure 4.S2A), and we found that PKA treatment eliminated the SL-dependence of pCa_{50} in native and WT trabeculae, in which both cTnI and cMyBP-C were phosphorylated. Since exchange with S23/24D Tn also eliminated the SL-dependence of pCa_{50}, the results indicate that phosphorylation of the cTnI N-terminus alone reduces cardiac length-dependent activation. Additionally, because PKA treatment reduced ΔpCa_{50} in S23/24A trabeculae, in which mutant cTnI cannot be phosphorylated by PKA, the

evidence suggests that phosphorylation of cMyBP-C likewise reduced or eliminated the length-dependence Ca^{2+}-sensitivity.

In addition to reducing ΔpCa_{50} in native, WT and S23/24A trabeculae, our data (Figure 4.5) indicate that PKA treatment increases myofilament lattice spacing and promotes crossbridge mass distribution towards thin filaments, as found in previous studies [88,150,166]. Changes in lattice spacing can alter pCa_{50} independent of changes in SL [65]. However, our data indicate that decreases in pCa_{50} and reduction of the SL-dependence of pCa_{50} by PKA do not result directly from alterations in $d_{1,0}$. For example, the SL-dependence of pCa_{50} is lost in S23/24D trabeculae, even though $d_{1,0}$ at longer SL is similar to that of S23/24A trabeculae (Figure 4.5), where pCa_{50} was dependent on SL (Figure 4.4A). $d_{1,0}$ did not differ for S23/24A trabeculae compared with PKA-treated native and WT trabeculae, which also exhibit reduced SL-dependence of pCa_{50}. Assuming the $d_{1,0}$ relationship between the conditions tested is not altered during contraction, these data would indicate the loss of SL-dependence of pCa_{50} resulted primarily from the influences of cTnI phosphorylation state and cMyBP-C/titin phosphorylation, and not from PKA induced changes in myofilament lattice spacing.

4.4.3 How does cTnI and cMyBP-C phosphorylation alter cardiac length-dependent activation?

A potential explanation for the disproportionate decrease in pCa_{50} at the longer SL (Table 4.1) may lie in the ability of strong-binding, force generating CB's to both displace tropomyosin into the activated position and the unique ability of CB's to enhance the Ca^{2+}-affinity of cTnC in cardiac muscle [27,65]. We previously suggested that enhanced strong-crossbridge binding with low [ATP] increased pCa_{50} more at the shorter SL because the crossbridge population available for recruitment and contribution to activation was greater at short SL [78]. Using this same reasoning, if phosphorylation of cTnI and/or cMyBP-C/titin reduced coupling between strong CB's and thin

filament activation, the effect should be more evident at longer SL since myosin S1 proximity to actin and potential for binding is greater with reduced lattice spacing [121]. Supporting this idea are observations that strong crossbridge binding decreases the distance between cTnI and cTnC [167] and is required to achieve the fully "open" conformation of the cTnC N-terminus [126]. Further, cTnI interaction with actin decreases with strong crossbridge binding, independent of the effects of Ca^{2+} [168]. Importantly, in the unphosphorylated state the N-terminus of cTnI interacts with the N-terminal regulatory domain of cTnC and stabilizes the Ca^{2+}-bound state [139,169]. Since cTnI N-terminal phosphorylation weakens cTnI-cTnC interaction, crossbridge mediated increases in cTnC Ca^{2+}-affinity may be reduced, consistent with a PKA mediated reduction of pCa_{50} at longer SL. However, this speculation remains to be tested directly. It should be noted that our Tn exchange was not complete (~80%), thus it is possible, however unlikely, that reduced Ca^{2+}-sensitivity and loss of pCa_{50} SL-dependence resulted from phosphorylation of the small of amount of un-exchanged (native) cTnI. This would require that the full effects of PKA on pCa_{50} and ΔpCa_{50} through cTnI S23/24 phosphorylation were caused by phosphorylation of 10-20% of the cTnI pool. Moreover, evidence from others also argues that there is a significant contribution of cMyBP-C phosphorylation in reducing Ca^{2+} sensitivity at the long SL. PKA treatment following alanine substitution at PKA phosphorylation sites of either cTnI or cMyBP-C results in a similar reduction of pCa_{50} at a long SL (~2.2μm) [164]. In cMyBP-C knock-out mice, pCa_{50} at the long SL was reduced by a lesser degree after PKA treatment [37].

Others have found that of cMyBP-C phosphorylation state can determine the level of maximal Ca^{2+}-activated force, possibly through cMyBP-C influence on myosin head orientation [170]. In fact, recent studies have reported that RLC phosphorylation influences myosin head orientation and force production [171]. However, we observed that F_{MAX} was unaffected by either phosphomimetic,

S23/24D, exchange or by PKA treatment (Table 4.1). A potential explanation may be that at higher [Ca^{2+}], thin filament state is dominated by strong crossbridge displacement of tropomyosin into its "on" position, such that weakening of cTnI-cTnC interaction (by cTnI phosphorylation) or increased myosin S1 proximity to thin filaments (cMyBP-C phosphorylation) would have reduced influence on force. Furthermore, the lack of PKA effect on F_{MAX} at 2.3 or 2.0 μm SL under all conditions tested indicates the effect of SL on force at sub-maximal pCa was present, but attenuated. Thus the Frank-Starling effect was not eliminated, just reduced.

The attenuation of SL-dependence of force at all levels of thin filament activation is illustrated by solid curves in Figure 4.6, which plots the difference in force at 2.3 vs. 2.0 μm SL at each activating pCa. As in our previous study [78], the sensitivity of force to decreasing SL reached a maximum over the physiologically relevant range of sub-maximal pCa for native (Figure 4.6A), WT (Figure 4.6B) and S23/24A trabeculae (Figure 4.6C). The peak in each force difference curve corresponds to increased force sensitivity to altered SL. We have suggested this peak results from optimal "tuning" of the interaction between Ca^{2+} binding to cTn and crossbridge binding to activate cardiac thin filaments [78]. Following treatment with PKA (corresponding dashed lines in Figure 4.6) these peaks were eliminated for native, WT and S23/24A preparations and the SL dependence of force was reduced over the physiologically relevant pCa range. It is also noteworthy that S23/24D trabeculae (Figure 4.6D) produced changes in these force difference curves that mimic the effects of PKA treatment, including loss of the peak (compare Figure 4.6D with dashed lines in A, B, and C).

4.4.4 Physiological consequence of PKA phosphorylation for the Frank-Starling relation

If the net effect of PKA mediated phosphorylation of cTnI, cMyBP-C and titin is to decrease the Ca^{2+}-sensitivity of force and its SL dependence, what is the physiological relevance? At normal levels of

activity the steep SL-dependence of myocardial force generation enables the heart to respond automatically to small alterations in venous return, without nervous or endocrine input. However, at heightened levels of activity, β-adrenergic stimulation increases heart rate, elevates intracellular [Ca^{2+}] and force, increases the kinetics for force development and shortening, and also increases the rate of ventricular relaxation and diastolic filling to maintain high cardiac output [53]. Furthermore, myofilament Ca^{2+}-sensitivity is reduced to support rapid resequestration of intracellular Ca^{2+} by the sarcoplasmic reticulum, allowing faster relaxation for increased diastolic filling. Under these conditions a steep dependence of cardiac force on sarcomere length or ventricular volume could limit ventricular output during a cardiac contractile cycle by reducing force and ventricular ejection fraction, as shortening proceeds in systole. Our results indicate that following PKA treatment, pCa_{50} at long SL is reduced (Figure 4.7, grey dashed line), with no effects on maximum force production, so that pCa_{50} at the long and short SL are identical (□,●) and the difference in force production between long and short SL is reduced. Reduction of the effect of shortening on the Ca^{2+}-sensitivity of contractile activation by PKA mediated myofilament protein phosphorylation, in combination with elevated intracellular [Ca^{2+}] during β-adrenergic stimulation, should help maintain ventricular force generation throughout systole. Thus, at a given [Ca^{2+}] the ability of PKA to blunt a relative reduction of force from shortening during systole could increase the ventricular ejection fraction and help maintain cardiac output per contraction cycle during periods of metabolic demand.

4.5 ACKNOWLEDGEMENTS

The authors would like to thank Drs. An-Yue Tu and Charles Luo for preparations of cTnI variant proteins and protein isolation, and Dr. Jin Dai for preparation of trabeculae and protein gels for characterization of protein content and phosphorylation. We would also like to thank Mengjie Zhang and Luping Xie for help with analyzing X-ray diffraction patterns. We are indebted to Martha

Mathiason for development data acquisition and analysis software. This research was supported by NIH RO1 HL-67071 (Martyn), NIH R01 HL-65497 (Regnier), and AHA 11POST7400069 (Rao). Use of the Advanced Photon Source, an Office of Science User Facility operated for the U.S. Department of Energy (DOE) Office of Science by Argonne National Laboratory, was supported by the U.S. DOE under Contract No. DE-AC02-06CH11357. BioCAT is a National Institutes of Health-supported Research Center RR-08630. The content is solely the responsibility of the authors and does not necessarily reflect the official views of the National Center for Research Resources or the National Institutes of Health.

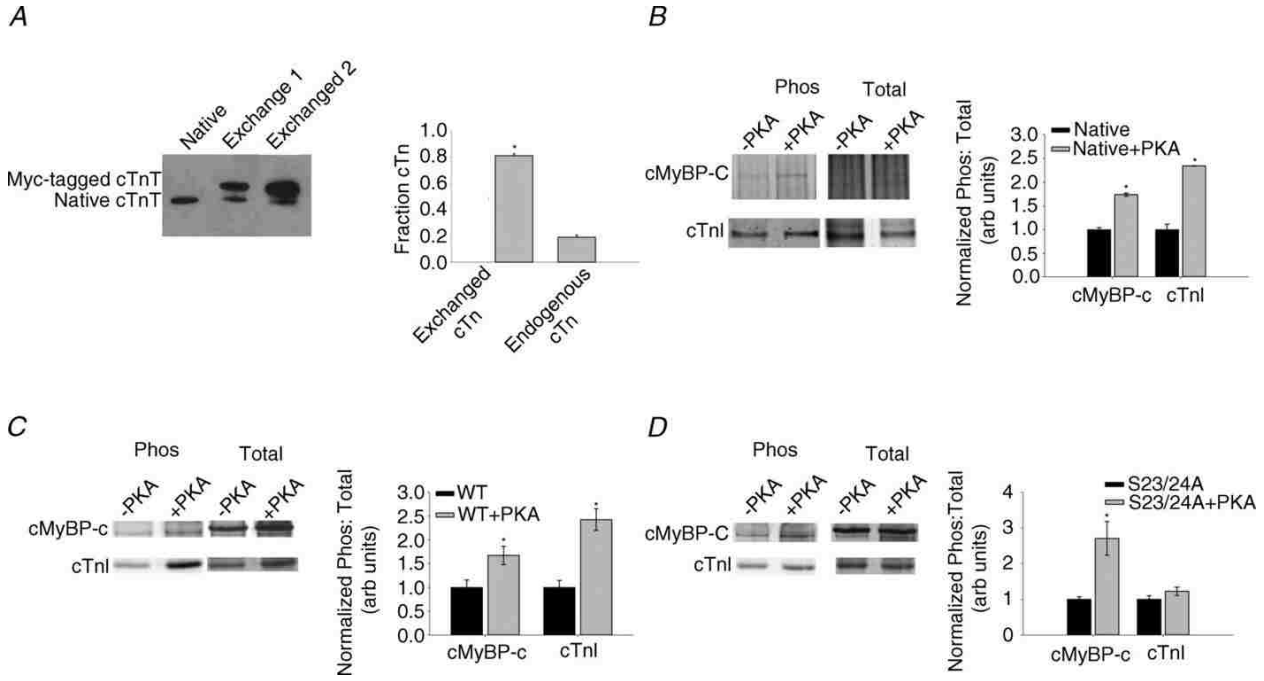

Figure 4.1: Exchange efficiency and phosphoprotein analysis. (A) Efficiency of exchange of recombinant cardiac troponin complex (Tn) into rat cardiac trabeculae. Representative Western blot against cTnT antibody (Santa Cruz Biotechnology, Santa Cruz, CA) in native trabeculae and two exchanged samples (left) and relative levels of exchanged Tn containing cTnT + myc-tag and endogenous, unexchanged Tn (right), *n* = 3 (Western blots). (B) Phosphorylation analysis of native cardiac trabeculae, +/- PKA. Pro-Q Diamond phosphoprotein and total protein (Coomassie blue) stain of cMyBP-C and cTnI, +/- PKA (left) and phosphorylation: total protein staining ratios of Native (black bars) and Native+PKA (gray bars) samples (right), *n* = 3 (gels), 10 exchanged trabeculae/lane. (C) Phosphorylation analysis of wild-type (WT) trabeculae, +/- PKA. Pro-Q Diamond phosphoprotein and total protein stain of cMyBP-C and cTnI, +/- PKA (left) and phosphorylation: total protein staining ratios of WT (black bars) and WT+PKA (gray bars) samples (right), *n* = 3. (D) Phosphorylation analysis S23/24A trabeculae +/-PKA. Pro-Q Diamond phosphoprotein and total protein stain of cMyBP-C and cTnI, +/- PKA (left) and phosphorylation: total protein staining ratios of S23/24A (black bars) and S23/24A+PKA (gray bars) samples (right), *n* = 3. Data (means +/- SEM) *p <0.05 compared to no PKA treatment.

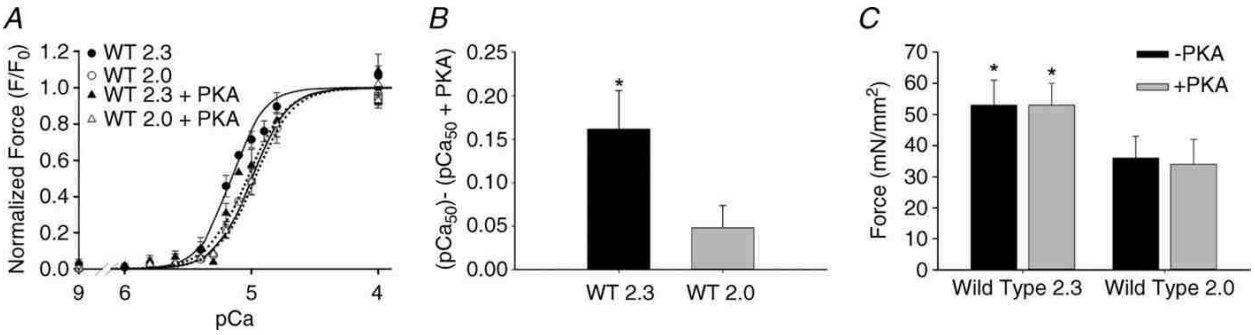

Figure 4.2: (A) Force-pCa relations are illustrated for WT trabeculae. Data (means +/- SEM) were obtained at 2.3 (○) and 2.0 (△) μm SL before (solid symbols; solid lines) and after treatment with the catalytic subunit of PKA (open symbols; dotted lines). (B) ΔpCa_{50} for WT trabeculae before and after PKA treatment at SL 2.3 μm (black bars) and 2.0 μm (grey bars), respectively. (C) Maximal Ca^{2+}-activated (pCa 4.5) force at 2.3 and 2.0 μm SL before (black bars) and after PKA treatment (grey bars). Data (means +/- SEM) were obtained from 8 trabeculae. *$p<0.05$ compared to SL 2.0 μm.

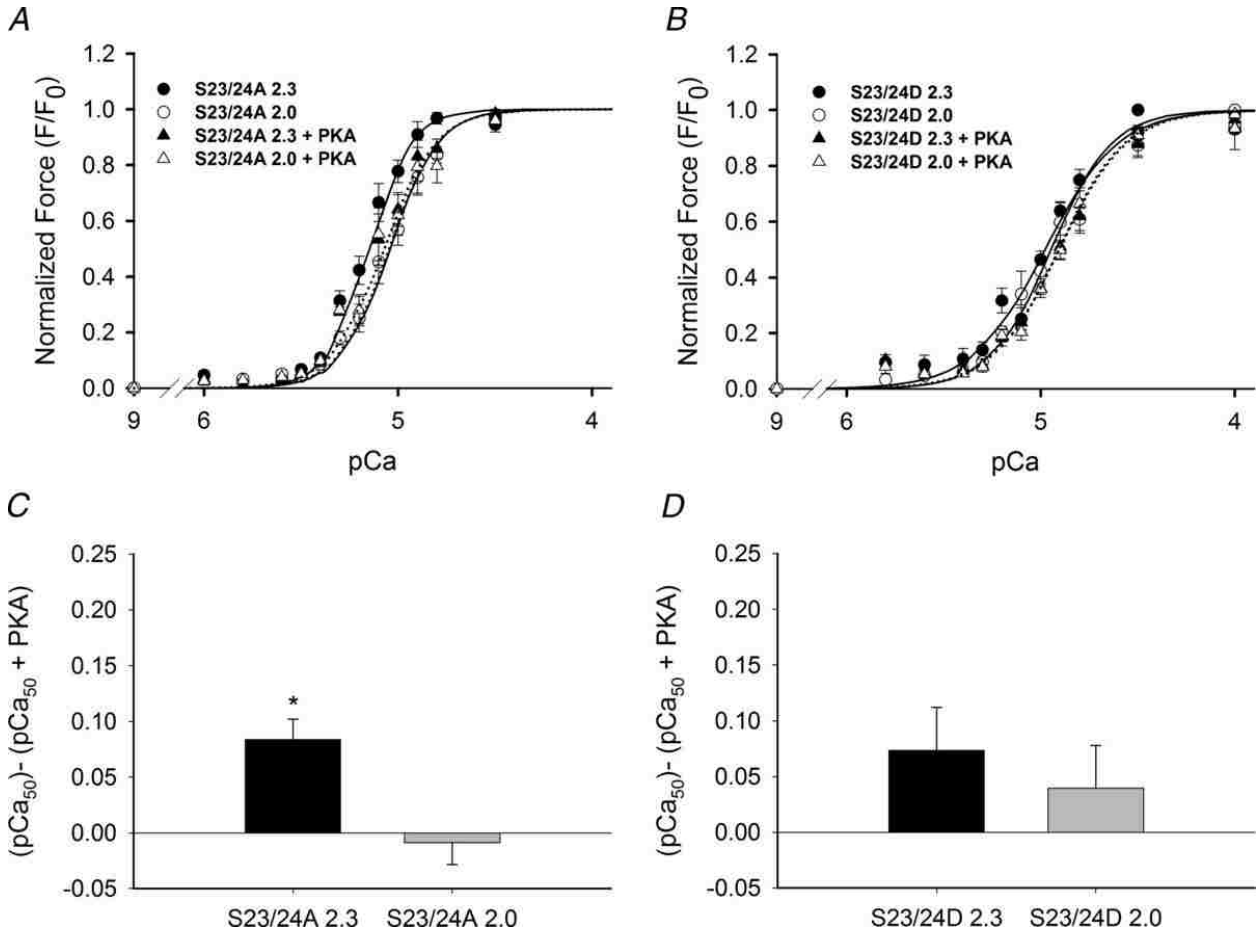

Figure 4.3: (A) Force-pCa relations for S23/24A trabeculae. Data (means +/- SEM; n = 8) were obtained at 2.3 (○) and 2.0 (△) μm SL before (solid symbols; solid lines) and after treatment with the catalytic subunit of PKA (open symbols; dotted lines). (B) Force-pCa relations for S23/24D trabeculae,. Data (means +/- SEM; n = 8) were obtained at 2.3 (○) and 2.0 (△) μm SL before (solid symbols; solid lines) and after treatment with the catalytic subunit of PKA (open symbols; dotted lines). ΔpCa_{50} for (C) S23/24A and (D) S23/24D trabeculae before and after PKA treatment at SL 2.3 μm (black bars) and 2.0 μm (grey bars), respectively. *p<0.05 compared to SL 2.0 μm.

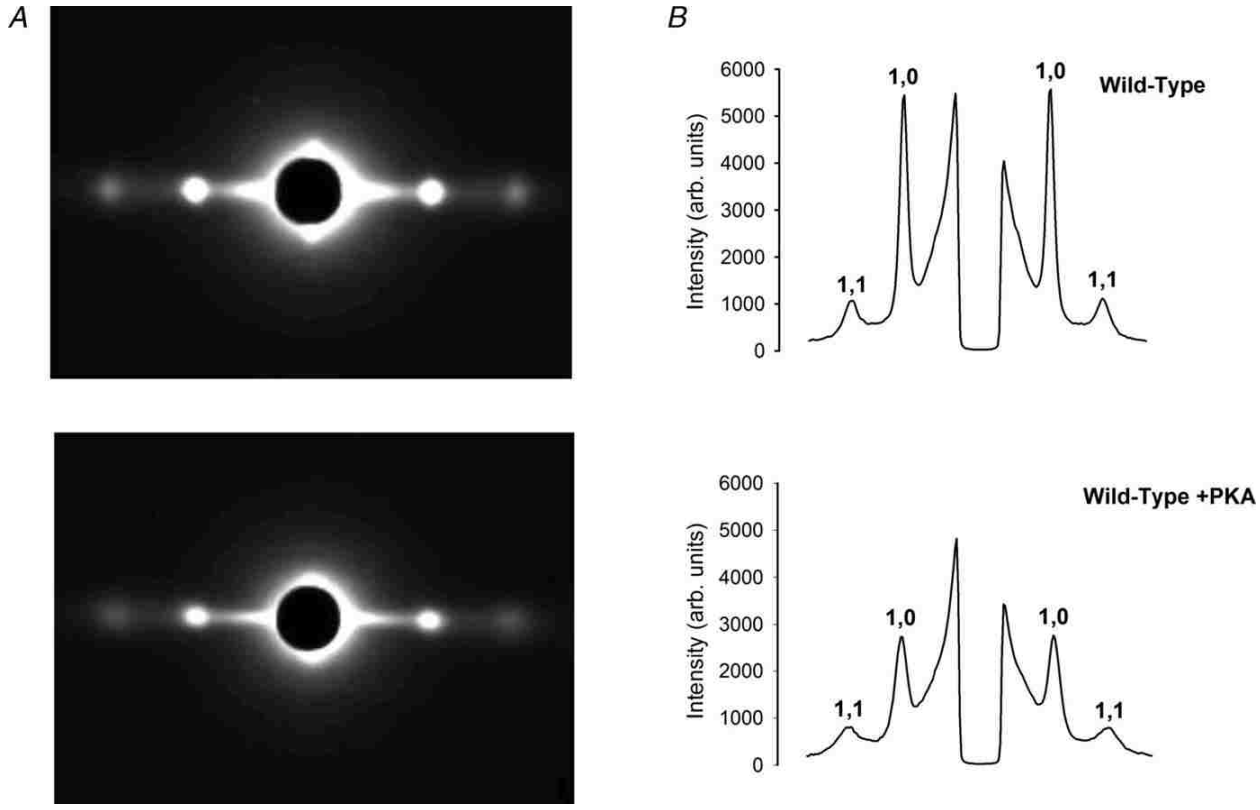

Figure 4.4: (A) Representative equatorial patterns from low angle X-ray diffraction were obtained from WT trabeculae before and after treatment with PKA. (B) The corresponding traces of diffraction intensities integrated along the equator vs. spacing in (A) are illustrated. The 1,0 and 1,1 diffraction peaks are labeled.

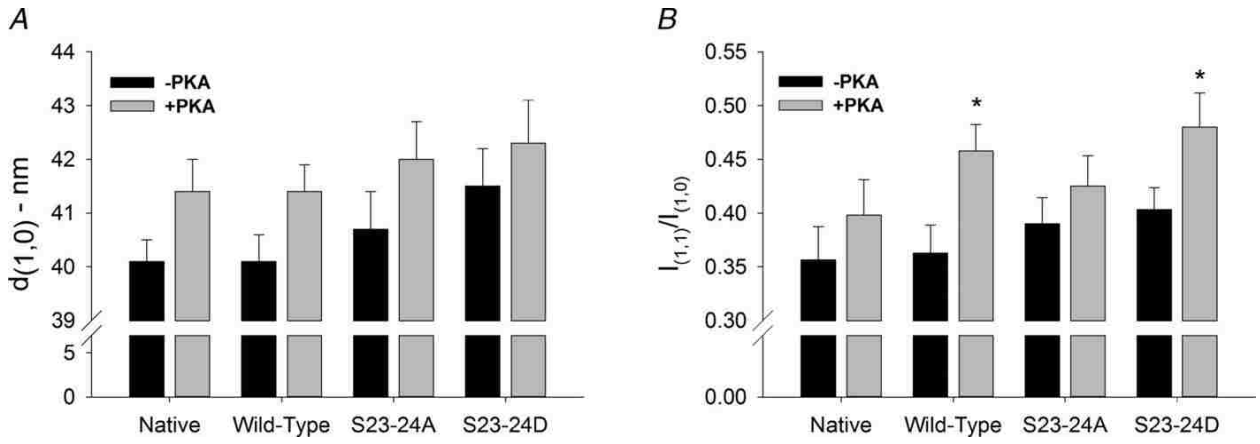

Figure 4.5: (A) Inter-thick filament spacing ($d_{1,0}$) and (B) the ratio of 1,1 to 1,0 peak intensities ($I_{1,1}/I_{1,0}$) obtained from native (n = 9, n=7 after PKA), WT (n = 15, n = 12 after PKA), S23/24A (n = 13, n=10 after PKA) or S23/24D (n =12, n=9 after PKA) trabeculae are summarized in (A) and (B), respectively. Values (means + SEM) are shown before (light bars) and after (solid bars) treatment with PKA for each condition. Data were analyzed by fitting the diffraction intensity profiles with Fityk to determine the position of the centroid of the peaks and the values of the integrated intensities. *$p<0.05$ compared to before PKA treatment.

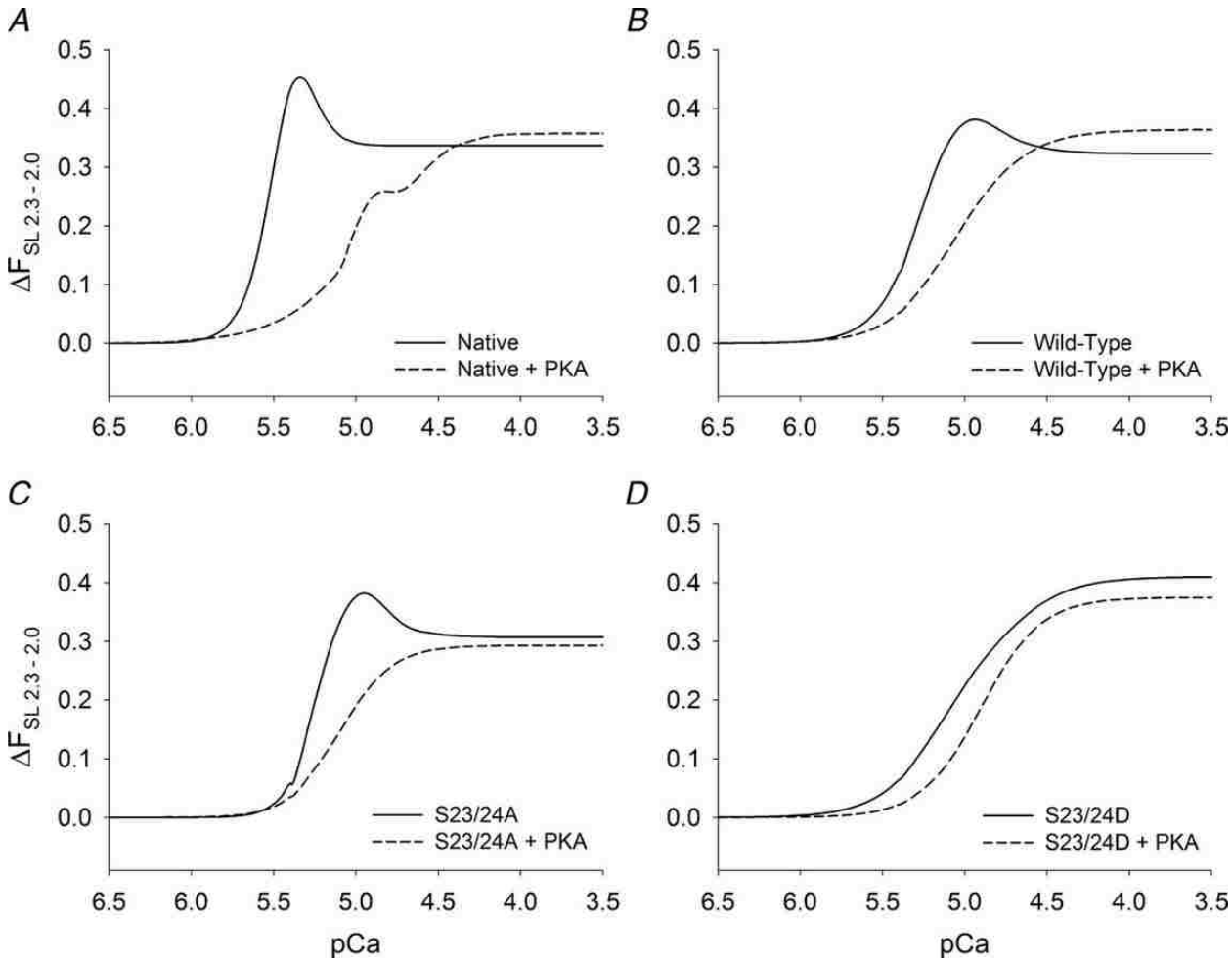

Figure 4.6: The difference in force-[Ca^{2+}] relations between Hill fit curves to data obtained at 2.3 and 2.0 μm SL from data illustrated in Figures 2, 3 and 4 are shown for (A) native (no exchange), (B) WT, (C) S23/24A and (D) S23/24D trabeculae. Data are shown before (solid curves) and after (dashed curves) treatment with PKA.

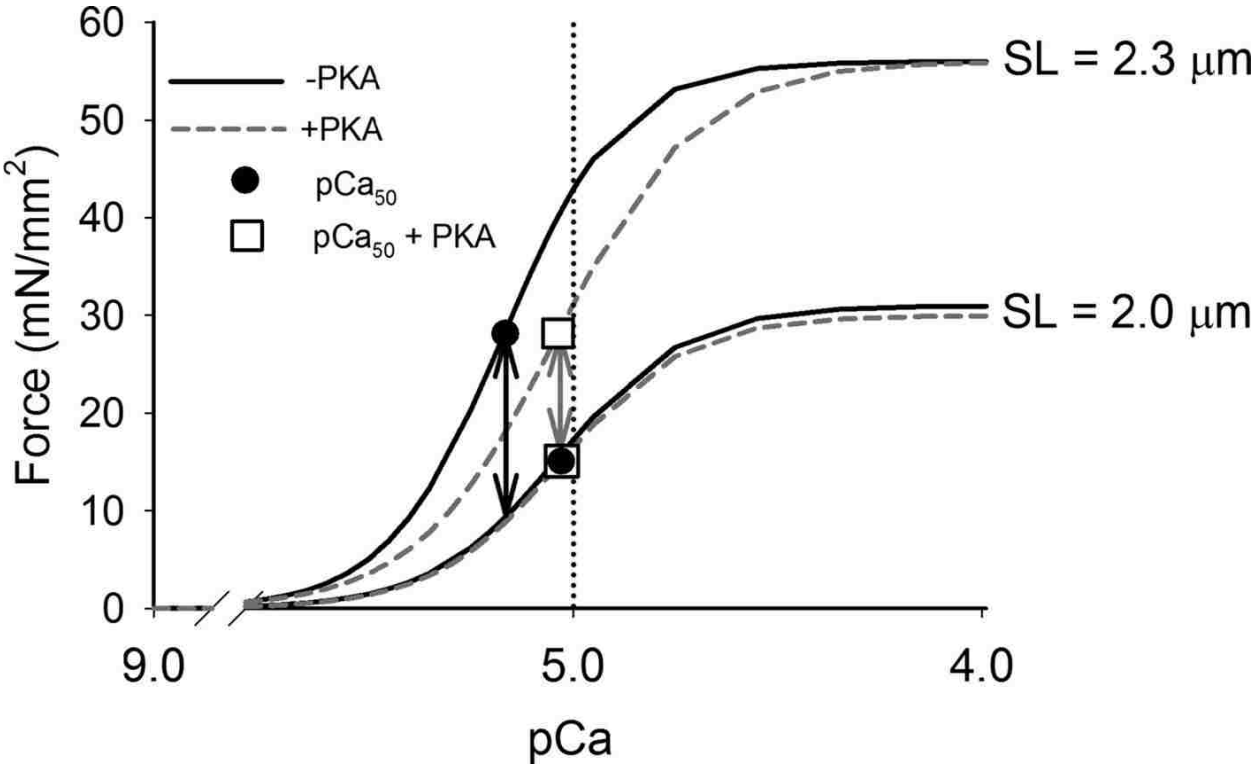

Figure 4.7: Physiological relevance of PKA phosphorylation of myofibrillar proteins. The effects of PKA treatment on the fitted force-pCa curves for WT trabeculae from Figure 2 are described. Prior to PKA treatment (black lines), pCa_{50} (black circles) at the long SL is greater than at the short SL. The difference in force production between long and short SL (black arrows) at the long SL pCa_{50} is illustrated. Following PKA treatment (gray, dashed lines), pCa_{50} at the long SL (open box) is reduced, with no effects on maximum force production. The pCa_{50} at the long and short SL (open boxes) are identical and the difference in force production (gray arrows) between long and short SL is reduced not only at long SL pC_{50}, but also over the range of submaximal activating $[Ca^{2+}]$.

Table 4.1: Hill fit parameters of force-pCa relations obtained from rat cardiac trabeculae before and after PKA treatment at sarcomere lengths (SL) 2.3 μm and 2.0 μm. *p < 0.05 compared to SL 2.0 μm, indicating length-dependent effects. †p < 0.05 compared to paired samples after PKA treatment.

Condition	SL (μm)	pCa_{50}	ΔpCa_{50}	EC_{50} (μM)	ΔEC_{50} (μM)	F_{MAX} (mN/mm²)	F_{pass} (mN/mm²)	n_H
Native (n=5)	2.3	5.45±0.05*†	0.13	3.55±0.36*†	1.2	56±8*	7.5±1.1*	4.4±0.7
	2.0	5.32±0.04		4.75±0.42		34±6	1.7±0.4	5.1±0.8
Native + PKA (n=5)	2.3	5.32±0.04	0.04	4.74±0.38	0.49	53±4*	5.9±1.7*	3.3±0.3
	2.0	5.28±0.05		5.22±0.58		31±6	1.8±0.6	5.0±0.5
Wild-Type (n=8)	2.3	5.17±0.04*†	0.13	6.77±0.55*†	2.5	56±8*	9.1±3.1*	2.9±0.4
	2.0	5.04±0.05		9.22±1.00		31±5	1.7±0.4	2.8±0.3
Wild-Type + PKA (n=8)	2.3	5.04±0.04	0.01	9.83±1.00	0.16	56±8*	5.8±0.8*	2.4±0.4
	2.0	5.03±0.05		10.3±1.10		30±4	1.6±0.4	2.6±0.3
S23/24A (n=7)	2.3	5.16±0.02*†	0.10	6.95±0.31*†	1.8	44±5*	10±2.4*	3.9±0.3
	2.0	5.06±0.03		8.76±0.54		31±3	2.5±0.6	3.5±0.2
S23/24A + PKA (n=7)	2.3	5.07±0.03	--	8.42±0.55	0.16	51±5*	5.7±1.5*	3.2±0.3
	2.0	5.07±0.04		8.59±0.73		34±4	2.4±0.7	3.4±0.2
S23/24D (n=8)	2.3	4.98±0.04	0.03	10.5±0.91	0.77	54±6*	9.7±2.6*	2.3±0.2
	2.0	4.95±0.04		11.3±0.94		32±3	3.6±1.1	2.8±0.4
S23/24D + PKA (n=8)	2.3	4.91±0.03	--	12.4±0.81	--	50±6*	8.3±1.8*	2.5±0.3
	2.0	4.91±0.02		12.4±0.54		31±4	3.5±1.1	2.6±0.2

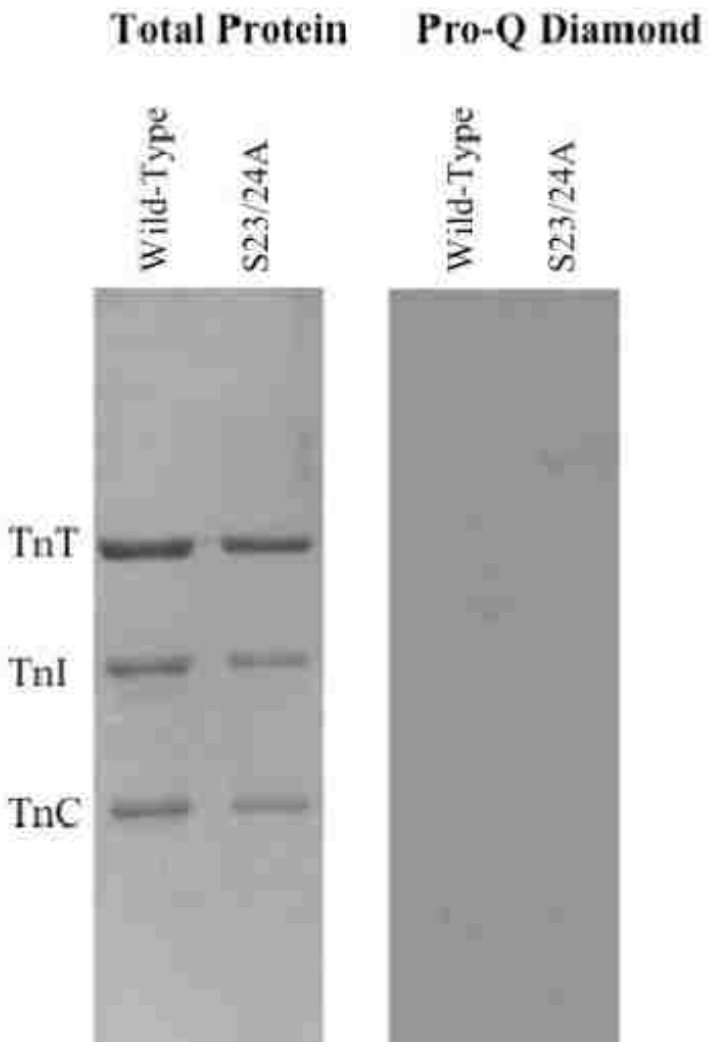

Figure 4.S1: Phosphorylation state of recombinant proteins. Total protein stain (left) of cardiac troponin complex (Tn) of wild-type and S23/24A. Pro-Q Diamond phosphoprotein stains (right).

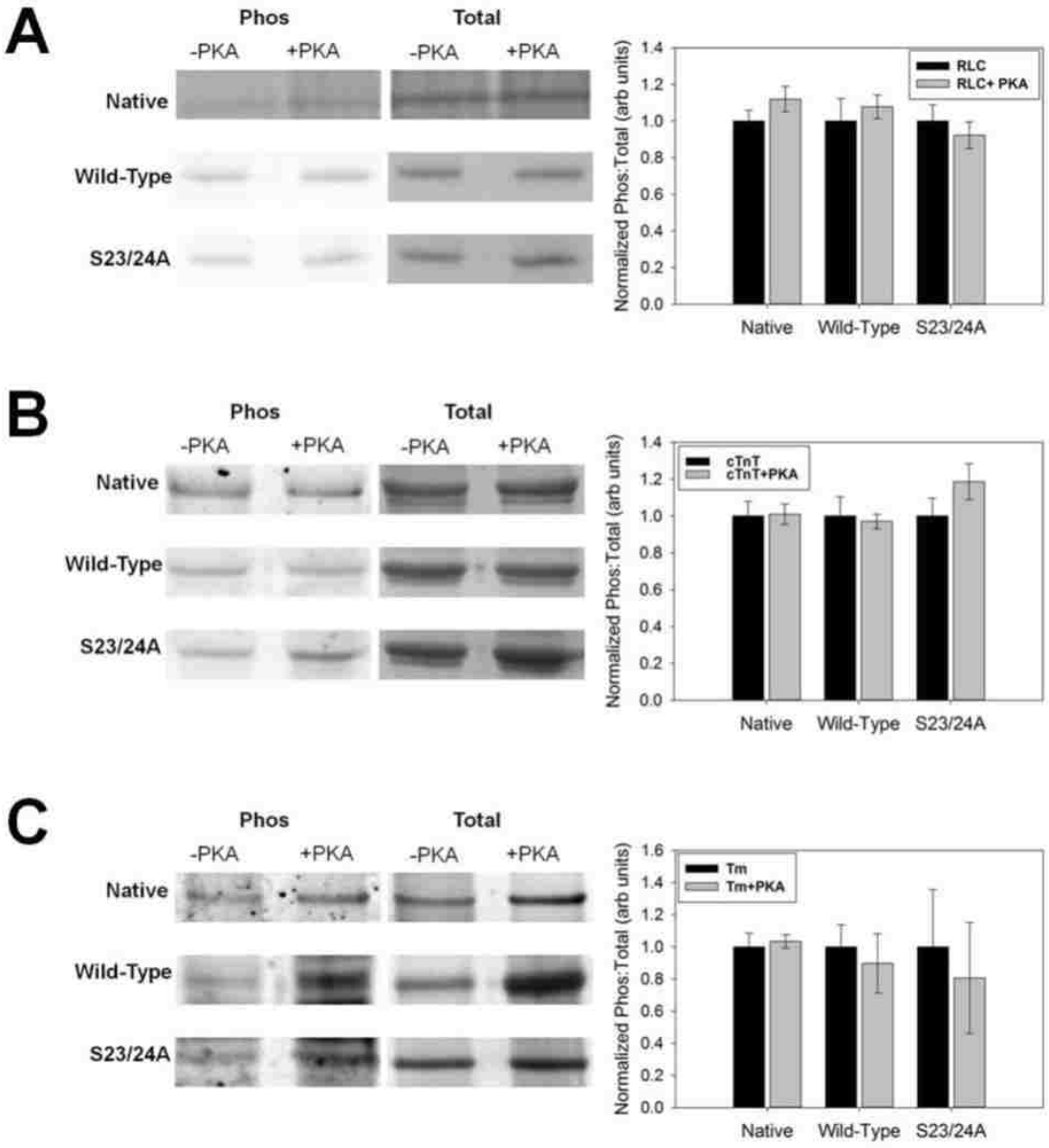

Figure 4.S2: Phosphorylation analysis of regulatory contractile proteins from cardiac trabeculae. (A) Representative Pro-Q Diamond phosphoprotein and total protein (Coomassie blue) stain of regulatory light chain 2 (RLC), +/- PKA (left) and phosphorylation: total protein staining ratios of Native, WT, and S23/24A trabeculae before (black bars) and after (gray bars) PKA treatment (right), n = 3 (gels), 10 exchanged trabeculae/lane. (B) Representative Pro-Q Diamond phosphoprotein and total protein (Coomassie blue) stain of cardiac troponin T (cTnT), +/- PKA (left) and phosphorylation: total protein staining ratios of Native, WT, and S23/24A trabeculae before (black bars) and after (gray bars) PKA treatment (right), n = 3. (C) Representative Pro-Q Diamond phosphoprotein and total protein (Coomassie blue) stain of tropomyosin (Tm), +/- PKA (left) and phosphorylation: total protein staining ratios of Native, WT, and S23/24A trabeculae before (black bars) and after (gray bars) PKA treatment (right), n = 3.

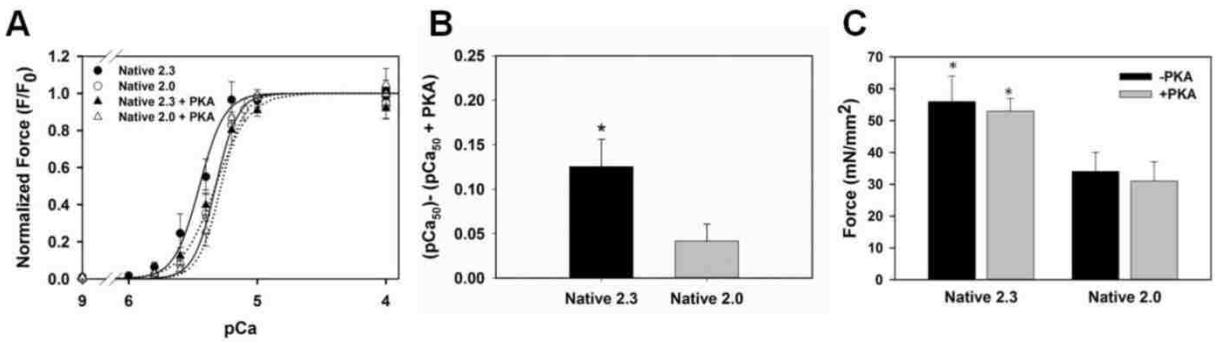

Figure 4.S3: In (A) force-pCa relations are illustrated for native trabeculae at 2.3 (circle) and 2.0 (triangle) μm SL before (solid symbols; solid lines) and after treatment with the catalytic subunit of PKA (open symbols; dotted lines). (B) ΔpCa50 for native trabeculae before and after PKA treatment at SL 2.3 μm (black bars) and 2.0 μm (grey bars), respectively. (C) Maximal Ca^{2+}-activated (pCa 4.5) force at 2.3 and 2.0 μm SL before (black bars) and after PKA treatment (grey bars). Data (means +/- SEM) were obtained from 7 trabeculae. *$p<0.05$ compared to SL 2.0 μm.

Chapter 5. Thin filament incorporation of an engineered cardiac troponin C variant (L48Q) enhances contractility in intact cardiomyocytes from healthy and infarcted hearts

Erik R. Feest, F. Steven Korte, An-yue Tu, Jin Dai, Charles E. Murry, Michael Regnier.

Manuscript submitted.

5.1 ABSTRACT

Many current pharmaceutical therapies for heart failure target intracellular [Ca^{2+}] ($[Ca^{2+}]_i$) metabolism, or cardiac troponin C (cTnC) on thin filaments, and can have significant side-effects such as arrhythmogenesis or adverse effects on diastolic function. In this study, we tested the feasibility of directly altering the Ca^{2+} binding properties of cTnC to enhance contraction independent of $[Ca^{2+}]_i$ in intact cardiomyocytes from healthy and infarcted hearts. Specifically, cardiac thin filament activation was enhanced through adenovirus-mediated over-expression of a cardiac troponin C (cTnC) variant designed to have increased Ca^{2+} binding affinity conferred by single amino acid substitution (L48Q). In skinned cardiac trabeculae and myofibrils we and others have shown that substitution of L48Q cTnC for native cTnC increases Ca^{2+} sensitivity of force and the maximal rate of force development. Therefore, we sought to directly target cardiac thin filaments to enhance the contractility of intact cardiomyocytes from healthy and infarcted hearts. Using video-microscopy to monitor cell shortening and intracellular Ca^{2+} transients (Fura-2), expression of L48Q cTnC (identified by co-expression of GFP) significantly increased healthy and MI cardiomyocyte contractility across various stimulation frequencies without adversely affecting Ca^{2+} transient properties or relaxation. The improvements in healthy and MI cardiomyocyte contractility from L48Q cTnC expression are likely the result of enhanced contractile efficiency, or cell shortening per Ca^{2+} released. Expression and incorporation of L48Q cTnC into myofilaments was confirmed by Western blot analysis of myofibrils from transduced cardiomyocytes, which indicated replacement

of 18±2% of native cTnC with L48Q cTnC. These experiments demonstrate the feasibility of directly targeting cardiac thin filament proteins to enhance cardiac contractility without impairing relaxation or Ca^{2+} transient properties.

5.2 INTRODUCTION

Heart failure is characterized by decreased systolic function and has a variety of etiologies with one of the most common being myocardial infarction (MI). In addition to the formation of a fibrotic scar that follows an MI, perturbations in normal cardiomyocyte processes, such as intracellular Ca^{2+} handling [172], β-adrenergic responsiveness [15], and contractile apparatus function [173,174], cause decreases in individual cardiomyocyte contractility in the non-infarcted region [175,176]. While there is still debate about the extent and mechanisms of changes in myofilament properties that occur post-MI, such changes in Ca^{2+} sensitivity, altered myofilament properties are thought to underlie, at least in part, the decreased contractility of failing myocardium [92,173,177–179].

Numerous strategies have been developed that attempt to compensate for the deleterious changes that occur in cardiomyocytes following MI. Most approaches have focused on increasing intracellular Ca^{2+} as a means to overcome decreased cardiomyocyte contractility, but these can be pro-arrhythmogenic and can further impair diastolic function [6]. Pharmaceutical agents that target the myofilaments, such as calmidazolium, bepridil, and levosimenden, have also been developed and tested. These agents improve the contractility of failing myocardium by increasing Ca^{2+} binding to the N-terminus of cardiac troponin C (cTnC) to enhance contractile activation. Unfortunately, they are not highly specific to cTnC and can have off-target effects on other similar EF-hand Ca^{2+} binding proteins and on other proteins involved in excitation-contraction coupling [10,180].

Another approach to enhance cardiac contractility without concomitant off-target effects is genetic manipulation of thin filament regulatory proteins to increase the Ca^{2+} sensitivity of cardiac myofilaments. cTnC is an attractive myofilament protein target because it binds Ca^{2+} to initiate myofilament contraction, and manipulation of its Ca^{2+} binding properties can result in enhanced cardiac contractility without requiring increased intracellular [Ca^{2+}]. Previous work by others [43] and us [42] has demonstrated that a single amino acid substitution of leucine at position 48 with glutamine (L48Q) in cTnC increases the Ca^{2+} binding affinity of the troponin complex. We have also demonstrated that when cardiac troponin containing L48Q cTnC (L48Q cTnC-cTn) was exchanged into demembranated cardiac muscle or cardiac myofibrils, the Ca^{2+} sensitivity of force and the rate of force development was increased without impairing maximal force generation or relaxation [41,45]. We recently reported that exchange of L48Q cTnC-cTn into demembranated cardiac muscle increased thin filament activation at submaximal Ca^{2+} concentrations independent of strong crossbridge binding. This effectively increased thin filament activation at Ca^{2+} levels that occur during cardiomyocyte twitch contraction [45]. We have also demonstrated that enhanced myofilament Ca^{2+} sensitivity in the uninjured myocardium of an MI heart after neonatal rat cardiomyocyte engraftment may be a major contributor to the improvement in whole heart function of MI hearts that was achieved [92]. Taken together, these studies suggest that enhancing myofilament Ca^{2+} sensitivity in cardiomyocytes from MI hearts, via L48Q cTnC incorporation into myofilaments, may improve contractility.

The potential of L48Q cTnC to improve the contractility of intact cardiomyocytes from healthy or failing (MI) hearts has yet to be determined and is what motivates the work presented here. In this study, we show that adenovirus-mediated *in vitro* expression of L48Q cTnC significantly improved the contraction of cardiomyocytes from healthy hearts without altering intracellular Ca^{2+} transients. It also increased the contraction of cardiomyocytes from hearts in failure following MI, even though

Ca^{2+} transients were depressed, thus restoring the magnitude of contraction to normal levels. These increases in contraction occurred without prolonging relaxation. Additionally, these increases in contractility occurred with only an ~20% myofilament incorporation of the L48Q cTnC variant, as indicated by Western blot analysis. Our results suggest that acute expression of L48Q cTnC and incorporation into sarcomeres of intact cardiomyocytes from either healthy or MI hearts increases myofilament responsiveness to Ca^{2+}, and this can occur without significant impairment of relaxation. Future *in vivo* studies will be required to determine whether this approach can be used to improve systolic function (without impairing diastolic function), and thus show promise as a myofilament-targeted gene therapy for heart failure.

5.3 RESULTS

5.3.1 In vivo cardiac functional assessment

Echocardiography was used to determine the *in vivo* cardiac function of control (sham operated, non-infarcted) and infarcted hearts (MI) 4-6 weeks post-surgery (permanent ligature of the left descending coronary artery), and the measurements are summarized in Figure 5.1. Similar to previous work by us [92] and others [175,181–184], there were no significant differences in average body weight or heart rate between sham control rats (180±3 g; 363±9 beats/min) and MI rats (181±2 g; 333±10 beats/min). Fractional shortening (FS) was significantly reduced ($p < 0.05$) in MI rats (30.0±1.9%) compared to control (53.5±6.7%) (Fig. 5.1A), which is in agreement with previous studies [92,175,181–184]. The decrease in cardiac function measured by echocardiography was characterized by both end-diastolic and end-systolic dilation in MI rats (Fig. 5.1B). Left-ventricular diameter at end-diastole (LVDD) was significantly larger in MI hearts (6.8±0.2 mm) compared to control hearts (5.3±0.4 mm). At end-systole, left ventricular diameter (LVSD) in MI hearts (4.8±0.3 mm) was also much larger than control hearts (2.5±0.5 mm) ($p < 0.05$), which indicates greatly reduced systolic function (Fig. 5.1B). There were no significant differences in septal wall or left-

ventricular posterior wall thickness between sham and MI rats (data not shown). These results demonstrate that the MI hearts were failing at the time of cardiomyocyte isolation for *in vitro* measures of contraction, relaxation, and intracellular Ca^{2+} transients.

5.3.2 Cardiomyocyte transduction and viability

Cardiomyocytes from healthy and MI hearts were enzymatically isolated and then transduced with adenovirus containing genes for L48Q + GFP (AV-L48Q cTnC) or WT cTnC + GFP (AV-WT cTnC)and incubated for 48-60 hours. At the end of the 48-60 hours, cell contractility and Ca^{2+} transient properties were measured. Cardiomyocyte numbers and sarcomere lengths are summarized in Table 5.1. There was no difference in cell length or sarcomere length between groups, which suggests that over-expression of L48Q or WT cTnC does not alter the resting state of cardiomyocytes or induce Ca^{2+} independent activation.

5.3.3 Contractile and Ca^{2+} transient analysis of isolated cardiomyocytes

The effects of L48Q cTnC over-expression on the contractile properties of cardiomyocytes from MI hearts measured at 1 Hz stimulation frequency are summarized in Figure 5.2A-C and Table 5.2. Example contractile traces for cardiomyocytes from control hearts and from MI hearts that were non-transduced, transduced with AV-WT cTnC, or transduced with AV-L48Q cTnC are shown in Fig. 5.2A. As these traces demonstrate, cellular shortening (percentage of cell length change) was significantly decreased in cardiomyocytes from MI hearts (5.5±0.4%) compared to cardiomyocytes from control hearts (11.2± 0.8%) (Fig. 5.2C; Table 5.2). Additionally, cardiomyocytes from MI hearts relaxed much slower, as indicated by significantly longer times to 50% (RT_{50}) and 90% of relaxation (RT_{90}) (Fig. 5.2D; Table 5.2). The depression of contractile and relaxation properties of cardiomyocytes from MI

hearts agrees with previously published results [92,175,181–184] and demonstrates that hallmarks of heart failure are observed at both the whole heart and individual cell levels.

Cardiomyocytes from MI hearts that were transduced with AV-L48Q cTnC (MI+L48Q cTnC) had significantly improved cell shortening (9.5±0.5%) that was nearly restored to healthy control levels. These cardiomyocytes also had significantly improved RT_{50} and RT_{90} times that were also nearly restored to healthy control levels (Fig 5.2A, 5.2C, 5.2D; Table 5.2). There was no significant difference in cell shortening, RT_{50}, or RT_{90} between MI+L48Q cTnC and healthy control cardiomyocytes. In contrast cardiomyocytes from MI hearts that were transduced with AV-WT cTnC (MI+WT cTnC) had decreased fractional shortening (5.3±0.4%) and prolonged relaxation times that were not different from non-treated MI cardiomyocytes (Fig. 5.2A, 2C,D; Table 5.2). The results of these control measurements suggest that it was the over-expression of the L48Q cTnC variant, and not simply over-expression of cTnC, that markedly improved the contractile properties of cardiomyocytes from both MI and healthy hearts.

To determine if changes in contractile properties resulted from altered myofilament properties *per se* or were due to changes in Ca^{2+} transient behavior, we simultaneously examined the Ca^{2+} transient properties of cardiomyocytes isolated from MI and control (sham operated) hearts. These data are summarized in Figure 5.2E-F and Table 5.2. Example intracellular Ca^{2+} transient traces are shown in Figure 5.2B. There was a significant decrease in the Ca^{2+} transient peak, measured by Fura-2, in cardiomyocytes from MI hearts compared to control hearts (Fig. 5.2E; Table 5.2). These cells from infarcted hearts also had a significantly slower Ca^{2+} transient decay, which was measured as the 50% (DT_{50}) and 90% (DT_{90}) time to return to baseline (Fig. 5.2F). The reduction in intracellular Ca^{2+} and prolongation of transient decay times for cardiomyocytes from MI hearts agrees with previously

published results [92,175,181–184], and suggests reduced contractility and slower relaxation may result (at least partially) from altered cardiomyocyte Ca^{2+} handling. Transduction of cardiomyocytes from MI hearts with either AV-L48Q cTnC or AV-WT cTnC did not affect the intracellular Ca^{2+} transient properties of the cells (Fig. 5.2E, 5.2F; Table 5.2). Interestingly, expression of L48Q cTnC in MI cardiomyocytes slightly improved DT_{50} and DT_{90} times (Fig. 5.2F; Table 5.2). These results suggest that over-expression of cTnC does not have adverse effects on the Ca^{2+} handling properties of cardiomyocytes from healthy or MI hearts. Furthermore, the improvements in contractile properties resulting from transduction with AV-L48Q cTnC appear to be primarily caused by enhancement of myofilament Ca^{2+} binding properties, not changes in intracellular Ca^{2+} handling.

5.3.4 Cellular response to stimulation frequency

Because changes in heart rate are normal adaptations to changes in physiological demand, we wanted to determine how transduction of cardiomyocytes with AV-L48Q cTnC affects cellular responsiveness to changes in stimulation frequency. After 48-72 hours in culture, the ability of adult cardiomyocytes to respond to higher frequencies found *in vivo* (4-6 Hz) is diminished, likely due to partial disruption of the T-tubule system over time in culture [185], however, we did monitor the effects at lower (0.5, 1, to 2 Hz) stimulation frequencies. The results of varying of stimulation frequency are summarized in Figure 5.3 and the values at 0.5 and 2 Hz stimulation are summarized in Supplemental Tables 5.S1 and 5.S2, respectively. Cardiomyocytes from MI hearts had significantly less cell shortening at all stimulation frequencies compared to control cardiomyocytes (Fig. 5.3A), and this was not improved at any frequency for MI cardiomyocytes transduced with AV-WT cTnC. Transduction with AV-L48Q cTnC, however, significantly improved cell shortening of MI cardiomyocytes at all stimulation frequencies. This improvement essentially returned the contractile properties of the MI+L48Q cTnC cardiomyocytes to a level that was not different from control cells at 0.5 and 1Hz but slight less at 2Hz (Fig. 5.3A). The slower relaxation of cardiomyocytes from MI

hearts occurred at all stimulation frequencies, as measured by RT_{90} times, and this was not improved by transduction with AV-WT cTnC. Transduction with AV-L48Q cTnC actually improved RT_{90} (Fig. 5.3B) at lower stimulation frequencies (0.5 and 1 Hz). These results demonstrate the improvement of contractility of cardiomyocytes from MI hearts by over-expression of L48Q cTnC persists at various stimulation frequencies.

As for 1 Hz stimulation, peak intracellular Ca^{2+} at 0.5 and 2 Hz was significantly reduced for cardiomyocytes from MI compared to control (sham operated) hearts, and this was not changed when MI cardiomyocytes were transduced with AV-L48Q or AV-WT cTnC (Fig. 5.3C; Table 5.2; Supplemental Tables 5.S1, 5.S2). Cardiomyocytes from MI hearts also had significantly prolonged Ca^{2+} transient decay times (DT_{90}) at all stimulation frequencies, and this was unaffected by transduction with AV-WT cTnC (Fig. 5.3D; Table 5.2; Supplemental Tables 5.S1, 5.S2). However, transduction of MI cardiomyocytes with AV-L48Q cTnC slightly improved Ca^{2+} transient decay times at lower stimulation frequencies (0.5 and 1 Hz), but not at 2 Hz (Fig. 5.3D). These data suggest that improvements in the contractile properties of cardiomyocytes by transduction with AV-L48Q cTnC occur via enhanced myofilament Ca^{2+} responsiveness, and not by having a significant effect on Ca^{2+} transient properties that are impaired following MI.

We chose to perform these experiments at room temperature (22-24°C) to compare with the predominant number of reports for cultured cardiomyocytes in the literature [25,96–100]. However, a subset of measurements was made at 37°C to determine if the effects persist at physiological temperature. At 37°C (Supplemental Tables 5.S3-5.S5), there were no significant differences in nearly all of the contractile and Ca^{2+} properties of any condition (MI, MI+WT cTnC, or MI+L48Q cTnC) at 37°C when compared the results at room temperature (22-24°C) for any stimulation frequency. In

some cases, the relaxation times and Ca^{2+} transient decay times were slightly faster at 37°C, but these were not statistically significant changes. The only significant changes were slightly faster Ca^{2+} transient decay times for MI+WT cTnC at 0.5 and 1 Hz stimulation frequencies at 37°C. These results comparing room temperature (22-24°C) and 37°C are similar to previous reports [25], and demonstrate that the effects of transduction with AV-L48Q cTnC on MI contractility and Ca^{2+} transient properties persist at physiological temperature as well.

5.3.5 Cardiomyocyte contractile efficiency

A measure of myofilament responsiveness to Ca^{2+} (Ca^{2+} sensitivity of contraction/relaxation) can be obtained by replotting the data in Figure 5.3 as the amount of cell shortening (contraction) per unit of peak intracellular Ca^{2+}. The summary of this analysis is illustrated as contractile responsiveness in Figure 5.4. Cardiomyocytes from MI hearts exhibit a significant decrease in contractile efficiency at all frequencies compared to cardiomyocytes from control (sham operated) hearts. This reduced efficiency was not affected when cardiomyocytes were transduced with AV-WT cTnC. However, cardiomyocytes from MI hearts that were transduced with AV-L48Q cTnC exhibited a significant improvement at all frequencies, such that contractile efficiency was almost completely restored to that of cardiomyocytes from control (sham operated) hearts. The significant improvement in the contractile efficiency with AV-L48Q cTnC supports the idea that there is an enhancement of myofilament responsiveness to activating Ca^{2+}.

5.3.6 Contraction and Ca^{2+} transient properties of isolated healthy cardiomyocytes

The effects of L48Q cTnC over-expression on the contractile properties of cardiomyocytes from healthy hearts measured at different stimulation frequencies (0.5, 1, to 2 Hz) are summarized in Supplemental Figure 5.1. Cardiomyocytes from healthy hearts that were transduced with AV-L48Q

cTnC had significantly improved cellular shortening and no adverse effects on relaxation times (RT_{90}) when compared to non-transduced cells at all stimulation frequencies tested (Supplemental Figure 5.1). The magnitude of increase of cell shortening in healthy cells transduced with AV-L48Q cTnC was similar to the improvements that occurred in MI cardiomyocytes. Transduction of healthy cardiomyocytes with AV-WT cTnC had no effects on cell shortening or and relaxation times (RT_{90}) as compared to non-transduced cells at all stimulation frequencies tested (Supplemental Figure 5.1). In healthy cardiomyocytes transduced with AV-L48Q cTnC or AV-WT cTnC, there were also no effects on the Ca^{2+} transient peak or Ca^{2+} transient decay times (DT_{90}) when compared to non-transduced cells at all stimulation frequencies examined (Supplemental Figure 5.1). The improvement in healthy cardiomyocyte contractility without altering relaxation or Ca^{2+} transient properties following expression of L48Q cTnC provides additional evidence that L48Q cTnC is able to enhance myofilament responsiveness to activating Ca^{2+}, and that the improvements in contractility are not limited to MI cardiomyocytes.

5.3.7 Myofilament protein analysis

To determine the level of WT or L48Q cTnC incorporation into the myofilaments resulting from adenovirus-mediated transduction, cardiomyocytes were transduced with AV constructs containing genes for WT or L48Q cTnC-Flag + GFP for 48-60 hours, or left non-transduced. Transduction with WT or L48Q cTnC-Flag and incorporation into the myofilaments was demonstrated by Western blot ratiometric analysis of purified myofibrils from transduced cardiomyocytes probed with anti-cTnC (Santa Cruz Biotechnology, Santa Cruz, CA) for total cTnC content and anti-Flag (Sigma-Aldrich, St. Louis, MO) for transduced protein content (Figure 5.5). Figure 5.5 shows a representative example of the anti-TnC and anti-Flag Western blots. To assess the approximate level of myofilament incorporation of transduced cTnC-Flag, Western blot bands from transduced cardiomyocyte myofibrils were quantified by densitometry to compare total cTnC content vs. cTnC-Flag (transduced

protein) content (Figure 5.5). Three batches of cardiomyocytes were run in duplicate and averaged results indicate equivalent replacement of native cTnC with either WT cTnC-Flag (22±5%) or L48Q cTnC-Flag (18±2%).

5.4 DISCUSSION

The main objective of this study was to determine if expression of L48Q cTnC and incorporation into myofibrils could improve the contractile properties of intact cardiomyocytes and rescue contractile properties of cardiomyocytes that are depressed following MI. We found that this was indeed the case, and it occurred when myofilament incorporation of L48Q cTnC was only ~20% of the total cTnC content. The improvement in contractile properties of cardiomyocytes from MI hearts occurred without adverse effects on relaxation times. This interesting finding could be predicted from previous solution measurements, and mechanical measurements from myofibrils and demembranated trabeculae, where L48Q cTnC enhanced the Ca^{2+} binding properties of troponin and thin filaments and the Ca^{2+} sensitivity of myofilament contraction [41,45]. It suggests that in the current study, ~20% myofilament content of the L48Q cTnC variant is sufficient to increase the Ca^{2+} sensitivity of myofibrils such that significantly greater contraction can occur without an increase in intracellular Ca^{2+}.

The mechanism by which L48Q cTnC is able to increase myofilament Ca^{2+} sensitivity and contractile function is not completely understood, but recent work by our group [42,45] and others [69,115,186] suggest that increased Ca^{2+} binding to troponin containing L48Q cTnC increases the ability to activate the thin filament. Our solution studies [42], and work by others [43], have demonstrated that the L48Q point mutation significantly increases the Ca^{2+} affinity of cTnC and increases the affinity of cTnC for cTnI in both the presence and absence of Ca^{2+}. Both magnetic resonance spectroscopy (NMR) and

molecular dynamic (MD) simulation data indicate that the N-terminal lobe of L48Q cTnC has a more open structure and exposure of the cTnC hydrophobic patch is stabilized following Ca^{2+} binding [42]. This should increase cTnC-cTnI interaction allowing enhanced movement of cTm and access to myosin binding sites on actin for a given submaximal [Ca^{2+}]. It may also reduce the requirement for crossbridges to stabilize the cTnC-cTnI state [187]. This effect should be more pronounced at submaximal [Ca^{2+}], where the slower dissociation rate of L48Q cTnC [41,43] should result in more Ca^{2+} being bound to cTn in thin filaments at any given time.

An important and promising aspect of L48Q cTnC is that, while it more effectively activated the thin filament and improved contraction, cardiomyocyte relaxation was mainly unaffected in both healthy and diseased cardiomyocytes. Increased Ca^{2+} binding affinity can lead to prolonged thin-filament activation and thus prolonged crossbridge attachment, which can hinder relaxation [188]. Prolonging systole and slowing diastole would have severe *in vivo* functional consequences by reducing diastolic filling and, subsequently, cardiac output. The relaxation time in cardiac muscle is also influenced by the restoring force supplied by titin, which increases in a linear manner as sarcomeres shorten [149]. Relaxation times observed in our study roughly correlate with cellular fractional shortening in healthy or diseased cardiomyocytes, which indicates that L48Q cTnC does not prolong crossbridge attachment in intact cells. It is also possible that the amount of replacement of endogenous cTnC with L48Q cTnC was sufficient to improve shortening without significantly affecting relaxation, while greater replacement may elicit different effects on relaxation. Additionally, any effect of L48Q cTnC on relaxation may be smaller at submaximal [Ca^{2+}] levels that occur in intact myocardium, and effects may also differ under loaded conditions (strain) such as those encountered *in vivo*. Further studies to investigate these questions are warranted.

Our results are in line with previous studies that have demonstrated that over-expression of different thin filament proteins in intact adult cardiomyocytes is able to effectively modulate thin filament properties and thus cardiac contractility. A number of studies with slow skeletal TnI (ssTnI) have shown that over-expression of ssTnI in adult cardiomyocytes significantly enhanced myofilament Ca^{2+} sensitivity, and that exogenous ssTnI is able to effectively incorporate into the myofilaments [188–191]. Furthermore, similar to results presented in our study, viral-mediated over-expression of ssTnI in cardiomyocytes significantly enhanced cardiac contractility without altering intracellular peak Ca^{2+}. However, in contrast to our findings, this study observed a prolongation in relaxation and Ca^{2+} transient decay times [188]. Interestingly, Lim et al., demonstrated that cardiomyocytes over-expressing mutant cTnC (E59D, D75Y), which is associated with idiopathic dilated cardiomyopathy, markedly decreased contractility while having no effect on intracellular Ca^{2+} homeostasis [192]. This study is another example that it is possible to manipulate thin filament Ca^{2+} binding affinity without affecting Ca^{2+} transient behavior. The results of these provide further support of our hypothesis that targeted increases in myofilament Ca^{2+} sensitivity through specific manipulation of thin filament Ca^{2+} binding properties can have a significant impact on cardiac contractility without perturbing intracellular Ca^{2+} handling.

MI and cardiac diseases of the sarcomere, such as dilated cardiomyopathy (DCM), commonly lead to heart failure [193–195]. Within these causes of heart failure, some patterns have emerged that demonstrate potential similarities in altered contractile properties and disease state. For example, most DCM mutations in one of several myofilament proteins result in decreased Ca^{2+} sensitivity of force [193,196–201]. Additionally, perturbations in myofilament properties, including altered Ca^{2+} sensitivity, are thought to underlie, at least in part, the decreased contractility of failing myocardium post-MI [92,173,177–179]. If one of the characteristics of failing myocardium from DCM or MI is altered myofilament Ca^{2+} sensitivity, a logical therapeutic approach would be to return the Ca^{2+}

sensitivity levels to normal in order to prevent further disease progression and to correct the dysfunction. However, little is known whether alterations that increase myofilament Ca^{2+} sensitivity, in our case expression of L48Q cTnC, might be beneficial in DCM or MI. One approach has shown that increasing myofilament Ca^{2+} sensitivity exhibits some promise as a means to treat DCM. In this study, the use of a Ca^{2+} sensitizing agent, pimobendan, demonstrated that administration to DCM transgenic mice with a deletion in troponin T significantly improved cardiac performance and morphology [202]. We have demonstrated that enhanced myofilament Ca^{2+} sensitivity in the uninjured myocardium of an MI heart after neonatal rat cardiomyocyte engraftment may be a major contributor to the improvement in whole heart function of MI hearts that was achieved [92]. These results are promising and suggest that expression of thin filament mutations that increase myofilament Ca^{2+} sensitivity, such as L48Q cTnC, may be able to improve function in failing hearts.

5.5 CONCLUSIONS

This study demonstrated that expression of L48Q cTnC and incorporation into cardiac myofibrils enhanced Ca^{2+} sensitivity of the myofilaments and markedly improved contractility in both healthy and MI cardiomyocytes without adverse effects on relaxation or Ca^{2+} transient behavior. This presents an alternative approach to other studies that have shown that myofilament Ca^{2+} sensitization through protein [203] or pharmacological [204,205] means have many off-target effects. Additional challenges and risks are encountered with some therapeutic strategies that have focused on increasing intracellular Ca^{2+} concentrations, which can be pro-arrhythmogenic and can further impair diastolic function [6]. It may be that the ~20% replacement of native cTnC by L48Q cTnC is insufficient to produce any of the deleterious off-target effects associated with current treatment options. Alternatively, L48Q cTnC may alter interactions with cTnI in a way that does precipitate delayed relaxation. Future *in vivo* work will be required to determine the effects of L48Q cTnC expression on whole heart function, and whether expression of L48Q cTnC can improve systolic

function (without impairing diastolic function), and thus show promise as a myofilament-targeted gene therapy.

5.6 ACKNOWLEDGMENTS

We thank Dr. Hans Reinecke, Dr. Jennifer Davis, and Dr. N. Scott Blair for their assistance in adenoviral design, production, and troubleshooting. We also thank Kate Buckley for her help with cardiomyocyte isolations and assessment of cardiomyocyte contractility.

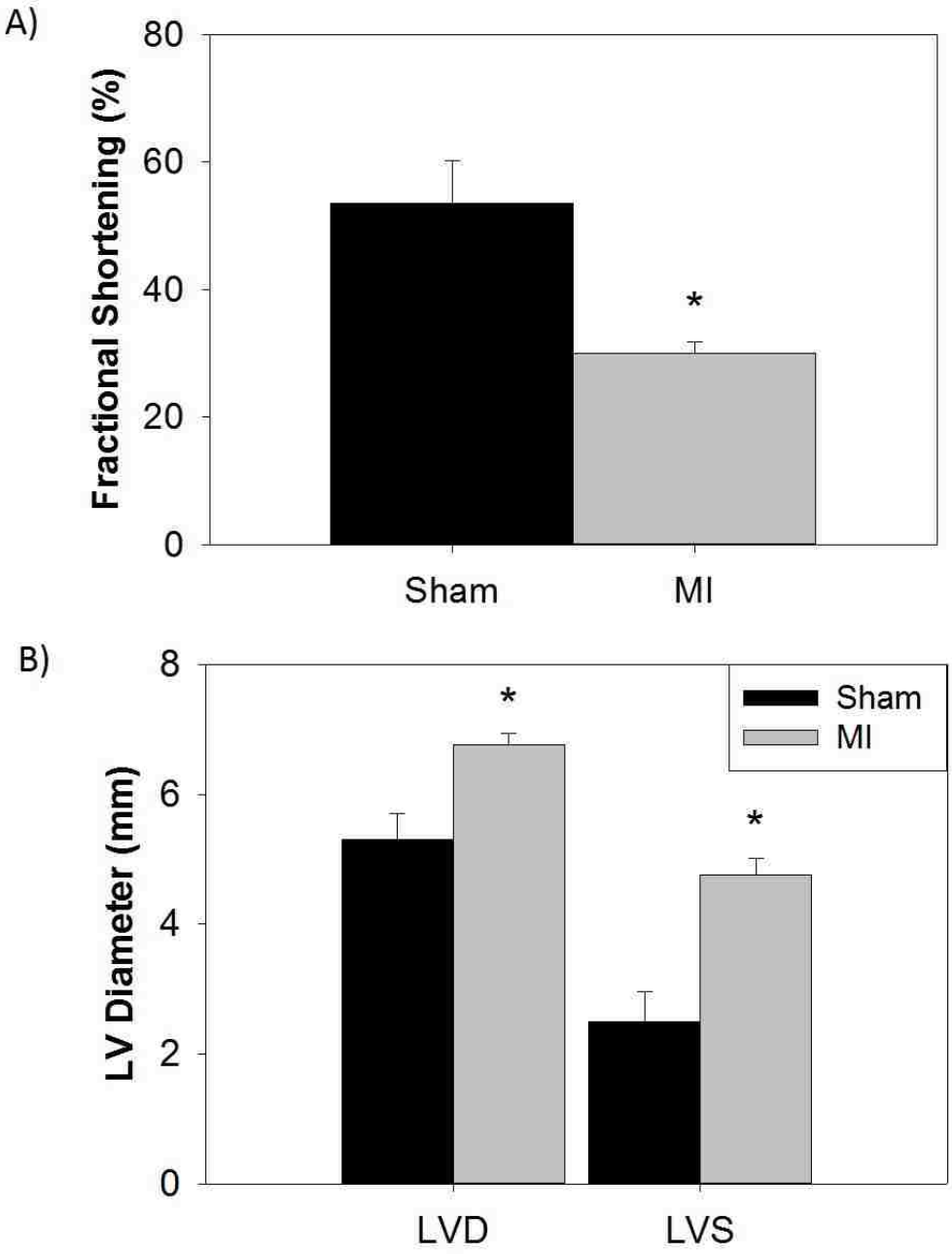

Figure 5.1: Assessment of cardiac function after myocardial infarction by echocardiography. Factional shortening of infarcted hearts (A, n= 6) was significantly reduced compared to healthy controls (sham, n = 3). Both diastolic and systolic LV diameters significantly increased after MI. Values are means ± S.E.M.; * = $p<0.05$ as compared to sham.

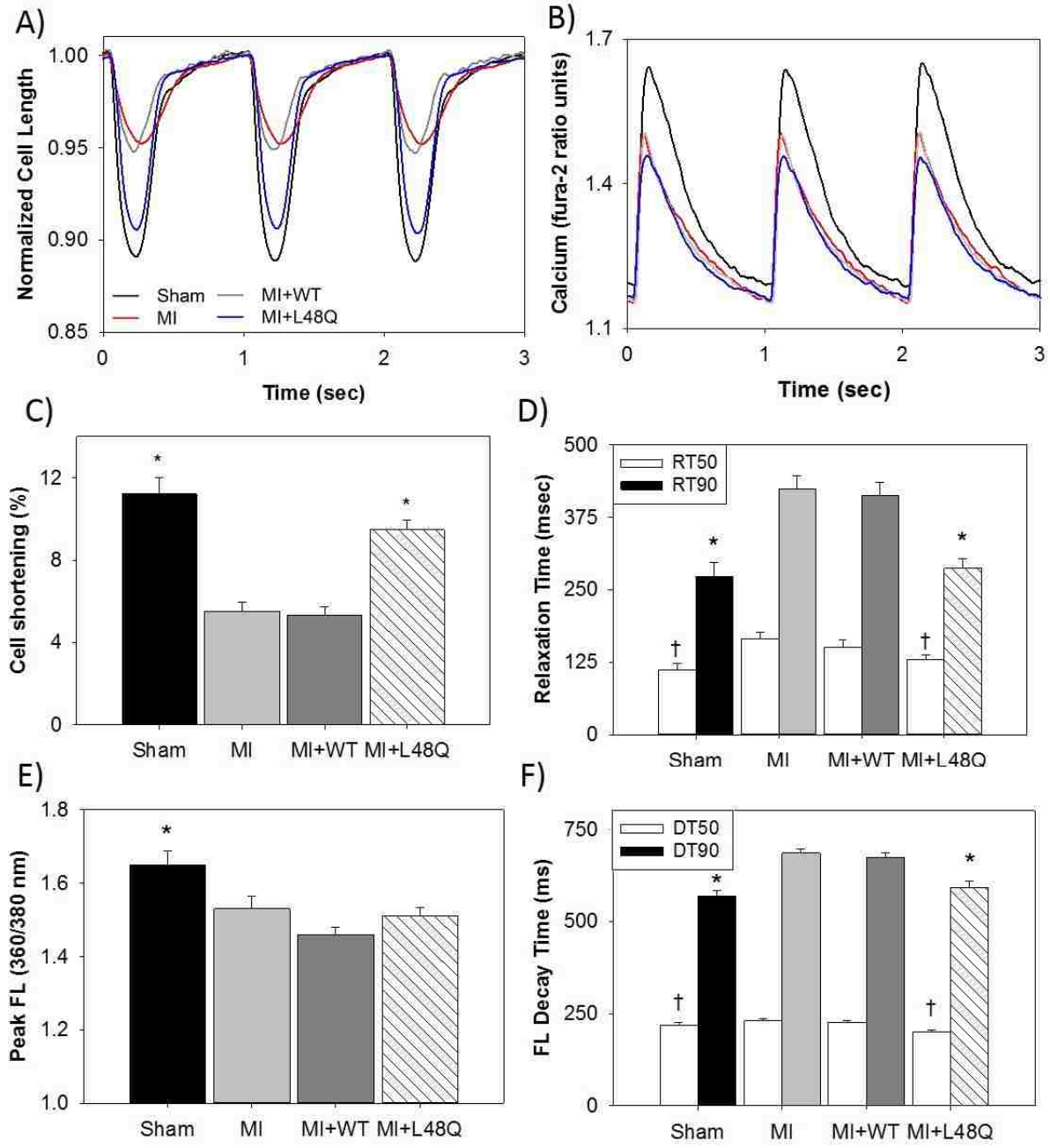

Figure 5.2: Contractile and intracellular Ca^{2+} transient properties of cardiomyocytes from MI hearts stimulated at 1Hz. Representative cell length traces (A) and Ca^{2+} transients (B, Fura-2 fluorescence) of healthy sham (black), MI non-transduced (red), MI+WT cTnC (grey), and MI+L48Q cTnC (blue) cardiomyocytes. MI cells had depressed cell shortening (C) and slowed RT_{50} (open bars) and RT_{90} (filled bars) times (D), which was partially rescued by expression of L48Q cTnC. Peak intracellular Ca^{2+} fluorescence was depressed (E) and intracellular Ca^{2+} decay times DT_{50} (open bars) and DT_{90} (filled bars) (F) were slowed in all MI conditions. L48Q cTnC had surprising slight improvements in DT_{50} and DT_{90} (F). Values are means ± S.E.M.; * = $p<0.05$ as compared to MI; † = $p<0.05$ as compared to MI for RT_{50} and DT_{50}.

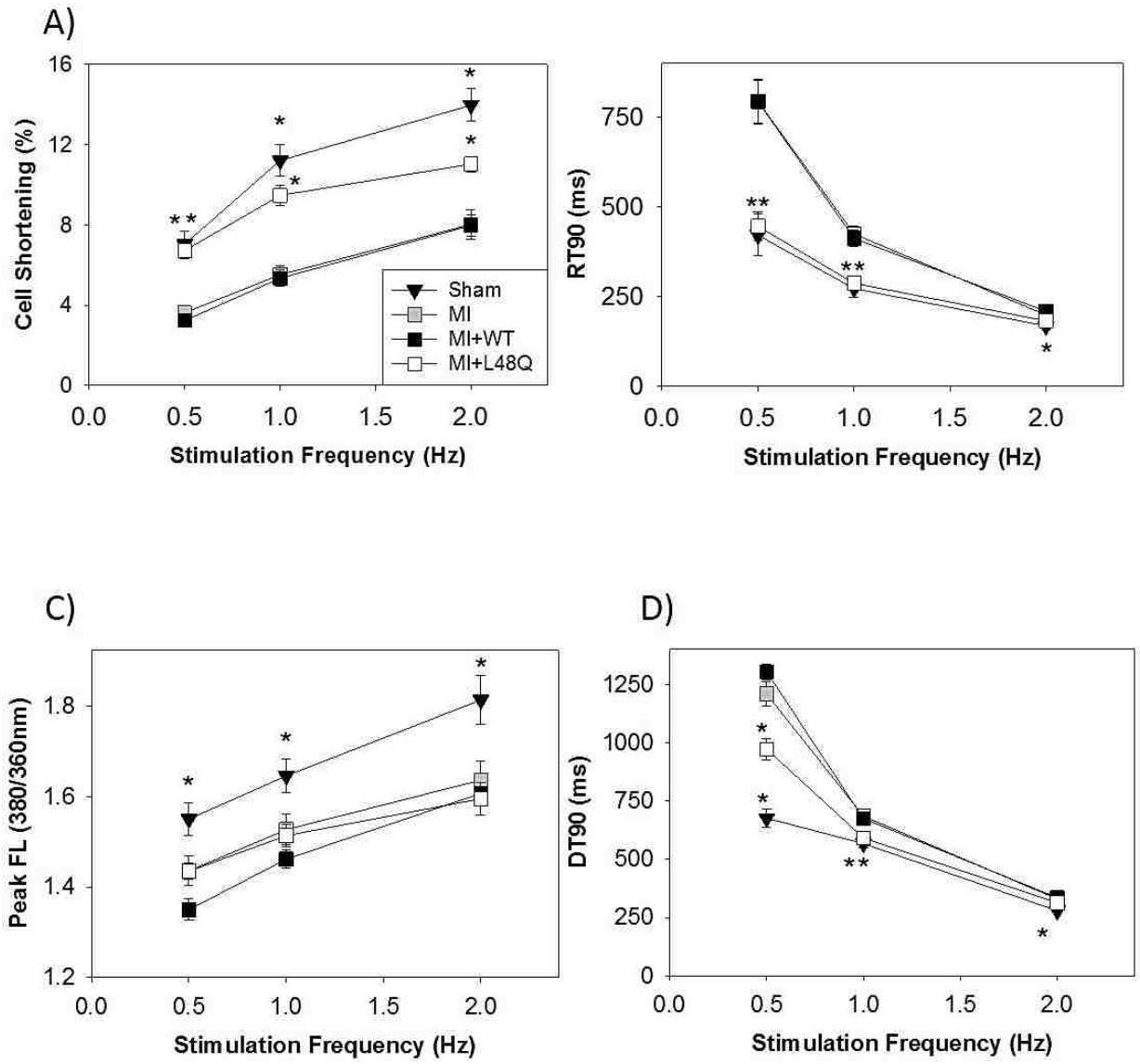

Figure 5.3: Effects of stimulation frequency on contractile and intracellular Ca^{2+} transient properties. Contractility is depressed and relaxation times are slowed at all frequencies for MI (grey squares) and MI+WT cTnC (black squares) myocytes (A,B) compared to sham. MI+L48Q cTnC (white squares) improves the contractility and relaxation times at all frequencies (A,B). Peak intracellular Ca^{2+} fluorescence was depressed in all MI conditions at all frequencies (C). Intracellular Ca^{2+} decay time was slowed in MI and MI+WT cTnC at all frequencies (D). Interestingly, MI+L48Q cTnC improved DT_{90} times at lower frequencies but this did not persist at 2 Hz (D). Values are means ± S.E.M while some error bars are concealed within data points; * = $p<0.05$ as compared to MI.

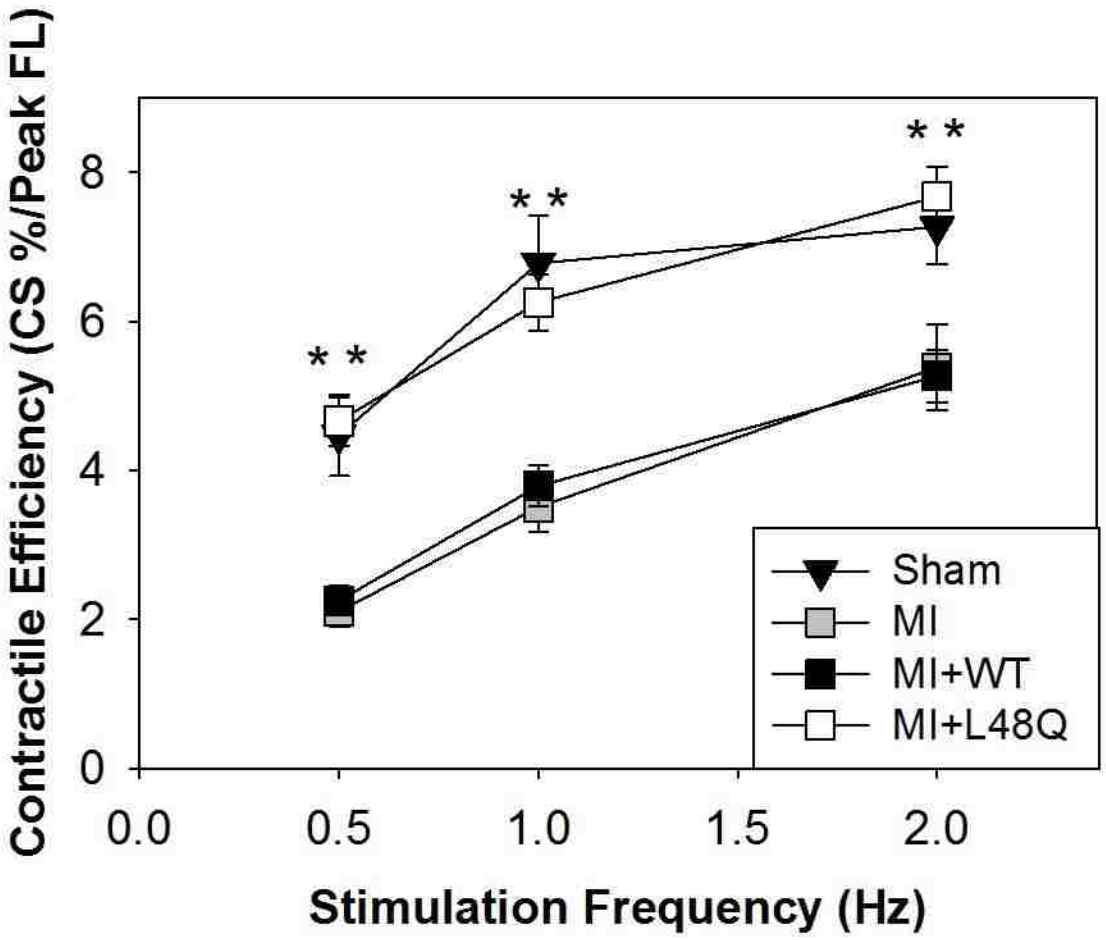

Figure 5.4: Contractile efficiency assessed as cell shortening divided by peak Fura-2 fluorescence (peak Ca^{2+}). MI+L48Q cTnC transduced cardiomyocytes (white squares) are significantly more responsive to Ca^{2+} at all stimulation frequencies, which is similar to responsiveness of sham control cells (black triangles). MI+WT cTnC transduced cardiomyocytes (black squares) respond to Ca^{2+} similarly to non-transduced MI cardiomyocytes (grey squares). Values are means ± S.E.M.; * = $p<0.05$ as compared to MI

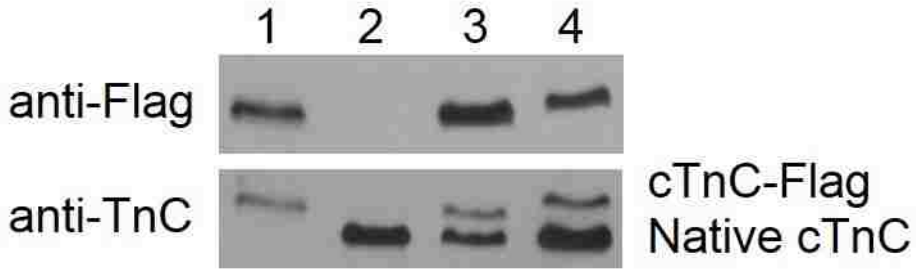

Figure 5.5: Analysis of myofilament incorporation of Flag-tagged WT and L48Q cTnC. Representative Western blots against Flag and TnC show that myofibrils contain 22±5% WT cTnC-Flag or 18±2% L48Q cTnC-Flag of the total myofilament cTnC content. Lane 1) WT cTnC-Flag from HEK 293 cells (positive control), 2) non-transduced cardiomyocytes (negative control), 3) WT cTnC-Flag transduced cardiomyocytes 4) L48Q cTnC-Flag transduced cardiomyocytes.

Table 5.1: Cell characteristics**.** n = # of cells; No statistical significance between any groups. The data are from 3 sham animals and 6-8 infarcted animals.

	n	SL (μm)	Cell length (μm)
Sham	27	1.77 ± 0.02	91.8 ± 2.9
MI	48	1.79 ± 0.02	95.2 ± 2.3
MI+WT cTnC	41	1.78 ± 0.02	95.9 ± 3.5
MI+L48Q cTnC	51	1.79 ± 0.02	91.7 ± 2.5

Table 5.2: Contractile and Ca^{2+} transient values at 1 Hz stimulation frequency. * = $p<0.05$ as compared to MI; ANOVA analysis and post-hoc tests with Dunnett's test for all MI conditions; independent t-test for MI vs. Sham.

	Fractional Shortening (%)	RT_{50} (ms)	RT_{90} (ms)	Baseline Ca^{2+} (Fura ratio units)	Peak Ca^{2+} (Fura ratio units)	DT_{50} (ms)	DT_{90} (ms)
Sham	11.2 ± 0.8*	111 ± 11*	272 ± 24*	1.21 ± 0.02*	1.65 ± 0.04*	217 ± 9	568 ± 17*
MI	5.5 ± 0.4	165 ± 12	425 ± 22	1.14 ± 0.01	1.53 ± 0.03	230 ± 6	685 ± 12
MI+WT cTnC	5.3 ± 0.4	151 ± 13	412 ± 23	1.14 ± 0.01	1.46 ± 0.02	226 ± 5	675 ± 11
MI+L48Q cTnC	9.5 ± 0.5*	129 ± 8*	287 ± 16*	1.18 ± 0.02	1.51 ± 0.02	200 ± 5*	591 ± 17*

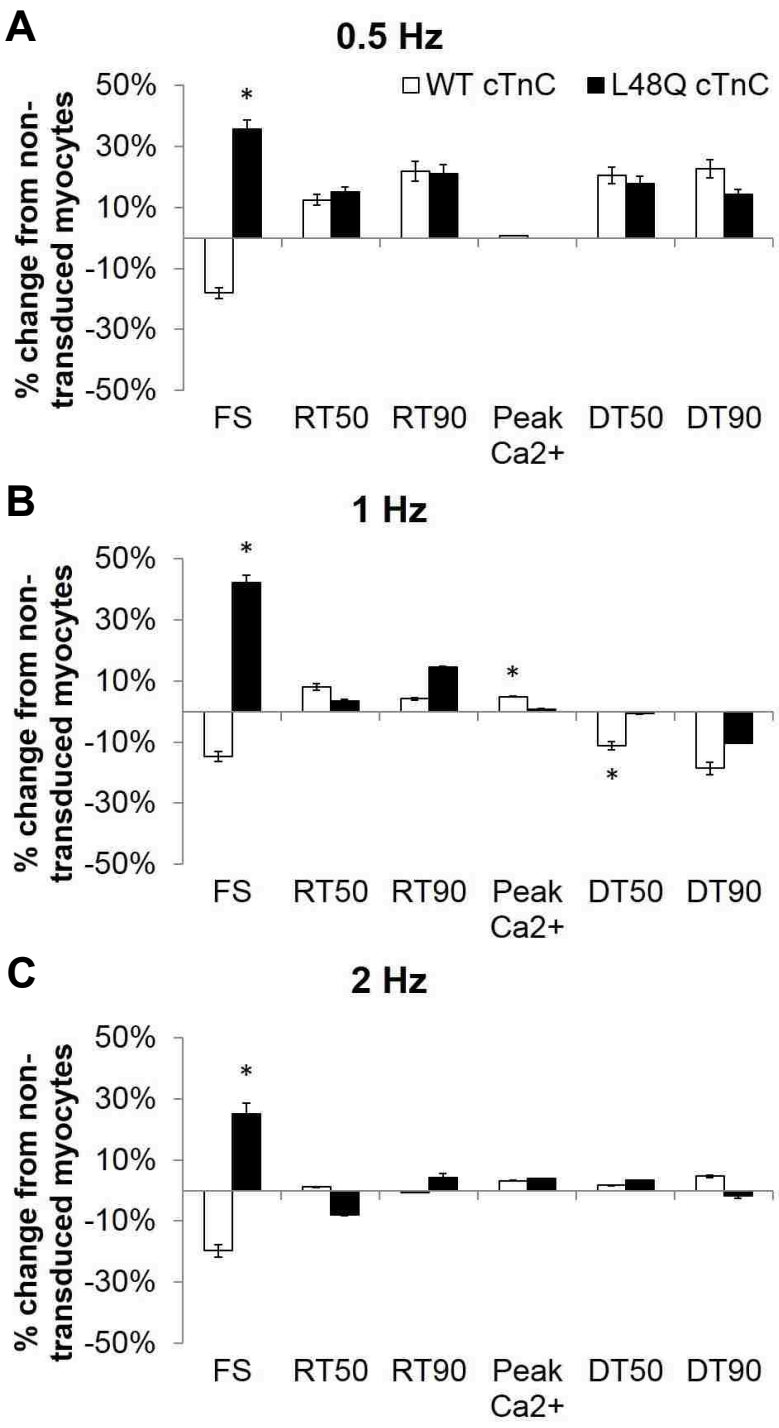

Figure 5.S1: Contractile and Ca^{2+} transient properties of healthy transduced cardiomyocytes. The percentage change in contractile and Ca^{2+} transient properties for WT cTnC (open bars) and L48Q cTnC (solid bars) at 0.5 Hz (A), 1 Hz (B), and 2 Hz (C) as compared to non-transduced cardiomyocytes. * = $p<0.05$ as compared to non-transduced cardiomyocytes.

Table 5.S1: Contractile and Ca^{2+} transient values at 0.5 Hz stimulation frequency. * = $p<0.05$ as compared to MI; ANOVA analysis and post-hoc tests with Dunnett's test for all MI conditions; independent t-test for MI vs. Sham.

	Fractional Shortening (%)	RT_{50} (ms)	RT_{90} (ms)	Baseline Ca^{2+} (Fura ratio units)	Peak Ca^{2+} (Fura ratio units)	DT_{50} (ms)	DT_{90} (ms)
Sham	7.0 ± 0.7*	146 ± 22*	421 ± 58*	1.21 ± 0.02*	1.55 ± 0.04*	244 ± 12*	676 ± 38*
MI	3.6 ± 0.3	265 ± 27	793 ± 59	1.12 ± 0.02	1.44 ± 0.03	366 ± 19	1209 ± 53
MI+WT cTnC	3.2 ± 0.3	262 ± 26	792 ± 62	1.09 ± 0.01	1.35 ± 0.02	390 ± 15	1304 ± 32
MI+L48Q cTnC	6.7 ± 0.4*	150 ± 13*	446 ± 40*	1.15 ± 0.02	1.43 ± 0.02	269 ± 11*	972 ± 46*

Table 5.S2: Contractile and Ca^{2+} transient values at 2 Hz stimulation frequency. * = $p<0.05$ as compared to MI; ANOVA analysis and post-hoc tests with Dunnett's test for all MI conditions; independent t-test for MI vs. Sham.

	Fractional Shortening (%)	RT_{50} (ms)	RT_{90} (ms)	Baseline Ca^{2+} (Fura ratio units)	Peak Ca^{2+} (Fura ratio units)	DT_{50} (ms)	DT_{90} (ms)
Sham	14 ± 0.8*	92 ± 7	168 ± 11*	1.35 ± 0.03*	1.81 ± 0.05*	150 ± 6	279 ± 10*
MI	8.0 ± 0.7	107 ± 5	199 ± 8	1.24 ± 0.02	1.64 ± 0.04	140 ± 3	329 ± 4
MI+WT cTnC	8.0 ± 0.6	115 ± 6	209 ± 8	1.23 ± 0.01	1.61 ± 0.02	142 ± 3	335 ± 3
MI+L48Q cTnC	11 ± 0.4*	100 ± 5	182 ± 7	1.24 ± 0.01	1.60 ± 0.04	140 ± 3	313 ± 5

Table 5.S3: Contractile and Ca^{2+} transient values at 0.5 Hz stimulation frequency and 37°C. No statistical significance between most groups when compared with independent t-test for each condition at 22-24°C vs. 37°C. * = $p<0.05$ as compared to the equivalent condition at 22-24°C for MI, MI+WT cTnC, or MI+L48Q cTnC.

	Fractional Shortening (%)	RT_{50} (ms)	RT_{90} (ms)	Baseline Ca^{2+} (Fura ratio units)	Peak Ca^{2+} (Fura ratio units)	DT_{50} (ms)	DT_{90} (ms)
MI	3.3 ± 0.8	241 ± 81	898 ± 117	1.08 ± 0.01	1.37 ± 0.06	327 ± 72	1123 ± 55
MI+WT cTnC	2.4 ± 0.3	184 ± 42	704 ± 90	1.11 ± 0.02	1.34 ± 0.03	288 ± 27*	1123 ± 55*
MI+L48Q cTnC	5.2 ± 1.1	198 ± 33	793 ± 97*	1.09 ± 0.01	1.42 ± 0.06	200 ± 5	1134 ± 102

Table 5.S4: Contractile and Ca^{2+} transient values at 1 Hz stimulation frequency and 37°C. No statistical significance between most groups when compared with independent t-test for each condition at 22-24°C vs. 37°C. * = $p<0.05$ as compared to the equivalent condition at 22-24°C for MI, MI+WT cTnC, or MI+L48Q cTnC.

	Fractional Shortening (%)	RT_{50} (ms)	RT_{90} (ms)	Baseline Ca^{2+} (Fura ratio units)	Peak Ca^{2+} (Fura ratio units)	DT_{50} (ms)	DT_{90} (ms)
MI	5.7 ± 1.6	132 ± 32	375 ± 33	1.12 ± 0.01	1.49 ± 0.07	209 ± 28	642 ± 39
MI+WT cTnC	5.8 ± 1.5	111 ± 17	360 ± 54	1.13 ± 0.02	1.44 ± 0.05	188 ± 12*	618 ± 24*
MI+L48Q cTnC	8.9 ± 1.9	142 ± 27	396 ± 44	1.14 ± 0.01	1.59 ± 0.09	210 ± 16	660 ± 31

Table 5.S5: Contractile and Ca^{2+} transient values at 2 Hz stimulation frequency and 37°C. No statistical significance between most groups when compared with independent t-test for each condition at 22-24°C vs. 37°C. * = $p<0.05$ as compared to the equivalent condition at 22-24°C for MI, MI+WT cTnC, or MI+L48Q cTnC.

	Fractional Shortening (%)	RT_{50} (ms)	RT_{90} (ms)	Baseline Ca^{2+} (Fura ratio units)	Peak Ca^{2+} (Fura ratio units)	DT_{50} (ms)	DT_{90} (ms)
MI	9.9 ± 2.2	84 ± 10	182 ± 31	1.23 ± 0.07	1.63 ± 0.08	122 ± 12*	290 ± 39
MI+WT cTnC	8.4 ± 0.6	96 ± 11	208 ± 9	1.20 ± 0.03	1.56 ± 0.07	129 ± 5	322 ± 8
MI+L48Q cTnC	10.1 ± 0.8	96 ± 16	180 ± 23	1.24 ± 0.03	1.72 ± 0.09	131 ± 6	334 ± 7

Table 5.S6: Cell characteristics for cTnC-Flag study. n = # of cells; No statistical significance between any groups.

	n	SL (μm)	Cell length (μm)
NA	11	1.79 ± 0.03	101 ± 3.8
WT cTnC-Flag	9	1.78 ± 0.08	97 ± 4.6
L48Q cTnC-Flag	9	1.79 ± 0.06	98 ± 4.5

Table 5.S7: cTnC-Flag transduced cardiomyocyte contractile and Ca^{2+} transient values at 0.5 Hz stimulation frequency. * = $p<0.05$ as compared to NA; ANOVA analysis and post-hoc tests with Dunnett's test for both cTnC-Flag conditions.

	Fractional Shortening (%)	RT_{50} (ms)	RT_{90} (ms)	Baseline Ca^{2+} (Fura ratio units)	Peak Ca^{2+} (Fura ratio units)	DT_{50} (ms)	DT_{90} (ms)
NA	7.1 ± 0.5	71 ± 8	209 ± 46	1.17 ± 0.06	1.31 ± 0.05	183 ± 34	690 ± 98
WT cTnC-Flag	7.2 ± 1.2	136 ± 22*	389 ± 90	1.06 ± 0.02	1.22 ± 0.02	241 ± 25	731 ± 95
L48Q cTnC-Flag	10.0 ± 1.1*	86 ± 9	214 ± 30	1.15 ± 0.02	1.31 ± 0.03	204 ± 18	739 ± 72

Table 5.S8: cTnC-Flag transduced cardiomyocyte contractile and Ca^{2+} transient values at 1 Hz stimulation frequency. * = $p<0.05$ as compared to NA; ANOVA analysis and post-hoc tests with Dunnett's test for both cTnC-Flag conditions.

	Fractional Shortening (%)	RT_{50} (ms)	RT_{90} (ms)	Baseline Ca^{2+} (Fura ratio units)	Peak Ca^{2+} (Fura ratio units)	DT_{50} (ms)	DT_{90} (ms)
NA	8.2 ± 0.7	70 ± 7	176 ± 33	1.22 ± 0.06	1.33 ± 0.04	132 ± 16	384 ± 40
WT cTnC-Flag	8.2 ± 1.4	105 ± 11*	251 ± 42	1.05 ± 0.02	1.25 ± 0.03	201 ± 9*	522 ± 33*
L48Q cTnC-Flag	12.1 ± 1.2*	83 ± 8	181 ± 19	1.19 ± 0.03	1.37 ± 0.04	157 ± 14	357 ± 37

Table 5.S9: cTnC-Flag transduced cardiomyocyte contractile and Ca^{2+} transient values at 2 Hz stimulation frequency. * = $p<0.05$ as compared to NA; ANOVA analysis and post-hoc tests with Dunnett's test for both cTnC-Flag conditions.

	Fractional Shortening (%)	RT_{50} (ms)	RT_{90} (ms)	Baseline Ca^{2+} (Fura ratio units)	Peak Ca^{2+} (Fura ratio units)	DT_{50} (ms)	DT_{90} (ms)
NA	10.4 ± 1.3	67 ± 6	134 ± 13	1.18 ± 0.06	1.33 ± 0.04	122 ± 15	241 ± 28
WT cTnC-Flag	11.6 ± 0.9	93 ± 5*	191 ± 12*	1.09 ± 0.02	1.30 ± 0.04	158 ± 3*	323 ± 10*
L48Q cTnC-Flag	14.5 ± 1*	82 ± 4	156 ± 7	1.24 ± 0.01	1.45 ± 0.05	132 ± 7	247 ± 14

Chapter 6. Upregulation of cardiomyocyte ribonucleotide reductase increases intracellular 2 deoxy-ATP, contractility, and relaxation

F. Steven Korte, Jin Dai, Kate Buckley, Erik R. Feest, Nancy Adamek, Michael A. Geeves, Charles E. Murry, Michael Regnier. 2011. *Journal of Molecular and Cellular Cardiology.* Vol. 51, 6: 894-901.

6.1 ABSTRACT

We have previously demonstrated that substitution of ATP with 2 deoxy-ATP (dATP) increased the magnitude and rate of force production at all levels of Ca^{2+}-mediated activation in demembranated cardiac muscle. In the current study we hypothesized that cellular [dATP] could be increased by viral-mediated over-expression of the ribonucleotide reductase (Rrm1 and Rrm2) complex, which would increase contractility of adult rat cardiomyocytes. Cell length and ratiometric (Fura-2) Ca^{2+} fluorescence were monitored by video microscopy. At 0.5 Hz stimulation, the extent of shortening was increased ~40% and maximal rate of shortening was increased ~80% in cardiomyocytes over-expressing Rrm1+Rrm2 as compared to non-transduced cardiomyocytes. The maximal rate of relaxation was also increased ~150% with Rrm1+Rrm2 over-expression, resulting in decreased time to 50% relaxation over non-transduced cardiomyocytes. These differences were even more dramatic when compared to cardiomyocytes expressing GFP-only. Interestingly, Rrm1+Rrm2 over-expression had no effect on minimal or maximal intracellular [Ca^{2+}] (Fura-2 fluorescence), indicating increased contractility is primarily due to increased myofilament activity without altering Ca^{2+} release from the sarcoplasmic reticulum. Additionally, functional potentiation was maintained with Rrm1+Rrm2 over-expression as stimulation frequency was increased (1 Hz and 2 Hz). HPLC analysis indicated cellular [dATP] was increased by approximately 10-fold following transduction, becoming ~1.5% of the adenine nucleotide pool. Furthermore, 2% dATP was sufficient to significantly increase crossbridge binding and contractile force during sub-maximal Ca^{2+} activation in demembranated

cardiac muscle. These experiments demonstrate the feasibility of directly targeting the actin-myosin chemomechanical crossbridge cycle to enhance cardiac contractility and relaxation without affecting minimal or maximal Ca^{2+}.

6.2 INTRODUCTION

Systolic and/or diastolic cardiac function is compromised in a number of cardiovascular diseases including myocardial infarction, ischemia/reperfusion injury, diabetes, high blood pressure and hypertrophic and dilated cardiomyopathy. These pathophysiological conditions often involve alterations in the Ca^{2+} cycle [172], β-adrenergic responsiveness [15], and/or the contractile apparatus of cardiomyocytes [173,174]. To date, therapeutic efforts have focused primarily on approaches that increase intracellular Ca^{2+} concentrations ($[Ca^{2+}]_i$) that can be pro-arrhythmogenic and may impair ventricular filling by slowing diastolic relaxation [6]. Other approaches involving adrenergic agents can have undesirable long-term consequences, including significant side-effects due to drug actions in non-target areas, pro-arrythmogenic triggered activity, and potential for accelerated progression into heart failure [15]. Thus, new approaches to combat cardiac dysfunction are desirable.

We have previously shown that replacing ATP with 2 deoxy-ATP (dATP) as the substrate for contraction of demembranated cardiac muscle increased isometric force and the rate of force development and shortening at all levels of Ca^{2+} activation, including saturating $[Ca^{2+}]$ (pCa 4.0) [74,77,78,206]. The presence of dATP results in enhanced myosin binding to actin and an increase in the rates of P_i and dADP release and myosin detachments. As such, contractile properties can be improved by >50% over the range of $[Ca^{2+}]_i$ seen *in vivo*. Thus, replacement of ATP with dATP offers the potential to improve contraction independent of changes in $[Ca^{2+}]_i$ or adrenergic signaling.

To date, the effect of dATP has only been studied in demembranated cardiac tissue and with isolated contractile proteins. As such, its potential to improve intact cardiomyocyte contraction or cardiac function in situ is unknown. Cellular production of dATP occurs in the cytoplasm of mammalian cells by ribonucleotide reductase (Rrm), which removes a hydroxyl moiety from the 2-position on the ribose ring of ADP to produce dADP. dADP is then rapidly converted to dATP. Rrm consists of two subunit proteins, a catalytic activator (Rrm1) and free radical containing (Rrm2) subunit and is regulated by nucleoside triphosphate allosteric effectors [207]. While the details of regulating cellular RR content, enzymatic activity and cellular concentration [dATP] are unclear, it is known that both subunits are necessary for activity [208].

In the current study, we produced adenoviral vectors expressing cytomegalovirus (CMV) promoter driven Rrm1 or Rrm2, each along with green fluorescent protein (GFP) as a transduction reporter. Cultured adult rat cardiomyocytes were transduced with these vectors, and the rate and extent of myocyte contraction and relaxation and Ca^{2+} transient rise and decay (Fura-2 fluorescence) were monitored by video microscopy following a 48 hour viral incubation period. Here we show that these treatments significantly increased cellular [dATP], rate and extent of shortening, and rate of relaxation, with minimal effects on Ca^{2+} transients, at 0.5 Hz, 1 Hz and 2 Hz stimulation. Additionally, the [dATP] found in transduced cells (1-2% of adenine nucleotide content) was sufficient to increase sub-maximal Ca^{2+} activated force in skinned cardiac trabeculae. These experiments suggest that increases in cardiac intracellular Rrm and/or the dATP pool can significantly alter the actin-myosin crossbridge cycle to enhance cardiac contractility without impairing diastolic function or cardiomyocyte Ca^{2+} handling.

6.3 RESULTS

Transduction with recombinant adenovirus containing appropriate cDNA constructs driven by the CMV promoter was used to induce over-expression of muscle ribonucleotide reductase 1 (Rrm1) and 2 (Rrm2) in cultured adult and neonatal rat cardiomyocytes. Each adenovirus also contained a second expression cassette for green fluorescent protein (GFP), which was used as a reporter protein identifying successful transduction. Cardiomyocytes were infected with adenovirus containing genes for Rrm1 + GFP and Rrm2 + GFP or GFP for 2 days. Successful gene transfer, grossly indicated by green fluorescence with microscopy, indicated nearly 100% transduction efficiency (Supplemental Figure 6.S1). This is consistent with previous studies using cardiomyocytes [95]. Cell survival over this period was similar for all groups, including non-transduced control cells, suggesting these viral vectors did not compromise cardiomyocyte viability. Cardiomyocyte numbers and sarcomere lengths are summarized in Table 6.1. There was no difference in resting sarcomere length between groups, indicating that over-expression of Rrm1+Rrm2 (or GFP) did not increase Ca^{2+} independent activation.

6.3.1 Contractile analysis of cultured cardiomyocytes

The effects of Rrm1+Rrm2 over-expression on extent and rate of stimulated shortening-relengthening of adult rat cardiomyocytes were determined using video length-detection (IonOptix). Figure 6.1a shows representative shortening traces, and Figure 6.1b shows representative Ca^{2+} transients (Fura-2 fluorescence), for non-transduced (black), GFP-only (green), and Rrm1+Rrm2 (red) transduced cardiomyocytes. The data for all measurements at 0.5 Hz is summarized in Table 6.2. Cardiomyocytes transduced with Rrm1+Rrm2 (+GFP) had a significantly greater magnitude and rate of shortening vs. non-transduced cardiomyocytes and GFP-only transduced controls. This is illustrated in Figure 6.1c, which shows % differences in rate and extent of shortening, relaxation rate,

and time to 50% and 90% relaxation. While GFP has been reported to have a deleterious [209] or no effect [101,210] on contractility, it did not appear to act as a contractile inhibitor in this study. However, GFP did slow the 90% relaxation time, which was accompanied by a slower time to 50% and 90% decay of the Ca^{2+} transient (Figure 6.1c, Table 6.2). Regardless, Rrm1+Rrm2 over-expression increased the rate of relaxation and decreased the time to 50% relaxation, and this effect may be somewhat underestimated due to the presence of GFP. Figure 6.1d illustrates the % difference in Ca^{2+} transient properties, including minimal and maximal Ca^{2+}, and the time to 50% and 90% Ca^{2+} decay. There was no significant effect from either GFP or Rrm1+Rrm2 + GFP on minimal and maximal Ca^{2+}, indicating that enhanced contractility with Rrm1+Rrm2 was primarily due to increased myofilament responsiveness to activating Ca^{2+}. Interestingly, Rrm1+Rrm2 over-expression did speed Ca^{2+} re-sequestration, as indicated by a reduction the time to 50% and 90% decay. This could be due to increased SERCA activity and, in part, explain the increased maximal rate of cardiomyocyte relaxation at 0.5 Hz (Table 6.2) stimulation. Faster relaxation in Rrm1+Rrm2 over-expressing cardiomyocytes could also be due to faster crossbridge cycling, that leads to shortening induced thin filament inactivation and Ca^{2+} release from troponin C.

It is important to determine whether Rrm1+Rrm2 over-expression affects normal cellular response to increased stimulation frequency, as changes in heart rate are a normal physiological adaptation to systemic demand. Figure 6.2 summarizes the effect of increased stimulation frequency (0.5 to 1 to 2 Hz) on fractional shortening (6.2a), shortening velocity (6.2b), relaxation velocity (6.2c), and time to 90% relaxation (6.2c). The contractile response to stimulation frequency was similar between groups, and Rrm1+Rrm2 transduced cardiomyocytes maintained functional potentiation at all frequencies. Importantly, increased pacing frequency is associated with a positive lusitropic effect, shortening the time to 90% relaxation in all groups. There was little difference in non-transduced

myocytes vs. GFP-only transduced myocytes, except that time to 90% relaxation is longer at 0.5 Hz in GFP-only myocytes. The effect of stimulation frequency on Ca^{2+} transients was also assessed, and is summarized in Figure 6.3 for minimal Ca^{2+} (6.3a), maximal Ca^{2+} (6.3b) and time to 50% (6.3c) and 90% (6.3d) Ca^{2+} decay (DT_{50}, DT_{90}). As with contraction, there was no difference in Ca^{2+} transient behavior with increased stimulation frequency between non-transduced and Rrm1+Rrm2 transduced myocytes. GFP-only transduced cardiomyocytes had a slight increase in minimal Ca^{2+} at 2 Hz, and an increase in maximal Ca^{2+} at 1 Hz and 2 Hz, as compared to non-transduced myocytes, but the times to 50% and 90% decay were similar. As at 0.5 Hz, the times to 50% and 90% decay were decreased (faster decay) in Rrm1+Rrm2 transduced myocytes at both 1 and 2 Hz. Most importantly, although higher stimulating frequencies increased relaxation parameters in all groups, the relative increase in relaxation kinetics was maintained with Rrm1+Rrm2 over-expression, such that relaxation was improved, not impaired. Results for 1 Hz and 2 Hz stimulation are summarized in Supplemental Table 6.S1 and 6.S2, respectively.

We chose to perform these experiments at room temperature (22-24° C) to compare with the predominant number of reports for cultured cardiomyocytes in the literature [96–100]. However, a subset of measurements was made at 37°C to determine if the effects persist at physiological temperature. At 37°C (Supplemental Table 6.S3), shortening and Ca^{2+} transients were faster than at 22-24°C, but were similarly increased in cardiomyocytes transduced with Rrm1+Rrm2 vs. GFP-only transduced and non-transduced cells. Similarly, the rates of Ca^{2+} release and re-uptake were also increased at 37°C vs. room temperature, but with Rrm1+Rrm2 over-expression resulting in faster Ca^{2+} transient decay as was observed at ambient temperature.

Since there was little difference between groups in minimal and maximal Ca^{2+}, changes in contractility can best be explained by a change in myofilament responsiveness to activating Ca^{2+}. This is illustrated in Figure 6.4 as contractile response, defined here as cardiomyocyte fractional shortening divided by maximal Fura-2 fluorescence (peak Ca^{2+}). Cardiomyocytes expressing Rrm1+Rrm2 had significantly higher contractile response than non-transduced or GFP transduced cardiomyocytes at all stimulation frequencies. There was no difference in contractile response between GFP only or non-transduced myocytes except at 2 Hz, which can be primarily be attributed to increased maximal Ca^{2+} in GFP only myocytes with no increase in fractional shortening, reducing response.

6.3.2 Protein and nucleotide analysis

To verify increased Rrm mRNA, Rrm protein, and dATP production in Rrm1+Rrm2 transduced cells, neonatal rat cardiomyocytes were collected and processed for RT-PCR, western blotting and HPLC analysis of intracellular [ATP] and [dATP]. Neonatal cardiomyocytes were used to achieve high enough cell density for accurate nucleotide content analysis, as intracellular [dATP] is known to be in the pM range. Although there are structural differences between neonatal and adult cardiomyocytes, it is important to note that Rrm1+Rrm2 over-expression increased contractility to a similar extent in both cell types (Supplemental Figure 6.S2, Supplemental Table 6.S4). Interestingly, as neonatal cardiomyocytes have been used to study the effects of cellular engraftment following myocardial infarction [92], improved contractility in these cells may be another mechanism to improve cardiac function following an infarct. Rrm1 and Rrm2 mRNA was significantly increased following adenoviral transduction (Supplemental Figure 6.S3). Concomitant with this, Figure 6.5a and .5b illustrate that Rrm1 and Rrm2 transduced cardiomyocytes had greater than 24-fold and 46-fold increased Rrm1 and Rrm2 protein content, respectively. GAPDH was used as a loading control.

Figure 6.5c illustrates that Rrm1+Rrm2 transduced cardiomyocytes had ~10-fold increased cellular [dATP] as compared to GFP transduced cardiomyocytes (an increase to 0.35 nmol/mg protein). While this is robust, since [dATP] normally comprises less than 0.2% of total adenine triphosphate nucleotide, this increase in [dATP] represents only ~1.5% of the total adenine nucleotide pool. This suggests that only a small amount of dATP is required to significantly increase cardiomyocyte contractility.

To determine how the relatively small increase in cellular [dATP] might influence crossbridge binding and contraction, we compared the rates of nucleotide binding + acto-myosin S1 dissociation (k_{obs}) for ATP vs. dATP. Figure 6.6 shows the effect of increasing [ATP] and [dATP] on k_{obs} at 10°C and 20°C for mouse cardiac (alpha) myosin. There was no difference in k_{obs} between ATP and dATP at any [NTP] at either temperature. This was also true for fast and slow skeletal S1 myosin (Supplemental Figure 6.S4). This data indicates NTP binding to S1, and subsequent S1 dissociation from actin, is not different for dATP vs. ATP. Thus, it appears that enhanced contractility of R1R2 over-expressing cardiomyocytes is not likely due to a greater myosin affinity for dATP.

6.3.3 Crossbridge binding and force in demembranated trabeculae

To determine if small amounts of dATP increase force production, we activated contraction of demembranated rat cardiac trabeculae at pCa 5.6 (sub-maximal) and pCa 4.0 (maximal) in solutions containing 5 mM NTP, composed of either 100% ATP or 2% dATP, 98% ATP. The sub-maximal Ca^{2+} activation approximates the force levels attained during twitch activity, and was 30 ± 7% of maximal force (88.4 ± 1.9 mN/mm2). The example force trace in Figure 6.7A demonstrates that moving a trabeculae from 100% ATP solution to the 2% dATP, 98% ATP solution resulted in a significant increase in force, which was reversible upon transfer back to the 100% ATP solution. Figure 6.7B

summarizes this increase for all trabeculae activated and shows that 2% dATP, 98% ATP increased force 17.1 ± 0.02% ($p<0.05$) at pCa 5.6 but not during maximal Ca2+ (pCa 4.0) activation. Similarly, crossbridge binding, assessed by high frequency sinusoidal stiffness measurements, increased 16.0 ± 0.03% ($p<0.05$), which indicates that the increased force with 2% dATP, 98% ATP is due to increased crossbridge binding. Thus the data demonstrate that a relatively small increase in cellular [dATP] (1-2% of adenine nucleotide) is sufficient to significantly increase the contractile strength of intact cardiomyocytes by increasing the number of strong crossbridges.

6.4 DISCUSSION

The main objective of this study was to determine if over-expression of ribonucleotide reductase (Rrm1+Rrm2) increases cellular [dATP] and, in turn, increases contractility in intact cardiomyocytes without adversely affecting cardiomyocyte relaxation. Over-expression of Rrm1+Rrm2 resulted in increased cellular [dATP] to ~1.5% of the total adenine nucleotide pool, and this dramatically increased the extent and rate of myocyte shortening and rate of myocyte relaxation, while having no apparent effect Ca^{2+} transient properties.

Previous experiments in our laboratory using skinned cardiac trabeculae showed dATP increased isometric force and the rate of force development and shortening at all levels of Ca^{2+} activation, including saturating [Ca^{2+}] (pCa 4.0), but these studies were performed with 100% replacement of 5 mM ATP with 5 mM dATP in bathing solutions [74,77,78]. For our current study in intact cardiomyocytes we did not expect over-expression of Rrm1+Rrm2 to result in high (mM) levels of dATP. Others have shown that as little as 10% replacement of ATP with dATP is sufficient to see a gain of force in demembranated porcine trabeculae (15°C) [211] and replacement of ~30% increased contractility in intact embryonic chick cardiomyocytes [212]. In our studies the observed large

increases in contractility of adult rat cardiomyocytes occurred with a relatively small increase in cellular [dATP] resulting from over-expression of Rrm1+Rrm2, and a similar amount (2% dATP) significantly increased sub-maximal force in dememembranated trabeculae. It is possible there was a small population of contaminating cells (e.g., fibroblasts) that were either not as easily transduced or over-expressed less Rrm1+Rrm2, which would lead to underestimation of cardiomyocyte [dATP] from the HPLC analysis. However, considering the relative scarcity of non-cardiomyocyte cells in our culture, this confounding effect should be minimal. Our force measurements with demembranated trabeculae suggest this relatively small concentration of cellular [dATP] is sufficient to result in the increased contractility seen in intact cardiomyocytes. This may be advantageous in that large increases in [dATP] are not required to achieve contractile potentiation, thus reducing the potential for negative side effects [212,213].

It is interesting to speculate on how a relatively small increase in cellular dATP can improve cardiomyocyte function. Contractile response estimations (Figure 6.4) indicate increased contractility in Rrm1+Rrm2 transduced myocytes is primarily myofilament based, thus dATP likely has its effect primarily by improving myosin binding (to actin) and crossbridge cycling. The increase in sub-maximal steady-state force and stiffness seen in demembranated trabeculae activated with 2% dATP, 98% ATP supports this idea. This is similar to experiments where faster (alpha) myosin has been expressed in cardiomyocytes that normally express slower (beta) myosin, resulting in functional potentiation with no effect on Ca^{2+} transient amplitude [210]. One possibility we examined was that dATP affinity for cardiac myosin is much greater than ATP affinity for myosin, such that the increased level in cells (with Rrm1+Rrm2 over-expression) was utilized almost specifically by myosin. We have previously shown that ATP and dATP have similar binding affinity to skeletal myosin and actomyosin and a similar γ-phosphate cleavage equilibrium by myosin [214]. Here we

report that NTP binding and subsequent dissociation of cardiac α-myosin from actin does not differ for dATP vs. ATP, as assessed by k_{obs} (Figure 6.6). This suggests dATP has a similar binding affinity for cardiac myosin as ATP. For skeletal myosin we have also shown post-hydrolysis crossbridge binding and the rate of crossbridge detachment is increased with dATP [214]. This can explain an increase in the Ca^{2+} sensitivity of tension development, and a faster rate of tension development and shortening velocity in skinned skeletal muscle [214–216]. While we have not performed a detailed chemo-mechanical analysis with dATP in cardiac muscle, we have shown that it increases maximal crossbridge binding (as indicated from stiffness measurements) and isometric force by >40%, in addition to increasing k_{tr} and unloaded shortening velocity [77]. We have also shown that dATP significantly increases isometric force and k_{tr} in cardiac muscle at all levels of Ca^{2+}, whether the demembranated cardiac muscle was expressing primarily α- or β- myosin heavy chain [78]. This is important because, unlike skeletal muscle, the intracellular [Ca^{2+}] during a cardiac muscle twitch only reaches a level that is approximately within the half-maximally activating range. Additionally, cooperative thin filament activation in cardiac muscle is strongly influenced by strong binding crossbridges [74]. Based on our results that 2% dATP, 98% ATP significantly enhanced crossbridge binding and force in demembranated trabeculae, we propose that dATP results in the formation of a few additional strong binding crossbridges early on during the twitch, which provides a positive feedback amplification of thin filament activation. This results in greater total crossbridge binding, including crossbridges using ATP, during the cardiomyocyte twitch. Therefore, for our current experiments with cultured cardiomyocytes, it may be that a small increase in initial binding of myosin S1 heads was enough to cooperatively increase thin filament activation, resulting in the increased magnitude and rate of shortening. Future studies will be required to determine how R1R2 over-expression and resulting increases in cellular [dATP] affect cardiac function in situ, but previous experiments have demonstrated that even demembranated cardiomyocyte function translates to cardiac organ function [217]. Interestingly, a recent study investigating a small molecule myosin

activator (omecamtiv mecarbil) demonstrated functional potentiation at the cardiomyocyte level, via increased crossbridge binding that was very similar to results in the present study [13]. However, this molecule appeared to slow the times to peak shortening and 50% and 90% relaxation, which would likely increase time spent in systole while decreasing time spent in diastole. In contrast, Rrm1+Rrm2 over-expression increased fractional shortening without increasing the time to peak shortening, and shortened the times to 50% and 90% relaxation (Figure 6.1a, Table 6.1, Supplemental Tables 6.S1-3), which would allow more time for ventricular filling.

There was no adverse effect on relaxation with over-expression of Rrm1+Rrm2 (and the subsequent increase in [dATP]), in fact myocyte relaxation was enhanced. It is possible that this resulted, at least in part, from a faster decay of the Ca^{2+} transient. dATP could be used by other ATPases (besides myosin) such as the sarcoplasmic Ca^{2+} ATPase (SERCA), the plasma membrane Ca^{2+} ATPase (PMCA), and may also indirectly effect activity of the Na^{+}/ Ca^{2+} exchanger (NCX) [218]. An increase in SERCA activity could explain the increased decay rate of the Ca^{2+} transient, especially at 0.5 and 1.0 Hz stimulation. However, increased SERCA activity is known to increase SR Ca^{2+} stores [219], making more Ca^{2+} available for release during activation, which was not observed in Rrm1+Rrm2 transduced cardiomyocytes (Figure 6.1d). Furthermore, increased PMCA and NCX activity should result in a Ca^{2+} transient decay over time by extruding Ca^{2+} out of the cell. Because ~95% of activating Ca^{2+} is released from the SR in rat cardiomyocytes [53,220], Ca^{2+} extrusion from the cell would lead to progressively decreased Ca^{2+} transient amplitudes and contraction, which was not observed over the duration of these experiments. However, the specific mechanism behind increased Ca^{2+} transient decay rate warrants future investigation.

Since dATP increases the rate of crossbridge detachment [77,215] this may also explain a faster rate of relaxation in the current experiments with cultured cardiomyocytes. Although specific mechanisms that govern relaxation in intact cardiac muscle are not known, early phase relaxation in cardiac and skeletal myofibrils has been shown to be governed by the rate of crossbridge dissociation [221–224]. This would also be consistent with our finding that cardiomyocyte contractility was increased with Rrm1+Rrm2, because shortening rate in unloaded cells (as in culture) is primarily determined by crossbridge detachment rates [225,226], although cultured cardiomyocytes still contract against a small internal load. It is also possible that increased crossbridge detachment rate with dATP accelerates cooperative thin filament inactivation, by more rapidly decreasing the bound crossbridge population as thin filament Ca^{2+} binding decreases during relaxation. A more rapid decrease in bound crossbridge population could also increase the rate of Ca^{2+} dissociation from troponin, as demonstrated by Tikunova et al. [44], further accelerating relaxation.

In summary, dATP provides a dual benefit of positive inotropy and lusitropy in cultured rat cardiomyocytes, with little alteration of Ca^{2+} transient properties, and also increases isometric force production at physiologically relevant [Ca^{2+}]. These results warrant progression to animal studies to determine its potential to improve global cardiac function in normal and diseased hearts.

6.5 ACKNOWLEDGMENTS

We thank Dr. Hans Reinecke for assistance in adenoviral production, and Scott Lundy for assistance in preparing the manuscript. Funding support for this work was provided by from NIH HL07828 and AHA 2310117 (FSK), NIHHL65497 (MR), R21 HL091368 (MR and CEM), R01 HL084642 (CEM) and P01HL094374 (CEM). MR is an Established Investigator of the American Heart Association.

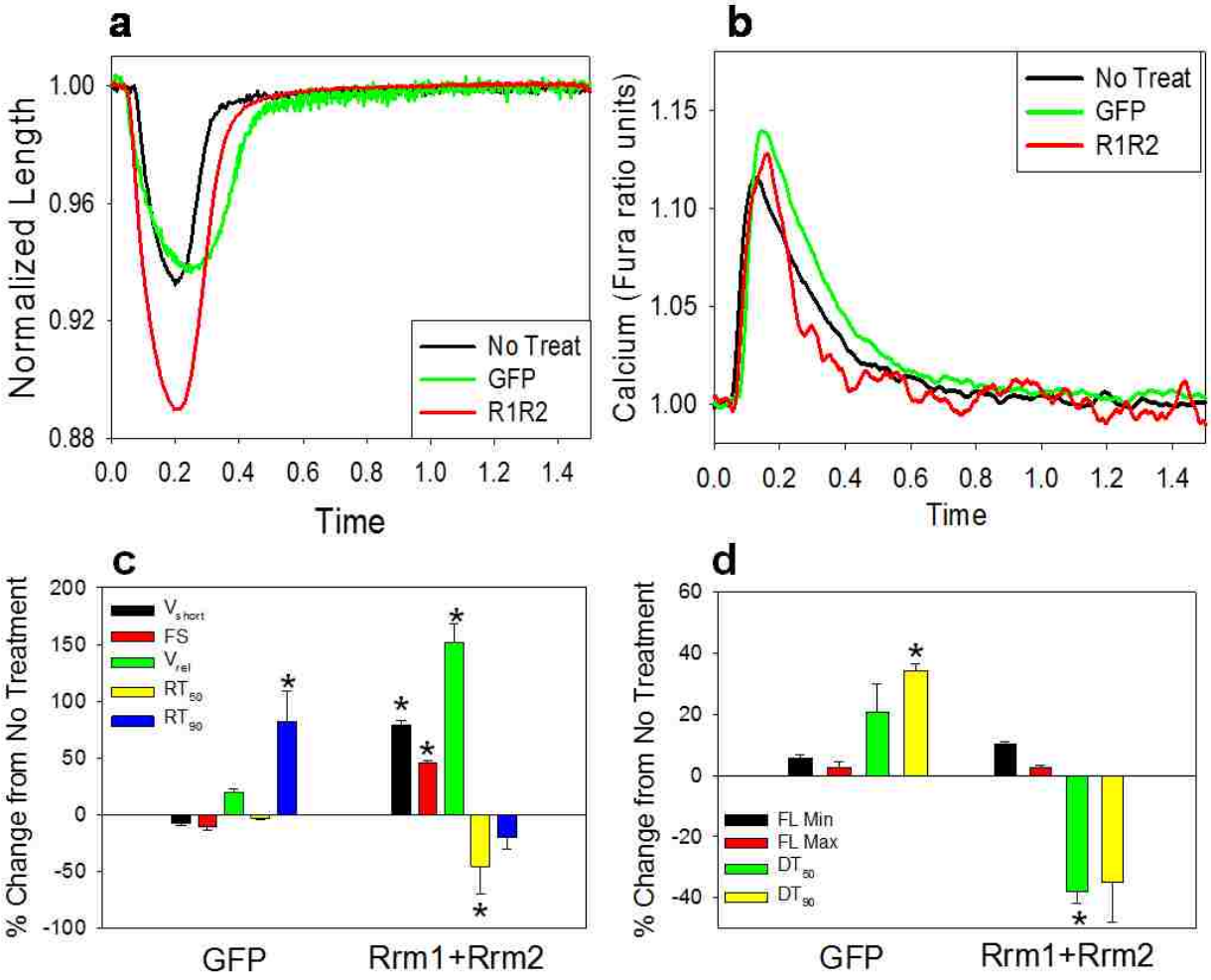

Figure 6.1: Representative traces and data summary. Representative cell length traces (a) and Ca2+ transients (b, Fura-2 fluorescence) of non-transduced (black), GFP-only (green), and Rrm1+Rrm2+GFP (red) transduced cardiomyocytes. Percentage change in contractile (c) and Ca^{2+} transient (d) properties of GFP-only and Rrm1+Rrm2+GFP transduced myocytes, stimulated at 0.5 Hz, as compared to non-transduced myocytes. V_{short} = velocity of shortening; FS = fractional shortening; V_{rel} = maximal relaxation velocity; $RT_{50,90}$ = time to 50% and 90% relaxation, respectively; FL = fluorescence; $DT_{50,90}$ = time to 50% and 90% Ca^{2+} decay, respectively *p<0.05 as compared to Non-Transduced.

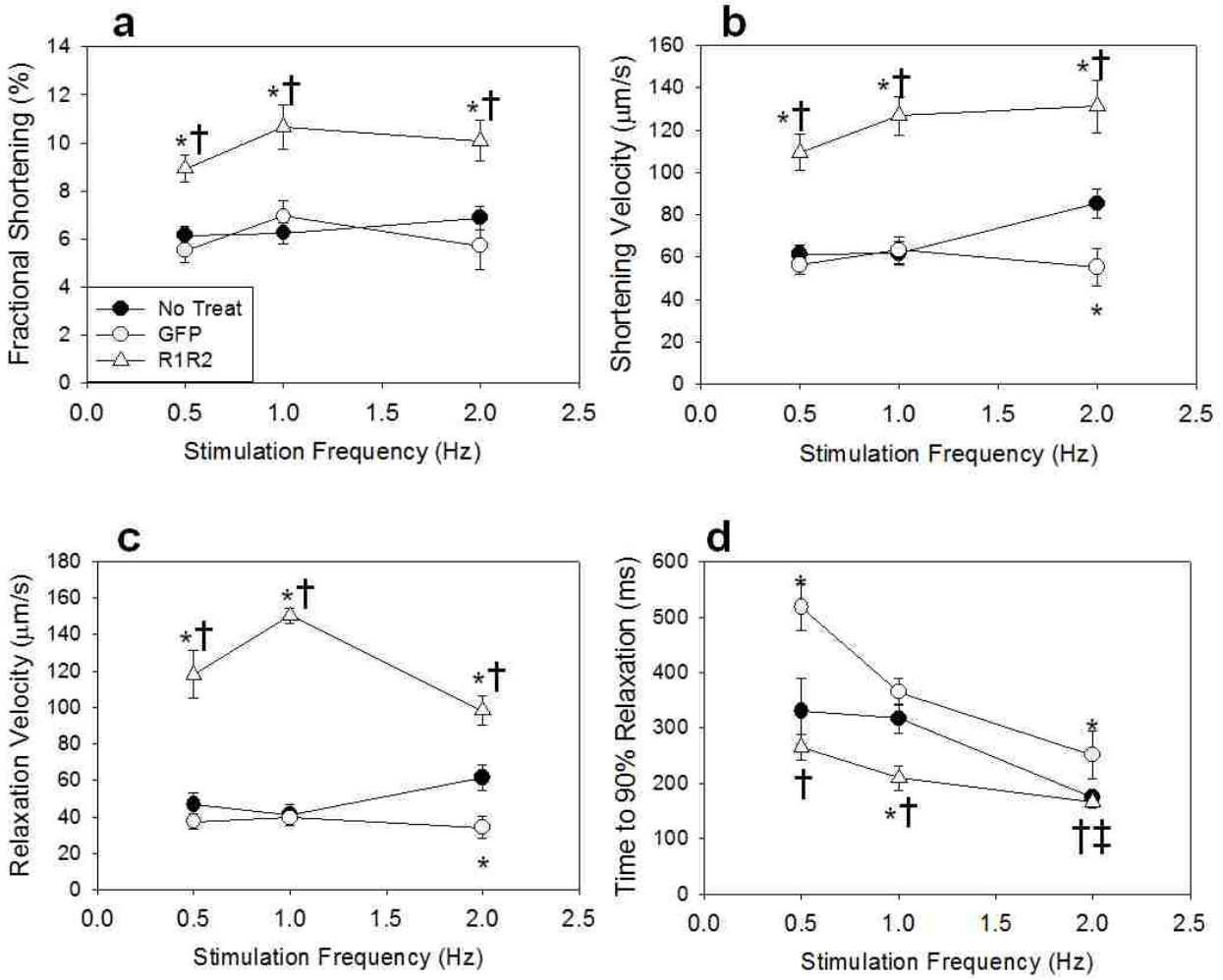

Figure 6.2: Effect of stimulation frequency on contractile properties. Rrm1+Rrm2 transduced myocytes (open triangles) respond similarly to stimulation frequency as GFP-only transduce open circles) and non-transduced myocytes (closed circles) but show elevated fractional shortening (a) and shortening velocity (b) at all frequencies. Relaxation velocity (c) and time to 90% relaxation (d) are also similar between groups, with time to relaxation shortening as stimulation frequency increases. * = $p<0.05$ as compared to Non-Transduced, † = $p<0.05$ as compared to GFP, ‡ = $p<0.05$ as compared to 0.5 Hz for all groups.

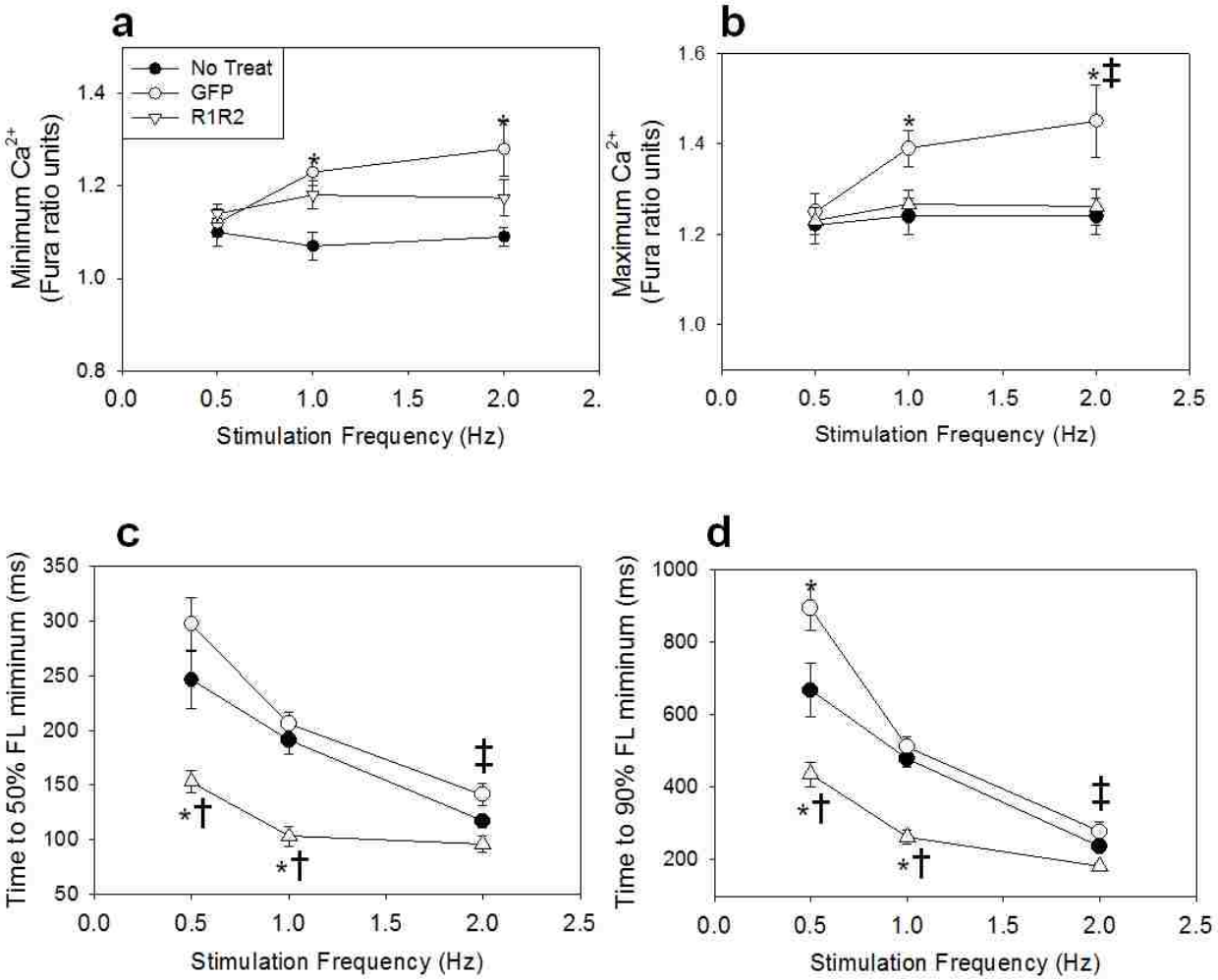

Figure 6.3: Effect of stimulation frequency on Ca^{2+} handling properties. Rrm1+Rrm2 transduced myocytes (open triangles) respond similarly to stimulation frequency as non-transduced myocytes (closed circles) in minimal (a) and maximal (b) fluorescence, while GFP-only transduced myocytes (closed circles) showed a greater increase in both as frequency increased. As with cardiomyocyte relaxation, Ca^{2+} transient decay time (DT) to 50% (c) and 90% (d) is shortened with increased stimulation frequency, but both are dramatically shortened in R1R2 transduced cardiomyocytes. * = $p<0.05$ as compared to Non-Transduced, † = $p<0.05$ as compared to GFP, ‡ = $p<0.05$ as compared to 0.5 Hz for all groups.

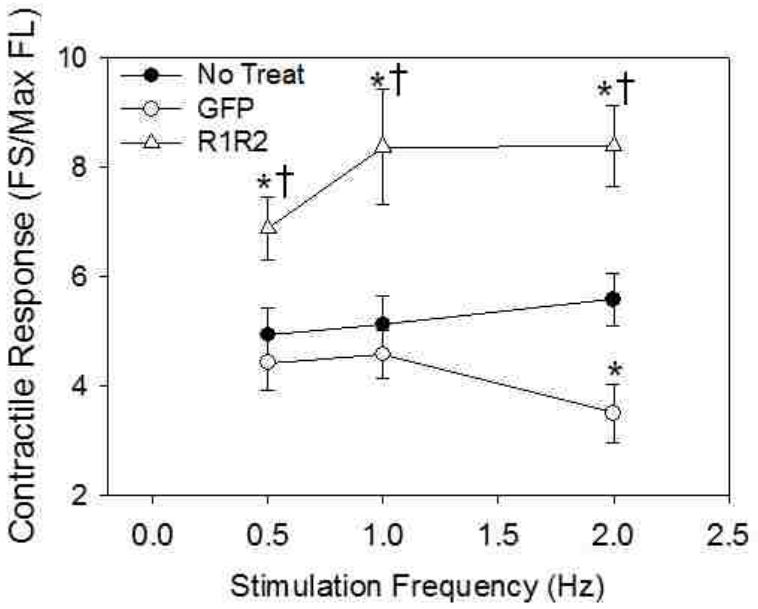

Figure 6.4: Contractile Responsiveness. Contractile response as assessed as fractional shortening divided by maximal Fura fluorescence (peak Ca^{2+}) indicates Rrm1+Rrm2 transduced cardiomyocytes (open triangles) are significantly more responsive to Ca^{2+} at all stimulation frequencies, while GFP-only transduced cardiomyocytes (open circles) are less responsive to Ca^{2+} only at 2Hz stimulation frequency as compared to non-transduced cardiomyocytes (closed circles). * = $p<0.05$ as compared to Non-transduced, † = $p<0.05$ as compared to GFP.

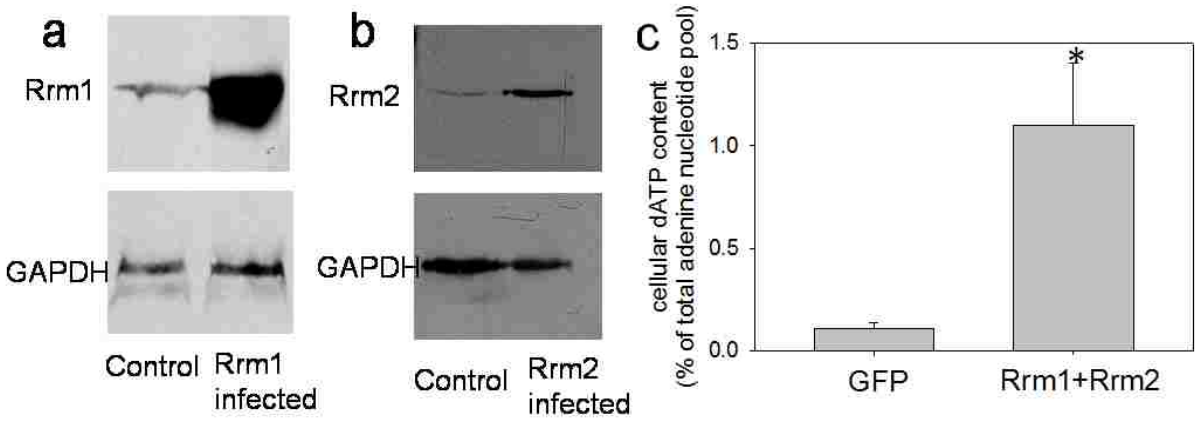

Figure 6.5: Increased Rrm and dATP. (a) Western blot of Rrm1 transduced neonatal rat cardiomyocytes probed with anti-Rrm1 antibody indicates a >24-fold increase in Rrm1. (b) Western blot of Rrm2 transduced neonatal rat cardiomyocytes probed with anti-Rrm2 antibody indicates a > 46-fold increase in Rrm2. (c) Rrm1+Rrm2 over-expression significantly increased intracellular [dATP] by >10-fold in neonatal rat cardiomyocytes as assessed by HPLC analysis. * = $p<0.05$ as compared to GFP transduced cardiomyocytes.

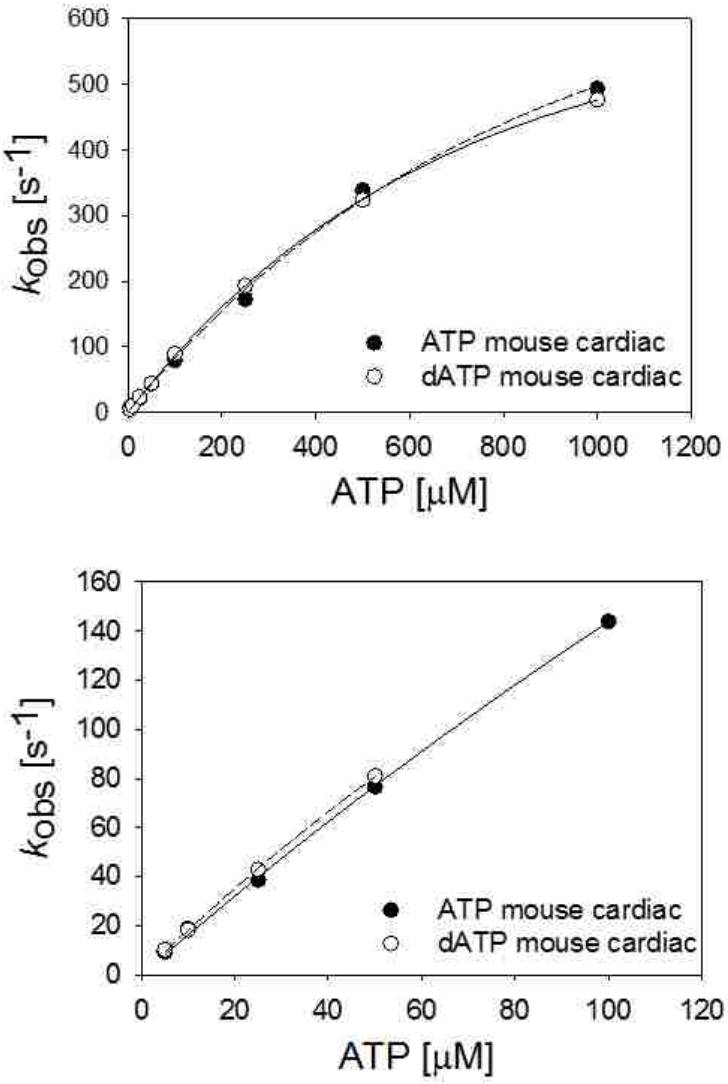

Figure 6.6: Nucleotide binding and actin-myosin dissociation. Rapid kinetic measurements of nucleotide binding and actin-myosin dissociation of mouse cardiac myosin taken at 10°C (top) and 20°C (bottom). There was no difference in k_{obs} between ATP and dATP at any [NTP] at either temperature.

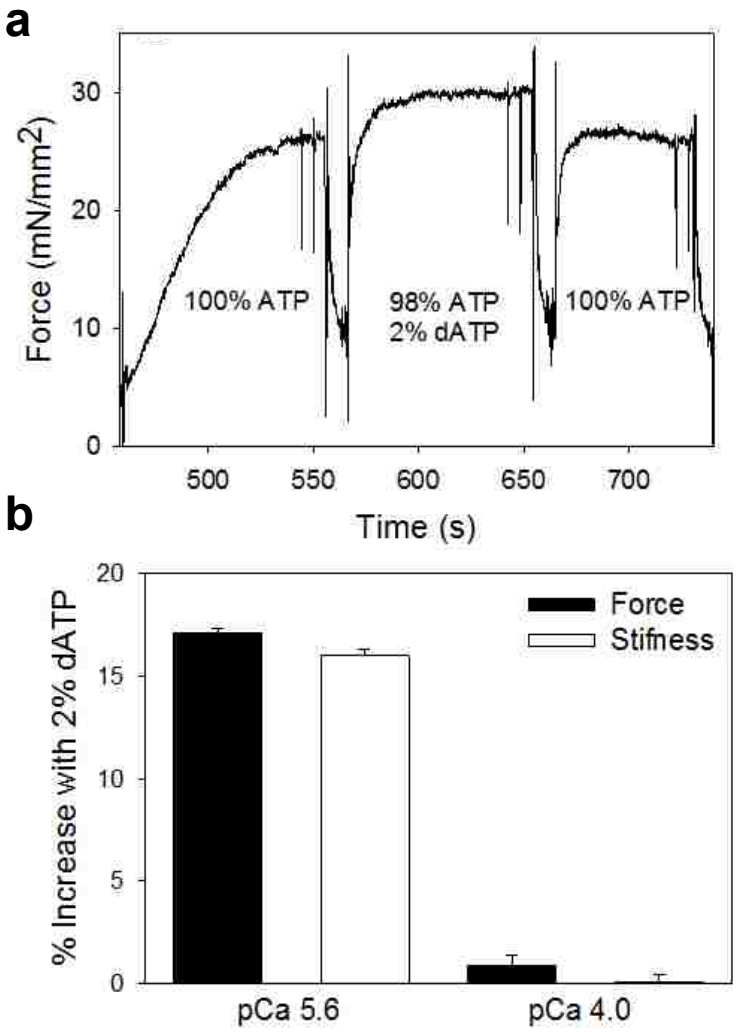

Figure 6.7: Isometric force increases with 2% dATP. Isometric force development of demembranated cardiac trabeculae activated with 2% dATP, 98% ATP vs. 100% ATP (5 mM [NTP] total). (a) Force trace with pCa 5.6 activation. (b) Summary of % increase in force with 2% dATP in activation solutions for sub-maximal (pCa 5.6), but not maximal (pCa 4.0) Ca^{2+} activation.

Table 6.1: Cell dimensions of experimental groups. N = number of hearts, n = number of cardiomyocytes.

	N	n	SL (μm)	Cell length (μm)
Non-transduced	5	51	1.88 ± 0.03	90.4 ± 1.8
Control (GFP)	5	50	1.84 ± 0.03	89.1 ± 1.5
R1R2 (GFP)	5	52	1.82 ± 0.02	91.6 ± 1.7

Table 6.2: Contractile and Ca^{2+} transient values at 0.5 Hz stimulation. * = $p<0.05$ as compared to No Treat, † = $p<0.05$ as compared to GFP, ‡ = $p<0.05$ as compared to 0.5 Hz for all groups.

	Fractional Shortening (%)	Maximal Shortening Rate (μm/s)	Time to Peak (ms)	Maximal Relaxation Rate (μm/s)	RT_{50} (ms)	RT_{90} (ms)	Minimal Ca^{2+} (Fura ratio units)	Maximal Ca^{2+} (Fura ratio units)	DT_{50} (ms)	DT_{90} (ms)
Non-transduced	6.2 ± 0.4	61.1 ± 4.4	173 ± 12	46.8 ± 6.5	208 ± 28	330 ± 59	1.10 ± 0.02	1.22 ± 0.04	246 ± 26	666 ± 74
Control (GFP)	5.5 ± 0.5	56.5 ± 4.4	217 ± 15*	37.5 ± 4.3	202 ± 25	518 ± 42*	1.12 ± 0.03	1.25 ± 0.04	297 ± 24	893 ± 63*
R1R2 (GFP)	8.9 ± 0.5*	109.5 ± 8.7*	177 ± 7	117.9 ± 13.1*	113 ± 7*†	265 ± 23†	1.14 ± 0.02	1.23 ± 0.03	153 ± 10*†	435 ± 34*†

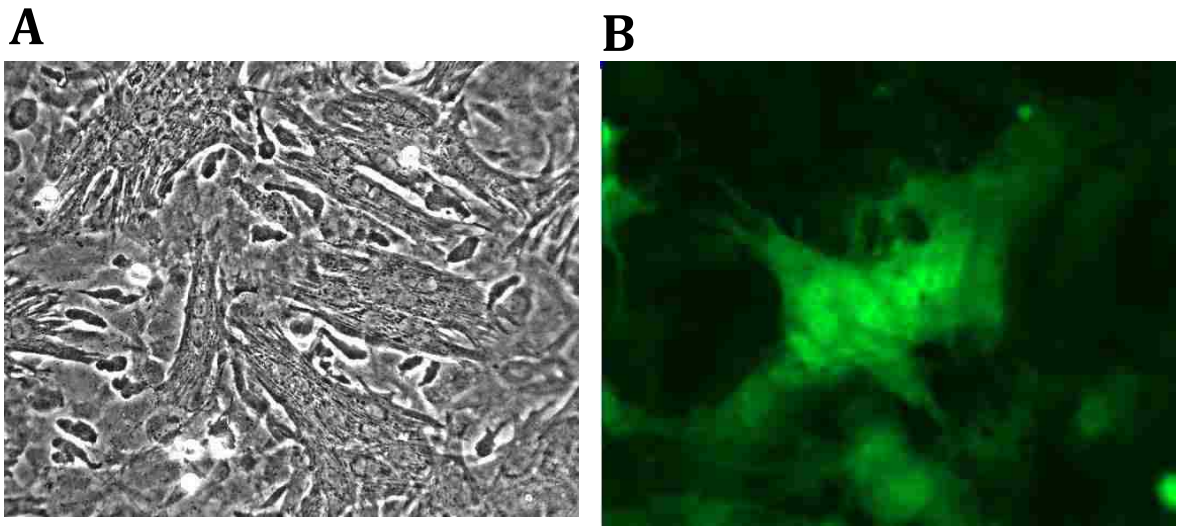

Figure 6.S1: Cultured NRCs following adenoviral transduction of Rrm1+GFP and Rrm2+GFP under white light (A) and fluorescence microscopy (B) at 20X magnification.

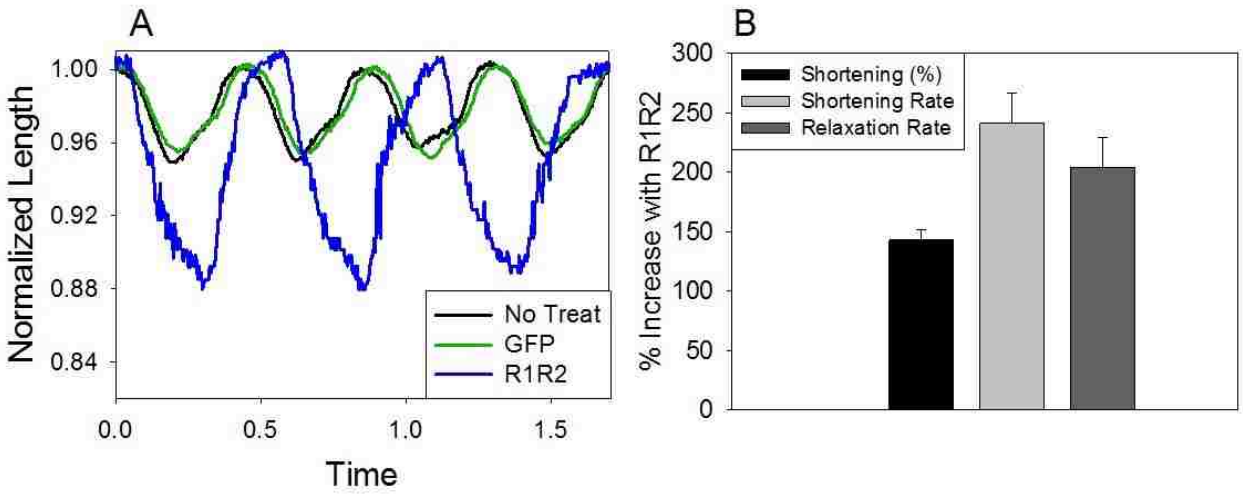

Figure 6.S2: (A) Representative neonatal cardiomyocyte shortening traces from non-transduced (black), GFP-only (green), and Rrm1+Rrm2 (blue) transduced cardiomyocytes. Rrm1+Rrm2 transduced cardiomyocytes had a significantly increased extent and rate of shortening (B), while the intrinsic beating frequency and time to relaxation were unaffected.

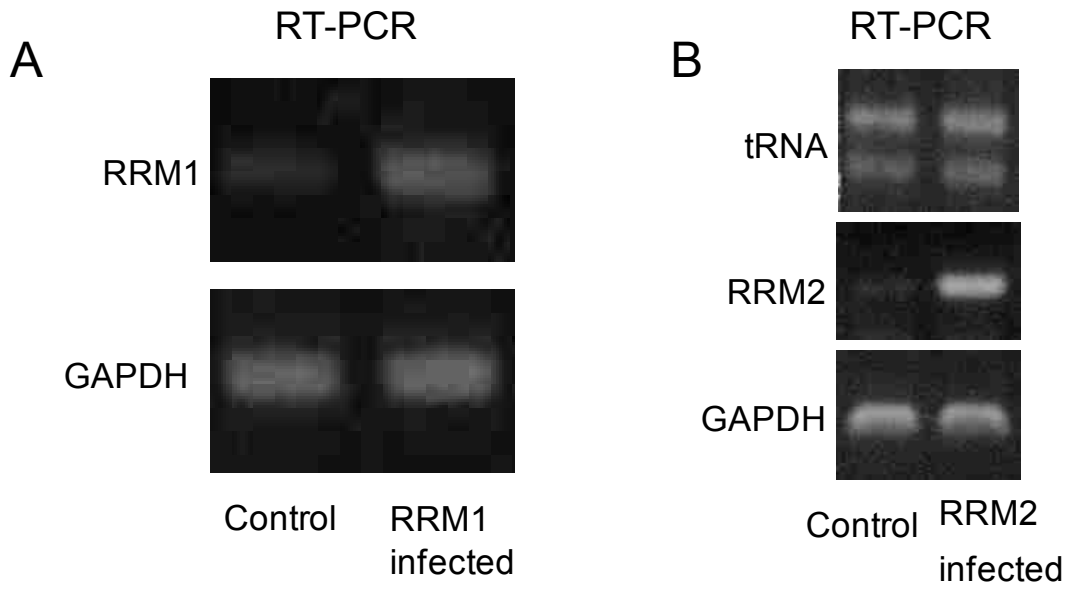

Figure 6.S3: (A) RT-PCR analysis of transduced neonatal cardiomyocytes demonstrated increased Rrm1 mRNA in transduced cells compared to control (non-transduced) cells. (B) RT-PCR analysis of transduced neonatal rat cardiomyocytes demonstrated increased Rrm2 mRNA in transduced cells compared to control (non-transduced) cells.

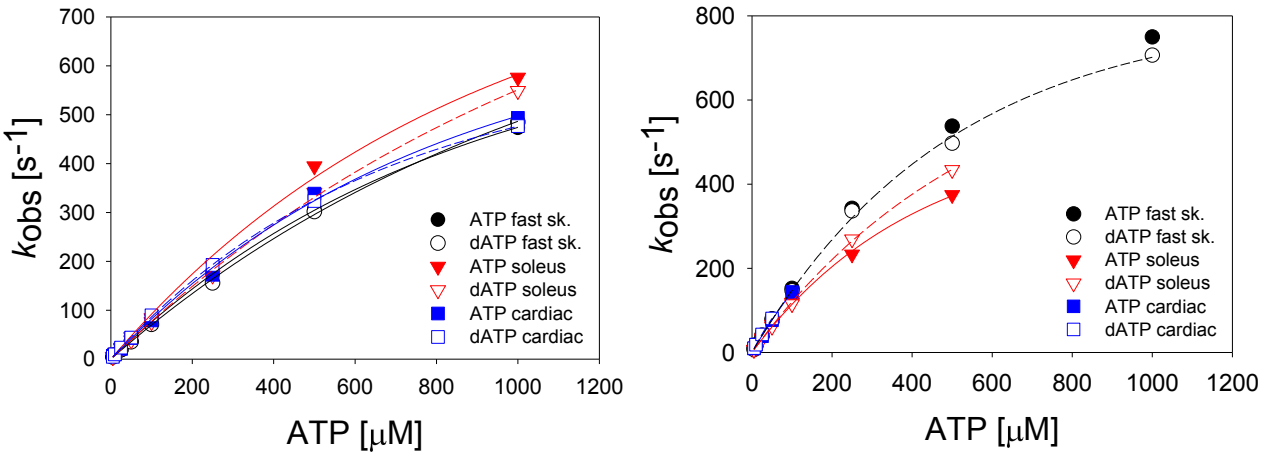

Figure 6.S4: Rapid kinetic measurements of nucleotide binding and actin-myosin dissociation taken at 10°C (A) and 20°C (B). There was no difference in kobs between ATP and dATP at any [NTP] at either temperature.

Table 6.S1: Contractile and Ca^{2+} transient values at 1 Hz stimulation. * = $p<0.05$ as compared to Non-Transduced, † = $p<0.05$ as compared to GFP, ‡ = $p<0.05$ as compared to 0.5 Hz for all groups.

	Fractional Shortening (%)	Maximal Shortening Rate (μm/s)	Time to Peak (ms)	Maximal Relaxation Rate (μm/s)	RT_{50} (ms)	RT_{90} (ms)	Minimal Ca^{2+} (Fura ratio units)	Maximal Ca^{2+} (Fura ratio units)	DT_{50} (ms)	DT_{90} (ms)
Non-transduced	6.2 ± 0.4	61.9 ± 5.7	189 ± 15	41.0 ± 5.5	191 ± 21	317 ± 27	1.07 ± 0.03	1.24 ± 0.04	191 ± 13	478 ± 23
Control (GFP)	6.9 ± 0.6	63.2 ± 6.4	184 ± 8	39.7 ± 4.7	156 ± 15	365 ± 25	1.23 ± 0.03	1.39 ± 0.04	206 ± 11	511 ± 27
R1R2 (GFP)	10.7 ± 0.9*†	126.8 ± 9.2*†	178 ± 13	150.2 ± 4.2*†	110 ± 12*	209 ± 22*†	1.14 ± 0.03	1.27 ± 0.03	103 ± 9*†	262 ± 20*†

Table 6.S2: Contractile and Ca^{2+} transient values at 2 Hz stimulation. * = $p<0.05$ as compared to Non-Transduced, † = $p<0.05$ as compared to GFP, ‡ = $p<0.05$ as compared to 0.5 Hz for all groups.

	Fractional Shortening (%)	Maximal Shortening Rate (μm/s)	Time to Peak (ms)	Maximal Relaxation Rate (μm/s)	RT_{50} (ms)	RT_{90} (ms)	Minimal Ca^{2+} (Fura ratio units)	Maximal Ca^{2+} (Fura ratio units)	DT_{50} (ms)	DT_{90} (ms)
Non-transduced	6.9 ± 0.5	85.3 ± 6.7	155 ± 6	61.6 ± 7.0	92 ± 5	174 ± 7	1.09 ± 0.02	1.24 ± 0.04	117 ± 6	237 ± 10
Control (GFP)	5.7 ± 1.0	55.3 ± 8.9	157 ± 8	34.3 ± 6.1	113 ± 10	251 ± 43	1.28 ± 0.06	1.45 ± 0.08	141 ± 10	277 ± 27
R1R2 (GFP)	10.1 ± 0.8*†	131.2 ± 12.3*†	163 ± 10	98.3 ± 7.7*†	96 ± 8	166 ± 11	1.17 ± 0.04	1.26 ± 0.04	96 ± 7*	182 ± 11*

Table 6.S3: Contractile and Ca^{2+} transient values at 37°C at 0.5 Hz stimulation. * = $p<0.05$ as compared to Non-transduced.

	Fractional Shortening (%)	Maximal Shortening Rate (µm/s)	Time to Peak (ms)	Maximal Relaxation Rate (µm/s)	RT_{50} (ms)	RT_{90} (ms)	Minimal Ca^{2+} (Fura ratio units)	Maximal Ca^{2+} (Fura ratio units)	DT_{50} (ms)	DT_{90} (ms)	Response (FS/Max Ca^{2+})
Control (GFP)	6.5 ± 0.9	152.7 ± 9.5	109 ± 6	134.1 ± 24.7	57 ± 8	176 ± 32	1.07 ± 0.02	1.16 ± 0.02	139 ± 27	275 ± 37	6.8 ± 0.8
R1R2 (GFP)	9.2 ± 0.7*	189.0 ± 9.6*	113 ± 7	156.8 ± 28.3	58 ± 10	176 ± 63	1.07 ± 0.02	1.17 ± 0.03	93 ± 15*	266 ± 33	9.3 ± 0.8

Table 6.S4: Contractile measurements of neonatal rat cardiomyocytes. CL/s = Cell lengths per second; RT10, RT50, RT90, times to 10%, 50%, and 90% relaxation, respectively. * Significant difference from non-transduced, † Significant difference from Control (GFP) ($p<0.05$).

	N	Beat Rate	Fractional Shortening (%)	Maximal Shortening Rate (CL/s)	Maximal Relaxation Rate (CL/s)	RT_{10} (ms)	RT_{50} (ms)	RT_{90} (ms)
Non-transduced	26	71 ± 3	4.7 ± 0.5	3.1 ± 0.5	2.3 ± 0.2	60 ± 1	156 ± 21	271 ± 45
Control (GFP)	20	71 ± 4	4.2 ± 0.5	2.7 ± 0.3	2.3 ± 0.3	57 ± 8	153 ± 24	237 ± 41
RRM1/2 + GFP	35	70 ± 3	10.2 ± 0.8*†	9.2 ± 1.2*†	7.0 ± 1.0*†	65 ± 8	142 ± 15	241 ± 23

Table 6.S5: Minimal and maximal [Ca^{2+}] as calculated by the Grynkiewicz equation. * = $p<0.05$ as compared to Non-transduced.

	Minimal Ca^{2+} @ 0.5 Hz (nmol/L)	Maximal Ca^{2+} @ 0.5 Hz (nmol/L)	Minimal Ca^{2+} @ 1 Hz (nmol/L)	Maximal Ca^{2+} @ 1 Hz (nmol/L)	Minimal Ca^{2+} @ 2 Hz (nmol/L)	Maximal Ca^{2+} @ 2 Hz (nmol/L)
Non-transduced	146 ± 17	324 ± 14	132 ± 14	327 ± 24	130 ± 18	307 ± 17
Control (GFP)	157 ± 13	305 ± 17	228 ± 14*	445 ± 21*	287 ± 18*	543 ± 16*
R1R2 (GFP)	157 ± 16	305 ± 7	201 ± 13	307 ± 12	190 ± 21	309 ± 22

Chapter 7. Development of a cardiac muscle-targeted viral gene delivery system

7.1 ABSTRACT

Current clinical treatments of heart failure are primarily palliative and attempt to manage the progression of the disease rather restore cardiac function and can often cause significant side-effects. Accordingly, gene therapy has been considered an alternative novel therapeutic approach to treat heart failure. While different gene delivery methods have their own advantages and challenges with targeting the heart, viral vectors, specifically adeno-associated virus serotypes (AAV), are among the most promising. AAVs possess important advantages over the other delivery methods and viral strategies: they have low immunogenicity and are not pathogenic in humans, and they provide significantly longer transgene expression including a sustained myocardial transduction. This work in conjunction with others suggests that AAV serotype 6 (AAV6) is an ideal candidate to use for development of a cardiac muscle gene therapy for heart failure. The goal of the work in this chapter was to engineer a novel cardiac muscle-specific *in vivo* gene delivery system to investigate how acute changes in myofilament Ca^{2+} binding properties (via L48Q cTnC) affect whole heart function. We made significant progress towards this goal by developing a novel AAV6 gene delivery system capable of effectively transducing the myocardium after systemic delivery. The AAV6 $cTnT_{455}$ mCherry-P2a-cTnC-Flag system produced uniform and robust mCherry expression throughout the myocardium, which demonstrates the $cTnT_{455}$ promoter is highly effective at driving gene expression in the heart. Additionally, the AAV6 serotype limited the transduction in off-target, non-cardiac tissues. These preliminary results suggest that our AAV6 is effective at targeting gene expression to cardiac muscle. Future work will focus on determining the L48Q cTnC-Flag expression profile in the myocardium, and the effects of L48Q cTnC-Flag expression on whole heart function.

7.2 INTRODUCTION

Heart failure is characterized by decreased systolic and/or diastolic function and has a variety of etiologies including myocardial infarction (MI), ischemia/reperfusion injury, diabetes, high blood pressure, and hypertrophic (HCM) and dilated cardiomyopathy (DCM). Current clinical treatments of heart failure are primarily palliative and attempt to manage the progression of the disease rather restore cardiac function, and these treatments can often cause significant side-effects [6]. The significant lack of effective clinical treatments underscores the need to develop new therapeutic strategies for heart failure focused on recovery of cardiac function.

Accordingly, gene therapy has been considered an alternative a novel therapeutic approach to treat heart failure. This strategy is able to modulate gene expression profiles and/or correct specific gene defects that are associated with development of heart failure [16,17]. Additionally, gene transfer, either through permanent modification of the host genome or expression of a transgene in target cells, is a powerful experimental tool for discovering the primary etiologies and mechanistic bases for disease pathogenesis as well as treating the disease. Different gene delivery methods have been explored, including naked DNA [227,228], non-viral vehicles such as liposomes and polymer-based DNA carriers [229,230], and viral vectors [231–234]. While each of the delivery methods have their own advantages and challenges, viral vectors, specifically adeno-associated virus serotypes (AAV), are among the most promising because they possess important advantages over the other delivery methods and viral strategies: they have low immunogenicity and are not pathogenic in humans [235], and they provide significantly longer transgene expression [233] including a sustained myocardial transduction [232–234].

All AAVs are Dependoviruses (belonging to the Parvoviridae viral family). As a Dependovirus, AAV is incapable of replicating in host cells under most physiological circumstances and requires coinfection

with a helper virus for replication [16]. The AAV capsid is a non-enveloped proteinaceous capsid made of three proteins termed VP1, VP2, and VP3, and the capsid seems to be devoid of most posttranslational modifications [16]. They contain a single-stranded DNA genome encoding two genes: the rep gene that encodes four critical proteins involved in DNA replication, integration, and packaging, and the cap gene that encodes three proteins which, via alternative splicing, make up the protein coat of the virus [236]. The AAV genome also contains two ITRs, which are important for genome packaging, replication, and stability [237–241]. Over 100 distinct serotypes of AAV have been identified while new serotypes are continuously being identified [242–246]. While AAV has distinct advantages that make it appealing for cardiac gene therapy, such as low immunogenicity, limited integration into the host genome, and long-term persistent expression in the target tissues, it is relatively limited in its cloning capacity [16]. The entire expression cassette of interest, including the open reading frame and transcriptional regulatory sequence, must not exceed ~4.5 kb, allowing for 300 bp of ITR sequence [239].

Despite their limited cloning capacity, AAV vectors have been widely used for cardiac gene transfer. A variety of work has been done investigating the effectiveness of different AAV serotypes (1-9) at cardiac gene transfer, and serotypes 1, 6, 7, 8, and 9 appeared to be the most efficient at transduction [247–253]. It has been, however, very difficult to identify the serotype that exhibits the highest efficacy for cardiac gene therapy because of that fact that in many of these studies different routes of administration, different animal models and ages of animals, and different virus titers and serotypes have been used. Recently, Zincarelli C, et al. [254] tackled this question and demonstrated that a comparison of AAV serotypes 1-9 delivered to the heart the same way (via intracoronary injection) elucidated that AAV6 achieved the highest transduction levels in the myocardium without negatively affecting cardiac function or causing local inflammation. This work in conjunction with others

[242,248,249,254–256] strongly suggests that AAV6 is an ideal candidate to use for development of a cardiac muscle gene therapy for heart failure.

The goal of this chapter was to engineer a novel cardiac muscle-specific *in vivo* gene delivery system to investigate how acute changes in myofilament Ca^{2+} binding properties (via L48Q cTnC) affect whole heart function. Based on the previous work that demonstrated the efficacy of AAV6 at transducing the myocardium, I designed and developed an AAV6 gene delivery system to express L48Q cTnC specifically in cardiac muscle *in vivo*. As demonstrated in previous work in our lab and in Chapters 3 and 5, L48Q cTnC increased the Ca^{2+} binding affinity of cTn and myofilament Ca^{2+} sensitivity, which enhanced overall contractility in cardiomyocytes from healthy and infarcted hearts. Based on the promising *in vitro* results from L48Q cTnC expression, the hypothesis driving this chapter is that acute expression of L48Q cTnC *in vivo* will enhance whole heart function. The design, development, and characterization of a novel cardiac muscle-targeted AAV6 gene delivery system for the expression of L48Q cTnC *in vivo* reached a significant milestone towards the goal and hypothesis of this chapter as well as the long-term goal of the project. Additional studies will be required to further investigate the therapeutic potential of L48Q cTnC and its ability to enhance whole heart function.

7.3 RESULTS

7.3.1 Adeno-associated viral vector (AAV6) design and production

To design a novel vector system capable of effectively targeting and transducing cardiac muscle *in vivo* for long-term, stable gene expression duration with minimal immunogenicity, I collaborated with Dr. Jeff Chamberlain's laboratory at UW. Based on the work from the Chamberlain lab [248,256,257] and work done by others [247–253], I designed a recombinant AAV6 virus for *in vivo*

delivery and expression of L48Q cTnC in the myocardium. Importantly, the AAV6 system was designed to enable systemic administration of the virus since this is one the most clinically relevant administration methods when considering potential therapeutic applications of a cardiac gene therapy.

In order to develop an AAV6 system capable of systemic delivery, it was necessary to make the AAV6 system targeted specifically to cardiac muscle to enable sufficient levels of L48Q cTnC expression only in the myocardium and to limit/prevent off-target expression in other tissues. To avoid expression of L48Q cTnC in off-target tissues, the CMV promoter in the rAVV6 backbone [248,256,257] was replaced with the cardiac specific $cTnT_{455}$ promoter (provided by Dr. Steven Hauschka's lab at UW). The $cTnT_{455}$ promoter is based on the human cTnT promoter and contains a truncated cTnT basal promoter with two truncated cTnT enhancers. The cTnT promoter has been shown to be very effective at cardiac muscle-specific expression *in vitro* and *in vivo* [258–263], while also having driven stronger gene expression in cardiac muscle than other cardiac muscle-targeted promoters, such as cardiac myosin light chain and β myosin heavy chain [264]. Furthermore, the cTnT promoter has been shown to be extremely effective at myocardial-specific gene expression following systemic delivery of an AAV system by increasing gene expression in the myocardium by nearly 100-fold as compared to other tissues while maintaining > 40% of the expression strength of CMV promoter [255].

Downstream of the $cTnT_{455}$ promoter, our two genes of interest– mCherry and WT or L48Q cTnC-Flag – were cloned in and separated by the P2a peptide. After multiple iterations of different AAV6 systems and *in vivo* testing, the final version used for the work in this dissertation was the following: $cTnT_{455}$ mCherry-P2a-cTnC-Flag. The fluorescent protein, mCherry, was included as a second

reporter of AAV6 virus expression, and provided another tool to assess the robustness and uniformity of vector transduction and expression throughout the myocardium and other tissues. Following mCherry, the P2a peptide was inserted, which is a relatively small peptide (20 amino acids) that permits co-translation of two proteins from a single mRNA strand. The P2a sequence prevents the formation of a peptide bond between the glycine and proline at the end of the peptide sequence resulting in the ribosome skipping to the next codon [265,266] and nascent peptide cleavage between glycine and proline. This ribosomal skip and peptide cleavage yields two separate proteins. After cleavage, the short P2A peptide (~18 amino acids) remains on the C-terminus of the upstream protein [267,268]. We inserted mCherry upstream the P2a peptide to place the residual P2a peptide on C-terminus of mCherry instead of cTnC-Flag, which may have interfered with cTnC function or Flag tag detectability in previous iterations. Following the P2a peptide, WT or L48Q cTnC with the Flag tag was included. Flag tag was attached to the C-terminus of the cTnC proteins to enable exogenous protein identification and quantification of myofilament incorporation. Flag tag is only 8 amino acids long, relatively charge neutral, and is a commonly used and commercially available tag (Sigma, St. Louis, MO). Based on previous work with Flag tag [269], we did not anticipate the Flag tag interfering with native cTnC protein folding or function. Because both mCherry and cTnC-Flag genes were driven by same promoter and translated from the same mRNA, they should be expressed at approximately a 1:1 ratio, thus providing two methods to determine the robustness of AAV6 expression in the myocardium [267,268,270].

The full rAAV6 $cTnT_{455}$ mCherry-P2a-cTnC-Flag was purified and then amplified in HEK 293 cells [256]. Vector genomes (vg) were determined relative to plasmid standards using a SV40 poly-adenylation region oligonucleotide ^{32}P end-labeled probe with Southern blot hybridization and

confirmed by quantitative RT-PCR [256]. Amplification and purification yielded an AAV6 viral titer of ~$1.2x10^{14}$ vector genomes (vg)/mL and 0.4 mL total of virus.

7.3.2 Ventricular cross-section mCherry fluorescence and immunohistochemistry

At the end of the 4 week *in vivo* expression study, a portion of the mouse hearts were used to examine mCherry fluorescence in the myocardium as an indication of robustness and uniformity of AAV6 transduction and gene expression in the heart. Representative ventricular cross-sections from AAV6 injected mice in Figure 7.1 demonstrate that there was very strong and uniform mCherry expression, and thus AAV6 expression throughout the myocardium. In the control mice that received only HBSS injection, there was no mCherry expression in the ventricle, which demonstrates that the mCherry signal in the AAV6 mouse ventricles was purely from the virus. These initial results were very promising and suggested that our AAV6 system was highly effective at transducing the myocardium and producing robust gene expression.

In light of the promising mCherry fluorescence results in the myocardium, we sought to also determine the expression profile of L48Q cTnC-Flag since it is the potential therapeutic gene we are truly trying to express to the myocardium. We attempted to determine the L48Q cTnC-Flag expression profile using anti-Flag tag immunohistochemistry (IHC) on ventricular cross-sections. Unfortunately, the results from the anti-Flag IHC were inconclusive. After repeated attempts to troubleshoot and optimize the IHC conditions and eliminate non-specific anti-Flag binding in negative control tissue (data not shown), the conclusion reached was that the anti-Flag antibody being used was not well-suited for the IHC assay even though it worked well for Western blots. As a result, additional studies will need to be done with different anti-Flag antibodies to characterize the L48Q cTnC-Flag ventricular expression profile. Overall, these initial results suggest that the AAV6

system was able to successfully transduce the mouse myocardium, and the $cTnT_{455}$ promoter was able to drive robust and uniform expression of mCherry *in vivo*.

7.3.3 AAV6 biodistribution analysis

At the end of the 4 week *in vivo* expression period, various tissues from the mice were collected to determine the biodistribution of AAV6 vector genomes from systemic delivery. The following tissues were collect for mCherry RT-PCR analysis of AAV6 vector genome presence and quantity: atria, ventricles, lung, liver, gastrocnemius, soleus, tibialis anterior, and extensor digitorum longus. The preliminary tissue battery (atria, ventricles, lung, liver, gastrocnemius) provided an initial indication of the number vector genomes that were present in the myocardium and in off-target tissues. The systemic administration of $6x10^{12}$ AAV6 vector genomes resulted in, on average, $7.6x10^5$ ± 2.2 $x10^5$ vg in the ventricles, $4.2x10^5$ ± 2.1 $x10^5$ vg in the atria, and $3.4x10^6$ ± 1.2 $x10^6$ vg in the liver, while the other tissues had noticeably fewer vector genomes with $7.4x10^4$ ± 4.9 $x10^4$ vg in the lung and $2.0x10^4$ ± 1.2 $x10^4$ vg in the gastrocnemius. Because of the function the liver plays within the body of filtering most entities in circulation, especially toxin-like substances, it is not surprising that the liver contained the highest number of vector genomes. This has also been observed by others with systemic administration of AAV systems [254,255].

The number of AAV6 vector genomes was normalized to the total number of host genome copies in each tissue to better understand approximately how many vector genomes were present on a per nuclei basis. The RT-PCR analysis of a housekeeping gene, such as Pax7, which was present in the host genome but not in the episomal AAV6 vector genome, enabled quantification of only the host genomes from each tissue sample. Using this data, it was possible to normalize the AAV6 vector genomes by the number of total host genomes. The normalized RT-PCR data for the preliminary

tissue battery for each AAV6 injected animal and an HBSS-injected control animal are shown in Figure 7.2. In the atria (pink bars) and ventricles (red bars), there were an average 13±1.4 AAV6 vg/host vg and 20±2.4 AAV6 vg/host vg, respectively. In contrast, there were only 1.4±0.2 AAV6 vg/host vg in the lung (yellow bars) and 0.76±0.08 AAV6 vg/host vg in the gastrocnemius (green bars). The liver again contained the highest ratio at 51±4.0 AAV6 vg/host vg (light blue bars). For comparison, the HBSS-injected control mouse data only contained negligible background levels of vg/host genomes in any tissue: atria 0.4±0.1 vg/host vg, ventricle 0.1±0.01 vg/host vg, lung 0.04±0.00 vg/host vg, liver 0.2±0.02 vg/host vg, and gastrocnemius 0.3±0.3 vg/host vg. Overall, the data demonstrate that the novel AAV6 delivery system successfully transduced the atria and ventricles more effectively than other tissues (excluding the liver), and limited transduction in off-target tissues, including skeletal muscle.

7.3.4 Western blot analysis of ventricular tissue

In order to characterize the protein expression levels that were achieved in the myocardium from systemic delivery of our AAV6 system, the ventricular tissue that was prepared for RT-PCR analysis was also prepared for Western blot analysis. Since the fluorescence and IHC analysis of ventricular cross-sections yielded promising evidence of vector expression based on mCherry fluorescence, I attempted to characterize the expression of other components of the AAV6 system downstream of mCherry: the P2a peptide and L48Q cTnC-Flag. I hypothesized that since there was robust mCherry expression in the myocardium, there should also be P2a peptide present in the ventricles since it is attached to the C-terminus of mCherry. The anti-2a peptide Western blot confirmed the presence of mCherry-P2a, and it also suggested the presence of a second protein containing the P2a peptide. In Figure 7.3, there are two P2a-positive bands that are only present in the ventricles from AAV6 injected mice, while there were no P2a-positive bands in the ventricle from HBSS control mice or the

L48Q cTnC-Flag positive control. These data demonstrate that P2a-positive proteins were indeed a result of AAV6 expression in the myocardium. Furthermore, mCherry is 28.8 kDa and the addition the residual P2a peptide increases the molecular weight of mCherry-P2a to ~30 kDa, which is the size of the larger P2a-positve protein. These data confirm that both mCherry and the P2a peptide were effectively expressed in the myocardium. Interestingly, the second P2a-postive band is ~20-25 kDa. It is unclear what protein this 2a peptide-positive band represents, but it is worth noting that L48Q cTnC-Flag is ~19 kDa and the addition of ~ 2kDa from P2a would increase the molecular weight of P2a-L48Q cTnC-Flag to approximately ~21 kDa, which is near the size of the second band.

I also attempted to characterize L48Q cTnC-Flag expression in the myocardium using an anti-Flag Western blot in the lower panel of Figure 7.3. Interestingly, both of the P2a-positve bands were also Flag tag positive in the ventricles from all AAV6 mice. Again, there was no Flag tag-positive signal in the ventricle from HBSS control mice, which demonstrates the Flag tag positive proteins are also only a product of AAV6 expression. The ~20-25kDa Flag tag positive band is slightly larger than the L48Q cTnC-Flag positive control sample (~19 kDa) in Figure 7.3, and the fact that this band was also P2a-positive suggests it could be P2a-L48Q cTnC-Flag. Overall, the anti-Flag Western blot data suggest that L48Q cTnC-Flag may be present in the myocardium of AAV6 mice, but additional studies are required to confirm and clarify these results.

7.3.5 In vivo heart function assessment via echocardiography

To preliminarily examine the *in vivo* effects of AAV6-mediated expression of L48Q cTnC on healthy whole heart function, echocardiography data from mice that received $6x10^{12}$ AAV6 $cTnT_{455}$ mCherry-P2a-L48Q cTnC-Flag vector genomes and HBSS injected control mice are summarized in Figure 7.4. The echocardiography data from mice was collected before delivery of AAV6 to establish a baseline

for all animals and collected each of the 4 weeks following the AAV6 injection. There were no significant differences in average body weight or average heart rate between control (24±0.2 g; 613±10 beats/min) and AAV6 mice (24±0.1 g; 621±7 beats/min) at the end of the 4 weeks. There were also no differences between HBSS control and AAV6 mice in fractional shortening, or left-ventricular diameter at end-diastole (LVDD) and end-systole (LVSD) at any point in the 4 week period (Figure 7.4). While these preliminary results suggest that acute *in vivo* expression the current version of the AAV6 system did not adversely affect healthy whole heart function, it is difficult to draw many insights from the echocardiography data at this point without knowing if sufficient expression of L48Q cTnC-Flag was achieved in the myocardium. Additional studies are required to more rigorously examine the effects acute AAV6 $cTnT_{455}$ mCherry-P2a-L48Q cTnC-Flag expression may have on whole heart function.

7.4 DISCUSSION

The goal of this chapter was to engineer a novel cardiac muscle-specific *in vivo* gene delivery system to investigate how acute changes in myofilament Ca^{2+} binding properties (via L48Q cTnC) affect whole heart function. Significant progress towards this goal was made by developing a novel AAV6 gene delivery system capable of successfully transducing the myocardium after systemic delivery. The mCherry-P2a data in various tissue and protein level assays demonstrated this through uniform and robust expression of mCherry throughout the ventricles. At this early stage in the development and application of the AAV6, it is difficult to speculate about how much of the myocardium would need to be transduced in order to produce a change in whole heart function. But, based on these results, I am confident that the ability transduce a sufficient amount myocardium will not be a limiting factor for the AAV6 system. The strong, robust mCherry signal also corroborates previous data by others [242,248,249,254–256] that the AAV6 serotype is highly effective at transducing the

myocardium, and that the $cTnT_{455}$ promoter is highly effective at driving gene expression in the heart [258–263]. Preliminary evidence that our AAV6 system limited off-target transduction in non-cardiac tissues was also demonstrated based on the biodistribution analysis of AAV6 vector genomes. The RT-PCR data indicated that the majority of the AAV6 vector genomes were present in the atria, heart, and liver while very few vector genomes were in the other non-cardiac tissues examined. When the vector genome transduction data are coupled with the cardiac-specific $cTnT_{455}$ promoter driving the gene expression, they suggest that the AAV6 system limited the gene expression in non-target tissues. Even if a very low number of vector genomes were present in non-target tissue, the $cTnT_{455}$ promoter would function as a method of preventing gene expression in non-cardiac tissue. Additional protein expression analysis for mCherry and/or L48Q cTnC-Flag in the non-cardiac tissue will be required in order to characterize and confirm the cardiac-specific expression properties of the AAV6 system.

An additional part of the goal for this chapter was to eventually use the AAV6 system to investigate how acute changes in myofilament Ca^{2+} binding properties (via L48Q cTnC) affect whole heart function. However, before it is possible to investigate the effects on whole heart function acute expression of L48Q cTnC may have, it is necessary to be able to demonstrate successful AAV6-mediated L48Q cTnC expression in the myocardium. While I was able to demonstrate high levels of mCherry-P2a expression, the data required to demonstrate *in vivo* L48Q cTnC-Flag expression is still inconclusive. The design of the AAV6 system to include the P2a peptide, which allowed both mCherry and L48Q cTnC-Flag to be driven by the same promoter and to be translated from the same mRNA, and previous work with 2a peptides [267,268,270] implied that our system should have achieved approximately 1:1 expression of mCherry and L48Q cTnC-Flag. Therefore, the robust expression profile of mCherry-P2a would suggest that L48Q cTnC-Flag is present in the myocardium at similar levels. While the anti-Flag Western blot results did suggest that this might be the case to some extent,

those same results were somewhat confusing since they suggested that what may be the L48Q cTnC-Flag band also contains the P2a peptide. However, the P2a peptide should only be present on mCherry and not on L48Q cTnC-Flag. Additional studies are required to determine if the anti-Flag Western blot results were caused by a lack of antibody binding specificity or actual L48Q cTnC-Flag expression. The initial attempts to demonstrate L48Q cTnC-Flag expression throughout the myocardium using IHC encountered issues with the efficacy of the anti-Flag antibody in the IHC assay. The results from that study need to be repeated with a different anti-Flag antibody in hopes that it will provide more meaningful insights into the L48Q cTnC-Flag expression profile in the myocardium. Alternatively, additional Western blot analysis may aid in the identification and clarification of the P2a and Flag tag-positive protein of ~20-25 kDa.

Because of the uncertainty about the level of *in vivo* L48Q cTnC-Flag expression achieved with the AAV6 system, it is difficult to draw any concrete conclusions from the preliminary *in vivo* whole heart function data. While the echocardiography data did not show any adverse changes in cardiac function as a result of acute AAV6 *in vivo* expression over the 4 week study, it is difficult to make any additional conclusions about the effects of L48Q cTnC-Flag expression on healthy heart function. There are a number of questions in regards to L48Q cTnC-Flag expression that still need to be answered before it is possible to conclude anything from the echocardiography data. Because of that, it is important to keep in mind that the goal of this chapter was two-fold: 1) to engineer and characterize the transduction and expression efficacy of our AAV6 system, and 2) to assess the impact L48Q cTnC-Flag expression has on whole heart function. Once L48Q cTnC-Flag expression in the myocardium has been demonstrated, additional *in vivo* studies will be required to examine the effects of L48Q cTnC-Flag expression on healthy and/or diseased whole heart function. These studies will also be crucial in determining whether the enhancement in contractility at the intact cardiomyocyte level

from L48Q cTnC expression and incorporation into the myofilaments (Chapter 5) is recapitulated at the whole organ level.

Taken together, the results in this chapter demonstrated the development of a novel cardiac muscle-targeted AAV6 gene delivery system that is able to successfully transduce the myocardium robustly and uniformly *in vivo* with limited off-target tissue expression after systemic administration. In doing so, I also reached significant milestones towards both the chapter and long-term project goals. Importantly, the work in this chapter set the stage for additional studies to characterize the L48Q cTnC-Flag expression profile and the therapeutic potential of the AAV6 $cTnT_{455}$ mCherry-P2a-L48Q cTnC-Flag system to enhance whole heart function.

7.5 ACKNOWLEDGMENTS

I would like to thank Jeff Chamberlain's lab for their help developing the AAV6 system. I would especially like to thank Guy Odom for his excellent help with the design, develop, and characterization of the AAV6 system. His insights and discussions were invaluable to this work. I would also like Stephen Hauskchka's lab for their development and assistance with the $cTnT_{455}$ promoter.

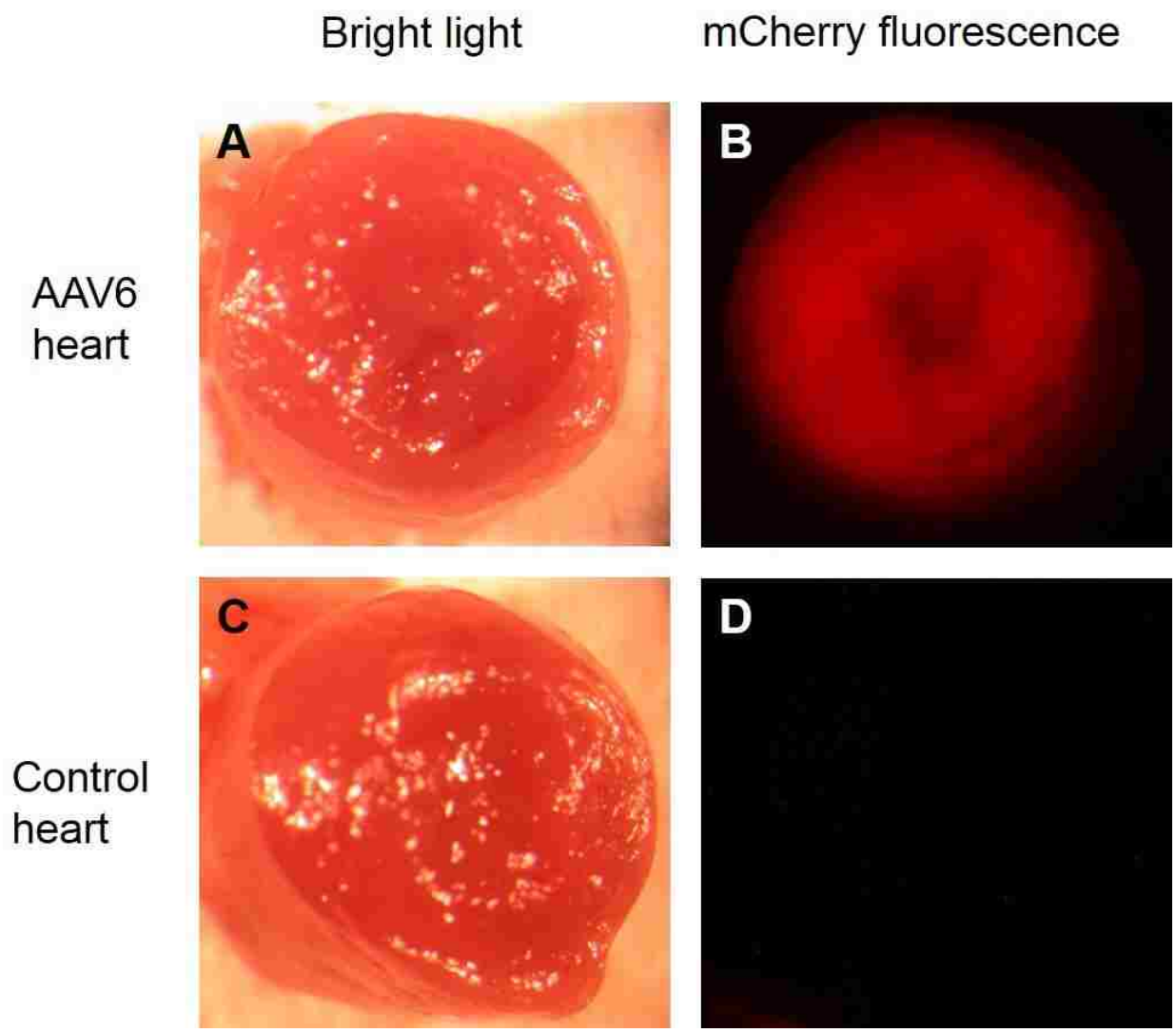

Figure 7.1: Myocardial AAV6 vector expression profile in ventricular cross-sections. Ventricular cross-sections of hearts from an AAV6 injected mouse (A, B) and an HBSS injected control mouse (C, D). Ventricular cross-sections under bright light (A) and mCherry fluorescent light (B) of an AAV6 injected mouse show robust and uniform vector expression throughout the myocardium. By comparison, ventricular cross-sections under bright light (C) and mCherry fluorescent light (D) of an HBSS injected mouse do not show any vector expression. 18X magnification.

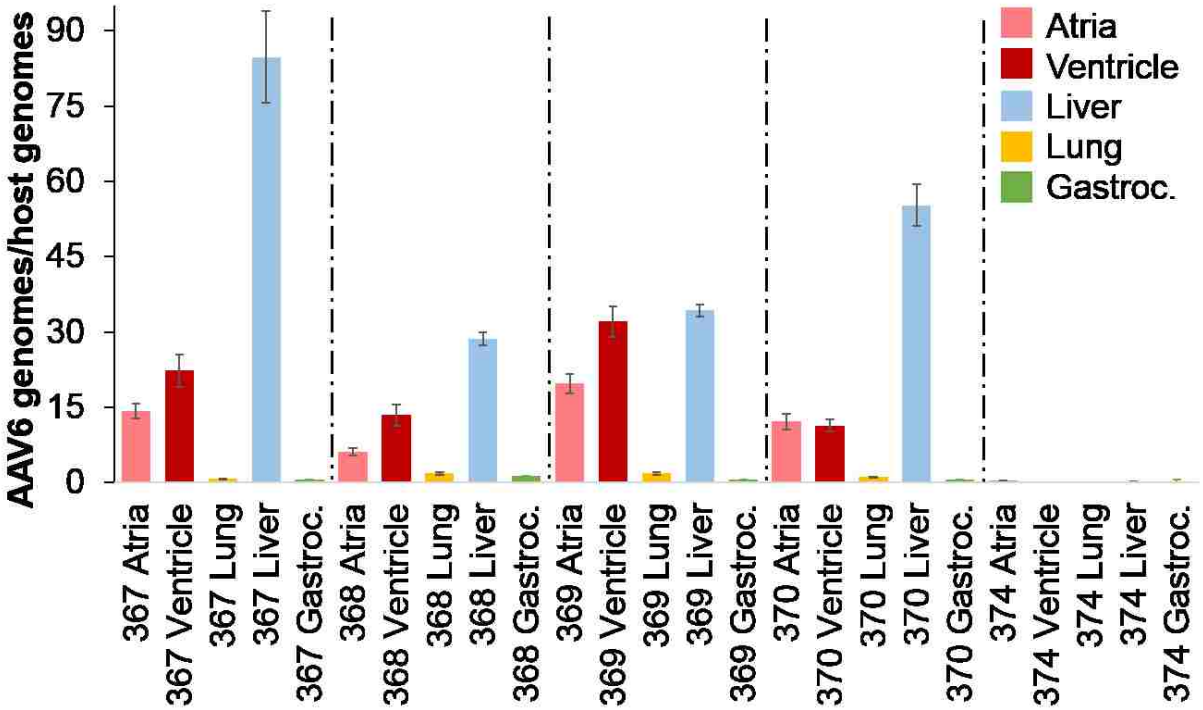

Figure 7.2: Analysis of AAV6 vector genome biodistribution in cardiac and non-cardiac tissue. Quantification of AAV6 vector genomes in the atria (pink), ventricles (red), lung (yellow), liver (light blue), and gastrocnemius (green) for AAV6 injected mice (367-370) and an HBSS injected control mouse (370) were normalized to the number of host genomes in each tissue sample. The liver contained the highest number of AAV6 genomes/host genomes follow by the ventricles and then the atria, which indicates effective transduction of all of those tissues. The lung and gastrocnemius contained similar numbers of AAV6 genomes/host genomes to that of an HBSS injected control mouse, which demonstrates limited off-target transduction in non-cardiac tissue (excluding the liver). Values are means ± S.D.

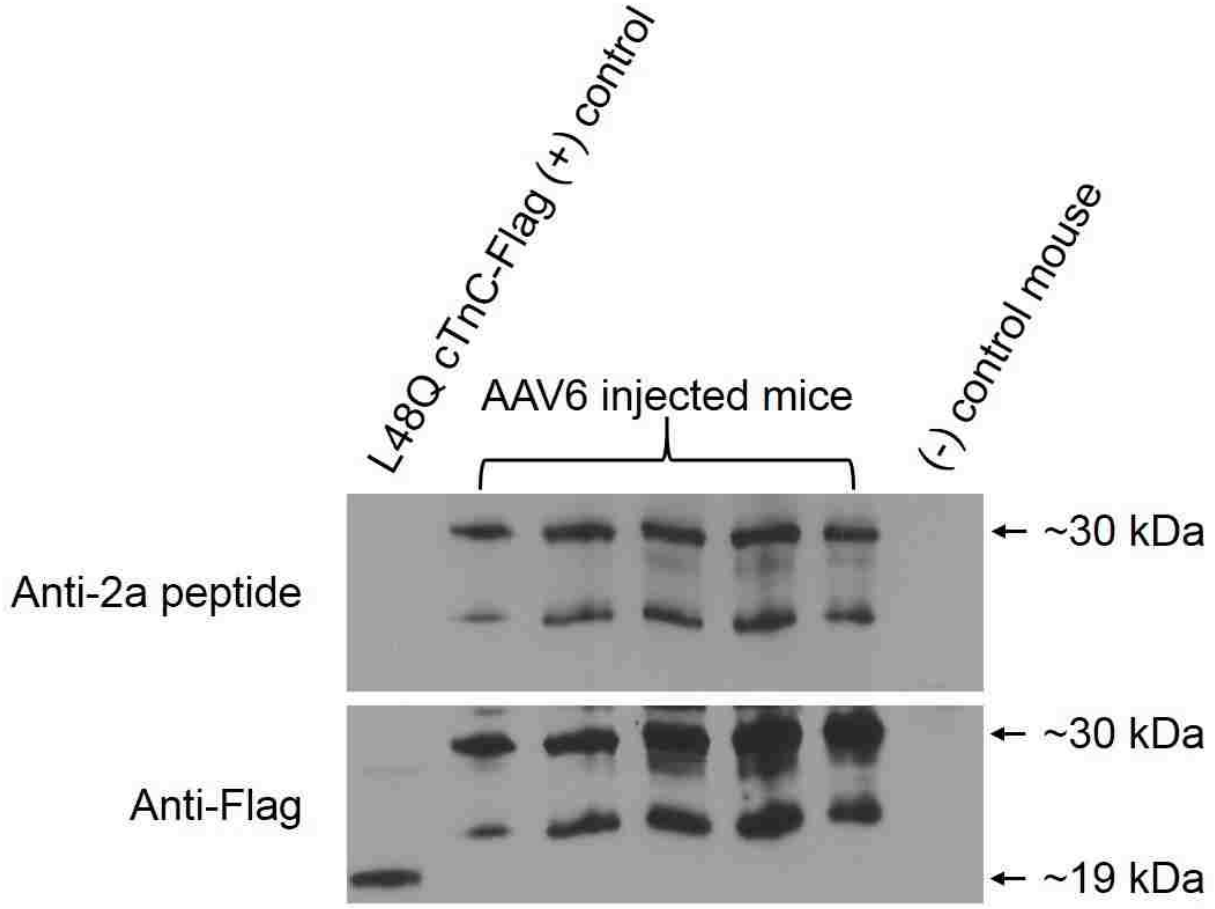

Figure 7.3: Western blot analysis of AAV6-mediated protein expression in ventricular tissue from AAV6 injected mice. Lane (left to right): 1) L48Q cTnC-Flag positive control from HEK 293 cell lysate; 2-6) AAV6 injected mice, 366-370; 7) HBSS injected negative control mouse, 374. The anti-2a peptide Western blot (top panel) shows 2a-positve bands only in AAV6 injected mice at ~30 kDa, which corresponds with the size of mCherry-P2a. It is unclear what the smaller band represents at this time. The anti-Flag Western blot (lower panel) shows two Flag-positive bands that are the identical sizes as the 2a-positve bands in the panel above. The small band at ~20-25 kDa is larger than the cTnC-Flag alone, which could suggest that some of the P2a peptide remained on the L48Q cTnC-Flag. The HBSS injected negative control mouse sample did not contain any 2a peptide or Flag-positive proteins.

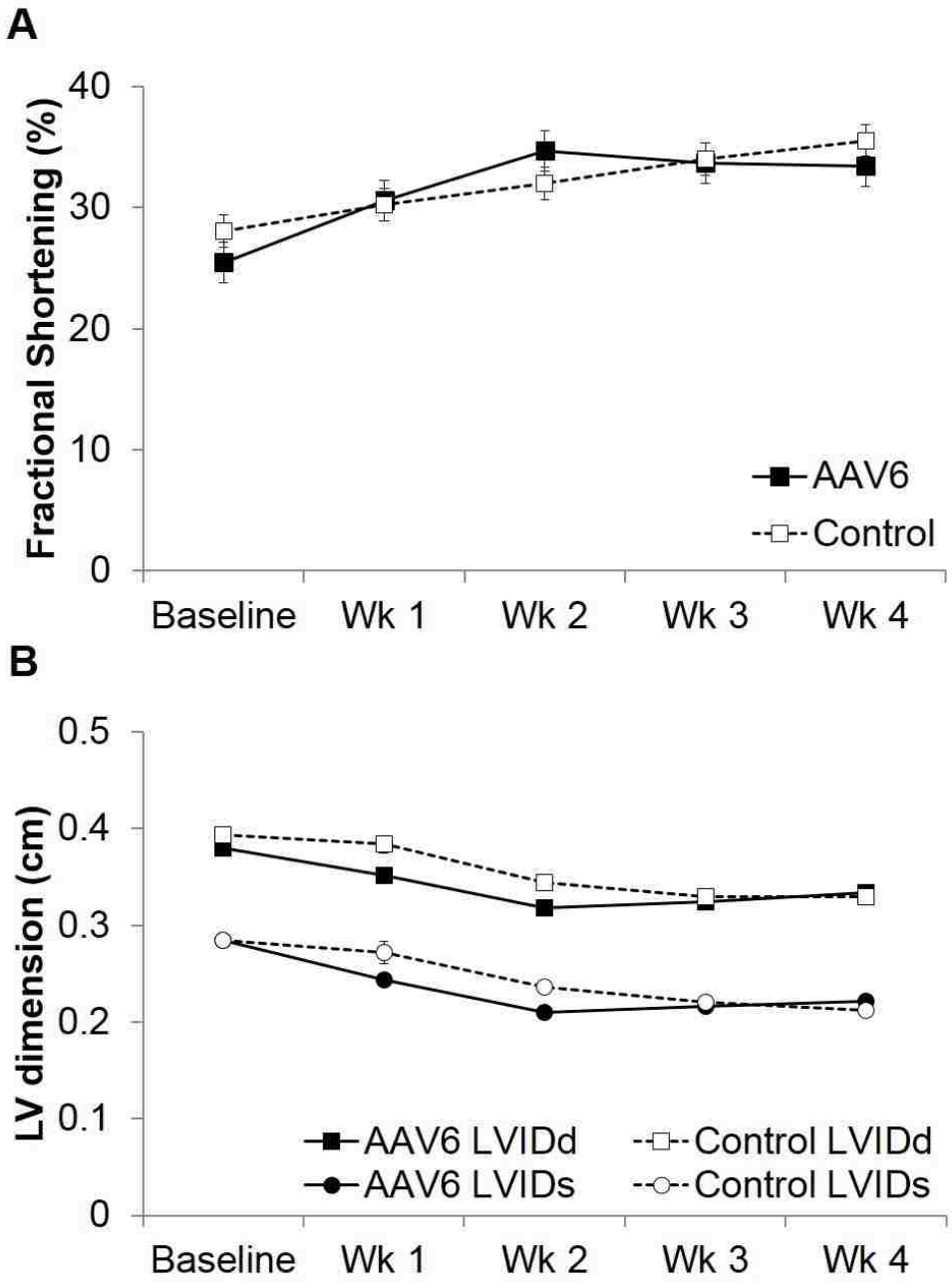

Figure 7.4: Assessment of cardiac function after systemic delivery of the AAV6 $cTnT_{455}$ mCherry-P2a-L48Q cTnC-Flag vector. A) Factional shortening of hearts in AAV6 injected mice (closed squares, solid line; n= 5) was unchanged when compared to HBSS injected control mice (open squares, dotted line; n = 5) over the 4 week expression period. B) Both diastolic and systolic LV diameters in AAV6 injected mice (closed squares and circles, solid lines) were also unchanged when compared to HBSS injected control mice (open squares and circles, dotted lines) over the same period. Values are means ± S.E.M.

Chapter 8. Conclusions and Future Work

8.1 CONCLUSIONS

This dissertation has combined the investigation of basic science questions and the translation of these findings to the development a potential therapeutic strategy to treat heart failure. The severe impact heart failure has directly on the lives of patients suffering from it and indirectly on the healthcare system – costs that total over $500 billion annually in the United States alone [1] – illustrates the need to improve heart failure treatment strategies. Furthermore, the lack of treatment options that restore functional capacity to a failing heart underscores the importance of developing novel therapies that are more than just palliative treatments. Motivated by these unmet needs and shortcomings, the long-term goal of this dissertation was to apply the improved mechanistic understanding of how modulating myofilament Ca^{2+} binding properties affects cardiac muscle contraction regulation to the development of a novel cardiac muscle-targeted gene therapy to improve heart function. While work is still on-going towards this long-term goal, this dissertation has reached significant milestones towards this goal and provided the foundation for the future investigations into the mechanisms of cardiac muscle contraction and therapeutic strategies for heart failure. More specifically, in this work I was able to:

1. Demonstrate that altering myofilament Ca^{2+} binding properties via troponin modulations (via L48Q cTnC or phosphorylated cTnI) sets thin filament activation levels and the SL dependence of Ca^{2+} sensitivity of force in cardiac muscle
2. Improve healthy and diseased intact cardiomyocyte contractility without adversely affecting relaxation or Ca^{2+} transient properties by acutely increasing myofilament Ca^{2+} binding properties (via L48Q cTnC) or crossbridge cycle kinetics (via dATP)

3. Engineer a cardiac muscle-specific *in vivo* gene delivery system to investigate of the effects of acute increased myofilament Ca^{2+} binding properties via L48Q cTnC expression on whole heart function

In Chapters 3 and 4, we tested the hypotheses that the intrinsic properties of cTn are important in determining 1) the Ca^{2+} sensitivity of thin filament activation in response to crossbridge binding, and 2) the SL dependence of force in cardiac muscle. The SL-dependence of the Ca^{2+} sensitivity of force is thought to be the molecular mechanism that, at least in part, underlies the Frank-Starling law of the heart, and it has been shown to be influenced by various components of the contractile apparatus. Changes in thin filament properties, such as substitution of ssTnI for cTnI [113–115] or point mutations in cTnC [112] and cTnT [116,117], as well as changes in thick filament properties [118] and factors affecting thin and thick filament interactions (lattice spacing [65,67,78,119–122], pH [118]) or the cross bridge cycle [70,123] have all been shown to influence the SL dependence of contraction. However, no single mechanism has emerged as the primary determinant of the Frank-Starling relationship. Since one of the hallmarks of heart failure is the loss of the Frank-Starling relationship, a better understanding of the molecular mechanism governing it may improve the ability to understand and treat heart failure.

In Chapter 3, we demonstrated that a cTnC variant with increased Ca^{2+} binding affinity (L48Q cTnC) eliminated crossbridge-mediated effects on the apparent SL-dependence of Ca^{2+} sensitivity of thin filament activation. In L48Q cTnC-cTn exchanged trabeculae the pCa_{50} was unaffected by perturbations of crossbridge activity/number. However, L48Q cTnC-cTn did not alter the SL-dependence of F_{MAX}, which suggests the SL-dependence of CB binding and force was maintained. The results with L48Q cTnC-cTn and PKA phosphorylation of cTnI corroborate the evidence presented by Sun YB et al. [69] that the intrinsic properties of the thin filament play a very significant role in the

cooperative Ca^{2+} activation and regulation of cardiac contractility. Furthermore, the results with L48Q cTnC-cTn suggest that by sensitizing the thin filament to Ca^{2+}, L48Q cTnC greatly reduces the crossbridge assistance required for thin filament activation in cardiac muscle by improving thin filament activation at submaximal Ca^{2+}. This, in turn, reduces and/or eliminates crossbridge induced changes in Ca^{2+} sensitivity. The data also suggest that the SL-dependence of cardiac force development is greatly influenced by the properties of native cTn. This is likely to have implications for many familial inherited cardiomyopathies associated with mutations in thin filament proteins that result in altered Ca^{2+} binding affinity and/or Ca^{2+} sensitivity of force. Additionally, since L48Q cTnC increases myofilament Ca^{2+} sensitivity and subsequently improves thin filament activation at submaximal Ca^{2+}, which is where the heart operates, it may also have implications as potential therapeutic strategy to improve cardiac muscle function in heart failure patients.

In Chapter 4, by replacing endogenous cTn with recombinant WT cTn, a nonphosphorylatable cTnI (S23/24A) cTn, or the phosphomimetic cTnI (S23/24D) cTn, we determined that phosphorylation of cTnI or cMyBP-C/titin, individually or in combination, significantly reduced the SL dependence of Ca^{2+} sensitivity of force. However, PKA phosphorylation did not alter the SL-dependence of F_{MAX}, suggesting the SL-dependence of CB binding and force was maintained. Taken together, our findings point to cTnC-cTnI interactions as a switch that sets the length dependence of Ca^{2+} sensitivity in cardiac muscle, in conjunction with PKA induced changes in crossbridge structure. The ability of heart to manipulate the Ca^{2+} sensitivity and thin filament activation in cardiac muscle through PKA induced changes in myofilament properties enables it to quickly adapt to the changes in the physiological demands of the body. This adaptability comes at a cost since β-adrenergic stimulation that leads to PKA phosphorylation also increases heart rate, elevates intracellular [Ca^{2+}] and force, increases the kinetics for force development and shortening, and also increases the rate of ventricular relaxation and diastolic filling to maintain high cardiac output [53]. While concomitant effects of β-

adrenergic stimulation and decreasing myofilament Ca^{2+} sensitivity through mediated PKA phosphorylation of cTnI or cMyBP-C/titin can improve cardiac output in the short term, they can contribute to the loss of the Frank-Starling relationship and exacerbate to the progression of heart failure when present chronically. Nevertheless, the studies in Chapters 3 and 4 helped elucidate the important role cTnC-cTnI interactions play as a switch that sets the length dependence of Ca^{2+} sensitivity and thin filament activation in cardiac muscle.

In Chapters 5 and 6, we tested the hypotheses that 1) increases in the Ca^{2+} sensitivity of the myofilaments via expression of L48Q cTnC, and/or 2) increases in the crossbridge cycle kinetics through elevated levels of dATP would improve intact cardiomyocyte contractility. Work in our lab had demonstrated that L48Q cTnC increased the Ca^{2+} binding affinity of cTn, which resulted in an increase in myofilament Ca^{2+} sensitivity, and this increase in myofilament Ca^{2+} sensitivity had minimal effects on relaxation of myofibrils [41,43,44]. When these results were combined with the mechanistic evidence in Chapter 3 that sensitizing the thin filament to Ca^{2+} via L48Q cTnC improved thin filament activation at submaximal Ca^{2+}, it suggested that L48Q cTnC may have the potential to enhance intact cardiomyocyte contractility and was explored further in Chapter 5. On the thick filament side, dATP had been shown to increase the magnitude and rate of force development, and increased the Ca^{2+} sensitivity of the force-pCa relationship in demembranated cardiac trabeculae [77,78]. These results suggested that increased crossbridge cycling kinetics via dATP as the myosin substrate may also have the potential to enhance intact cardiomyocyte contractility and was explored in Chapter 6. Because both L48Q cTnC and dATP are myofilament targeted approaches that have demonstrated the potential to increase cardiac contractility in demembranated muscle, it was important to determine for the first time, to our knowledge, the effects each of these approaches had on intact cardiomyocyte function; this was also a crucial first step in the exploration of their potential therapeutic application.

In Chapter 5, transduction with L48Q cTnC significantly improved the contractile function of cardiomyocytes from healthy and infarcted hearts. The use of adenoviral-mediated over-expression of L48Q cTnC in cardiomyocytes resulted in 18±2% replacement of native cTnC with L48Q cTnC. This level of L48Q cTnC myofilament incorporation markedly improved contractile properties of healthy and diseased cardiomyocytes while not adversely affecting relaxation properties. This study corroborates previous results that demonstrated L48Q cTnC is able to enhance the Ca^{2+} binding properties of the myofilaments and likely increases the ability of submaximal Ca^{2+} to activate the thin filament [41,75], and supports the hypothesis that L48Q cTnC can enhance cardiomyocyte contractility without prolonging relaxation. Furthermore, the improvement in the contractile properties of cardiomyocytes from healthy and infarcted hearts after L48Q cTnC transduction did not adversely affect the Ca^{2+} transient properties. Because the Ca^{2+} transient properties were unaffected, these results demonstrated that the improvement in contractility from L48Q cTnC transduction is the result of an enhancement in the Ca^{2+} sensitivity of the myofilaments and contractile efficiency – the extent of contraction per a given release of Ca^{2+}.

The mechanism by which L48Q cTnC is able to increase myofilament Ca^{2+} sensitivity and contractile function is not completely understood, but recent work by our group [41,42,75] and others (44) suggest that increased Ca^{2+} binding to troponin containing L48Q cTnC increases the ability to activate the thin filament. Our solution studies, and work by others (44), have demonstrated that the L48Q point mutation significantly increases the Ca^{2+} affinity of cTnC and increases the affinity of cTnC for cTnI in both the presence and absence of Ca^{2+}. Both magnetic resonance spectroscopy (NMR) and molecular dynamic (MD) simulation data indicate that the N-terminal lobe of L48Q cTnC has a more open structure and exposure of the cTnC hydrophobic patch is stabilized following Ca^{2+} binding. This should increase cTnC-cTnI interaction allowing enhanced movement of cTm and access to myosin

binding sites on actin for a given submaximal [Ca^{2+}]. It may also reduce the requirement for crossbridges to stabilize the cTnC-cTnI state [271]. This effect should be more pronounced at submaximal [Ca^{2+}], where the slower dissociation rate of L48Q cTnC [41,43] should result in more Ca^{2+} being bound to cTn in thin filaments at any given time. Taken together, these results suggest that acute expression of a cTnC variant with increased Ca^{2+} binding properties, such as L48Q cTnC, in intact cardiomyocytes is able to improve myofilament Ca^{2+} sensitivity and cellular contractility.

The potential for L48Q cTnC as a therapeutic strategy to treat heart failure, caused by DCM or MI, is encouraging because it markedly improved contractility in both healthy and diseased cardiomyocyte without adverse effects on Ca^{2+} transient behavior or relaxation. L48Q cTnC is especially promising considering the fact that other studies have shown that myofilament Ca^{2+} sensitization through protein [203] or pharmacological [204,205] means have many off-target effects. Additional challenges and risks are also encountered with some therapeutic strategies have that focused on increasing intracellular Ca^{2+} concentrations, which can cause arrhythmias and can further impair diastolic function [6]. Expression of L48Q cTnC in cardiac muscle possesses the potential to be an effective myofilament-targeted therapy because of its ability to enhance cardiac contractile properties without off-target effects. Interestingly, previous work by Lim et al., provides evidence that supports this potential of limited off-target effects by demonstrating that over-expressing a mutant cTnC (E59D, D75Y), which is associated with idiopathic DCM, in adult rat cardiomyocytes significantly decreased contractility while having no effects on intracellular Ca^{2+} homeostasis [272]. This study further demonstrates it is possible to manipulate thin filament Ca^{2+} binding affinity without affecting Ca^{2+} transient behavior. Little is known, however, whether alterations that increase myofilament Ca^{2+} sensitivity, such as expression of L48Q cTnC, may be beneficial in treating DCM and/or MI. One approach has shown that increasing myofilament Ca^{2+} sensitivity exhibits some promise as a means to treat DCM. In this study, the use of a Ca^{2+} sensitizing agent, pimobendan,

demonstrated that administration to DCM transgenic mice with a deletion in troponin T significantly improved cardiac performance and morphology [202]. We demonstrated that enhanced myofilament Ca^{2+} sensitivity in the uninjured myocardium of an MI heart after neonatal rat cardiomyocyte engraftment may be a major contributor to the improvement in whole heart function of MI hearts that was achieved [92]. The combination of these studies, the results in Chapter 5, and the shortcomings of current treatment strategies for heart failure suggest that expression of thin filament mutations that increase myofilament Ca^{2+} sensitivity, such as L48Q cTnC, may be able to rescue failing heart function.

In Chapter 6, we showed that increasing cellular dATP concentrations in intact healthy cardiomyocytes enhanced the contractile properties of the cells. Adenoviral-mediated over-expression of Rrm1 and Rrm2 resulted in significant elevation of dATP content within the cells. The increase in dATP content in intact cells dramatically increased the rate and magnitude of contraction, and the rate of relaxation with minimal effects on intracellular Ca^{2+} transients. These results also corroborate the previous results in embryonic chick cardiomyocytes where ~30% replace of ATP with dATP increase contractility in these cells as well [211]. Importantly, the increased contractile properties we observed in cardiomyocytes resulted from a much lower replacement of the ATP pool with our over-expression Rrm1+Rrm2 as compared to that which was used in the embryonic chick cardiomyocytes. This may be advantageous in that large increases in intracellular dATP content are not required to achieve contractile potentiation, thus reducing the potential for negative side effects [212,213]. It is important to consider that dATP could be used by other ATPases (besides myosin) such as the sarcoplasmic Ca^{2+} ATPase (SERCA2a), the plasma membrane Ca^{2+} ATPase (PMCA), and may also indirectly effect activity of the Na^{+}/ Ca^{2+} exchanger (NCX) [218]. Ongoing work in our laboratory is investigating these potential off-target effects.

The improvements in contractility did not perturb Ca^{2+} transient properties and even enhanced relaxation in some cases. Since dATP increases the rate of crossbridge detachment [77,215] and thus crossbridge cycling kinetics, it is likely that this explains both the enhancement in contraction and relaxation in intact caridomyocytes. At least in the case of acute elevation of dATP via Rrm1+Rrm2 over-expression, the evidence we have so far suggests that it elicits minimal off-target effects. Although the exact mechanism by which dATP increases crossbridge cycling kinetics is still currently under investigation and the potential off-target effects require additional investigation yet, the dual benefit of positive inotropy and lusitropy that elevation of dATP content in cardiac muscle provides still holds much promise as a myofilament targeted strategy to improve cardiac contractility and potentially treat heart failure.

In order to further investigate the effects of L48Q cTnC expression on whole heart function and explore its therapeutic potential, I engineered a novel cardiac muscle-specific AVV6 *in vivo* gene delivery system that was described in Chapter 7. The work in this chapter on the design, development, and characterization of our AAV6 system reached significant milestones towards the long-term goal of this dissertation: to apply the improved mechanistic understanding of how modulating myofilament Ca^{2+} binding properties (via L48Q cTnC) affects cardiac muscle contraction regulation to the development of a novel cardiac muscle-targeted gene therapy to improve heart function. The novel AAV6 gene delivery system was designed with a specific purpose in mind for each element included in it. Based on the previous work that demonstrated the efficacy and the preferential transduction of the myocardium with AAV6 compared to other AAV serotypes [242,248,249,254–256], recombinant AAV6 was used as the viral backbone. The $cTnT_{455}$ promoter was included to limit gene expression in off-target tissues and drive strong gene expression of mCherry – a fluorescent reporter protein – and L48Q cTnC accompanied by a C-terminal Flag tag specifically in cardiac muscle [255,258–264]. L48Q cTnC was included to examine its effects on whole

heart function, while the C-terminal Flag was included to measure the extent of *in vivo* myofilament incorporation of L48Q cTnC. In order to fit both genes into the AAV6 viral backbone and to enable expression of mCherry and L48Q cTnC-Flag by the same promoter at approximately a 1:1 ratio [267,268,270], the small P2a peptide was included between the mCherry and L48Q cTnC-Flag genes. The preliminary data in Chapter 7 demonstrated that the AAV6 $cTnT_{455}$ mCherry-P2a-L48Q cTnC-Flag system was able to transduce the myocardium uniformly and robustly as indicated by mCherry-P2a expression. The biodistribution data also demonstrated that the robust myocardial expression was achieved in a targeted manner with limited transduction of off-target tissues. The expression level in the non-cardiac tissue still needs to be investigated even though it is anticipated that the $cTnT_{455}$ promoter will prevent gene expression in those tissues. While I was able to demonstrate high levels of mCherry-P2a expression, the demonstration of *in vivo* L48Q cTnC-Flag expression is still ongoing. The preliminary *in vivo* whole heart functional data demonstrated that expression of the AAV6 system in the myocardium did not adversely affect healthy whole heart function. However, because confirmation of L48Q cTnC-Flag expression still requires additional work, it is difficult to glean any additional insights into the effects of *in vivo* expression of L48Q cTnC-Flag. Once the levels of L48Q cTnC-Flag expression in the myocardium have been demonstrated, additional *in vivo* studies will be able to elucidate the effects of L48Q cTnC-Flag expression on healthy and/or diseased whole heart function.

8.2 FUTURE WORK

The work in this dissertation improved the mechanistic understanding of cardiac muscle contraction regulation and the role modulation of cTn Ca^{2+} binding affinity via cTnC properties plays in thin filament activation. By doing so, it also provided unique insights into an innovative target for therapeutic strategies to treat heart failure. This unique combination of basic science questions and the translation of these findings to the development a potential therapeutic strategy to treat heart

failure has set the stage for many interesting future studies. Since much of the work in this dissertation focused on *in vitro* studies with L48Q cTnC and developing an AAV6 system to express the engineered L48Q cTnC variant *in vivo*, some of the most interesting future work should focus on the effects *in vivo* expression of L48Q cTnC has on cardiac muscle regulation and whole heart function.

In vivo expression of an engineered cTnC variant that enhances cTn Ca^{2+} binding affinity and myofilament Ca^{2+} sensitivity, such as L48Q cTnC, opens the door to many questions from the mechanistic and disease development perspectives. The work in this dissertation showed that L48Q cTnC increased myofilament Ca^{2+} sensitivity, reduced crossbridge-mediated effects on the apparent SL dependence of Ca^{2+} sensitivity, and subsequently improved thin filament activation at submaximal [Ca^{2+}], which is physiological condition where the heart operates *in vivo*. Based on these findings, it would be important to examine if these effects are recapitulated at the whole heart level. It would also be interesting to determine if cardiac muscle from myocardium transduced *in vivo* with L48Q cTnC exhibits the same SL properties that we observed in our L48Q cTnC-cTn exchange experiments in Chapter 3. If the Frank-Starling relationship is eliminated or significantly reduced *in vivo*, it could have interesting effects on heart function. It would also be interesting to investigate from a heart failure perspective since loss of the Frank-Starling relationship is a hallmark of heart failure. Furthermore, since the heart can use many compensatory mechanisms to match cardiac output to the physiological demands of the body, it will be important to determine if *in vivo* expression of L48Q cTnC elicits any compensatory mechanisms in both the short and long-term.

Increased myofilament Ca^{2+} sensitivity has also been associated with many clinical phenotypes of HCM. With HCM, it is unclear if the increase in myofilament Ca^{2+} sensitivity is causative, concomitant, or compensatory with the disease state [273]. Because L48Q cTnC is an engineered cTnC variant and

is not associated with a clinical HCM phenotype, it could be useful in identifying the role the increased myofilament Ca^{2+} sensitivity plays in HCM development. Additionally, it could be used to examine the causes of other complications with HCM, such as changes in excitation-contraction coupling and activation of signaling pathways typically associated with pathological hypertrophy. It would also be interesting to compare the effects of acute vs. chronic expression of L48Q cTnC on heart function and possible disease development. These are just a few of the mechanistic and disease development questions *in vivo* expression of a cTnC variant with increased Ca^{2+} binding properties like L48Q cTnC could shed light on.

In addition to improving the understanding of cardiac disease development, future work should also examine the therapeutic potential of *in vivo* expression of L48Q cTnC as a treatment for heart failure. The work in this dissertation demonstrated that enhancement of cTn Ca^{2+} binding affinity and myofilament Ca^{2+} sensitivity through the expression of L48Q cTnC improved the contractility of cardiomyocytes from healthy and infarcted hearts. Moreover, these results suggest that the potential of L48Q cTnC as a therapeutic strategy to treat heart failure is encouraging because it markedly improved contractility in both healthy and diseased cardiomyocytes without adverse effects on Ca^{2+} transient behavior or relaxation (Chapter 5). It will be important to determine the effects of AAV6-mediated L48Q cTnC expression on whole heart function, and whether expression of L48Q cTnC is able to rescue whole heart function post-MI or in a DCM model. Equally as important will be the determination of any off-target effects of *in vivo* L48Q cTnC expression in both cardiac and non-cardiac tissue. Specifically in cardiac muscle, it will be crucial to examine the effects of L48Q cTnC expression on whole heart Ca^{2+} handling properties, diastolic function, and cardiac metabolism. Similarly, it will also be important to look at the differences between acute vs. chronic expression of L48Q cTnC in healthy and diseased myocardium. Differences in expression duration could have drastic effects on the ability of L48Q cTnC to improve heart function and on any deleterious effects

that may be associated with L48Q cTnC expression in the heart. Finally, when considering the therapeutic potential of any heart failure treatment, the questions around dose administered, and the duration and frequency of administration need to be considered. The improvements in contractile properties in healthy and MI cardiomycoytes were produced by acute expression of L48Q cTnC and only 18±2% of L48Q cTnC relative to native cTnC present in the myofilaments. It will be interesting to examine whether increasing the amount of L48Q cTnC results in even greater improvements in cardiac function, or if a point of diminishing returns is met where increasing replacement of native cTnC with L48Q cTnC produces no additional gain in function, or possibly even impairs cardiac function. The effects of various extents of myofilament incorporation of L48Q cTnC and the long-term effects of different levels of L48Q cTnC expression will need to be well-understood going forward. Many additional studies will be required to truly evaluate the therapeutic potential of L48Q cTnC expression to treat heart failure, and the aforementioned studies are some of the most crucial ones to begin with.

In closing, this work represents the combination of the investigation of basic science questions and the translation of these findings to the development a potential therapeutic strategy to treat heart failure. It has tackled a variety of different questions about cardiac muscle contraction regulation and investigated these questions at a multitude of different levels ranging from sub-cellular to the whole organ. While different but related questions were investigated and various milestones were reached, the long-term goal of applying an improved mechanistic understanding of how modulating myofilament Ca^{2+} binding properties affects cardiac muscle contraction to the development of a novel cardiac muscle-targeted gene therapy to improve heart function still remains as the motivation for this and future work. In doing so, the work in this dissertation has set the stage for a number of additional studies, including the characterization of the *in vivo* L48Q cTnC-Flag expression profile and determination of the therapeutic potential of the AAV6 system to enhance whole heart function.

It has also pioneered and developed many of the tools that many collaborative projects in the lab are currently using to investigate additional questions. As an engineer who has been focused on the application of science and engineering to tackle unsolved problems, I have gained invaluable insights and skills from learning how to also investigate basic science questions and translate the improvements in fundamental understanding to unmet scientific and clinical needs. I can only hope that someday the contributions of this work, to both the mechanistic understanding of cardiac muscle contraction regulation and to the development of a potential therapy for heart failure, will improve the efficacy of treatments for patients with heart failure and reduce the associated costs.

References

[1] Lloyd-Jones D, Adams RJ, Brown TM, Carnethon M, Dai S, De Simone G, et al. Executive summary: heart disease and stroke statistics--2010 update: a report from the American Heart Association. Circulation 2010;121:948–54.

[2] Laflamme MA, Murry CE. Regenerating the heart. Nature Biotechnology 2005;23:845–56.

[3] Bristow MR, Ginsburg R, Umans V, Fowler M, Minobe W, Rasmussen R, et al. Beta 1- and beta 2-adrenergic-receptor subpopulations in nonfailing and failing human ventricular myocardium: coupling of both receptor subtypes to muscle contraction and selective beta 1-receptor down-regulation in heart failure. Circ Res 1986;59:297–309.

[4] Bristow MR, Ginsburg R, Minobe W, Cubicciotti RS, Sageman WS, Lurie K, et al. Decreased catecholamine sensitivity and beta-adrenergic-receptor density in failing human hearts. N Engl J Med 1982;307:205–11.

[5] Rockman HA, Koch WJ, Lefkowitz RJ. Seven-transmembrane-spanning receptors and heart function. Nature 2002;415:206–12.

[6] Rubart M, Zipes DP. Mechanisms of sudden cardiac death. The Journal of Clinical Investigation 2005;115:2305–15.

[7] Tuttle RR, Mills J. Dobutamine: development of a new catecholamine to selectively increase cardiac contractility. Circ Res 1975;36:185–96.

[8] Farah AE, Frangakis CJ. Studies on the mechanism of action of the bipyridine milrinone on the heart. Basic Research in Cardiology 1989;84 Suppl 1:85–103.

[9] Kass D a, Solaro RJ. Mechanisms and use of calcium-sensitizing agents in the failing heart. Circulation 2006;113:305–15.

[10] Wyskovsky W, Hauptner R, Suko J. Drug-induced calcium release from heavy sarcoplasmic reticulum of skeletal muscle. Biochimica et Biophysica Acta 1988;938:89–96.

[11] Cleland JGF, Teerlink JR, Senior R, Nifontov EM, Mc Murray JJ V, Lang CC, et al. The effects of the cardiac myosin activator, omecamtiv mecarbil, on cardiac function in systolic heart failure: a double-blind, placebo-controlled, crossover, dose-ranging phase 2 trial. Lancet 2011;378:676–83.

[12] Shen Y-T, Malik FI, Zhao X, Depre C, Dhar SK, Abarzúa P, et al. Improvement of cardiac function by a cardiac Myosin activator in conscious dogs with systolic heart failure. Circulation Heart Failure 2010;3:522–7.

[13] Malik FI, Hartman JJ, Elias K a, Morgan BP, Rodriguez H, Brejc K, et al. Cardiac myosin activation: a potential therapeutic approach for systolic heart failure. Science (New York, NY) 2011;331:1439–43.

[14] Mebazaa A, Nieminen MS, Packer M, Cohen-Solal A, Kleber FX, Pocock SJ, et al. Levosimendan vs dobutamine for patients with acute decompensated heart failure: the SURVIVE Randomized Trial. JAMA : the Journal of the American Medical Association 2007;297:1883–91.

[15] Sabbah HN. Biologic rationale for the use of beta-blockers in the treatment of heart failure. Heart Failure Reviews 2004;9:91–7.

[16] Davis J, Westfall M V, Townsend D, Blankinship M, Herron TJ, Guerrero-Serna G, et al. Designing heart performance by gene transfer. Physiological Reviews 2008;88:1567–651.

[17] Isner JM. Myocardial gene therapy. Nature 2002;415:234–9.

[18] Gwathmey JK, Yerevanian AI, Hajjar RJ. Cardiac gene therapy with SERCA2a: from bench to bedside. Journal of Molecular and Cellular Cardiology 2011;50:803–12.

[19] Minamisawa S, Hoshijima M, Chu G, Ward CA, Frank K, Gu Y, et al. Chronic phospholamban-sarcoplasmic reticulum calcium ATPase interaction is the critical calcium cycling defect in dilated cardiomyopathy. Cell 1999;99:313–22.

[20] Ritterhoff J, Most P. Targeting S100A1 in heart failure. Gene Therapy 2012;19:613–21.

[21] Jessup M, Greenberg B, Mancini D, Cappola T, Pauly DF, Jaski B, et al. Calcium Upregulation by Percutaneous Administration of Gene Therapy in Cardiac Disease (CUPID): a phase 2 trial of intracoronary gene therapy of sarcoplasmic reticulum Ca2+-ATPase in patients with advanced heart failure. Circulation 2011;124:304–13.

[22] Hajjar RJ, Zsebo K, Deckelbaum L, Thompson C, Rudy J, Yaroshinsky A, et al. Design of a phase 1/2 trial of intracoronary administration of AAV1/SERCA2a in patients with heart failure. Journal of Cardiac Failure 2008;14:355–67.

[23] Elledge SJ, Zhou Z, Allen JB. Ribonucleotide reductase: regulation, regulation, regulation. Trends in Biochemical Sciences 1992;17:119–23.

[24] Regnier M, Rivera a J, Chen Y, Chase PB. 2-deoxy-ATP enhances contractility of rat cardiac muscle. Circulation Research 2000;86:1211–7.

[25] Korte FS, Dai J, Buckley K, Feest ER, Adamek N, Geeves MA, et al. Upregulation of cardiomyocyte ribonucleotide reductase increases intracellular 2 deoxy-ATP, contractility, and relaxation. Journal of Molecular and Cellular Cardiology 2011;51:894–901.

[26] Nowakowski SG, Kolwicz SC, Korte FS, Luo Z, Robinson-Hamm JN, Page JL, et al. Transgenic overexpression of ribonucleotide reductase improves cardiac performance. Proceedings of the National Academy of Sciences of the United States of America 2013;110:6187–92.

[27] Gordon a M, Homsher E, Regnier M. Regulation of contraction in striated muscle. Physiological Reviews 2000;80:853–924.

[28] Seidman JG, Seidman C. The genetic basis for cardiomyopathy: from mutation identification to mechanistic paradigms. Cell 2001;104:557–67.

[29] Gillis TE, Martyn D a, Rivera AJ, Regnier M. Investigation of thin filament near-neighbour regulatory unit interactions during force development in skinned cardiac and skeletal muscle. The Journal of Physiology 2007;580:561–76.

[30] McKillop DF, Geeves MA. Regulation of the interaction between actin and myosin subfragment 1: evidence for three states of the thin filament. Biophysical Journal 1993;65:693–701.

[31] Lehman W, Hatch V, Korman V, Rosol M, Thomas L, Maytum R, et al. Tropomyosin and actin isoforms modulate the localization of tropomyosin strands on actin filaments. Journal of Molecular Biology 2000;302:593–606.

[32] Vibert P, Craig R, Lehman W. Steric-model for activation of muscle thin filaments. Journal of Molecular Biology 1997;266:8–14.

[33] Guatimosim S, Dilly K, Santana LF, Saleet Jafri M, Sobie EA, Lederer WJ. Local Ca(2+) signaling and EC coupling in heart: Ca(2+) sparks and the regulation of the [Ca(2+)](i) transient. J Mol Cell Cardiol 2002;34:941–50.

[34] Strang KT, Sweitzer NK, Greaser ML, Moss RL. Beta-adrenergic receptor stimulation increases unloaded shortening velocity of skinned single ventricular myocytes from rats. Circulation Research 1994;74:542–9.

[35] Sumandea MP, Pyle WG, Kobayashi T, de Tombe PP, Solaro RJ. Identification of a functionally critical protein kinase C phosphorylation residue of cardiac troponin T. The Journal of Biological Chemistry 2003;278:35135–44.

[36] Kunst G, Kress KR, Gruen M, Uttenweiler D, Gautel M, Fink RH. Myosin binding protein C, a phosphorylation-dependent force regulator in muscle that controls the attachment of myosin heads by its interaction with myosin S2. Circulation Research n.d.;86:51–8.

[37] Cazorla O, Szilagyi S, Vignier N, Salazar G, Krämer E, Vassort G, et al. Length and protein kinase A modulations of myocytes in cardiac myosin binding protein C-deficient mice. Cardiovascular Research 2006;69:370–80.

[38] Olsson MC, Patel JR, Fitzsimons DP, Walker JW, Moss RL. Basal myosin light chain phosphorylation is a determinant of Ca2+ sensitivity of force and activation dependence of the kinetics of myocardial force development. American Journal of Physiology Heart and Circulatory Physiology 2004;287:H2712–8.

[39] Wang YP, Fuchs F. Length, force, and Ca(2+)-troponin C affinity in cardiac and slow skeletal muscle. The American Journal of Physiology 1994;266:C1077–82.

[40] Hofmann PA, Fuchs F. Effect of length and cross-bridge attachment on Ca2+ binding to cardiac troponin C. The American Journal of Physiology 1987;253:C90–6.

[41] Kreutziger KL, Piroddi N, McMichael JT, Tesi C, Poggesi C, Regnier M. Calcium binding kinetics of troponin C strongly modulate cooperative activation and tension kinetics in cardiac muscle. Journal of Molecular and Cellular Cardiology 2011;50:165–74.

[42] Wang D, Robertson IM, Li MX, McCully ME, Crane ML, Luo Z, et al. Structural and functional consequences of the cardiac troponin C L48Q Ca(2+)-sensitizing mutation. Biochemistry 2012;51:4473–87.

[43] Tikunova SB, Davis JP. Designing calcium-sensitizing mutations in the regulatory domain of cardiac troponin C. The Journal of Biological Chemistry 2004;279:35341–52.

[44] Tikunova SB, Liu B, Swindle N, Little SC, Gomes A V, Swartz DR, et al. Effect of calcium-sensitizing mutations on calcium binding and exchange with troponin C in increasingly complex biochemical systems. Biochemistry 2010;49:1975–84.

[45] Korte FS, Feest ER, Razumova M V, Tu A-Y, Regnier M. Enhanced Ca2+ binding of cardiac troponin reduces sarcomere length dependence of contractile activation independently of strong crossbridges. American Journal of Physiology Heart and Circulatory Physiology 2012;303:H863–70.

[46] Gordon a M, Regnier M, Homsher E. Skeletal and cardiac muscle contractile activation: tropomyosin "rocks and rolls". News in Physiological Sciences : an International Journal of Physiology Produced Jointly by the International Union of Physiological Sciences and the American Physiological Society 2001;16:49–55.

[47] Goldman YE, Hibberd MG, Trentham DR. Relaxation of rabbit psoas muscle fibres from rigor by photochemical generation of adenosine-5'-triphosphate. The Journal of Physiology 1984;354:577–604.

[48] Chalovich JM, Chock PB, Eisenberg E. Mechanism of action of troponin . tropomyosin. Inhibition of actomyosin ATPase activity without inhibition of myosin binding to actin. The Journal of Biological Chemistry 1981;256:575–8.

[49] Brenner B. Effect of Ca2+ on cross-bridge turnover kinetics in skinned single rabbit psoas fibers: implications for regulation of muscle contraction. Proceedings of the National Academy of Sciences of the United States of America 1988;85:3265–9.

[50] Regnier M, Morris C, Homsher E. Regulation of the cross-bridge transition from a weakly to strongly bound state in skinned rabbit muscle fibers. Am J Physiol 1995;269:C1532–9.

[51] Tesi C, Colomo F, Piroddi N, Poggesi C. Characterization of the cross-bridge force-generating step using inorganic phosphate and BDM in myofibrils from rabbit skeletal muscles. The Journal of Physiology 2002;541:187–99.

[52] Yount RG, Lawson D, Rayment I. Is myosin a "back door" enzyme? Biophysical Journal 1995;68:44S–47S; discussion 47S–49S.

[53] Bers DM. Cardiac excitation-contraction coupling. Nature 2002;415:198–205.

[54] Reuter H, Pott C, Goldhaber JI, Henderson S a, Philipson KD, Schwinger RHG. Na(+)--Ca2+ exchange in the regulation of cardiac excitation-contraction coupling. Cardiovascular Research 2005;67:198–207.

[55] DiPolo R, Beaugé L. Sodium/calcium exchanger: influence of metabolic regulation on ion carrier interactions. Physiological Reviews 2006;86:155–203.

[56] Bers DM. Calcium and cardiac rhythms: physiological and pathophysiological. Circ Res 2002;90:14–7.

[57] Holubarsch C, Ruf T, Goldstein DJ, Ashton RC, Nickl W, Pieske B, et al. Existence of the Frank-Starling mechanism in the failing human heart. Investigations on the organ, tissue, and sarcomere levels. Circulation 1996;94:683–9.

[58] Kitzman DW, Higginbotham MB, Cobb FR, Sheikh KH, Sullivan MJ. Exercise intolerance in patients with heart failure and preserved left ventricular systolic function: failure of the Frank-Starling mechanism. Journal of the American College of Cardiology 1991;17:1065–72.

[59] Schwinger RH, Böhm M, Koch A, Schmidt U, Morano I, Eissner HJ, et al. The failing human heart is unable to use the Frank-Starling mechanism. Circ Res 1994;74:959–69.

[60] Jacob R, Dierberger B, Kissling G. Functional significance of the Frank-Starling mechanism under physiological and pathophysiological conditions. Eur Heart J 1992;13 Suppl E:7–14.

[61] Komamura K, Shannon RP, Ihara T, Shen YT, Mirsky I, Bishop SP, et al. Exhaustion of Frank-Starling mechanism in conscious dogs with heart failure. The American Journal of Physiology 1993;265:H1119–31.

[62] Nejad NS, Klein MD, Mirsky I, Lown B. Assessment of myocardial contractility from ventricular pressure recordings. Cardiovascular Research 1971;5:15–23.

[63] Ross J, Sonnenblick EH, Taylor RR, Spotnitz HM, Covell JW. Diastolic geometry and sarcomere lengths in the chronically dilated canine left ventricle. Circulation Research 1971;28:49–61.

[64] Farman GP, de Tombe PP, Irving TC. Radial head position of cardiac muscle affects calcium sensitivity. 2003;84:139a.

[65] Fuchs F, Martyn D a. Length-dependent Ca(2+) activation in cardiac muscle: some remaining questions. Journal of Muscle Research and Cell Motility 2005;26:199–212.

[66] Hanft LM, Korte FS, McDonald KS. Cardiac function and modulation of sarcomeric function by length. Cardiovascular Research 2008;77:627–36.

[67] Konhilas JP, Irving TC, de Tombe PP. Myofilament calcium sensitivity in skinned rat cardiac trabeculae: role of interfilament spacing. Circ Res 2002;90:59–65.

[68] Sun YB, Irving M. The molecular basis of the steep force-calcium relation in heart muscle. J Mol Cell Cardiol 2010;48:859–65.

[69] Sun YB, Lou F, Irving M. Calcium- and myosin-dependent changes in troponin structure during activation of heart muscle. J Physiol 2009;587:155–63.

[70] Fitzsimons DP, Moss RL. Strong binding of myosin modulates length-dependent Ca2+ activation of rat ventricular myocytes. Circ Res 1998;83:602–7.

[71] Gordon AM, Ridgway EB. Cross-bridges affect both TnC structure and calcium affinity in muscle fibers. Adv Exp Med Biol 1993;332:183–4.

[72] Morimoto S, Ohtsuki I. Ca2+ binding to cardiac troponin C in the myofilament lattice and its relation to the myofibrillar ATPase activity. Eur J Biochem 1994;226:597–602.

[73] Farman GP, Allen EJ, Schoenfelt KQ, Backx PH, de Tombe PP. The role of thin filament cooperativity in cardiac length-dependent calcium activation. Biophys J 2010;99:2978–86.

[74] Regnier M, Martin H, Barsotti RJ, Rivera AJ, Martyn DA, Clemmens E. Cross-bridge versus thin filament contributions to the level and rate of force development in cardiac muscle. Biophysical Journal 2004;87:1815–24.

[75] Korte FS, Feest ER, Razumova M V, Regnier M. Sarcomere Length Dependent Contractile Activation is Reduced in Rat Trabeculae Exchanged with cTn Containing the L48Q cTnC Variant Independently of Strong Binding Cross-Bridges. Biophysical Journal 2010;98:356a.

[76] Rao VS, Korte FS, Razumova M V, Feest ER, Hsu H, Irving TC, et al. N-terminal phosphorylation of cardiac troponin-I reduces length-dependent calcium sensitivity of contraction in cardiac muscle. The Journal of Physiology 2013;591:475–90.

[77] Regnier M, Rivera AJ, Chen Y, Chase PB. 2-deoxy-ATP enhances contractility of rat cardiac muscle. Circ Res 2000;86:1211–7.

[78] Adhikari BB, Regnier M, Rivera AJ, Kreutziger KL, Martyn D a. Cardiac length dependence of force and force redevelopment kinetics with altered cross-bridge cycling. Biophysical Journal 2004;87:1784–94.

[79] Köhler J, Chen Y, Brenner B, Gordon AM, Kraft T, Martyn DA, et al. Familial hypertrophic cardiomyopathy mutations in troponin I (K183D, G203S, K206Q) enhance filament sliding. Physiol Genomics 2003;14:117–28.

[80] Potter JD. Preparation of troponin and its subunits. Methods Enzymol 1982;85 Pt B:241–63.

[81] Fabiato A. Computer programs for calculating total from specified free or free from specified total ionic concentrations in aqueous solutions containing multiple metals and ligands. Methods in Enzymology 1988;157:378–417.

[82] Martyn DA, Chase PB, Hannon JD, Huntsman LL, Kushmerick MJ, Gordon AM. Unloaded shortening of skinned muscle fibers from rabbit activated with and without Ca2+. Biophys J 1994;67:1984–93.

[83] Regnier M, Rivera AJ, Wang CK, Bates MA, Chase PB, Gordon AM. Thin filament near-neighbour regulatory unit interactions affect rabbit skeletal muscle steady-state force-Ca(2+) relations. J Physiol 2002;540:485–97.

[84] Brenner B, Eisenberg E. Rate of force generation in muscle: correlation with actomyosin ATPase activity in solution. Proc Natl Acad Sci U S A 1986;83:3542–6.

[85] Wojdyr M. Fityk : a general-purpose peak fitting program. Journal of Applied Crystallography 2010;43:1126–8.

[86] Fischetti R, Stepanov S, Rosenbaum G, Barrea R, Black E, Gore D, et al. The BioCAT undulator beamline 18ID: a facility for biological non-crystalline diffraction and X-ray absorption spectroscopy at the Advanced Photon Source. Journal of Synchrotron Radiation 2004;11:399–405.

[87] Irving TC, Konhilas J, Perry D, Fischetti R, de Tombe PP. Myofilament lattice spacing as a function of sarcomere length in isolated rat myocardium. American Journal of Physiology Heart and Circulatory Physiology 2000;279:H2568–73.

[88] Colson BA, Locher MR, Bekyarova T, Patel JR, Fitzsimons DP, Irving TC, et al. Differential roles of regulatory light chain and myosin binding protein-C phosphorylations in the modulation of cardiac force development. The Journal of Physiology 2010;588:981–93.

[89] Irving TC, Millman BM. Changes in thick filament structure during compression of the filament lattice in relaxed frog sartorius muscle. Journal of Muscle Research and Cell Motility 1989;10:385–94.

[90] Tachampa K, Kobayashi T, Wang H, Martin AF, Biesiadecki BJ, Solaro RJ, et al. Increased cross-bridge cycling kinetics after exchange of C-terminal truncated troponin I in skinned rat cardiac muscle. The Journal of Biological Chemistry 2008;283:15114–21.

[91] Santana LF, Kranias EG, Lederer WJ. Calcium sparks and excitation-contraction coupling in phospholamban-deficient mouse ventricular myocytes. The Journal of Physiology 1997;503 (Pt 1:21–9.

[92] Moreno-Gonzalez A, Korte FS, Dai J, Chen K, Ho B, Reinecke H, et al. Cell therapy enhances function of remote non-infarcted myocardium. Journal of Molecular and Cellular Cardiology 2009;47:603–13.

[93] He TC, Zhou S, da Costa LT, Yu J, Kinzler KW, Vogelstein B. A simplified system for generating recombinant adenoviruses. Proceedings of the National Academy of Sciences of the United States of America 1998;95:2509–14.

[94] Luo J, Deng Z-L, Luo X, Tang N, Song W-X, Chen J, et al. A protocol for rapid generation of recombinant adenoviruses using the AdEasy system. Nature Protocols 2007;2:1236–47.

[95] Badrian B, Bogoyevitch MA. Changes in the transcriptional profile of cardiac myocytes following green fluorescent protein expression. DNA and Cell Biology 2007;26:727–36.

[96] Cazorla O, Lucas A, Poirier F, Lacampagne A, Lezoualc'h F. The cAMP binding protein Epac regulates cardiac myofilament function. Proceedings of the National Academy of Sciences of the United States of America 2009;106:14144–9.

[97] Sheehan KA, Arteaga GM, Hinken AC, Dias FA, Ribeiro C, Wieczorek DF, et al. Functional effects of a tropomyosin mutation linked to FHC contribute to maladaptation during acidosis. Journal of Molecular and Cellular Cardiology 2011;50:442–50.

[98] Kawashima H, Satoh H, Saotome M, Urushida T, Katoh H, Hayashi H. Protein phosphatase inhibitor-1 augments a protein kinase A-dependent increase in the Ca2+ loading of the

sarcoplasmic reticulum without changing its Ca2+ release. Circulation Journal : Official Journal of the Japanese Circulation Society 2009;73:1133–40.

[99] Shah AM, Prendergast BD, Grocott-Mason R, Lewis MJ, Paulus WJ. The influence of endothelium-derived nitric oxide on myocardial contractile function. International Journal of Cardiology 1995;50:225–31.

[100] Vogelpohl I, Vetter R, Heger J, Ebermann L, Euler G, Schultheiss H-P, et al. Transgenic overexpression of heart-specific adenine nucleotide translocase 1 positively affects contractile function in cardiomyocytes. Cellular Physiology and Biochemistry : International Journal of Experimental Cellular Physiology, Biochemistry, and Pharmacology 2011;27:121–8.

[101] Herron TJ, Vandenboom R, Fomicheva E, Mundada L, Edwards T, Metzger JM. Calcium-independent negative inotropy by beta-myosin heavy chain gene transfer in cardiac myocytes. Circulation Research 2007;100:1182–90.

[102] Grynkiewicz G, Poenie M, Tsien RY. A new generation of Ca2+ indicators with greatly improved fluorescence properties. The Journal of Biological Chemistry 1985;260:3440–50.

[103] Iorga B, Adamek N, Geeves MA. The slow skeletal muscle isoform of myosin shows kinetic features common to smooth and non-muscle myosins. The Journal of Biological Chemistry 2007;282:3559–70.

[104] Margossian SS, Lowey S. Preparation of myosin and its subfragments from rabbit skeletal muscle. Methods in Enzymology 1982;85 Pt B:55–71.

[105] Weeds AG, Taylor RS. Separation of subfragment-1 isoenzymes from rabbit skeletal muscle myosin. Nature 1975;257:54–6.

[106] Spudich JA, Watt S. The regulation of rabbit skeletal muscle contraction. I. Biochemical studies of the interaction of the tropomyosin-troponin complex with actin and the proteolytic fragments of myosin. The Journal of Biological Chemistry 1971;246:4866–71.

[107] Bradford MM. A rapid and sensitive method for the quantitation of microgram quantities of protein utilizing the principle of protein-dye binding. Analytical Biochemistry 1976;72:248–54.

[108] Zor T, Selinger Z. Linearization of the Bradford protein assay increases its sensitivity: theoretical and experimental studies. Analytical Biochemistry 1996;236:302–8.

[109] Yardeni T, Eckhaus M, Morris HD, Huizing M, Hoogstraten-Miller S. Retro-orbital injections in mice. Lab Animal 2011;40:155–60.

[110] Geeves MA, Holmes KC. Structural mechanism of muscle contraction. Annu Rev Biochem 1999;68:687–728.

[111] Moss RL, Razumova M, Fitzsimons DP. Myosin crossbridge activation of cardiac thin filaments: implications for myocardial function in health and disease. Circ Res 2004;94:1290–300.

[112] Liang B, Chung F, Qu Y, Pavlov D, Gillis TE, Tikunova SB, et al. Familial hypertrophic cardiomyopathy-related cardiac troponin C mutation L29Q affects Ca2+ binding and myofilament contractility. Physiol Genomics 2008;33:257–66.

[113] Tachampa K, Wang H, Farman GP, de Tombe PP. Cardiac troponin I threonine 144: role in myofilament length dependent activation. Circulation Research 2007;101:1081–3.

[114] Arteaga GM, Palmiter K a, Leiden JM, Solaro RJ. Attenuation of length dependence of calcium activation in myofilaments of transgenic mouse hearts expressing slow skeletal troponin I. The Journal of Physiology 2000;526 Pt 3:541–9.

[115] Konhilas JP, Irving TC, Wolska BM, Jweied EE, Martin AF, Solaro RJ, et al. Troponin I in the murine myocardium: influence on length-dependent activation and interfilament spacing. J Physiol 2003;547:951–61.

[116] Chandra M, Rundell VL, Tardiff JC, Leinwand L a, De Tombe PP, Solaro RJ. Ca(2+) activation of myofilaments from transgenic mouse hearts expressing R92Q mutant cardiac troponin T. American Journal of Physiology Heart and Circulatory Physiology 2001;280:H705–13.

[117] Chandra M, Tschirgi ML, Rajapakse I, Campbell KB. Troponin T modulates sarcomere length-dependent recruitment of cross-bridges in cardiac muscle. Biophys J 2006;90:2867–76.

[118] Fukuda N, O-Uchi J, Sasaki D, Kajiwara H, Ishiwata S, Kurihara S. Acidosis or inorganic phosphate enhances the length dependence of tension in rat skinned cardiac muscle. J Physiol 2001;536:153–60.

[119] Fuchs F, Wang YP. Sarcomere length versus interfilament spacing as determinants of cardiac myofilament Ca2+ sensitivity and Ca2+ binding. J Mol Cell Cardiol 1996;28:1375–83.

[120] Fukuda N, Wu Y, Farman G, Irving TC, Granzier H. Titin isoform variance and length dependence of activation in skinned bovine cardiac muscle. J Physiol 2003;553:147–54.

[121] Martyn D a, Adhikari BB, Regnier M, Gu J, Xu S, Yu LC. Response of equatorial x-ray reflections and stiffness to altered sarcomere length and myofilament lattice spacing in relaxed skinned cardiac muscle. Biophysical Journal 2004;86:1002–11.

[122] Wang YP, Fuchs F. Osmotic compression of skinned cardiac and skeletal muscle bundles: effects on force generation, Ca2+ sensitivity and Ca2+ binding. J Mol Cell Cardiol 1995;27:1235–44.

[123] Houmeida A, Heeley DH, Belknap B, White HD. Mechanism of regulation of native cardiac muscle thin filaments by rigor cardiac myosin-S1 and calcium. J Biol Chem 2010;285:32760–9.

[124] Gillis TE, Martyn D a, Rivera AJ, Regnier M. Investigation of thin filament near-neighbour regulatory unit interactions during force development in skinned cardiac and skeletal muscle. The Journal of Physiology 2007;580:561–76.

[125] Smith L, Tainter C, Regnier M, Martyn DA. Cooperative cross-bridge activation of thin filaments contributes to the Frank-Starling mechanism in cardiac muscle. Biophys J 2009;96:3692–702.

[126] Dong W-J, Jayasundar JJ, An J, Xing J, Cheung HC. Effects of PKA phosphorylation of cardiac troponin I and strong crossbridge on conformational transitions of the N-domain of cardiac troponin C in regulated thin filaments. Biochemistry 2007;46:9752–61.

[127] Arteaga GM, Kobayashi T, Solaro RJ. Molecular actions of drugs that sensitize cardiac myofilaments to Ca2+. Ann Med 2002;34:248–58.

[128] Hanft LM, McDonald KS. Sarcomere length dependence of power output is increased after PKA treatment in rat cardiac myocytes. American Journal of Physiology Heart and Circulatory Physiology 2009;296:H1524–31.

[129] Kajiwara H, Morimoto S, Fukuda N, Ohtsuki I, Kurihara S. Effect of troponin I phosphorylation by protein kinase A on length-dependence of tension activation in skinned cardiac muscle fibers. Biochemical and Biophysical Research Communications 2000;272:104–10.

[130] Layland J, Solaro RJ, Shah AM. Regulation of cardiac contractile function by troponin I phosphorylation. Cardiovasc Res 2005;66:12–21.

[131] Burkart EM, Sumandea MP, Kobayashi T, Nili M, Martin AF, Homsher E, et al. Phosphorylation or glutamic acid substitution at protein kinase C sites on cardiac troponin I differentially depress myofilament tension and shortening velocity. The Journal of Biological Chemistry 2003;278:11265–72.

[132] Sumandea MP, Burkart EM, Kobayashi T, De Tombe PP, Solaro RJ. Molecular and integrated biology of thin filament protein phosphorylation in heart muscle. Annals of the New York Academy of Sciences 2004;1015:39–52.

[133] Kobayashi T, Solaro RJ. Calcium, thin filaments, and the integrative biology of cardiac contractility. Annual Review of Physiology 2005;67:39–67.

[134] Moir AJ, Solaro RJ, Perry S V. The site of phosphorylation of troponin I in the perfused rabbit heart. The effect of adrenaline. The Biochemical Journal 1980;185:505–13.

[135] Zhang R, Zhao J, Potter JD. Phosphorylation of both serine residues in cardiac troponin I is required to decrease the Ca2+ affinity of cardiac troponin C. The Journal of Biological Chemistry 1995;270:30773–80.

[136] Chandra M, Dong WJ, Pan BS, Cheung HC, Solaro RJ. Effects of protein kinase A phosphorylation on signaling between cardiac troponin I and the N-terminal domain of cardiac troponin C. Biochemistry 1997;36:13305–11.

[137] Kentish JC, McCloskey DT, Layland J, Palmer S, Leiden JM, Martin AF, et al. Phosphorylation of troponin I by protein kinase A accelerates relaxation and crossbridge cycle kinetics in mouse ventricular muscle. Circulation Research 2001;88:1059–65.

[138] Zhang R, Zhao J, Mandveno A, Potter JD. Cardiac troponin I phosphorylation increases the rate of cardiac muscle relaxation. Circulation Research 1995;76:1028–35.

[139] Finley N, Abbott MB, Abusamhadneh E, Gaponenko V, Dong W, Gasmi-Seabrook G, et al. NMR analysis of cardiac troponin C-troponin I complexes: effects of phosphorylation. FEBS Letters 1999;453:107–12.

[140] Li MX, Wang X, Lindhout DA, Buscemi N, Van Eyk JE, Sykes BD. Phosphorylation and mutation of human cardiac troponin I deferentially destabilize the interaction of the functional regions of troponin I with troponin C. Biochemistry 2003;42:14460–8.

[141] Robertson SP, Johnson JD, Holroyde MJ, Kranias EG, Potter JD, Solaro RJ. The effect of troponin I phosphorylation on the Ca2+-binding properties of the Ca2+-regulatory site of bovine cardiac troponin. The Journal of Biological Chemistry 1982;257:260–3.

[142] Moolman-Smook J, Flashman E, de Lange W, Li Z, Corfield V, Redwood C, et al. Identification of novel interactions between domains of Myosin binding protein-C that are modulated by hypertrophic cardiomyopathy missense mutations. Circulation Research 2002;91:704–11.

[143] Flashman E, Redwood C, Moolman-Smook J, Watkins H. Cardiac myosin binding protein C: its role in physiology and disease. Circulation Research 2004;94:1279–89.

[144] Stelzer JE, Larsson L, Fitzsimons DP, Moss RL. Activation dependence of stretch activation in mouse skinned myocardium: implications for ventricular function. The Journal of General Physiology 2006;127:95–107.

[145] Granzier H, Labeit S. Cardiac titin: an adjustable multi-functional spring. The Journal of Physiology 2002;541:335–42.

[146] Cazorla O, Wu Y, Irving TC, Granzier H. Titin-based modulation of calcium sensitivity of active tension in mouse skinned cardiac myocytes. Circulation Research 2001;88:1028–35.

[147] Granzier H, Labeit D, Wu Y, Labeit S. Titin as a modular spring: emerging mechanisms for elasticity control by titin in cardiac physiology and pathophysiology. Journal of Muscle Research and Cell Motility 2002;23:457–71.

[148] Yamasaki R, Wu Y, McNabb M, Greaser M, Labeit S, Granzier H. Protein kinase A phosphorylates titin's cardiac-specific N2B domain and reduces passive tension in rat cardiac myocytes. Circulation Research 2002;90:1181–8.

[149] Fukuda N, Wu Y, Nair P, Granzier HL. Phosphorylation of titin modulates passive stiffness of cardiac muscle in a titin isoform-dependent manner. The Journal of General Physiology 2005;125:257–71.

[150] Colson BA, Bekyarova T, Locher MR, Fitzsimons DP, Irving TC, Moss RL. Protein kinase A-mediated phosphorylation of cMyBP-C increases proximity of myosin heads to actin in resting myocardium. Circulation Research 2008;103:244–51.

[151] Shaffer JF, Kensler RW, Harris SP. The myosin-binding protein C motif binds to F-actin in a phosphorylation-sensitive manner. The Journal of Biological Chemistry 2009;284:12318–27.

[152] Krüger M, Linke WA. Protein kinase-A phosphorylates titin in human heart muscle and reduces myofibrillar passive tension. Journal of Muscle Research and Cell Motility 2006;27:435–44.

[153] Noland TA, Guo X, Raynor RL, Jideama NM, Averyhart-Fullard V, Solaro RJ, et al. Cardiac troponin I mutants. Phosphorylation by protein kinases C and A and regulation of Ca(2+)-stimulated MgATPase of reconstituted actomyosin S-1. The Journal of Biological Chemistry 1995;270:25445–54.

[154] Dohet C, al-Hillawi E, Trayer IP, Rüegg JC. Reconstitution of skinned cardiac fibres with human recombinant cardiac troponin-I mutants and troponin-C. FEBS Letters 1995;377:131–4.

[155] Millman BM. The filament lattice of striated muscle. Physiological Reviews 1998;78:359–91.

[156] Winegrad S. Myosin binding protein C, a potential regulator of cardiac contractility. Circulation Research n.d.;86:6–7.

[157] Granzier HL, Labeit S. The giant protein titin: a major player in myocardial mechanics, signaling, and disease. Circulation Research 2004;94:284–95.

[158] Li MX, Wang X, Sykes BD. Structural based insights into the role of troponin in cardiac muscle pathophysiology. Journal of Muscle Research and Cell Motility 2004;25:559–79.

[159] Howarth JW, Meller J, Solaro RJ, Trewhella J, Rosevear PR. Phosphorylation-dependent conformational transition of the cardiac specific N-extension of troponin I in cardiac troponin. Journal of Molecular Biology 2007;373:706–22.

[160] Sadayappan S, Finley N, Howarth JW, Osinska H, Klevitsky R, Lorenz JN, et al. Role of the acidic N' region of cardiac troponin I in regulating myocardial function. FASEB Journal : Official Publication of the Federation of American Societies for Experimental Biology 2008;22:1246–57.

[161] Wattanapermpool J, Guo X, Solaro RJ. The unique amino-terminal peptide of cardiac troponin I regulates myofibrillar activity only when it is phosphorylated. Journal of Molecular and Cellular Cardiology 1995;27:1383–91.

[162] Harris SP, Rostkova E, Gautel M, Moss RL. Binding of myosin binding protein-C to myosin subfragment S2 affects contractility independent of a tether mechanism. Circulation Research 2004;95:930–6.

[163] Tong CW, Stelzer JE, Greaser ML, Powers PA, Moss RL. Acceleration of crossbridge kinetics by protein kinase A phosphorylation of cardiac myosin binding protein C modulates cardiac function. Circulation Research 2008;103:974–82.

[164] Chen PP, Patel JR, Rybakova IN, Walker JW, Moss RL. Protein kinase A-induced myofilament desensitization to Ca(2+) as a result of phosphorylation of cardiac myosin-binding protein C. The Journal of General Physiology 2010;136:615–27.

[165] Verduyn SC, Zaremba R, van der Velden J, Stienen GJM. Effects of contractile protein phosphorylation on force development in permeabilized rat cardiac myocytes. Basic Research in Cardiology 2007;102:476–87.

[166] Colson BA, Bekyarova T, Fitzsimons DP, Irving TC, Moss RL. Radial displacement of myosin cross-bridges in mouse myocardium due to ablation of myosin binding protein-C. Journal of Molecular Biology 2007;367:36–41.

[167] Robinson JM, Dong W-J, Xing J, Cheung HC. Switching of troponin I: Ca(2+) and myosin-induced activation of heart muscle. Journal of Molecular Biology 2004;340:295–305.

[168] Dong W-J, Xing J, Ouyang Y, An J, Cheung HC. Structural kinetics of cardiac troponin C mutants linked to familial hypertrophic and dilated cardiomyopathy in troponin complexes. The Journal of Biological Chemistry 2008;283:3424–32.

[169] Gaponenko V, Abusamhadneh E, Abbott MB, Finley N, Gasmi-Seabrook G, Solaro RJ, et al. Effects of troponin I phosphorylation on conformational exchange in the regulatory domain of cardiac troponin C. The Journal of Biological Chemistry 1999;274:16681–4.

[170] Kulikovskaya I, McClellan G, Flavigny J, Carrier L, Winegrad S. Effect of MyBP-C binding to actin on contractility in heart muscle. The Journal of General Physiology 2003;122:761–74.

[171] Farman GP, Gore D, Allen E, Schoenfelt K, Irving TC, de Tombe PP. Myosin head orientation: a structural determinant for the Frank-Starling relationship. American Journal of Physiology Heart and Circulatory Physiology 2011;300:H2155–60.

[172] Benitah J-P, Alvarez JL, Gómez AM. L-type Ca(2+) current in ventricular cardiomyocytes. Journal of Molecular and Cellular Cardiology 2010;48:26–36.

[173] LeWinter MM. Functional consequences of sarcomeric protein abnormalities in failing myocardium. Heart Fail Rev 2005;10:249–57.

[174] Palmer BM. Thick filament proteins and performance in human heart failure. Heart Failure Reviews 2005;10:187–97.

[175] Holt E, Tønnessen T, Lunde PK, Semb SO, Wasserstrom J a, Sejersted OM, et al. Mechanisms of cardiomyocyte dysfunction in heart failure following myocardial infarction in rats. Journal of Molecular and Cellular Cardiology 1998;30:1581–93.

[176] Li P, Park C, Micheletti R, Li B, Cheng W, Sonnenblick EH, et al. Myocyte performance during evolution of myocardial infarction in rats: effects of propionyl-L-carnitine. The American Journal of Physiology 1995;268:H1702–13.

[177] Belin RJ, Sumandea MP, Kobayashi T, Walker LA, Rundell VL, Urboniene D, et al. Left ventricular myofilament dysfunction in rat experimental hypertrophy and congestive heart

failure. American Journal of Physiology Heart and Circulatory Physiology 2006;291:H2344–53.

[178] Belin RJ, Sumandea MP, Allen EJ, Schoenfelt K, Wang H, Solaro RJ, et al. Augmented protein kinase C-alpha-induced myofilament protein phosphorylation contributes to myofilament dysfunction in experimental congestive heart failure. Circulation Research 2007;101:195–204.

[179] Hamdani N, Kooij V, van Dijk S, Merkus D, Paulus WJ, Remedios CD, et al. Sarcomeric dysfunction in heart failure. Cardiovascular Research 2007;77:649–58.

[180] Kass D a, Solaro RJ. Mechanisms and use of calcium-sensitizing agents in the failing heart. Circulation 2006;113:305–15.

[181] Li RK, Jia ZQ, Weisel RD, Mickle DA, Zhang J, Mohabeer MK, et al. Cardiomyocyte transplantation improves heart function. The Annals of Thoracic Surgery 1996;62:654–60; discussion 660–1.

[182] Müller-Ehmsen J, Whittaker P, Kloner RA, Dow JS, Sakoda T, Long TI, et al. Survival and development of neonatal rat cardiomyocytes transplanted into adult myocardium. Journal of Molecular and Cellular Cardiology 2002;34:107–16.

[183] Scorsin M, Hagege AA, Marotte F, Mirochnik N, Copin H, Barnoux M, et al. Does transplantation of cardiomyocytes improve function of infarcted myocardium? Circulation 1997;96:II–188–93.

[184] Huwer H, Winning J, Vollmar B, Welter C, Löhbach C, Menger MD, et al. Long-term cell survival and hemodynamic improvements after neonatal cardiomyocyte and satellite cell transplantation into healed myocardial cryoinfarcted lesions in rats. Cell Transplantation 2003;12:757–67.

[185] Sacconi L, Ferrantini C, Lotti J, Coppini R, Yan P, Loew LM, et al. Action potential propagation in transverse-axial tubular system is impaired in heart failure. Proceedings of the National Academy of Sciences of the United States of America 2012;109:5815–9.

[186] Liang B, Chung F, Qu Y, Pavlov D, Gillis TE, Tikunova SB, et al. Familial hypertrophic cardiomyopathy-related cardiac troponin C mutation L29Q affects Ca2+ binding and myofilament contractility. Physiological Genomics 2008;33:257–66.

[187] Dong WJ, Jayasundar JJ, An J, Xing J, Cheung HC. Effects of PKA phosphorylation of cardiac troponin I and strong crossbridge on conformational transitions of the N-domain of cardiac troponin C in regulated thin filaments. Biochemistry 2007;46:9752–61.

[188] Fentzke RC, Buck SH, Patel JR, Lin H, Wolska BM, Stojanovic MO, et al. Impaired cardiomyocyte relaxation and diastolic function in transgenic mice expressing slow skeletal troponin I in the heart. The Journal of Physiology 1999;517 (Pt 1:143–57.

[189] Westfall M V, Rust EM, Albayya F, Metzger JM. Adenovirus-mediated myofilament gene transfer into adult cardiac myocytes. Methods Cell Biol 1997;52:307–22.

[190] Westfall M V, Rust EM, Metzger JM. Slow skeletal troponin I gene transfer, expression, and myofilament incorporation enhances adult cardiac myocyte contractile function. Proceedings of the National Academy of Sciences of the United States of America 1997;94:5444–9.

[191] Westfall M V. Myofilament Calcium Sensitivity and Cardiac Disease: Insights From Troponin I Isoforms and Mutants. Circulation Research 2002;91:525–31.

[192] Lim CC, Yang H, Yang M, Wang C-K, Shi J, Berg E a, et al. A novel mutant cardiac troponin C disrupts molecular motions critical for calcium binding affinity and cardiomyocyte contractility. Biophysical Journal 2008;94:3577–89.

[193] Maron BJ, Towbin JA, Thiene G, Antzelevitch C, Corrado D, Arnett D, et al. Contemporary definitions and classification of the cardiomyopathies: an American Heart Association Scientific Statement from the Council on Clinical Cardiology, Heart Failure and Transplantation Committee; Quality of Care and Outcomes Research and Functio. Circulation 2006;113:1807–16.

[194] Elliott P, Andersson B, Arbustini E, Bilinska Z, Cecchi F, Charron P, et al. Classification of the cardiomyopathies: a position statement from the European Society Of Cardiology Working Group on Myocardial and Pericardial Diseases. European Heart Journal 2008;29:270–6.

[195] Maron BJ. Hypertrophic cardiomyopathy: a systematic review. JAMA : the Journal of the American Medical Association 2002;287:1308–20.

[196] Kamisago M, Sharma SD, DePalma SR, Solomon S, Sharma P, McDonough B, et al. Mutations in sarcomere protein genes as a cause of dilated cardiomyopathy. The New England Journal of Medicine 2000;343:1688–96.

[197] Molkentin JD, Lu JR, Antos CL, Markham B, Richardson J, Robbins J, et al. A calcineurin-dependent transcriptional pathway for cardiac hypertrophy. Cell 1998;93:215–28.

[198] Nicol RL, Frey N, Olson EN. From the sarcomere to the nucleus: role of genetics and signaling in structural heart disease. Annual Review of Genomics and Human Genetics 2000;1:179–223.

[199] Ahmad F, Seidman JG, Seidman CE. The genetic basis for cardiac remodeling. Annual Review of Genomics and Human Genetics 2005;6:185–216.

[200] Chang AN, Potter JD. Sarcomeric protein mutations in dilated cardiomyopathy. Heart Failure Reviews 2005;10:225–35.

[201] Mestroni L, Rocco C, Gregori D, Sinagra G, Di Lenarda A, Miocic S, et al. Familial dilated cardiomyopathy: evidence for genetic and phenotypic heterogeneity. Heart Muscle Disease Study Group. Journal of the American College of Cardiology 1999;34:181–90.

[202] Du CK, Morimoto S, Nishii K, Minakami R, Ohta M, Tadano N, et al. Knock-in mouse model of dilated cardiomyopathy caused by troponin mutation. Circ Res 2007;101:185–94.

[203] Baudenbacher F, Schober T, Pinto JR, Sidorov VY, Hilliard F, Solaro RJ, et al. Myofilament Ca2+ sensitization causes susceptibility to cardiac arrhythmia in mice. The Journal of Clinical Investigation 2008;118:3893–903.

[204] Solaro RJ, Gambassi G, Warshaw DM, Keller MR, Spurgeon HA, Beier N, et al. Stereoselective actions of thiadiazinones on canine cardiac myocytes and myofilaments. Circulation Research 1993;73:981–90.

[205] White J, Lee JA, Shah N, Orchard CH. Differential effects of the optical isomers of EMD 53998 on contraction and cytoplasmic Ca2+ in isolated ferret cardiac muscle. Circulation Research 1993;73:61–70.

[206] Clemmens EW, Regnier M. Skeletal regulatory proteins enhance thin filament sliding speed and force by skeletal HMM. Journal of Muscle Research and Cell Motility 2004;25:515–25.

[207] Kashlan OB, Cooperman BS. Comprehensive model for allosteric regulation of mammalian ribonucleotide reductase: refinements and consequences. Biochemistry 2003;42:1696–706.

[208] Kashlan OB, Scott CP, Lear JD, Cooperman BS. A comprehensive model for the allosteric regulation of mammalian ribonucleotide reductase. Functional consequences of ATP- and dATP-induced oligomerization of the large subunit. Biochemistry 2002;41:462–74.

[209] Nishimura S, Nagai S, Sata M, Katoh M, Yamashita H, Saeki Y, et al. Expression of green fluorescent protein impairs the force-generating ability of isolated rat ventricular cardiomyocytes. Molecular and Cellular Biochemistry 2006;286:59–65.

[210] Herron TJ, Devaney E, Mundada L, Arden E, Day S, Guerrero-Serna G, et al. Ca2+-independent positive molecular inotropy for failing rabbit and human cardiac muscle by alpha-myosin motor gene transfer. FASEB Journal : Official Publication of the Federation of American Societies for Experimental Biology 2010;24:415–24.

[211] Schoffstall B, Clark A, Chase PB. Positive inotropic effects of low dATP/ATP ratios on mechanics and kinetics of porcine cardiac muscle. Biophysical Journal 2006;91:2216–26.

[212] Schoffstall B, Chase PB. Increased intracellular [dATP] enhances cardiac contraction in embryonic chick cardiomyocytes. Journal of Cellular Biochemistry 2008;104:2217–27.

[213] Xu X, Page JL, Surtees JA, Liu H, Lagedrost S, Lu Y, et al. Broad overexpression of ribonucleotide reductase genes in mice specifically induces lung neoplasms. Cancer Research 2008;68:2652–60.

[214] Regnier M, Lee DM, Homsher E. ATP analogs and muscle contraction: mechanics and kinetics of nucleoside triphosphate binding and hydrolysis. Biophys J 1998;74:3044–58.

[215] Regnier M, Homsher E. The effect of ATP analogs on posthydrolytic and force development steps in skinned skeletal muscle fibers. Biophys J 1998;74:3059–71.

[216] Regnier M, Martyn D a, Chase PB. Calcium regulation of tension redevelopment kinetics with 2-deoxy-ATP or low [ATP] in rabbit skeletal muscle. Biophysical Journal 1998;74:2005–15.

[217] Korte FS, Herron TJ, Rovetto MJ, McDonald KS. Power output is linearly related to MyHC content in rat skinned myocytes and isolated working hearts. American Journal of Physiology Heart and Circulatory Physiology 2005;289:H801–12.

[218] Hilgemann DW, Ball R. Regulation of cardiac Na+,Ca2+ exchange and KATP potassium channels by PIP2. Science (New York, NY) 1996;273:956–9.

[219] Janssen PML, Periasamy M. Determinants of frequency-dependent contraction and relaxation of mammalian myocardium. Journal of Molecular and Cellular Cardiology 2007;43:523–31.

[220] Bassani JW, Bassani RA, Bers DM. Relaxation in rabbit and rat cardiac cells: species-dependent differences in cellular mechanisms. The Journal of Physiology 1994;476:279–93.

[221] Luo Y, Davis JP, Smillie LB, Rall JA. Determinants of relaxation rate in rabbit skinned skeletal muscle fibres. The Journal of Physiology 2002;545:887–901.

[222] Luo Y, Davis JP, Tikunova SB, Smillie LB, Rall JA. Myofibrillar determinants of rate of relaxation in skinned skeletal muscle fibers. Advances in Experimental Medicine and Biology 2003;538:573–81; discussion 581–2.

[223] Piroddi N, Belus A, Scellini B, Tesi C, Giunti G, Cerbai E, et al. Tension generation and relaxation in single myofibrils from human atrial and ventricular myocardium. Pflügers Archiv : European Journal of Physiology 2007;454:63–73.

[224] Tesi C, Piroddi N, Colomo F, Poggesi C. Relaxation kinetics following sudden Ca(2+) reduction in single myofibrils from skeletal muscle. Biophysical Journal 2002;83:2142–51.

[225] Edman KA. The velocity of unloaded shortening and its relation to sarcomere length and isometric force in vertebrate muscle fibres. The Journal of Physiology 1979;291:143–59.

[226] Hinken AC, McDonald KS. Inorganic phosphate speeds loaded shortening in rat skinned cardiac myocytes. American Journal of Physiology Cell Physiology 2004;287:C500–7.

[227] Lin H, Parmacek MS, Morle G, Bolling S, Leiden JM. Expression of recombinant genes in myocardium in vivo after direct injection of DNA. Circulation 1990;82:2217–21.

[228] Buttrick PM, Kass A, Kitsis RN, Kaplan ML, Leinwand LA. Behavior of genes directly injected into the rat heart in vivo. Circulation Research 1992;70:193–8.

[229] Iwata A, Sai S, Nitta Y, Chen M, de Fries-Hallstrand R, Dalesandro J, et al. Liposome-mediated gene transfection of endothelial nitric oxide synthase reduces endothelial activation and leukocyte infiltration in transplanted hearts. Circulation 2001;103:2753–9.

[230] Miyagawa S, Sawa Y, Taketani S, Kawaguchi N, Nakamura T, Matsuura N, et al. Myocardial regeneration therapy for heart failure: hepatocyte growth factor enhances the effect of cellular cardiomyoplasty. Circulation 2002;105:2556–61.

[231] French BA, Mazur W, Geske RS, Bolli R. Direct in vivo gene transfer into porcine myocardium using replication-deficient adenoviral vectors. Circulation 1994;90:2414–24.

[232] Chu D, Sullivan CC, Weitzman MD, Du L, Wolf PL, Jamieson SW, et al. Direct comparison of efficiency and stability of gene transfer into the mammalian heart using adeno-associated virus versus adenovirus vectors. The Journal of Thoracic and Cardiovascular Surgery 2003;126:671–9.

[233] Vassalli G, Büeler H, Dudler J, von Segesser LK, Kappenberger L. Adeno-associated virus (AAV) vectors achieve prolonged transgene expression in mouse myocardium and arteries in vivo: a comparative study with adenovirus vectors. International Journal of Cardiology 2003;90:229–38.

[234] Wright MJ, Wightman LM, Lilley C, de Alwis M, Hart SL, Miller A, et al. In vivo myocardial gene transfer: optimization, evaluation and direct comparison of gene transfer vectors. Basic Research in Cardiology n.d.;96:227–36.

[235] Berns KI, Linden RM. The cryptic life style of adeno-associated virus. BioEssays : News and Reviews in Molecular, Cellular and Developmental Biology 1995;17:237–45.

[236] Flotte TR. Gene therapy progress and prospects: recombinant adeno-associated virus (rAAV) vectors. Gene Therapy 2004;11:805–10.

[237] Berns KI, Adler S. Separation of two types of adeno-associated virus particles containing complementary polynucleotide chains. Journal of Virology 1972;9:394–6.

[238] Lusby E, Fife KH, Berns KI. Nucleotide sequence of the inverted terminal repetition in adeno-associated virus DNA. Journal of Virology 1980;34:402–9.

[239] Srivastava A, Lusby EW, Berns KI. Nucleotide sequence and organization of the adeno-associated virus 2 genome. Journal of Virology 1983;45:555–64.

[240] Straus SE, Sebring ED, Rose JA. Concatemers of alternating plus and minus strands are intermediates in adenovirus-associated virus DNA synthesis. Proceedings of the National Academy of Sciences of the United States of America 1976;73:742–6.

[241] Xiao X, Xiao W, Li J, Samulski RJ. A novel 165-base-pair terminal repeat sequence is the sole cis requirement for the adeno-associated virus life cycle. Journal of Virology 1997;71:941–8.

[242] Rutledge EA, Halbert CL, Russell DW. Infectious clones and vectors derived from adeno-associated virus (AAV) serotypes other than AAV type 2. Journal of Virology 1998;72:309–19.

[243] Gao G-P, Alvira MR, Wang L, Calcedo R, Johnston J, Wilson JM. Novel adeno-associated viruses from rhesus monkeys as vectors for human gene therapy. Proceedings of the National Academy of Sciences of the United States of America 2002;99:11854–9.

[244] Muramatsu S, Mizukami H, Young NS, Brown KE. Nucleotide sequencing and generation of an infectious clone of adeno-associated virus 3. Virology 1996;221:208–17.

[245] Chiorini JA, Kim F, Yang L, Kotin RM. Cloning and characterization of adeno-associated virus type 5. Journal of Virology 1999;73:1309–19.

[246] Chiorini JA, Yang L, Liu Y, Safer B, Kotin RM. Cloning of adeno-associated virus type 4 (AAV4) and generation of recombinant AAV4 particles. Journal of Virology 1997;71:6823–33.

[247] Gregorevic P, Allen JM, Minami E, Blankinship MJ, Haraguchi M, Meuse L, et al. rAAV6-microdystrophin preserves muscle function and extends lifespan in severely dystrophic mice. Nature Medicine 2006;12:787–9.

[248] Gregorevic P, Blankinship MJ, Allen JM, Crawford RW, Meuse L, Miller DG, et al. Systemic delivery of genes to striated muscles using adeno-associated viral vectors. Nature Medicine 2004;10:828–34.

[249] Palomeque J, Chemaly ER, Colosi P, Wellman J a, Zhou S, Del Monte F, et al. Efficiency of eight different AAV serotypes in transducing rat myocardium in vivo. Gene Therapy 2007;14:989–97.

[250] Su H, Huang Y, Takagawa J, Barcena A, Arakawa-Hoyt J, Ye J, et al. AAV serotype-1 mediates early onset of gene expression in mouse hearts and results in better therapeutic effect. Gene Therapy 2006;13:1495–502.

[251] Wang Z, Zhu T, Qiao C, Zhou L, Wang B, Zhang J, et al. Adeno-associated virus serotype 8 efficiently delivers genes to muscle and heart. Nature Biotechnology 2005;23:321–8.

[252] Inagaki K, Fuess S, Storm TA, Gibson GA, Mctiernan CF, Kay MA, et al. Robust systemic transduction with AAV9 vectors in mice: efficient global cardiac gene transfer superior to that of AAV8. Molecular Therapy : the Journal of the American Society of Gene Therapy 2006;14:45–53.

[253] Pacak CA, Mah CS, Thattaliyath BD, Conlon TJ, Lewis MA, Cloutier DE, et al. Recombinant adeno-associated virus serotype 9 leads to preferential cardiac transduction in vivo. Circulation Research 2006;99:e3–9.

[254] Zincarelli C, Soltys S, Rengo G, Koch WJ, Rabinowitz JE. Comparative cardiac gene delivery of adeno-associated virus serotypes 1-9 reveals that AAV6 mediates the most efficient transduction in mouse heart. Clin Transl Sci 2010;3:81–9.

[255] Prasad K-MR, Xu Y, Yang Z, Acton ST, French B a. Robust cardiomyocyte-specific gene expression following systemic injection of AAV: in vivo gene delivery follows a Poisson distribution. Gene Therapy 2011;18:43–52.

[256] Blankinship MJ, Gregorevic P, Allen JM, Harper SQ, Harper H, Halbert CL, et al. Efficient transduction of skeletal muscle using vectors based on adeno-associated virus serotype 6. Molecular Therapy : the Journal of the American Society of Gene Therapy 2004;10:671–8.

[257] Allen JM, Halbert CL, Miller a D. Improved adeno-associated virus vector production with transfection of a single helper adenovirus gene, E4orf6. Molecular Therapy : the Journal of the American Society of Gene Therapy 2000;1:88–95.

[258] Tidyman WE, Sehnert AJ, Huq A, Agard J, Deegan F, Stainier DYR, et al. In vivo regulation of the chicken cardiac troponin T gene promoter in zebrafish embryos. Developmental Dynamics an Official Publication of the American Association of Anatomists 2003;227:484–96.

[259] Iannello RC, Mar JH, Ordahl CP. Characterization of a promoter element required for transcription in myocardial cells. The Journal of Biological Chemistry 1991;266:3309–16.

[260] Cooper TA, Ordahl CP. A Single Cardiac TroponinT Gene Generates Embryonic and Adult Isoforms via Developmentally Regulated Alternate Splicing. Journal of Biological Chemistry 1986;260.

[261] Wang G, Yeh HI, Lin JJ. Characterization of cis-regulating elements and trans-activating factors of the rat cardiac troponin T gene. The Journal of Biological Chemistry 1994;269:30595–603.

[262] Wang Q, Sigmund CD, Lin JJ. Identification of cis elements in the cardiac troponin T gene conferring specific expression in cardiac muscle of transgenic mice. Circulation Research 2000;86:478–84.

[263] Wang Q. A Novel TCTG(G/C) Direct Repeat and an A/T-Rich HMG2-Binding Site Control the Expression of the RatCardiacTroponin T Gene. Journal of Molecular and Cellular Cardiology 2002;34:1667–79.

[264] Ma H, Sumbilla CM, Farrance IK, Klein MG, Inesi G. Cell-specific expression of SERCA, the exogenous Ca2+ transport ATPase, in cardiac myocytes. Am J Physiol Cell Physiol 2004;286:C556–64.

[265] Donnelly ML, Luke G, Mehrotra A, Li X, Hughes LE, Gani D, et al. Analysis of the aphthovirus 2A/2B polyprotein "cleavage" mechanism indicates not a proteolytic reaction, but a novel translational effect: a putative ribosomal "skip". The Journal of General Virology 2001;82:1013–25.

[266] Donnelly ML, Hughes LE, Luke G, Mendoza H, ten Dam E, Gani D, et al. The "cleavage" activities of foot-and-mouth disease virus 2A site-directed mutants and naturally occurring "2A-like" sequences. The Journal of General Virology 2001;82:1027–41.

[267] Trichas G, Begbie J, Srinivas S. Use of the viral 2A peptide for bicistronic expression in transgenic mice. BMC Biology 2008;6:40.

[268] De Felipe P, Luke G a, Hughes LE, Gani D, Halpin C, Ryan MD. E unum pluribus: multiple proteins from a self-processing polyprotein. Trends in Biotechnology 2006;24:68–75.

[269] Unal R, Ahmed BA, Jeffus BC, Harney JT, Lyle CS, Wu Y-K, et al. At diabetes-like concentration, glucose down-regulates the placental serotonin transport system in a cell-cycle-dependent manner. Journal of Neurochemistry 2007;101:937–48.

[270] Kim JH, Lee S-R, Li L-H, Park H-J, Park J-H, Lee KY, et al. High cleavage efficiency of a 2A peptide derived from porcine teschovirus-1 in human cell lines, zebrafish and mice. PloS One 2011;6:e18556.

[271] Dong W-J, Jayasundar JJ, An J, Xing J, Cheung HC. Effects of PKA phosphorylation of cardiac troponin I and strong crossbridge on conformational transitions of the N-domain of cardiac troponin C in regulated thin filaments. Biochemistry 2007;46:9752–61.

[272] Lim CC, Yang H, Yang M, Wang C-K, Shi J, Berg E a, et al. A novel mutant cardiac troponin C disrupts molecular motions critical for calcium binding affinity and cardiomyocyte contractility. Biophysical Journal 2008;94:3577–89.

[273] Tardiff JC. Sarcomeric proteins and familial hypertrophic cardiomyopathy: linking mutations in structural proteins to complex cardiovascular phenotypes. Heart Failure Reviews 2005;10:237–48.